Physics Reports 466 (2008) 1–103

Contents lists available at ScienceDirect

Physics Reports

journal homepage: www.elsevier.com/locate/physrep

Electron impact dissociation of oxygen-containing molecules–A critical review

J.W. McConkey [a,b,*], C.P. Malone [a], P.V. Johnson [a], C. Winstead [c], V. McKoy [c], I. Kanik [a,**]

[a] *Jet Propulsion Laboratory, California Institute of Technology, Pasadena, CA 91109, USA*

[b] *Physics Department, University of Windsor, Ontario N9B 3P4, Canada*

[c] *A.A.Noyes Laboratory of Chemical Physics, California Institute of Technology, Pasadena, CA 91125, USA*

ARTICLE INFO

Article history:
Accepted 9 May 2008
Available online 17 May 2008
editor: J. Eichler

PACS:
34.80.Ht
34.80.Gs
34.80.My
34.80–i

Keywords:
Dissociation
Oxygen
Electron impact
Cross sections

ABSTRACT

The dissociation of a wide range of oxygen-containing molecules following impact with electrons of carefully controlled energy is critically reviewed. Molecules considered range from diatomics, like O_2 and CO, to large molecules of biological and technological interest. Dissociation mechanisms are discussed and, where possible, quantitative data for the various possible processes, ionization, attachment, dissociation, excitation, emission etc., are presented. Gaps and discrepancies in our current data base are highlighted. Both graphical and tabular data are presented.

Contents

* Corresponding address: University of Windsor, Sunset Avenue, Windsor, Ontario, N9B 3P4, Canada. Tel.: +1 519 253 3000; fax: +1 519 973 7075.
** Corresponding author. Tel.: +1 818 354 7233; fax: +1 818 393 4445.
E-mail addresses: mcconk@uwindsor.ca (J.W. McConkey), isik.kanik@jpl.nasa.gov (I. Kanik).

0370-1573/$ – see front matter © 2008 Elsevier B.V. All rights reserved.
doi:10.1016/j.physrep.2008.05.001

1. Introduction

Dissociation of oxygen-containing molecules is an important process in a wide range of environments and applications. Data relating to such processes form an important input into the understanding and modelling of such varied situations as the physics and chemistry of planetary atmospheres (particularly our own planet Earth), electrical discharges, radiation damage in biological materials and plasma waste disposal techniques [see Becker et al. (2000)]. Often an electron is the dissociation agent.

The present work represents an attempt to present and critically review the data that are currently available in the literature, particularly recent work that has not been reviewed previously. We note that it is much more than a collection of data; rather, it includes a detailed discussion of the dissociation processes, dynamics etc. Other reviews have dealt with subsections of this material or with individual oxygen-containing molecules, e.g. H_2O (Itikawa and Mason, 2005). Sometimes these reviews deal with scattering processes such as differential or total cross sections and do not consider dissociation explicitly. In these instances, this work represents an important and timely update. The reviews by Zecca et al. (1996, 1992) emphasized total cross section measurements but made reference to dissociative processes only where the cross sections were significant.

For this review we have considered material published up to mid-2007 though some more recent work known to the authors has been included also.

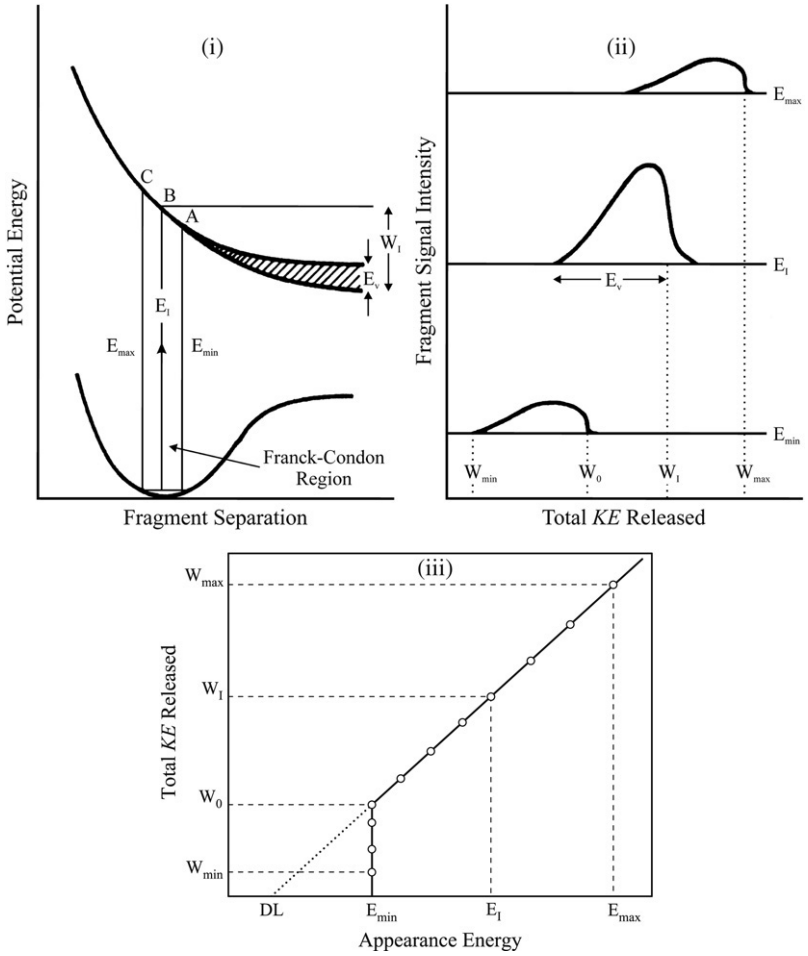

Fig. 1. (i) Cross section through the potential energy surfaces of a polyatomic molecule for dissociation into two fragments. One fragment is a molecule that can possess internal energy from zero to E_v. (ii) Kinetic energy distributions obtained for excitation to points A, B and C in the Franck–Condon region. (iii) Resultant plot of total released kinetic energy against appearance energy. Adapted from Allcock and McConkey (1978a).

2. Experimental considerations

When dissociation occurs it is often of interest not only to obtain the cross sections involved but also to determine the particular fragments, their kinetic energies and their state of internal excitation (electronic, vibrational, rotational). The details of the dissociation dynamics, the particular repulsive surfaces involved and other molecular information may also be of interest. The particular experimental set-up will be geared to the type of measurement being undertaken and to the nature of the fragment being studied, e.g. charged or uncharged.

To gain appreciation of the various parameters involved, consider the simplified diagram (Fig. 1), which illustrates the excitation of a molecule to a repulsive state followed by two-fragment dissociation. The excitation is governed by the so-called Franck–Condon Principle, which basically says that electronic excitation in a molecule occurs very quickly, in fact in a time period that is short compared to any nuclear motion in the molecule, vibration or rotation. Thus, in a potential energy versus fragment separation diagram like Fig. 1(i), the excitation occurs vertically. Because of the spreading of the ground state probability density distribution, excitation could occur to the region of the upper repulsive curve defined by ABC. If one of the fragments produced in the dissociation is a molecule it can possess internal energy, rotational and/or vibrational. Fig. 1(ii) shows the various kinetic energy distributions obtained following excitation to points A, B and C on the repulsive surface. We note that the shapes of the distributions are modified by the amount of available energy that is partitioned into internal rather than into kinetic energy, and also by any energy spread that may exist in the exciting electron beam. Often it is possible to measure fragment kinetic energies using time-of-flight (TOF) or other techniques (Zipf, 1984; Köllmann, 1978; Allan et al., 1996a).

If the kinetic energy released is plotted against the appearance energy, AE, when those fragments were first detected, a graph is obtained as shown in Fig. 1(iii). For two-fragment break-up this is linear and the extrapolation to where it cuts the appearance energy axis gives the dissociation limit for the process in question. The dissociation limit, DL, or asymptotic

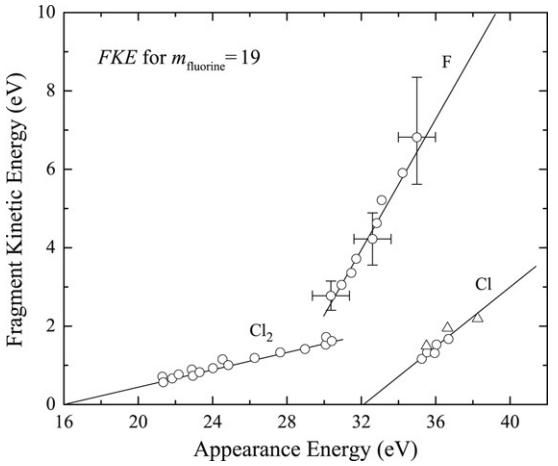

Fig. 2. Plots of appearance energies against fragment (assumed to be F) kinetic energy for three of the processes observed during the study of CCl_2F_2. The different slopes are indicative of different fragments shown, as discussed in the text. Adapted from Allcock and McConkey (1978b).

energy as it is sometimes called, may be defined as the energy required to break a bond and separate two fragments to infinite separation, plus the internal excitation energy of these fragments. Often fragment, rather than total, kinetic energy is displayed since the two quantities are linearly related.

For two-fragment break-up of, for instance, molecule XYZ into X + YZ, the situation is simplified. If no energy goes into internal energy of YZ, conservation of momentum leads to

$$\mathrm{KE_X} = m_{\mathrm{YZ}}/M_{\mathrm{XYZ}}[\mathrm{AE} - \mathrm{DL}] \tag{1}$$

where $\mathrm{KE_X}$ is the kinetic energy of the observed fragment and m_{YZ} and M_{XYZ} are the masses of the undetected fragment and parent molecule, respectively. Clearly a plot of $\mathrm{KE_X}$ against AE will have a slope, $m_{\mathrm{YZ}}/M_{\mathrm{XYZ}}$, characteristic of the mass being detected and an intercept that gives DL directly. If some of the available energy goes into internal (vibrational or rotational) energy of YZ and if this changes with impact energy, then the slope of the plot will be reduced.

Extensive measurements of diatomic molecular break-up illustrating this have been presented for both charged [e.g. the work of Locht et al. (1974) on N^+ production from N_2] and uncharged fragments [e.g. Rydberg production from N_2 and H_2 by Smyth et al. (1973) and Schiavone et al. (1975) respectively]. We note that in studies of polyatomic break-up of CH_4 (Schiavone et al., 1977) and CO_2 (Allcock and McConkey, 1976), Eq. (1) was found to describe the situation rather well, particularly when the incident electron energy was close to threshold.

For polyatomic molecules a plot of fragment KE against AE serves as a very useful first step towards fragment identification if this is not possible by other means. It is easy to show that if a particular mass is assumed for all fragments in such a plot, then lines of characteristic slope will be obtained for the individual masses being detected. This is illustrated in Fig. 2 adapted from the work of Allcock and McConkey (1978b) on the break up of CCl_2F_2. The detected fragment is assumed to be F and its appearance energy is plotted as a function of measured kinetic energy. The expected slope (Eq. (1)) is 0.84. Inspection of the figure reveals that one of the dissociation channels has this slope and hence must be the result of fragmentation into F + CCl_2F. Any other possible fragment with the exception of C would have a larger mass and hence a maximum slope of less than this.

Note that if the detected fragment (Eq. (1)) had been Y instead of X, the calculated KE would need to be modified by the ratio $m_{\mathrm{Y}}/m_{\mathrm{X}}$ and the slope modified to $m_{\mathrm{XZ}}/M_{\mathrm{XYZ}}$. Hence, Eq. (1) for the fragment kinetic energy would become, with some rearrangement,

$$\mathrm{KE} = [m_{\mathrm{X}}/m_{\mathrm{Y}}][m_{\mathrm{XZ}}/M_{\mathrm{XYZ}}][\mathrm{AE} - \mathrm{DL}]. \tag{2}$$

Thus under these conditions, Cl and Cl_2 detection would yield slopes of 0.38 and 0.11 respectively. These are indeed evidenced as shown in Fig. 2.

We note further that if total fragmentation of a polyatomic molecule occurs, there is no preferred energy sharing among the fragments, and fragments with a whole range of kinetic energies are observed at the same appearance energy. This gives lines of infinite slope on such graphs as in Fig. 1(iii) and 2. Examples of such a situation were found by Schiavone et al. (1977) for H Rydberg production from CH_4 and C_2H_6 dissociation and by Locht and Davister (1995) who investigated dissociative ionization in CO_2. Other possible scenarios that would produce lines of infinite slope have been discussed by Allcock and McConkey (1978a).

When the fragments and their internal energy status are identifiable and the dissociation limit and kinetic energy released have been established, it is possible to partially reconstruct the relevant potential energy surface such as in Fig. 1(i). Some examples of this for the break up of N_2O have been given by Allcock and McConkey (1978a) and by Cordaro et al. (1986) for H_2O. We note that for optically allowed dissociation channels, much more accurate probing of potential energy surfaces can

be accomplished by optical, laser-related techniques. Use of ultra-fast excitation pulses enables dissociation dynamics to be probed with unparalleled precision (Kling et al., 2006). Electron impact techniques come into their own when investigating optically forbidden channels, particularly those where a spin flip accompanies the excitation.

Recently, the development of multi-detector systems, covariance mapping and COLTRIMS ('Reaction Microscope')-type experiments have enabled molecular break-ups to be probed with greater precision by identifying the momenta and directions of the fragments, at least when charged particles are being considered [see e.g. Ullrich et al. (1997), Dörner et al. (2000) and Tian and Vidal (1998a,b)].

2.1. Symmetry considerations

Products of the electron impact dissociation process are emitted isotropically except at near-threshold energies where the momentum transfer direction (which takes the place of the photon polarization direction in the analogous photodissociation process) lies preferentially along the electron beam direction, particularly for electron attachment. At high electron energies it is perpendicular to this. Depending on the symmetries of the initial and final states, the transition moment can lie parallel or perpendicular to the internuclear axis. Thus the excitation process can pick out a subset of the target molecules whose internuclear axes are oriented favourably with respect to the electron beam direction. Because dissociation occurs on the time scale of a molecular vibration, molecular rotation is essentially "frozen" and the products of dissociation reflect the orientation of the parent molecule with respect to the electron beam at the instant of excitation. This is particularly so if the fragments possess significant translational kinetic energy. This situation was analysed first by Dunn (1962) based on symmetry considerations alone. He established rules that defined the various excitations that could occur and what level of anisotropy could result. van Brunt and Zare (1968) pointed out that the light emitted by dissociation fragments could be polarized. Further development of these ideas by O'Malley and Taylor (1968), van Brunt (1974), Teillet-Billy and Gauyacq (1984) and Ostrawsky et al. (1995) should be noted.

In practice, measured anisotropies tend to be small except for the simplest diatomics and for dissociative attachment. Usually for energies away from the near-threshold region, repulsive states of different symmetries contribute to the observed signals leading to a "washing out" of anisotropic effects (see Section 4 for specific examples).

2.2. Detection techniques

When the products of the dissociation are charged, or excited such that they subsequently emit optical radiation, conventional techniques are used to monitor them. Details of these techniques can be obtained from standard texts on mass or optical spectroscopy. Lindsay and Mangan (2003) have reviewed the various experimental techniques relative to ionization measurements and they have discussed the various problems that could affect the measurements, such as accurate pressure determination and discrimination effects in the collection of (often energetic) fragment ions. They emphasized the distinction between total ionization cross section measurements, which are the sum of the individual partial ionization cross sections, and total charge production cross section measurements, which are the sum of the partial ionization cross sections weighted by the charges of the respective ions. Most of the early experiments were of the latter, charge production, type.

For dissociative ionization, where identification of the fragment ions is necessary, some form of mass spectrometric detection system is required. Lindsay and Mangan point out some of the difficulties and possible errors that can occur with the use of quadrupole (or monopole) mass spectrometers and indirect normalization techniques to obtain absolute cross sections. They also highlight the need to demonstrate that total collection of all fragment ions is occurring.

If optical emissions from the fragments are being considered, care must be taken to take account of possible polarization of the radiation and polarization sensitivity of the detection equipment, though these effects are normally small ($<5\%$) and can be neglected relative to other, more substantial, errors in the measurements. Other secondary effects, such as trapping of resonance radiation, are usually negligible where dissociation occurs. Absolute calibration of optical emission data is a serious problem particularly in the VUV spectral region. Here secondary standards, in particular the emission of Lyman-α following electron impact on H_2 targets, are often used. van der Burgt et al. (1989) suggested correction factors that needed to be applied to earlier data following revisions to this standard in the 1980s. Additional work since that time has necessitated some further revision to the Lyman-α standard. This is discussed in Section 4.1.6.2.

Very helpful information can be obtained from such books as Moore et al. (2002), Märk and Dunn (1985), McDaniel (1989) and Massey et al. (1969) and such reviews as van der Burgt et al. (1989).

Neutral metastable fragments can be monitored using surface detectors where a process somewhat analogous to photoelectric emission occurs. Channel electron multipliers can be used where the internal energy is greater than about 8 eV and this can be extended to lower energies using a low work function surface as the primary electron emitter. Absolute calibration of these detectors is difficult and varies with the internal energy of the fragment. Both the nature and the cleanliness of the detecting surface are important.

If the internal energy of the fragment is lower than about 6 eV, other detection techniques are used. For example the atmospherically important species, $O(^1S_0)$, has an internal energy of 4.2 eV and a lifetime of just less than one second (Itikawa and Ichimura, 1990). Attempts to detect it by techniques such as Auger emission from a low work function surface (Gilpin

and Welge, 1971), by a chemi-ionization process (Stone et al., 1976), or by detection of inelastically scattered electrons, were limited by a lack of discrimination against other metastable atomic or molecular species or ground state, $O(^3P)$, and generally suffered from poor signal to background ratios.

Based in part on some earlier work by Kiefl et al. (1983), LeClair and McConkey (1993) used a TOF technique with a unique detector in order to observe $O(^1S_0)$ following electron impact on molecular parents (N_2O and O_2). The novel detector they developed consisted of a layer of Xe freshly deposited on a cryogenically cooled (∼65 K) surface. $O(^1S_0)$ atoms impinging on the surface formed excimers with Xe, which quickly decayed. This is a natural extension of the use of high pressure gaseous detection techniques, such as had been exploited by Cooper et al. (1961) and Simmons et al. (1979). Use of pulsed excitation and TOF techniques enabled separation of signal due to production of photons via dissociative excitation of the target molecules (observed synchronously with the exciting electron pulse) and the photons, emitted from the XeO^* excimers, which were delayed by the transit time of the $O(^1S_0)$ atoms to the Xe surface. LeClair and McConkey were able to take advantage of the fact that one channel dominated $O(^1S_0)$ production in N_2O targets and the fact that the oscillator strength relative to this process was accurately known, to put their cross section data for $O(^1S_0)$ production on an absolute basis with an error of less than 10%, using a Bethe–Born normalization procedure. This detector has the dual benefits of high sensitivity [>25% quantum efficiency to $O(^1S_0)$] and good selectivity (completely insensitive to all other O and O_2 species). The only other species to which the detector has exhibited sensitivity are $S(^1S_0)$ and $CO(a\,^3\Pi)$ (Kedzierski et al., 2001; LeClair and McConkey, 1994; LeClair et al., 1994). Since these species give rise to different spectral signatures than $O(^1S_0)$, they can be isolated, or discriminated against, readily using appropriate optical filters. Having established an accurate cross section for $O(^1S_0)$ from N_2O, the cross sections for production of this species from other targets can be established using relative flow techniques.

For very low lying metastable or ground state fragments the only detection possibilities, apart from the fast neutral beam technique discussed below, are via laser-related techniques. Examples are Harb et al. (2001) who exploited laser induced fluorescence (LIF) to probe the production of OH(X) following dissociation of H_2O and Kimmel and Orlando (1995) who used resonance-enhanced, multi-photon ionization (REMPI) to study the electron stimulated desorption of ground state and $O(^1D)$ metastable fragments from ice.

Cosby (1993) has exploited a different approach to study the fragmentation of diatomic molecules into neutral ground state or low-lying metastable state fragments. First, charge transfer involving a fast (keV) molecular ion beam is used to produce a fast neutral molecular beam, which is then crossed with the dissociating electron beam. Being formed with several keV of translational energy, the dissociation fragments can be detected readily by secondary electron emission at an electron multiplier detector. At high impact velocities, the secondary emission efficiencies of individual atomic states are roughly the same; hence fragments produced at the lower dissociation limits can be detected. The high velocity of the molecules further serves to constrain the spatial dispersion of the fragments such that all of the fragments, or at least a known fraction of them, can be detected. The fragments are detected in multiple coincidence with respect to their spatial and temporal separations, allowing a discrete pair of atomic fragments to be directly associated with the dissociation of a single molecule and to obtain an explicit measurement of the translational energy release. Charged dissociation products are explicitly excluded from detection and hence products of the electron impact dissociation reaction are observed without contributions from dissociative ionization processes.

3. Theoretical considerations

Electron impact dissociation of molecules poses severe challenges to theory. In the Born–Oppenheimer picture, dissociative excitation and dissociative ionization comprise two difficult problems in succession: first, the inelastic collision of an electron with a nonspherical, many-electron target; next, a unimolecular dissociation reaction that occurs on an excited-state or ionic potential-energy surface, with the possibility of radiative and non-radiative transitions to, or conical intersections with, still other surfaces. In the case of ionization, there is the further complication of a three-particle final state in which the Coulomb interaction strongly couples all three particles. Dissociative attachment, on the other hand, leads to a comparatively simple final state, but it is typically a negligible channel except when mediated by long-lived resonances, in which case it becomes a problem in non-Born–Oppenheimer dynamics, with attendant complications of its own. As a result, it is fair to say that computational study of electron-driven dissociation is still at a fairly primitive stage. We briefly describe here some of the principal methods for treating aspects of this problem and a few relevant applications.

3.1. Electron impact excitation

At sufficiently high projectile energies, electron impact excitation may be treated within the first Born approximation. At projectile energies on the order of 100 eV or less, however, more accurate methods are required. Several computational approaches, including the *R*-matrix method (Burke and Berrington, 1993), the Schwinger multichannel method (Winstead and McKoy, 1995), and the complex Kohn variational method (Rescigno et al., 1995), have been applied to low-energy electron impact excitation of molecules. Most calculations have been carried out only at the molecule's ground-state equilibrium nuclear geometry, with no attempt to follow nuclear motion subsequent to excitation. Connection to dissociation cross sections is thus possible only in cases where the fate of the excited state is known from other evidence. In

many alkanes and haloalkanes, for example, it is a reasonable approximation to take all electronic excitation as dissociative, in which case the summed electron impact excitation cross sections for the channels with low thresholds gives an estimate of the low-energy total cross section for neutral dissociation [e.g. Flaherty et al. (2006)].

3.2. Electron impact ionization

Electron impact ionization is conceptually an even more difficult problem than electron impact excitation of discrete states. The presence of two free electrons in the final state complicates the boundary conditions and makes a first-principles computational treatment extremely difficult. Although some excellent work has been done recently on simple atoms (Bray et al., 2002; McCurdy et al., 2004; Pindzola et al., 2007), computational treatments of electron impact ionization of molecules have mostly been confined to elementary models (Margreiter et al., 1990, 1994; Kim and Rudd, 1994; Hwang et al., 1996; Saksena et al., 1997; Khare et al., 1999) that rely in various ways on the binary-encounter (Vriens, 1966) and Born–Bethe (Bethe, 1930) approximations. One such model in wide use is that known as the Deutsch–Märk formalism (Margreiter et al., 1990, 1994), which implements an additivity rule for atomic ionization cross sections. Another widely used model that does not employ an additivity rule and requires fewer inputs is the binary-encounter/Bethe (BEB) model (Kim and Rudd, 1994; Hwang et al., 1996). These models are easy to apply and have proven generally successful at predicting total ionization cross sections, but once again they provide no direct information on dissociation following ionization.

3.3. Dissociative attachment

The great difference in time scales between nuclear and electronic motion implies that dissociative attachment (DA) occurs with significant probability only in very slow collisions or when the electron is trapped in a metastable (resonant) state long enough for the nuclei to reach a geometry at which autodetachment is no longer energetically possible. Vibrational [e.g. Domcke (1991), Schramm et al. (1999), Hotop et al. (2003) and Scheer et al. (2004)] and electronic [e.g. Stepanovic et al. (1994) and Allan et al. (1996a)] Feshbach resonances, electronically elastic shape resonances [e.g. Allan et al. (1996a) and Martin et al. (2004)], and core-excited shape resonances [e.g. Allan et al. (1996a) and Skalicky and Allan (2004)] have all been implicated in promoting DA.

Computational treatments of DA are usually formulated in terms of a nuclear dynamics problem involving a complex, non-local potential (O'Malley, 1966; Bardsley, 1968). As discussed by Fabrikant et al. (2002), it is almost always found necessary to simplify the problem to make calculations tractable. Most commonly one ignores the non-locality and thereby obtains a local complex potential whose real part is the resonance energy and imaginary part the resonance width. One can then proceed at various levels of sophistication, from simply letting the nuclei "roll down" the potential classically toward dissociation (in competition with autodetachment), to carrying out a fully quantum-mechanical study of wave-packet propagation on the complex surface. Likewise, resonance energies and widths are sometimes treated as adjustable parameters and sometimes treated as empirical constants, but they are ideally obtained from accurate scattering calculations that are repeated at every relevant nuclear geometry. Although the first *ab initio* calculation of DA to H_2 appeared some time ago (Mundel et al., 1985), only very recently have fully *ab initio* studies of more complicated molecules appeared. Trevisan et al. (2005) reported DA cross sections for NO below 2 eV computed from a full quantum-mechanical treatment of nuclear motion on complex, non-local potential surfaces determined from Kohn scattering calculations (Zhang et al., 2004). The same group has also carried out extensive calculations on H_2O, beginning with the construction of potential surfaces (Haxton et al., 2004a, 2005) and continuing on to calculations of DA cross sections within the local-potential approximation (Haxton et al., 2006, 2007a,b).

4. Data and discussion

4.1. O_2

Knowledge of electron interactions with molecular oxygen is of fundamental importance in many fields. It is basic to our understanding of atmospheric processes on Earth and other planets [see e.g. Matejcik et al. (1997)]. A detailed knowledge of the various electron impact cross sections is required for modelling electrical discharges that include oxygen (Gousset et al., 1991; Eliasson and Kogelschatz, 1986) and for optimizing many technological applications [e.g. Ricard et al. (1983), Zecca et al. (1992)].

A number of reviews and data compilations have been forthcoming dealing with various aspects of this subfield [see Itikawa et al. (1989), van der Burgt et al. (1989), Kanik et al. (1993b), Zecca et al. (1996), Itikawa (2003)]. The present work deals specifically with dissociative processes.

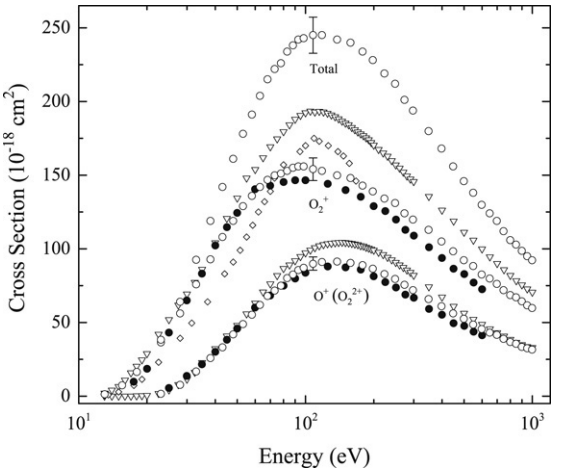

Fig. 3. Partial ionization cross sections for electron impact on O_2. Solid circles, Tian and Vidal (1998d); open circles, Straub et al. data from Table 1; triangles, Krishnakumar and Srivastava (1988); diamonds, Märk (1975).

4.1.1. Dissociative ionization

Lindsay and Mangan (2003) have critically evaluated the various cross section data sets that are available from the early measurements of Tate and Smith (1932) onward. Many of the earlier experiments were not able to demonstrate conclusively that total collection of fragment ions was obtained and many were not independently calibrated absolutely but depended on normalization to another cross section. For these reasons Lindsay and Mangan recommend the Straub et al. (1996b) data set (or rather a data set that had been reduced by a few percent to reflect a recalibration of their apparatus). These data are listed in Table 1. The good agreement between these data and other relatively recent measurements by Krishnakumar and Srivastava (1992) and Tian and Vidal (1998d) is illustrated by Fig. 3. The earlier work of Rapp et al. (1965) was not included because total collection of fragment ions was not achieved. Lindsay and Mangan claim that these partial cross sections are accurate to about the 5% level.

Tian and Vidal (1998d) were able to use their technique of covariance mapping mass spectroscopy to help isolate some of the individual channels. Thus they were able to separately quantify the following single, double and triple ionization channels:

$$e + O_2 \rightarrow (O_2)^+ + e' \rightarrow O^+ + O \quad (3a)$$

$$e + O_2 \rightarrow (O_2)^{2+} + 2e' \rightarrow O^+ + O^+ \quad (3b)$$

$$\rightarrow O^{2+} + O \quad (3c)$$

$$e + O_2 \rightarrow (O_2)^{+3+} + 3e' \rightarrow O^{2+} + O^+. \quad (3d)$$

Ionization of oxygen dimers has been studied by Kreil et al. (1998). They reported no evidence for atomic ion production.

4.1.2. Appearance energies and fragment energy distributions

Ion fragment energy distributions and appearance energies have been studied by a large number of workers over the years [see Matsuo et al. (1998), Zhukov et al. (1990), van Brunt et al. (1974), Schopman and Locht (1974), Stockdale and Deleanu (1973, 1974), Ehrhardt and Kresling (1967) and references therein]. It is difficult to compare the ion kinetic energy distributions because in some cases energy discrimination effects in the detection optics were not clearly identified and, in addition, not all data sets were taken at comparable incident electron energies. However a number of points can be made. A broad multi-structured ion energy distribution, which extends up to 10 eV at electron energies greater than about 50 eV, is observed. Four main O^+ ion groups are present with peak energies of 0.8, 2, 3 and 5 eV. Evidence for additional processes yielding ions with energies less than 0.6 eV has also been presented (Matsuo et al., 1998; Schopman and Locht, 1974) but the relative magnitude of these processes is unclear due to difficulties of accurately determining ion transmission functions in this low energy region.

Angular distributions of O^+ following dissociation have been studied by Stockdale and Deleanu (1973), van Brunt et al. (1974), Zhukov et al. (1990) and Matsuo et al. (1998). There is general agreement that, above an incident energy of 50 eV, distributions of ions of any and all energies are essentially isotropic. At energies closer to threshold some anisotropies are observed (see van Brunt et al.) for certain ion energies. These usually favoured the forward and backward directions (with respect to the electron beam) though Matsuo et al. identified one process where the 90° direction was strongly favoured. In these cases possible symmetries of the parent dissociating states could be identified using Dunn's (1962) rules.

Table 1
O_2 partial and total ionization cross sections

Energy (eV)	$\sigma(O_2^+)$ (10^{-18} cm^2)	$\sigma(O^+ + O_2^{2+})$ (10^{-18} cm^2)	$\sigma(O^{2+})$ (10^{-18} cm^2)	σ(total) (10^{-18} cm^2)
13	1.17			1.17
15.5	7.30			7.30
18	16.4			16.4
23	36.6	1.67		38.3
28	56.3	7.81		64.1
33	75.8	16.9		92.7
38	92.9	25.8		119
43	108	33.3		142
48	119	41.9		161
53	129	49.0		178
58	136	55.3		191
63	142	62.1		204
68	147	67.9		215
73	150	71.7	0.118	222
78	151	75.1	0.189	226
83	153	80.1	0.241	234
88	155	82.7	0.352	238
93	156	85.5	0.438	242
98	156	87.1	0.610	243
108	154	90.0	0.808	245
118	153	91.0	0.956	245
138	150	91.3	1.37	242
158	148	90.5	1.80	240
178	143	89.1	2.00	234
198	139	86.4	2.11	228
223	134	83.0	2.30	219
248	131	79.4	2.26	212
273	124	75.5	2.13	201
298	120	72.1	2.07	194
348	113	65.9	1.89	180
398	105	61.1	1.71	168
448	98.3	56.2	1.53	156
498	92.3	52.6	1.36	146
548	88.2	48.7	1.23	138
598	82.7	45.7	1.11	130
648	80.0	43.2	1.08	124
698	76.1	41.5	0.987	119
748	72.0	38.8	0.977	112
798	68.6	36.9	0.837	106
848	67.1	35.5	0.799	103
898	64.3	33.6	0.770	98.7
948	61.7	32.6	0.740	95.0
998	59.7	31.7	0.743	92.2

From Lindsay and Mangan (2003).

These angular distribution data plus extensive measurements of appearance energies of the different ions have enabled unambiguous assignment of the following predissociation process to the 0.8 eV peak:

$$e + O_2(X\,^3\Sigma_g^-) \rightarrow O_2^+(B\,^2\Sigma_g^-) + e' \rightarrow O^+(^4S) + O(^3P) \tag{4}$$

with a dissociation limit of 18.73 eV. This is confirmed by photodissociation work [see e.g. Richard-Viard et al. (1985) and Doolittle et al. (1968)]. Identification of the processes responsible for the other peaks in the fragment ion distribution curves is less certain and, in many cases, numerous repulsive curves are clearly involved.

Ion pair formation has been studied by Rapp and Briglia (1965) who established that the total cross section for the process reached a broad maximum of 0.48×10^{-18} cm^2 at about 34 eV. The threshold for the process is at 17.28 eV. van Brunt and Kieffer (1974) measured energy and angular distributions of the fragment anions and showed that the kinetic energy distributions exhibited well defined maxima near 1.9 and 3.3 eV with appearance energies, respectively at 20.0 and 23.0 eV. They presented strong evidence that the dominant, 1.9 eV, feature was the result of multistate processes.

4.1.3. Dissociative attachment

Rapp and Briglia (1965) measured total absolute cross sections for O^- production from O_2. Particular attention was placed on the total collection of the product anions. Data were made absolute by comparison with the cross section for cation production measured in the same apparatus. Their results are given in Table 2 and displayed in Fig. 4. The cross section exhibits a single broad resonance peak centred around 6.5 eV, where it amounts to 0.1% of the total cross section for electron impact on O_2 (Zecca et al., 1996). Data are given for a room temperature (300 K) O_2 target. Spence and Schulz (1969) have

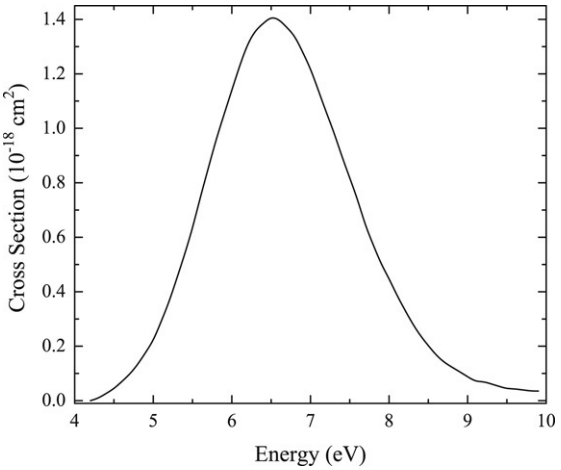

Fig. 4. Attachment cross section for the production of O^- from O_2 at a target gas temperature of 300 K. Data from Table 2.

Table 2
Cross sections for production of O^- from O_2 at a target gas temperature of 300 K

Energy (eV)	Cross section (10^{-18} cm^2)	Energy (eV)	Cross section (10^{-18} cm^2)	Energy (eV)	Cross section (10^{-18} cm^2)
4.2	0	6.1	1.23	8.0	0.449
4.3	0.0088	6.2	1.31	8.1	0.387
4.4	0.0264	6.3	1.36	8.2	0.334
4.5	0.0440	6.4	1.31	8.3	0.282
4.6	0.0704	6.5	1.41	8.4	0.238
4.7	0.0968	6.6	1.40	8.5	0.202
4.8	0.132	6.7	1.37	8.6	0.167
4.9	0.176	6.8	1.34	8.7	0.141
5.0	0.220	6.9	1.28	8.8	0.123
5.1	0.290	7.0	1.22	8.9	0.106
5.2	0.361	7.1	1.14	9.0	0.0880
5.3	0.449	7.2	1.06	9.1	0.0704
5.4	0.537	7.3	0.985	9.2	0.0704
5.5	0.633	7.4	0.897	9.3	0.0616
5.6	0.748	7.5	0.818	9.4	0.0528
5.7	0.853	7.6	0.739	9.5	0.0440
5.8	0.959	7.7	0.642	9.6	0.0440
5.9	1.05	7.8	0.572	9.8	0.0352
6.0	1.14	7.9	0.501	9.9	0.0352

From Lindsay and Mangan (2003).

showed that the dissociative attachment process is strongly affected by temperature, i.e. by the ro-vibrational distribution of the target.

van Brunt and Kieffer (1970) studied the angular distribution of the O^- fragments as a function of ion and incident electron energies and confirmed earlier suggestions (O'Malley, 1967), that a repulsive $O_2^-(^2\Pi_u)$ state is responsible for the observations. Only contributions from the first two allowed partial waves, $L = 1$ and 3, of the incoming electron are involved.

More recent studies of attachment in O_2 clusters have concentrated on the low incident electron energy region, 0–2 eV, where associative rather than dissociative attachment predominates and evaporation accompanies the process [see e.g. Matejcik et al. (1997, 1999), Barsotti et al. (2002) and Kreil et al. (1998) for details].

4.1.4. Dissociation into ground state fragments

Although there has been a considerable body of work on photodissociation of O_2 into ground state fragments [see e.g. Stone et al. (1976), Lee et al. (1977), Matsumi and Kawasaki (1990), Huang and Gordon (1991), Lin et al. (1998), Balakrishnan et al. (2000) and Parker (2000)], and an attempt to use a chemi-ionization technique to monitor O-atom production, Stone et al. (1975), the only direct quantitative electron impact study seems to be that of Cosby (1993) using his fast neutral beam technique. His target neutral beam had vibrationally excited components with $v < 4$. Since the cross section goes down with vibrational excitation, (Cosby, 1993), Cosby's data should represent a lower limit to the dissociation cross section for ground-state ($v = 0$) targets. His data are listed in Table 3 and displayed in Fig. 5. Cosby compared his measurements with data obtained from electron energy loss spectroscopy (EELS) by Trajmar et al. (1972) and by Wakiya (1978) as well as theoretical curves due to Chung and Lin (1980) and to Garrett et al. (1985). Reasonable agreement was obtained. Differences between Cosby's data and those obtained from EELS measurements are most likely due to differences

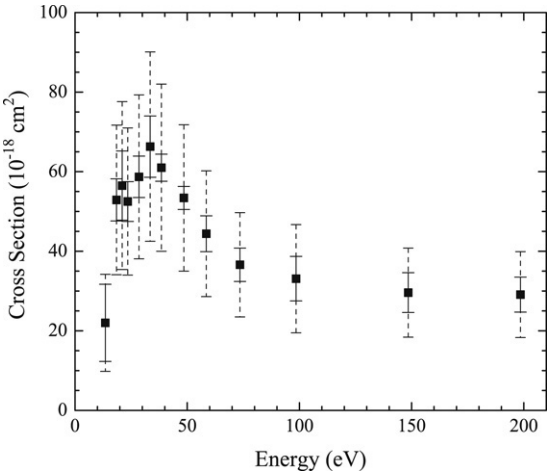

Fig. 5. Dissociation cross sections for electron impact on O_2. The relative uncertainties in the measurements are shown by the solid error bars, while the absolute uncertainties are shown by the dashed error bars. Data from Table 3.

Table 3
Cross sections for electron impact dissociation of O_2

Energy (eV)	Total dissociation cross section			Partial dissociation cross section ($W > 2.7$ eV)	
	(10^{-18} cm^2)	Relative uncertainty (10^{-18} cm^2)	Absolute uncertainty (10^{-18} cm^2)	(10^{-18} cm^2)	Absolute uncertainty (10^{-18} cm^2)
13.5	22.0	9.7	12.2		
18.5	52.9	5.3	18.8		
21.0	56.5	8.7	21.1		
23.5	52.5	5.0	18.5		
28.5	58.7	5.2	20.6	4.9	1.7
33.5	66.3	7.7	23.8	5.6	2.0
38.5	61.0	3.4	21.0	5.2	1.8
48.5	53.4	2.9	18.4	4.6	1.6
58.5	44.4	4.5	15.8	3.9	1.4
73.5	36.6	4.2	13.1	3.2	1.4
98.5	33.1	5.6	13.6	3.0	1.2
148.5	29.6	5.0	11.2	2.8	1.1
198.5	29.1	4.4	10.8	2.9	1.1

Partial dissociation cross sections for production of fragments with translational energy releases $W > 2.7$ eV are also given. Adapted from Cosby (1993).

in the target vibrational distributions. More recent EELS work (Teillet-Billy et al., 1989; Allan, 1995; Campbell et al., 2000) essentially confirms the magnitude of the earlier electron scattering data. We note also that an indirect confirmation of the electron scattering data comes from the gas discharge, ozone production measurements of Eliasson and Kogelschatz (1986).

From measurements of fragment kinetic energies released in the dissociation, Cosby was able to identify the dominant dissociation channels as leading to $O(^3P) + O(^3P)$ and $O(^3P) + O(^1D)$. The repulsive states involved are $B\,^3\Sigma_u^-$, $B'\,^3\Sigma_u^-$, and $2\,^3\Pi_u$ in the latter case, and $c\,^1\Sigma_u^-$, $A'\,^3\Delta_u$ and $A\,^3\Sigma_u^+$ in the former. This is consistent with the photodissociation work.

4.1.5. Dissociation into neutral metastable fragments

In addition to the $O(^1D)$ metastable atom product discussed in the previous section, there is also the $O(^1S)$ metastable atom within the ground configuration and the $O(^5S)$ metastable atom with an internal energy of 9.14 eV. Rydberg atoms with high enough n values can also be classified as metastables. All of these species have been investigated in O_2 dissociation studies.

LeClair and McConkey (1993) used their Xe-matrix detector to measure the cross section for $O(^1S)$ production from threshold to 1000 eV. Data were made absolute using production from N_2O as a secondary standard (see Section 2.2). Their data are listed in Table 4 and shown in Fig. 6. The cross section has a maximum at 2.1×10^{-18} cm^2 at an impact energy of 80 eV. Use of TOF techniques allowed them to extract $O(^1S)$ kinetic energy distributions and a sample of these is shown in Fig. 7. A group of atoms with kinetic energies near 3.5 eV dominates the spectra at all incident energies studied, though there are other features present indicating other production mechanisms. These spectra are very typical of metastable fragment kinetic energies released in O_2 dissociation [see e.g. Freund (1971b)].

Production of $O(^5S)$ metastables has been studied by Freund (1971b), by Zipf's group (Borst and Zipf, 1971; Wells et al., 1971; Erdman and Zipf, 1987), by Mason and Newell (1990) and, most recently, by the JPL group (Noren et al., 2001; Kanik

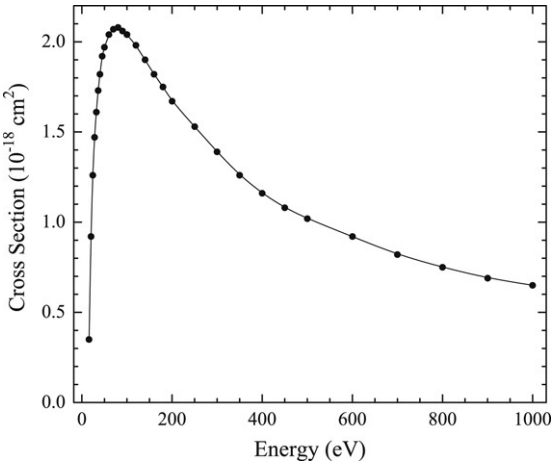

Fig. 6. Absolute cross section for the production of O(^{1}S) following electron impact on O_2. Data from Table 4.

Table 4
Absolute cross sections for the production of O(^{1}S) following electron impact on O_2

Energy (eV)	Cross section (10^{-18} cm^2)	Energy (eV)	Cross section (10^{-18} cm^2)
16	0.35	140	1.90
20	0.92	160	1.82
24	1.26	180	1.75
28	1.47	200	1.67
32	1.61	250	1.53
36	1.73	300	1.39
40	1.82	350	1.26
45	1.92	400	1.16
50	1.97	450	1.08
60	2.04	500	1.02
70	2.07	600	0.92
80	2.08	700	0.82
90	2.06	800	0.75
100	2.04	900	0.69

Data from LeClair and McConkey (1993).

et al., 2003). High-Rydberg, O(R), production has been studied by Freund (1971b) and by Ohshima et al. (1989) using a quenching technique to isolate the Rydberg species.

Using TOF techniques, Freund (1971b) and Borst and Zipf (1971) measured the kinetic energy distributions of metastable atoms following dissociation and identified "slow" and "fast" groups with peak energies near 0.3 and 2 eV respectively. The threshold energy for the appearance of the "slow" O(^{5}S) atoms was approximately 14.5 eV, i.e. very close to the energy required for dissociation into O(^{5}S) + O(^{3}P). Very similar data were obtained by Mason and Newell (1990). Since the kinetic energy distribution indicated that a significant fraction of the atoms had energies very close to zero, it was concluded that excitation was taking place to the repulsive inner wall of a potential energy curve. Excitation function data suggested that curves of $^3\Pi_u$ and $^3\Pi_g$ symmetry were involved. At energies away from threshold additional processes contribute either directly or via cascade, e.g. from 3p ^{5}P [see Erdman and Zipf (1987)].

Production of the "fast" O(^{5}S) atoms occurred at energies higher than about 21 eV. Evidence for a number of production channels, including cascade from 3p ^{5}P, was presented [see e.g. Mason and Newell (1990)]. The kinetic energy distributions pointed to dissociation via purely repulsive potential curves in the Franck–Condon region. The shape of the excitation cross section suggested that excitation of optically allowed parent molecular states was important.

It is difficult to calibrate absolutely the cross section for O(^{5}S) production. The long radiative lifetime precludes the use of normal optical techniques using the 135.6 nm, 3p(^{5}P) $\rightarrow$ 3s(^{5}S), transition. Initial attempts to obtain a reasonable estimate of its value were not successful as pointed out by Erdman and Zipf (1987). A lower limit to the excitation cross section (of 4.25×10^{-18} cm^2 at 100 eV) was obtained from measurements of the 777.4 nm cascade transition, where there was very good agreement between work by Erdman and Zipf (1987) and Schulman et al. (1985). Recently Noren et al. (2001) and Kanik et al. (2003) have been able to use a large, 1.5 m diameter, excitation chamber with a moveable optical detection system to allow integration of 135.6 nm radiation from a large volume surrounding the electron beam. In this way they were able to obtain an accurate ratio for the excitation of the 135.6 and 130.4 nm transitions. Using this, they derived a value of $6.4 \pm 2.2 \times 10^{-18}$ cm^2 at 100 eV for the absolute emission cross section of the 135.6 nm feature. Thus about 2/3 of the excitation of 3s(^{5}S) is via cascade.

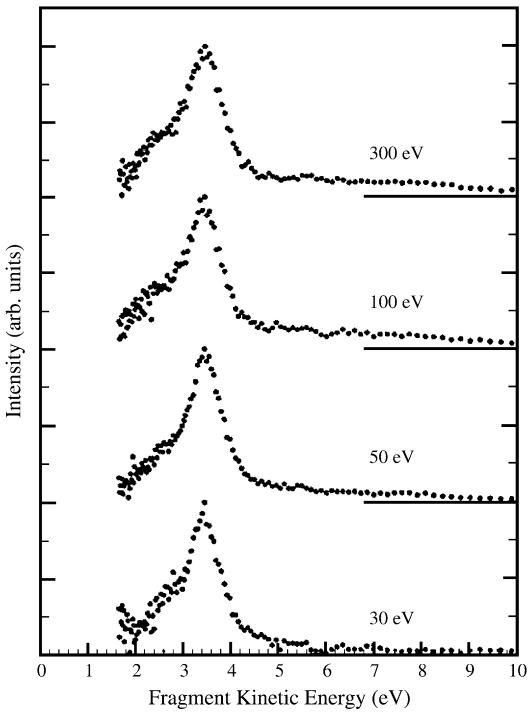

Fig. 7. $O(^1S)$ fragment kinetic energy spectra from O_2 at the incident electron energies indicated. The spectra are normalized to the same intensity at their maximum. Reused with permission from Lance R. LeClair, Journal of Chemical Physics, 99, 4566 (1993).

A detailed study of O(R) production from O_2 was made by Freund (1971b) and some additional work in the impact energy range 50–100 eV, with particular emphasis on fragment angular distributions was carried out by Ohshima et al. (1989). From fragment kinetic energy distributions and excitation functions at least four different processes were identified. Appearance energies suggested that both single and double electron excitation processes were active. The precursors of the fast (>4 eV) fragments were ascribed to Rydberg states converging to the $^3\Sigma_g^-$, and $^3\Pi_g$ states of O_2^{2+}, while those of the slower fragments were ascribed to Rydberg states converging to the $^3\Sigma_u^-$ state.

4.1.6. Dissociative excitation

A large amount of work has gone into measurements of dissociative excitation of O_2 because of its importance in the atmospheres of Earth and other bodies in the solar system such as the Jovian moons, Io, Europa and Ganymede [see Noren et al. (2001) and references therein]. Early VUV measurements were reviewed by van der Burgt et al. (1989) and additional tabular and graphical data have been given by Avakyan et al. (1998). Fig. 8, taken from Schulman et al. (1985), is a partial energy level diagram for atomic oxygen, which shows many of the transitions for which data are available. Additional dissociative excitation features, particularly in the spectral ranges 40–100 and 390–540 nm, are given by Wilhelmi and Schartner (2000) and Ajello and Franklin (1985).

4.1.6.1. Near-UV and longer wavelength region. In this spectral region energetic electron impact on O_2 produces a rich spectrum of emissions, both atomic and molecular. This is illustrated in Fig. 9 taken from Wilhelmi and Schartner (2000), which covers the 330–610 nm region. In some reports, concentration is on one or a few important transitions (Lawrence, 1970; Koppe et al., 1972; Zipf et al., 1979; Erdman and Zipf, 1987) while Schulman et al. (1985) and Wilhelmi and Schartner (2000) present data on a wide range of spectral features.

A key measurement was that of Lawrence (1970) for the 844.7 nm ($3p^3P \rightarrow 3s\ ^3S^o$) transition. By carefully measuring this cross section and the decay lifetime of the 130.4 nm resonance transition, which is fed by the 844.7 nm cascade, he was able to benchmark both these features. These values have been widely accepted and used as secondary standards by other workers. The only other independent measurement of this 844.7 nm multiplet was by Zipf et al. (1979), who obtained a value at 100 eV that was 15% larger but within the combined error limits of the two experiments.

The most intense feature in this spectral region is the 777.4 nm ($3p\ ^5P \rightarrow 3s\ ^5S^o$) multiplet. Very good agreement between the measurements of Erdman and Zipf (1987) and Schulman et al. (1985) is obtained for the peak cross section though Erdman and Zipf's cross section falls off somewhat more rapidly towards higher energies. Both data sets are referenced to the 844.7 nm emission. Table 5 lists Erdman and Zipf's data set. Erdman and Zipf also measured the Doppler profiles of the individual components of the multiplet and showed that both "slow" and "fast" groups of fragments were responsible for

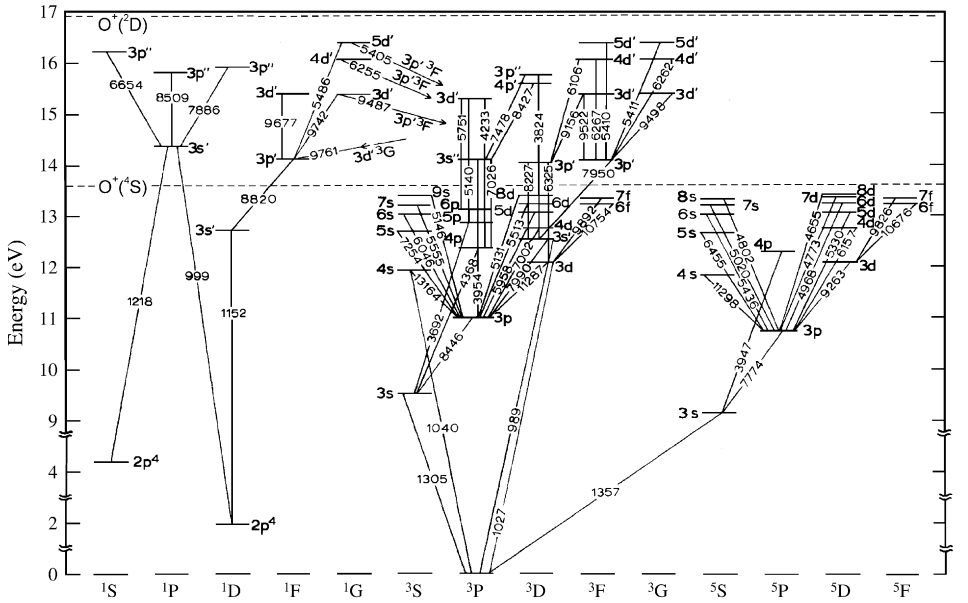

Fig. 8. Partial energy-level diagram for atomic oxygen showing some of the transitions that have been studied. Reused with permission from M. B. Schulman, Physical Review A, 32, 2100 (1985).

Table 5
Cross sections for the excitation of the OI (777.4 nm) multiplet by electron impact on O_2

Energy (eV)	Cross section (10^{-18} cm^2)	Energy (eV)	Cross section (10^{-18} cm^2)
16	0.044	375	1.72
17	0.35	400	1.65
18	0.618	425	1.58
19	0.888	450	1.50
20	1.10	475	1.44
22	1.52	500	1.39
24	1.75	600	1.20
26	1.91	700	1.06
28	2.05	800	0.954
30	2.16	900	0.868
35	2.40	1 000	0.797
40	2.62	1 200	0.687
50	3.19	1 400	0.605
60	3.83	1 600	0.542
70	3.99	1 800	0.492
80	4.07	2 000	0.451
90	4.31	2 200	0.416
100	4.23	2 400	0.387
125	3.87	2 600	0.362
150	3.42	2 800	0.340
175	3.06	3 000	0.321
200	2.76	4 000	0.251
225	2.56	5 000	0.208
250	2.34	6 000	0.178
275	2.20	7 000	0.156
300	2.04	8 000	0.139
325	1.94	9 000	0.125
350	1.82	10 000	0.114

Values above 400 eV were extrapolated from a Bethe–Oppenheimer relation. From Erdman and Zipf (1987).

the observations, with average kinetic energies of 0.13 and 2.5 eV respectively. The energy threshold for the "fast" group was around 20 eV. The significance of this multiplet in connection with the overall excitation of the 3s $^5S^o$ level has been discussed in 4.1.5 above.

Additional information about transitions to the 3p ^3P level from the 3s′ $^3D^o$, 3d $^3D^o$ and 4s $^3S^o$ at 799.0, 1128.7 and 1316.4 nm respectively have been given by Zipf's group (Zipf et al., 1979; Erdman and Zipf, 1983a). These levels are important because they also decay to the ground state emitting radiation in the VUV (see the next section).

Table 6
Optical excitation cross sections for O emissions resulting from electron impact dissociative excitation of O_2

O multiplet[a]	Wavelength (air) (nm)	$\sum_{J,J'} Q_{opt}(J' \rightarrow J)$[b] ($10^{-18}$ cm^2)
$4s\ ^5S^0 \rightarrow 3p\ ^5P$	1129.51–1130.24	0.61
$5s\ ^5S^0 \rightarrow 3p\ ^5P$	645.36–645.60	0.037[c]
$6s\ ^5S^0 \rightarrow 3p\ ^5P$	543.52–543.69	0.0075[c]
$7s\ ^5S^0 \rightarrow 3p\ ^5P$	501.88–502.02	0.0029[c]
$8s\ ^5S^0 \rightarrow 3p\ ^5P$	480.18–480.30	<0.0017
$3p\ ^5P \rightarrow 3s\ ^5S^0$	777.19–777.54	4.3[c]
$4p\ ^5P \rightarrow 3s\ ^5S^0$	394.73–394.76	0.011[c,d]
$3d\ ^5D^0 \rightarrow 3p\ ^5P$	926.08–926.60	1.24[c]
$4d\ ^5D^0 \rightarrow 3p\ ^5P$	615.60–615.82	0.11[c]
$5d\ ^5D^0 \rightarrow 3p\ ^5P$	532.91–615.82	0.034[c]
$7d\ ^5D^0 \rightarrow 3p\ ^5P$	477.24–533.07	0.0058
$8d\ ^5D^0 \rightarrow 3p\ ^5P$	465.41–465.54	0.0025 (50 eV)
$6f\ ^5F \rightarrow 3d\ ^5D^0$	1067.57–1067.59	0.045
$7f\ ^5F \rightarrow 3d\ ^5D^0$	982.58–982.60	0.024
$6s\ ^3S^0 \rightarrow 3p\ ^3P$	604.62–604.65	0.0030[c]
$7s\ ^3S^0 \rightarrow 3p\ ^3P$	555.48–555.50	<0.019[c]
$9s\ ^3S^0 \rightarrow 3p\ ^3P$ $3d'\ ^3P^0_2 \rightarrow 5p\ ^3P$	514.61	<0.0002[e]
$3p\ ^3P \rightarrow 3s\ ^3S^0$	844.62–844.68	2[c]
$4p\ ^3P \rightarrow 3s\ ^3S^0$	436.82	0.022 (50 eV)
$5p\ ^3P \rightarrow 3s\ ^3S^0$	369.24	0.0004
$3s''\ ^3P^0 \rightarrow 3p\ ^3P$	395.19–395.46	<0.0001 (50 eV)
$3s''\ ^3P^0_2 \rightarrow 4p\ ^3P$	702.55	<0.001
$3d'\ ^3P^0_2 \rightarrow 4p\ ^3P$	423.33	<0.0001[e]
$3d'\ ^3P^0_2 \rightarrow 6p\ ^3P$	575.06	<0.0003[e]
$3d\ ^3D^0 \rightarrow 3p\ ^3P$	1128.63–1128.73	0.52
$3s'\ ^3D^0 \rightarrow 3p\ ^3P$	798.19–798.73 799.51	<0.0010
$4d\ ^3D^0 \rightarrow 3p\ ^3P$	700.19–700.22	0.014[c]
$5d\ ^3D^0 \rightarrow 3p\ ^3P$	595.84–595.86	<0.020[c]
$6d\ ^3D^0 \rightarrow 3p\ ^3P$	551.26–551.28	<0.0025
$8d\ ^3D^0 \rightarrow 3p\ ^3P$ $3d'\ ^3P^0_1 \rightarrow 5p\ ^3P$	513.04–513.07	<0.0003
$3p'\ ^3D \rightarrow 3d\ ^3D^0$	632.34–632.48	<0.011
$3p'\ ^3D \rightarrow 3s'\ ^3D^0$	822.18 822.77–823.54	0.086[c,f]
$4p'\ ^3D \rightarrow 3s''\ ^3P^0$	842.09 842.47–842.91	<0.0065
$3p''\ ^3D \rightarrow 3s'\ ^3D^0$	382.26–382.55	<0.0002
$3p''\ ^3D \rightarrow 3s''\ ^3P^0$	747.14–747.32 747.64–748.07	<0.011
$6f\ ^3F \rightarrow 3d\ ^3D^0$	1075.35	0.037
$7f\ ^3F \rightarrow 3d\ ^3D^0$	989.17	0.015
$3p'\ ^3F \rightarrow 3s'\ ^3D^0$	795.2–794.72 793.95, 794.32	<0.0059
$3d'\ ^3F^0_4 \rightarrow 3p'\ ^3D_3$	915.60	0.029
$3d'\ ^3F^0 \rightarrow 3p'\ ^3F$	951.70–952.86	0.02
$4d'\ ^3F^0 \rightarrow 3p'\ ^3D$	610.63–610.76	0.0031[c]
$4d'\ ^3F^0_4 \rightarrow 3p'\ ^3F_4$	626.69	0.0029[e]
$3d'\ ^3G^0 \rightarrow 3p'\ ^3F$	949.27–950.56	0.068[g]
$3d'\ ^3G^0_4 \rightarrow 3p'\ ^1F$	976.07	0.020
$4d'\ ^3G^0 \rightarrow 3p'\ ^3F$	625.92–626.45	0.0046[e,g]
$5d'\ ^3G^0 \rightarrow 3p'\ ^3F$ $5d'\ ^3F^0 \rightarrow 3p'\ ^3F$	540.86–541.46	0.0017[c]
$3p''\ ^1S \rightarrow 3s''\ ^1P^0$	665.38	<0.0022[c]
$3p''\ ^1P \rightarrow 3s''\ ^1P^0$	850.86	<0.0008
$3p''\ ^1D \rightarrow 3s''\ ^1P^0$	788.63	<0.0015
$3p'\ ^1F \rightarrow 3s'\ ^1D^0$	882.04	0.044
$3d'\ ^1F^0 \rightarrow 3p'\ ^1F$	967.74	<0.0046[e]
$3d'\ ^1G^0 \rightarrow 3p'\ ^1F$	974.15	0.03
$3d'\ ^1G^0 \rightarrow 3p'\ ^3F$	948.12–948.74	0.043
$4d'\ ^1G^0 \rightarrow 3p'\ ^1F$	625.41–625.68	0.0027[e]
$5d'\ ^1G^0 \rightarrow 3p'\ ^1F$	548.65	<0.0005

The most extensive study in this spectral region was by Schulman et al. (1985) who list emission cross sections and show excitation function data for a large number of excited oxygen lines. These are given in Table 6 and Fig. 10. The figure illustrates that all of the excitation functions have the same basic structure — a fairly rapid rise from threshold followed

Table 6 (*continued*)

O multiplet[a]	Wavelength (air) (nm)	$\sum_{J,J'} Q_{opt}(J' \rightarrow J)$[b] ($10^{-18}$ cm^2)
$5d'\ ^1G^0 \rightarrow 3p'\ ^3F$	540.50	0.0004

Incident electron energy is 100 eV except where noted. Each cross section is for the sum over all J′ → J components of a transition, unless otherwise specified. From Schulman et al. (1985).

[a] Upper states are listed in order of energy within groups of increasing *L* and *S*, except where unrelated transitions are not resolved. A prime (′) on the configuration notation indicates the corresponding state of $O^+(^2D^0)$ as core; a double-prime symbol (″) indicates $O^+(^2P^0)$ as core; otherwise, an $O^+(^4S^0)$ core.

[b] Estimated uncertainty 20%, except those with superscripts c and e. See Schulman et al. (1985) for more details.

[c] Estimated uncertainty 15%.

[d] Falls near $O^+(3p\ ^2P^0_{3/2} \rightarrow 3s\ ^2P_{1/2})$at 394.5 nm, and a slight contamination is possible. At 50 eV the measured cross section is 0.0064×10^{-18} cm$^2 \pm 15\%$.

[e] Estimated uncertainty of up to 50% because of very low signal-to-noise ratio, or contamination from overlapping O_2^+ bands.

[f] Some J′ → J components of this multiplet were partially resolved and measurable. The cross section presented is the sum of the partially resolved components. See Table II in Schulman et al. (1985) also.

[g] $J\prime = 3 \rightarrow J = 4$ excluded.

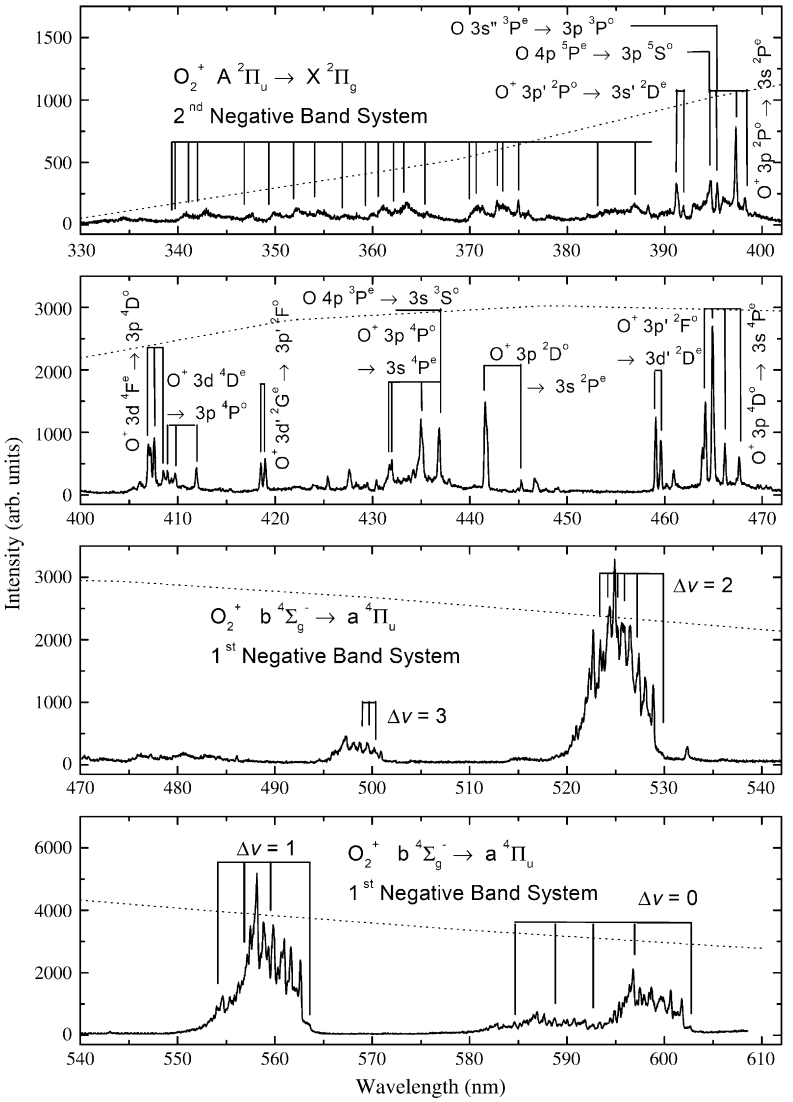

Fig. 9. Visible and near-UV spectrum resulting from 2 keV electron impact on O_2. Prominent emission lines from O and O^+ are indicated. The relative quantum efficiency of the detector is indicated by the dotted line. Reproduced with permission from Wilhelmi and Schartner (2000). With kind permission of The European Physical Journal (EPJ).

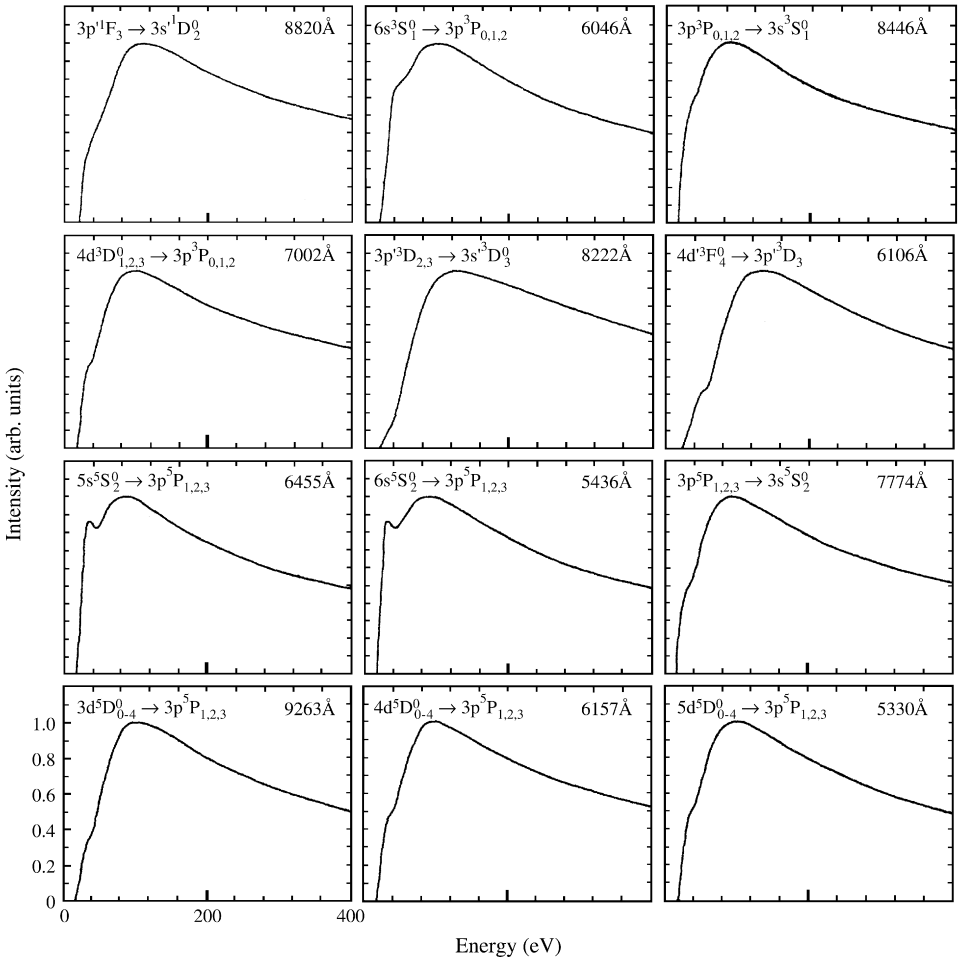

Fig. 10. Shape of optical-emission excitation functions for oxygen multiplet radiation. The curves shown are cubic spline fits to the experimental data, and have been normalized to a maximum value of 1.0 in each case. All curves are plotted to the same energy scale. See Table 6 for absolute cross section values corresponding to 100 eV. Reused with permission from M. B. Schulman, Physical Review A, 32, 2100 (1985).

by a shoulder in the 35–40 eV region, followed in turn by a rise to a broad maximum close to 90 eV. Near threshold, dissociative excitation through partly bound Rydberg states is the major production mechanism whereas, at higher energies, simultaneous ionization and excitation leading to dissociation are important. The initial thresholds were consistent with the minimum energies required to excite these transitions.

In addition to measurements of excited neutral O atoms, a number of O^+ emissions in the 370–500 nm region have been investigated by Koppe et al. (1972) and Wilhelmi and Schartner (2000) (see Figs. 9 and 10).

4.1.6.2. VUV Region. The only relevant input since van der Burgt et al. (1989) surveyed this sub-field has been the work of the JPL group (Noren et al., 2001; Makorov et al., 2003; Kanik et al., 2003) and of Wilhelmi and Schartner (2000). Problems of absolute calibration of emission cross sections persist, as discussed by Jans et al. (1995, 1997). Use of electron storage rings as primary radiation standards (McPherson et al., 1986; Wilhelmi and Schartner, 2000) and spinning rotor pressure gauges for target gas density measurement have removed a lot of the uncertainties inherent in less direct calibration methods. However this improvement has been offset, at least partly, by the extra difficulty of the calibration procedure itself. The Wilhelmi and Schartner (2000) calibration was carried out at 2 keV whereas lower energies (100 or 200 eV) were used in the other experiments. A more direct comparison would have been preferable as the shape of a measured excitation function, and hence the ratio of measurements at low and high energies can be affected by any low energy secondary electron component in the electron beam. Relative wavelength calibration using the molecular branching-ratio technique has improved significantly also, as the precision of modelling of molecular band systems has developed [see e.g. Jonin et al. (2000), Malone et al. (2008a,b)].

In summary, the number of electron-beam-excited secondary standards in the VUV is still very limited. Two that have been generally accepted are the 121.6 nm and 120.0 nm atomic transitions following electron impact on H_2 and N_2

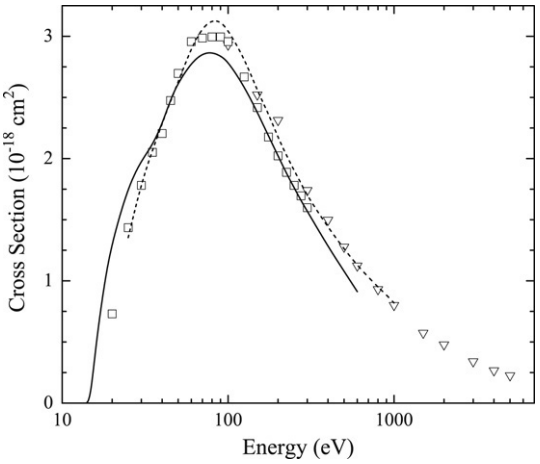

Fig. 11. O I (130.4 nm) excitation function of Kanik et al. (2003) [solid line] compared with earlier data of Lawrence (1970) [dashed line], Aarts and de Heer (1971) [open triangles] and Zipf (1986) [open squares]. See Table 7 for renormalizations and note that the results of Aarts and de Heer were normalized to our recommended value.

Table 7
Absolute emission cross sections at 100 eV for electron impact dissociative excitation of H_2 yielding H I ($2p\ ^2P^o \rightarrow 1s\ ^2S$; Lyman-$\alpha$; 121.6 nm)

Source	Cross section (10^{-18} cm^2)
Van Zyl et al. (1985)	7.22 ± 1.30
Ligtenberg et al. (1985)	6.57 ± 0.53
Liu et al. (1998)[a]	7.16 ± 0.95
Woolsey et al. (1986)[b]	6.81 ± 0.56
de Heer and Carrière (1971)[c]	7.37 ± 1.50
Recommended[d]	7.03 ± 0.47

[a] Liu et al.'s (1998) cross section has been used, superseding the earlier result of Shemansky et al. (1985).
[b] Woolsey et al.'s (1986) cross section was renormalized as discussed in Liu et al. (1998).
[c] de Heer and Carrière's (1971) cross section was renormalized as discussed in Liu et al. (1998).
[d] The recommended value is the average of rows 1–5.

respectively [see van der Burgt et al. (1989)]. As mentioned in Section 2.2, additional work has necessitated a revision of the Lyman-α secondary standard. The JPL group, Liu et al. (1998), have carried out a careful reanalysis of $e^- + H_2$ excitation and obtained a cross section value of $7.16 \pm 0.095 \times 10^{-18}$ cm^2 at 100 eV. This updates the earlier Shemansky et al. (1985) measurement. Further, Liu et al. (1998) have carefully reanalysed the Lyman-α cross section measurement of Long et al. (1968) on which the Windsor experiment (Woolsey et al., 1986) was based. This leads to a 4% reduction in the Windsor value. Finally, Liu et al. (1998) have reanalysed the early de Heer and Carrière (1971) data to obtain a revised datum to include in the overall average. These values along with the others included in van der Burgt et al.'s (1989) original average are given in Table 7. Using these values results in a recommended Lyman-α from H_2 cross section at 100 eV of 7.03×10^{-18} cm^2. This replaces the van der Burgt et al. (1989) recommendation of 7.3×10^{-18} cm^2 and represents a 4% reduction. We note that correction factors listed in Table 4–7 of van der Burgt et al. need to be modified to take account of this update.

A further VUV emission, which qualifies for consideration as a secondary standard, is the 130.4 nm oxygen transition as discussed next.

130.4 nm ($3s\ ^3S^o \rightarrow g\ ^3P$) *transition.* van der Burgt et al. (1989) noted that there was close agreement between different experimental groups regarding the cross section for this emission at 200 eV. Lawrence's (1970) original work was confirmed by Ajello and Franklin (1985) and Zipf (1986). Kanik et al. (2003) present a comparison of the different data sets including that of Aarts and de Heer (1971) that illustrates the level of agreement regarding the shape of the emission cross section. This is given in Fig. 11. Note that all the data sets have been renormalized at 200 eV to the Kanik et al. (2003) data.

In recommending a cross section value that may be considered as a secondary standard, we prefer to use an electron energy of 100 eV as any small secondary electron component in an electron beam will have a less significant effect here than at higher energies. Thus in Table 8 we list the 100 eV data from Lawrence (1970) and updated data from the Pittsburgh and JPL groups that are based on the revised Lyman-α standard. We recommend the average of these three values namely 2.93×10^{-18} cm^2. Note that the Aarts and de Heer (1971) cross section of 3.5×10^{-18} cm^2 was not included in the average because of the relatively large uncertainty (30%) associated with this value.

The lower energy region of the emission cross section exhibits an initial threshold and then a shoulder at higher energy indicating the existence of further contributing processes [see e.g. Mumma and Zipf (1971) and Makorov et al. (2003)]. The most careful study of this energy region seems to have been that of Makarov et al. who also made a detailed study of the emission linewidths so that they could obtain the kinetic energy spectrum of the $3s^3S^o$ source atoms. The measured

Table 8
Absolute cross sections at 100 eV for electron impact dissociative excitation of O_2 yielding O I ($3s\ ^3S^o \rightarrow 2p\ ^3P$; 130.4 nm)

Source	Cross section (10^{-18} cm^2)
Lawrence (1970)	3.05 ± 14%
Zipf (1986)[a]	2.96 ± 15%
Kanik et al. (2003)[b]	2.79 ± 23%
Recommended[c]	2.93 ± 10%

[a] Zipf's (1986) cross section was established using a Lyman-α from H_2 cross section of 7.5×10^{-18} cm^2 at 100 eV. This has been renormalized to reflect the new recommended value of 7.03×10^{-18} cm^2 (see text Section 4.1.6.2).
[b] Kanik et al.'s (2003) cross section was established using a Lyman-α value of 7.29×10^{-18} cm^2 (Pang et al., 1987; James et al., 1988). This has been renormalized to reflect the new recommended value of 7.03×10^{-18} cm^2.
[c] The recommended value is the average of rows 1–3.

Table 9
Absolute cross sections for electron impact dissociative excitation of O_2 to give the OI multiplets at 135.6 and 115.2 nm

Energy (eV)	σ (135.6 nm)[a] (10^{-18} cm^2)	σ (115.2 nm)[b] (10^{-18} cm^2)
14.3	0.0003	
16	1.70	0.00188
18	2.76	0.0234
20	3.40	0.0426
25	4.15	0.100
30	4.22	0.132
35	4.36	0.151
40	4.77	0.179
45	5.29	0.212
50	5.80	0.248
60	6.52	0.308
70	6.81	0.342
80	6.83	0.355
90	6.72	0.358
100	6.47	0.354
125	6.04	0.331
150	5.58	0.305
175	5.18	0.278
200	4.84	0.256
225	4.54	0.236
250	4.27	0.219
275	4.04	0.204
300	3.83	0.191
400	3.16	0.154
500	2.65	0.130
600	2.23	0.114

Data have been renormalized as indicated.
[a] The 135.6 nm data are from Kanik et al. (2003), which were normalized relative to the 130.4 nm cross section. This has been renormalized to reflect the new recommended value for the 130.4 nm emission cross section at 100 eV (see Table 7): 2.93×10^{-18} cm^2/2.90×10^{-18} cm^2 = 1.01.
[b] The 115.2 nm data are from Kanik et al. (2003), which were normalized to the 200 eV measurement of Ajello and Franklin (1985). We have renormalized their data by a factor of 7.03×10^{-18} cm^2/8.18×10^{-18} cm^2 = 0.86 to take account of changes in the Lyman-α from the H_2 standard since 1985.

appearance energy of 14.6 eV is consistent with the minimum energy for production of $O(3s\ ^3S^o)$ plus another ground state $O(g\ ^3P)$ atom. Although Zipf (1986) suggests that the shoulder in the excitation function is due to cascade effects, it could also be due to the onset of dissociative ionization and excitation. Since the minimum energy for this process is between 28 eV and 32 eV, depending on the state of the ionic fragment, excitation must be to fully repulsive potential energy curves in the Franck–Condon region and the resulting fragments must be quite energetic. Makarov et al. confirmed that this was the case. Thus the main production mechanisms may be specified as:

$$e + O_2(X\ ^3\Sigma_g^-) \rightarrow O(3s\ ^3S^o) + O + e' \tag{5a}$$

$$e + O_2(X\ ^3\Sigma_g^-) \rightarrow O(3s\ ^3S^o) + O^+ + e'. \tag{5b}$$

135.6 nm ($3s\ ^5S^o \rightarrow g\ ^3P$) *transition.* Excitation of $3s\ ^5S^o$ has been discussed in Section 4.1.5 and so only some additional relevant details need be mentioned here. Table 9 presents the absolute data obtained by Kanik et al. (2003) renormalized to reflect the change in the 130.4 nm cross section as discussed in the previous section. The shape of the excitation function is very similar to that discussed above for the $3s\ ^3S^o$ level (Makorov et al., 2003) and so similar conclusions can be drawn about the excitation processes that must be occurring. The magnitude of the cross section indicates that excitation is dominated by cascade from $3p(^5P)$ (see discussion in Section 4.1.5). Line profile analysis reveals the production of fast (0–7 eV) fragments at energies greater than 38 eV (Makorov et al., 2003).

121.8 nm ($3s''\ ^1P^o \rightarrow g\ ^1S$) *transition.* The only absolute data that seems to be available for this transition are from Ajello and Franklin (1985). Their emission cross section [renormalized as suggested by van der Burgt et al. (1989)] is 1.28×10^{-19} cm^2 at 200 eV. This transition is important as it is a feeder transition for the aurorally important O(^{1}S) metastable state. Using LeClair and McConkey's (1993) measurement for the total dissociative excitation cross section of O(^{1}S) at 200 eV fixes this cascade component at 7.6%.

115.2 nm ($3s'\ ^1D^o \rightarrow g\ ^1D$) *transition.* Data for this transition are listed in Table 9. These are from Kanik et al. (2003) but have been renormalized by a factor 7.03/8.18 to reflect the currently proposed value for the Lyman-α (from H_2) transition, which was used as a secondary standard in that work. We note that the 100 eV value of 3.54×10^{-19} cm^2 so obtained compares favourably with the value of 3.4×10^{-19} cm^2 given by Makorov et al. (2003). The shape of the excitation function is very similar to that for the previous two transitions and similar arguments about production processes apply. Makorov et al. (2003) demonstrated a rather wide kinetic energy spectrum (0–7 eV) for the fragments, particularly at the higher incident electron energies.

102.7 nm ($3d\ ^3D^o \rightarrow g\ ^3P$) *transition.* One new measurement of this transition has been made (Wilhelmi and Schartner, 2000) since the van der Burgt et al. (1989) review. At 200 eV their value of 9.0×10^{-19} cm^2 is 42% larger than the renormalized data of Morgan and Mentall (1983) and Ajello and Franklin (1985) but agrees very well with the renormalized data of Mumma and Zipf (1971). In all cases the renormalizations were due to the revision in the accepted value of the Lyman-α secondary standard. This is an unsatisfactory situation that requires further work.

98.9 nm ($3s'\ ^3D^o \rightarrow g\ ^3P$) *transition.* The situation here is somewhat similar to the previous case. As pointed out by van der Burgt et al. (1989), very good agreement existed between a number of workers on the magnitude of the cross section at 200 eV, once renormalization to take account of the revised Lyman-α standard had occurred [see Zipf et al. (1979), Morgan and Mentall (1983), Ajello and Franklin (1985)]. Unfortunately this value ($\sim 9 \times 10^{-19}$ cm^2) is more than a factor of two lower than the most recent data of Wilhelmi and Schartner (2000) based on the synchrotron radiation standard.

87.9 nm ($3s''\ ^3P^o \rightarrow g\ ^3P$) *transition.* Here there is a factor of approximately 3 between the lowest (Morgan and Mentall, 1983) and highest (Wilhelmi and Schartner, 2000) emission cross section values at 200 eV. Ajello and Franklin's (1985) renormalized value (4.1×10^{-19} cm^2) lies in the middle. Wilhelmi and Schartner have noted that their data below 100 nm are on average a factor of 1.5 times larger than those of Ajello and Franklin. Estimated errors in both experiments are approximately 25%. Clearly additional work is required in the spectral region below 100 nm to try and resolve these disagreements.

83.3 nm ($O^+(2s^{-1}\ ^4P^e \rightarrow g\ ^4S^o$) *transition.* This is the most intense emission where simultaneous excitation and ionization accompany the dissociation of O_2. We note that an inner shell electron is ejected, leaving the ion in an excited state. As with other transitions in this wavelength region discussed above, considerable uncertainty persists in the magnitude of the emission cross section of this important multiplet. This was already evident in the review of van der Burgt et al. (1989) where good agreement was indicated between experiments by Zipf et al. (1985) and Ajello and Franklin (1985) but earlier results by Morgan and Mentall (1983) and Aarts and de Heer (1971) seemed to be anomalously low. Morgan and Mentall's excitation function shape was also suspect below 100 eV as discussed by Ajello and Franklin (1985) and by Zipf et al. (1985). Wilhelmi and Schartner's (2000) result for this transition is almost 80% higher than these latter two data sets at 200 eV. This difference is considerably outside of the quoted error limits.

This transition is the only one where Wilhelmi and Schartner (2000) have provided data over an extended energy range from 200 to 2000 eV. They point out that the shape of their cross section at lower energies differs from that of the other workers listed. Thus agreement between them and Ajello and Franklin (1985) improves somewhat at higher energies. Very recently Malone et al. (2008b) have carefully remeasured this emission cross section at 100, 200 and 300 eV incident electron energies. They used the 130.4 nm emission as a secondary standard together with a modified branching ratio technique to obtain the relative sensitivity of their detection system between 80 and 130 nm. They obtained good agreement with Ajello and Franklin (1985) and Zipf et al. (1985) and suggest a benchmark value of $(1.50 \pm 0.17) \times 10^{-18}$ cm^2 for the emission cross section at 100 eV.

Other transitions. Both Ajello and Franklin (1985) and Wilhelmi and Schartner (2000) present data for other transitions, either from O* or $(O^+)^*$, in the VUV range from 37 to 136 nm. Where both groups measured these same features, the Wilhelmi and Schartner data are, on average, about 75% higher than the Ajello and Franklin (1985) results renormalized to reflect improvements in the Lyman-α calibration standard. We note that Ajello and Franklin checked their short wavelength (<60 nm) calibration by remeasuring the He 58.4 nm line and getting good agreement with the accepted value (Donaldson et al., 1972).

4.1.7. O_2^-

We note that Pedersen et al. (1999) have studied detachment plus dissociation of O_2^- by electron impact in a merged beam experiment at the ASTRID storage ring though absolute data were not determined.

4.2. CO

Carbon monoxide is a very important molecule in many applications, both terrestrially, e.g. as a feed gas for high power laser systems [e.g. Sato et al. (1985)], and extra-terrestrially where its spectral features have been observed from the Sun, the

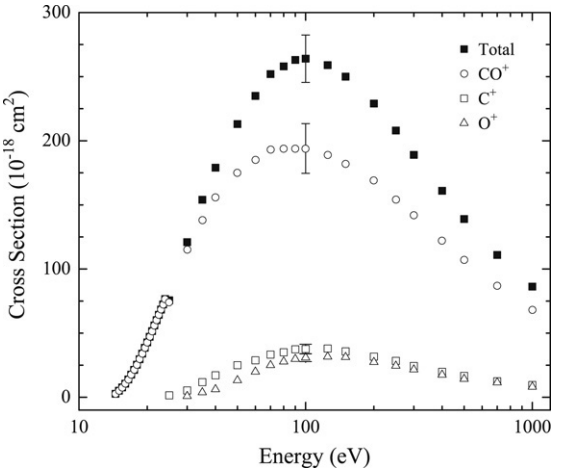

Fig. 12. CO partial and total electron impact ionization cross sections. Data from Table 10.

planets, comets, galaxies, quasi-stellar objects and the interstellar medium [see e.g. Beegle et al. (1999), Gusten et al. (2006), Carilli et al. (2002), Oliversen et al. (2002) and Lara et al. (2004)]. After hydrogen, CO is the most abundant molecule in the interstellar medium (van Dishoeck and Black, 1988). In Earth's atmosphere it represents an important pollutant species.

A number of reviews have dealt with various aspects of electron interactions leading to dissociation of the molecule. Thus, Lindsay and Mangan (2003) have discussed recommended absolute data for dissociative ionization and dissociative attachment, van der Burgt et al. (1989) considered dissociative excitation, Kanik et al. (1993b) reviewed total electron scattering and electronic state excitation cross sections, and Zecca et al. (1996) briefly described dissociative processes in the light of the broader picture where all electron-driven processes were considered. Avakyan et al. (1998) present averaged data for some VUV transitions following dissociative excitation of CO in both tabular form and in figures.

4.2.1. Dissociative ionization

A large number of measurements of dissociative ionization have been carried out over the years, most recently by Mangan et al. (2000) who give extensive references to earlier work. As pointed out by Mangan et al. (2000) and by Lindsay and Mangan (2003), only a few of the reported measurements were truly absolute and only a very few were demonstrably free from fragment ion energy discrimination effects. Measurements made with quadrupole mass spectrometers were particularly suspect in this regard. Based on their analysis, Lindsay and Mangan recommended data for fragment and total ion production. They found excellent agreement between their summed partial ionization cross sections and the absolute total ionization cross section measurements of Rapp and Englander-Golden (1965) and Srinivasa and Rees (1967). Overall uncertainties in the cross sections for fragment ion production were $\pm$6%. For doubly charged ionic fragments, the data of Tian and Vidal (1998c), with uncertainties of $\pm$15%, were preferred. Table 10 lists the recommended cross sections in the energy range from threshold to 1000 eV and some of the data are displayed in Fig. 12.

4.2.2. Appearance energies and fragment energy distributions

Extensive work on ion appearance energies and kinetic energies has been carried out by Köllmann (1975a,b) and by Locht and Durer (1975) and Locht (1977). Köllmann used a system in which the ions produced by electron impact were first energy analysed using a 90° cylindrical condenser and then mass analysed in a 60° sector field electromagnet. Constancy of transmission to within 20% was estimated for ions in the kinetic energy range 2–12 eV. Locht and colleagues used a retarding field kinetic energy analyzer followed by a quadrupole mass spectrometer. They did not give details of the transmission of their system as a function of fragment ion energy but it was probably biased in favour of low energy, particularly thermal, ions. TOF measurements on high-Rydberg fragments following CO dissociation, which should yield rather similar information on fragment kinetic energies to the dissociative ionization experiments, were carried out by Smyth et al. (1974).

For C^+ ion production there is reasonable agreement regarding the positions but not the relative magnitudes of the main features in the kinetic energy spectra. At 100 eV incident energy, Köllmann noted four distinct structures in KE spectra — a peak at thermal energy, a shoulder at 0.5 eV, a broad peak at 3 eV and a shoulder at 5.5 eV. At the same incident energy Locht identified three features — a thermal peak, a shoulder at around 0.3 eV and a broad structure around 2.5 eV. At low incident energies, $\sim$25 eV, only the thermal energy peak was observed, (Locht, 1977).

For O^+ ions Köllmann observed a single peak that broadened and moved from around 1 eV at 35 eV incident energy to about 3 eV at 200 eV. Locht also saw this peak develop and move from around 1 eV at 30 eV incident energy to more than 2 eV at 100 eV. In addition Locht observed a thermal energy peak that dominated the spectrum for energies below 30 eV. (Köllmann observed a very small thermal energy structure.)

Table 10
CO partial and total ionization cross sections

Energy (eV)	$\sigma(CO^+)$ (10^{-18} cm^2)	$\sigma(C^+)$ (10^{-18} cm^2)	$\sigma(O^+)$ (10^{-18} cm^2)	$\sigma(CO^{2+})$ (10^{-18} cm^2)	$\sigma(C^{2+})$ (10^{-18} cm^2)	$\sigma(O^{2+})$ (10^{-18} cm^2)	σ(total) (10^{-18} cm^2)
14.5	2.7						2.7
15	5.1						5.1
15.5	7.7						7.7
16	10.6						10.6
16.5	13.9						13.9
17	17.7						17.7
17.5	21.4						21.4
18	25.4						25.4
18.5	29.7						29.7
19	34.0						34.0
19.5	38.6						38.6
20	42.8						42.8
20.5	47.2						47.2
21	51.6						51.6
21.5	56						56.0
22	60.1						60.1
22.5	64.3						64.3
23	68.4						68.4
23.5	72.4						72.4
24	76.6						76.6
25	74.1	1.50					75.6
30	115	5.32	0.90				121
35	138	11.8	3.80				154
40	156	17.1	6.18				179
50	175	25.0	13.2	0.085			213
60	185	28.8	19.9	0.263	0.04		235
70	193	33.3	25.0	0.534	0.096		252
80	194	35.1	27.8	0.622	0.243	0.023	258
90	194	37.4	29.8	0.757	0.444	0.051	263
100	194	37.6	30.9	0.821	0.539	0.073	264
125	189	38.0	31.6	0.860	0.944	0.184	259
150	182	35.8	31.3	0.788	1.16	0.241	250
175				0.851	1.24	0.345	
200	169	31.7	27.4	0.697	1.25	0.367	229
225				0.745	1.21	0.335	
250	154	28.4	24.5	0.669	1.19	0.338	208
275				0.585	1.16	0.335	
300	142	24.4	21.6	0.548	1.10	0.334	189
350				0.457	0.978	0.245	
400	122	19.8	17.5	0.450	0.904	0.266	161
450				0.372	0.816	0.241	
500	107	16.7	14.3	0.331	0.762	0.200	139
550				0.329	0.757	0.216	
600				0.335	0.708	0.177	
700	87.1	12.5	11.5				111
1000	68.3	9.52	8.16				86.3

From Lindsay and Mangan (2003).

Smyth et al. (1974) observed a number of structures in their translational energy spectra of high-Rydberg atoms in this same kinetic energy range below 6 eV.

From plots of fragment kinetic energy against appearance energy as discussed in Section 2, a number of dissociation channels were definitely established. These were:

$$e + CO \rightarrow (CO)^* + e' \rightarrow C^+(^2P^o) + O^-(^2P^o) \tag{6a}$$

$$e + CO \rightarrow (CO)^+ + 2e' \rightarrow C^+(^2P^o) + O(^3P) \tag{6b}$$

$$e + CO \rightarrow (CO)^+ + 2e' \rightarrow C^+(^2P^o) + O(1D) \tag{6c}$$

$$e + CO \rightarrow (CO)^+ + 2e' \rightarrow O^+(^4S^o) + C(^3P) \tag{6d}$$

$$e + CO \rightarrow (CO)^+ + 2e' \rightarrow O^+(^4S^o) + C(^1D) \tag{6e}$$

$$e + CO \rightarrow (CO)^+ + 2e' \rightarrow O^+(^2D^o) + C(^3P). \tag{6f}$$

In their work on Rydberg states (Smyth et al., 1974), processes analogous to (6b)–(6d) were identified. In addition to the ones listed above, many other possible processes could be contributing, particularly at the higher incident energies. Various reaction models were discussed in terms of potential energy curves and their positions in the Franck–Condon region.

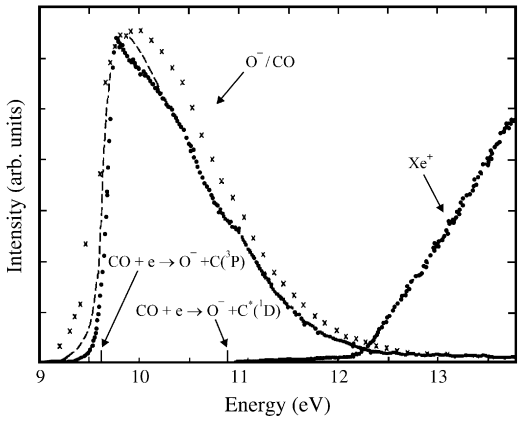

Fig. 13. Formation of O^- from CO by electron impact. The arrows point to the thresholds of the processes indicated. Solid dots, Stamatovic and Schulz (1970); dashed line, Chantry (1968); crosses, Rapp and Briglia (1965). The data sets have been normalized at their peaks. Also shown is Xe data used for energy calibration. Reused with permission from A. Stamatovic, Journal of Chemical Physics, 53, 2663 (1970).

Köllmann (1975a) was able also to measure the angular distribution of the fragment O^+ and C^+ ions. He found that at high electron energies the distributions were fairly isotropic but, at low incident energies (∼40 eV), they were peaked in the forward and backward directions. The isotropic part could be ascribed to $\Sigma^+ \rightarrow \Sigma^+$ transitions in the parent molecule, but the anisotropies were inconsistent with predictions of Dunn (1962) or others [e.g. van Brunt (1974)] for $\Sigma^+ \rightarrow \Pi, \Delta$ transitions.

Senn et al. (1999d) measured appearance energies for the monomer, dimer and trimer cations following electron impact on a clustered beam.

4.2.3. Dissociative attachment

Dissociative attachment in CO has been studied by numerous workers over the years. Both O^- and C^- anions have been observed. Lindsay and Mangan (2003) have reviewed the available data and recommend the absolute cross section measurements of Rapp and Briglia (1965) for O^- production with a maximum value of 2×10^{-19} cm^2 at 9.9 eV. Because of the relatively broad energy distribution (∼0.4 eV) in Rapp and Briglia's electron beam, the resonance feature is probably somewhat narrower and with a sharper threshold than their data indicate. Work by Chantry (1968) and by Stamatovic and Schulz (1970) using better energy resolution (70 meV) confirms this. Fig. 13, taken from Stamatovic and Schulz, illustrates this point.

This figure also illustrates the fact that two channels contribute to O^- production, namely,

$$e + CO \rightarrow (CO)^- \rightarrow C(^3P) + O^-(^2P^o) \tag{7a}$$

and

$$e + CO \rightarrow (CO)^- \rightarrow C(^1D) + O^-(^2P^o). \tag{7b}$$

The existence of channel (7b) has been confirmed in more recent work by Hall et al. (1977) and by Denifl et al. (1998). These latter authors observed a clear peak at the expected appearance energy of channel (7b), but state that its magnitude was enhanced by energy discrimination effects in their ion detection system. Hall et al. (1977) measured O^- angular distributions that enabled them to propose symmetries and configurations for the intermediate negative ion states. Chantry (1968) estimated that the peak cross section of process (7b) was 9.5×10^{-21} cm^2. He also demonstrated that O^- kinetic energies, from processes (7a) and (7b), were in the ranges 0–0.8 and 0–0.3 eV respectively. Similar results were obtained by Hall et al. (1977). Stamatovic and Schulz (1970) also investigated the production of C^-. They found two small peaks in the C^- cross section curve, at 10.4 and 10.9 eV. They estimated the cross section at 10.4 eV to be $6 \pm 1.5 \times 10^{-23}$ cm^2. From energetic considerations the fragments in both cases must be $C^-(^4S)$ and $O(^3P)$.

4.2.4. Dissociation into ground state fragments

Cosby (1993) provides the only report of CO dissociation into ground state fragments. He used the fast neutral beam technique described in Section 2.2 and measured absolute cross sections over the energy range from threshold to 200 eV. The data are given in Table 11 and displayed in Fig. 14. The process studied was

$$e + CO \rightarrow (CO)^* + e' \rightarrow C(^3P) + O(^3P) + W. \tag{8}$$

Explicit measurement of the translational energy release, W, allowed the intermediate $(CO)^*$ states to be identified and the atomic states of the products to be confirmed. A maximum cross section for the process was measured to be

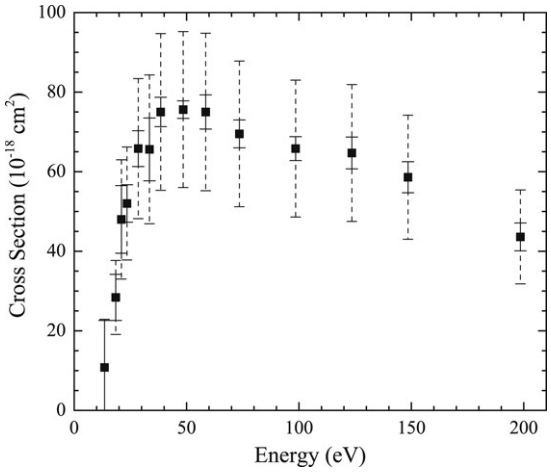

Fig. 14. Total cross section for the reaction $e + CO \rightarrow C + O + e'$ as a function of incident electron energy. The relative and absolute uncertainties in the measurements are shown by the solid and dashed error bars, respectively. From Cosby (1993).

Table 11
Electron impact dissociation cross sections of CO

Energy (eV)	Cross section (10^{-18} cm^2)	Relative error (10^{-18} cm^2)	Absolute error (10^{-18} cm^2)
13.5	10.8	11.8	12.1
18.5	28.4	5.8	9.3
21.0	48.0	8.5	15.0
23.5	52.0	4.7	14.2
28.5	65.8	4.5	17.6
33.5	65.6	7.9	18.7
38.5	75.0	3.7	19.7
48.5	75.6	2.2	19.6
58.5	75.0	4.3	19.8
73.5	69.5	3.5	18.3
98.5	65.8	3.0	17.2
123.5	64.7	4.0	17.2
148.5	58.6	3.9	15.6
198.5	43.6	3.5	11.8

From Cosby (1993).

75.6×10^{-18} cm^2 at an electron impact energy of 50 eV. This is about a factor of five lower than the total excitation cross section of all the electronic states of CO but about a factor of two larger than the dissociative ionization cross section of CO at this energy. The C and O atoms possess kinetic energies in the range of 0–1.66 and 0–1.24 eV respectively.

4.2.5. Dissociation into neutral metastable fragments

Fragmentation of CO into metastable atoms following electron impact has been studied by Smyth et al. (1974), Wells et al. (1978), Barnett et al. (1992) and LeClair and McConkey (1994). Smyth et al.'s data are particular to high-Rydberg fragments whereas LeClair et al. focused on O(^{1}S). The other two groups detected a combination of high-Rydbergs and O(^{5}S). TOF spectroscopy was used in all of the experiments with various detectors.

A large number of processes were observed to contribute to the data. For example, Smyth et al. identified seven distinct processes that yielded Rydberg fragments and Wells et al. found three additional ones that yielded O(^{5}S) either directly or via cascade from higher lying states. Significant amounts of kinetic energy release accompanied the dissociation. For example, Barnett et al. show broad kinetic energy distributions for the oxygen fragments, which peak at around 4 eV. These are indicative of parent molecular states that are steeply repulsive in the Franck–Condon region.

The only work, where absolute cross section data were obtained, was the experiment of LeClair and McConkey (1994) on O(^{1}S) production. They used their solid xenon matrix detector, described in 2.2. Their data are given in Table 12 and displayed in Fig. 15. They identified five different processes giving rise to O(^{1}S). At an incident electron energy of 100 eV, kinetic energy releases of up to 20 eV were observed. The main production process was accompanied by a kinetic energy release of around 5 eV. From the shape of the excitation cross section curve (Fig. 15), the dominant production mechanisms are optically allowed in the parent molecule. Thus:

$$e + CO(X\,^1\Sigma^+) \rightarrow CO^*(^1\Sigma^+, {}^1\Pi, {}^1\Delta) \rightarrow C(^1D) + O(^1S) + W. \quad (9)$$

Table 12
Absolute cross sections for the production of O(^{1}S) following electron impact on CO

Energy (eV)	Cross section (10^{-18} cm^2)
16	Threshold
18	0.03
20	0.05
25	0.11
30	0.16
35	0.22
40	0.28
45	0.32
50	0.36
60	0.42
70	0.47
80	0.48
90	0.49
100	0.50
120	0.50
140	0.49
160	0.48
180	0.47
200	0.45
250	0.40
300	0.36
350	0.33
400	0.30
450	0.28
500	0.26

From LeClair and McConkey (1994).

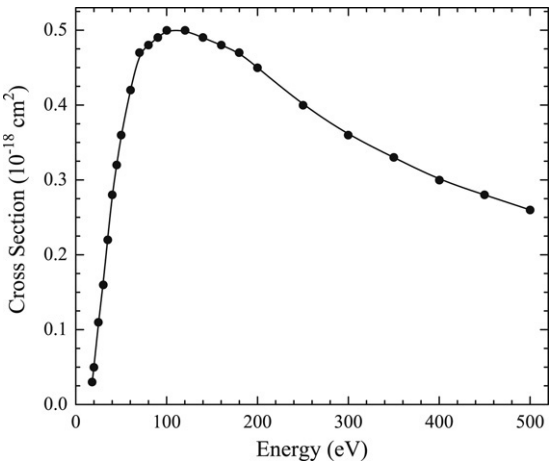

Fig. 15. Absolute cross section for production of O(^{1}S) following electron impact dissociation of CO as a function of incident electron energy. Data from Table 12.

4.2.6. Dissociative excitation

There have been a number of studies of electron impact excitation of CO since van der Burgt et al. (1989) reviewed the field of dissociative excitation leading to VUV emissions. Unfortunately there does not appear to have been any work done on excitation of atomic transitions in the visible or near-infrared spectral regions apart from the 100 eV cross section data, listed by Zipf (1984), for which no experimental details are given. Excellent agreement exists between Zipf's listed value for the 844.7 nm OI line of 5.7×10^{-19} cm^2 and the earlier measurement by Lawrence (1970) of 5.9×10^{-19} cm^2.

Since 1989 considerable effort has gone into establishing the cross sections for exciting the main molecular band systems of CO using both electron scattering [see Kato et al. (2007) and references therein] and optical techniques (James et al., 1992; Kanik et al., 1995; Ciocca et al., 1997; Beegle et al., 1999). These have resulted in some revisions to the earlier data of Ajello (1971), Aarts and de Heer (1970) and Mumma and Zipf (1971).

As far as dissociative excitation is concerned, the situation is rather unsatisfactory. Much spectral overlap occurs between atomic emissions and background CO bands [see James et al. (1992)]. Data are only available for a very limited number of atomic transitions and often cannot be directly compared because excitation functions, which allow comparison of cross sections at different electron energies, are not available. In the case of the OI lines at 130.4 and 102.6 nm where comparisons

can be made, significant disagreements between different laboratories are apparent. Thus, as pointed out by van der Burgt et al. (1989), reasonable agreement is seen between pre-1975 measurements of the 130.4 nm multiplet, whereas Zipf's (1984) measurement is about twice as large. On the other hand, Zipf's cross section for the 102.7 nm multiplet is only about one third that of James et al. (1992) at 100 eV.

In the case of the OI 115.2 nm ($^1D - {}^1D^o$) transition, a high resolution experiment by Kanik et al. (1995) enabled them to isolate this line and measure its cross section to be 3.7×10^{-19} cm^2 at 200 eV. This may be compared with a lower resolution measurement by James et al. (1992) of blended features, at this same wavelength and energy, of 19.0×10^{-19} cm^2. Beegle et al. (1999) measured the Doppler profile of this line and deduced that the O(^{1}D) atoms had kinetic energies ranging from zero to 3 eV at 30 eV incident electron energy and from zero to about 5 eV at 100 eV incident energy.

4.2.7. CO^+

Lecointre et al. (2006) have used a crossed electron–ion beam arrangement to make absolute measurements of the dissociative excitation and dissociative ionization of CO^+ into C^+ and O^+ fragments in the impact energy range 5–2500 eV. Kinetic energy distributions of the fragments were measured as were anisotropies in their angular distributions. Dissociative excitation cross sections were observed to peak around 35 eV. Maximum cross sections for C^+ and O^+ production by this mechanism were found to be $9.7 \pm 2.1 \times 10^{-17}$ cm^2 and $6.2 \pm 1.3 \times 10^{-17}$ cm^2 respectively and the corresponding threshold energies were 8.5 ± 0.5 and 14.8 ± 0.5 eV. C^+ production by this mechanism is dominant at low electron energies. For dissociative ionization the peak cross section of $12.6 \pm 2.4 \times 10^{-17}$ cm^2 occurs around 125 eV. Fragment kinetic releases of up to 24 eV were observed.

Very recently Lecointre et al. (2007) have revised and extended an earlier investigation from this laboratory (Belic et al., 1997) on the production of C^{2+} and O^{2+} from this same target molecular cation. Data for C^{3+} and O^{3+} were also obtained. Threshold energies and fragment kinetic energies were measured.

4.3. NO

NO is a minor but important component of the atmospheres of Earth, Mars and Venus. It is important for the studies of the ionosphere and of auroras, Ajello et al. (1989a,b). In Earth's lower atmosphere, it is an important ingredient in major photochemical reactions involving ozone (Crutzen, 1971).

Avakyan et al. (1998) and Lindsay and Mangan (2003) have recommended values for dissociative ionization of NO and the latter authors have also provided recommendations for dissociative attachment. Zecca et al. (1996) have discussed the broader context of electron collisions with NO while van der Burgt et al. (1989) have surveyed the VUV dissociative excitation data available at that time. Generally speaking, NO has not been as widely studied as many of the other simple oxygen-containing molecules.

4.3.1. Dissociative ionization

Recent measurements of dissociative ionization of NO have been carried out by Lopez et al. (2003), Lindsay et al. (2000) and Iga et al. (1996b). Lopez et al. used their fast neutral beam technique and quote error limits of ±18%. Lindsay et al. used their parallel plate apparatus with TOF mass spectroscopy and position-sensitive detection of product ions. They quote an error of ±5% for total fragment ion production. Iga et al. used their crossed beam system with quadrupole mass analysis and normalization to known He absolute data. They quote errors of ±15%. Lindsay and Mangan (2003) recommend the Lindsay et al. data set as it was demonstrably free of ion kinetic energy discrimination effects and was independently absolute. They did not consider the Lopez et al. (2003) data set.

Fig. 16, adapted from Lopez et al. shows the level of agreement between the three recent data sets for ($N^+ + O^+$) production. We note that the Iga et al. data lie significantly below the other two data sets, probably indicating incomplete collection of fast ion fragments in their system. Above about 125 eV the other two experiments overlap, though differences are evident at lower energies. The Lopez et al. data only extend to 200 eV electron energy.

Interestingly, if total single ionization is considered, a similar level of (dis)agreement between the data sets is observed. The older work of Rapp and Englander-Golden (1965) lies in the middle of the other data sets. The measurements of Lindsay et al. (2000) lie lowest in magnitude but in quite good agreement with the calculated cross section of Hwang et al. (1996) using a BEB formalism. The Iga et al. data are the largest but are supported by very recent calculations by Joshipura et al. (2007a) using their complex scattering potential method. The situation is rather unsatisfactory. The data set of Lindsay and Mangan (2003) is included for convenience in Table 13.

4.3.2. Appearance energies and fragment energy distributions

No detailed study of appearance energies or fragment ion energy distributions has been made. Inspection of the TOF data (Lindsay et al., 2000) indicates that fragment kinetic energies are significant, extending to greater than 5 eV at the higher incident energies.

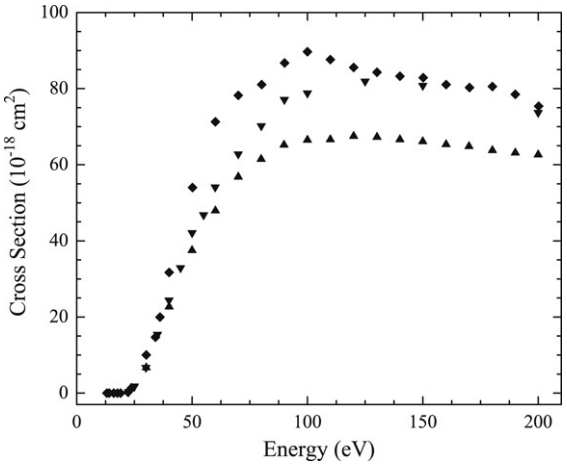

Fig. 16. $[N^+ + O^+]$ partial ionization cross section of NO from threshold to 200 eV. Diamonds, Lopez et al. (2003); triangles, Iga et al. (1996b); inverted triangles from Lindsay and Mangan (2003). Note that the Lindsay and Mangan data indicate a small component of NO^{2+} above 60 eV.

Table 13
NO partial and total ionization cross sections

Energy (eV)	$\sigma(NO^+)$ (10^{-18} cm^2)	$\sigma(N^+ + O^+ + NO^{2+})$ (10^{-18} cm^2)	$\sigma(N^+)$ (10^{-18} cm^2)	$\sigma(O^+)$ (10^{-18} cm^2)	$\sigma(NO^{2+})$ (10^{-18} cm^2)	σ(total) (10^{-18} cm^2)
12.5	4.8 ± 1.2					4.8 ± 1.2
15	21 ± 3					21 ± 3
17.5	48 ± 5					48 ± 5
20	59					59
22.5	75	0.35 ± 0.07				76
25	98	1.8 ± 0.3	1.4 ± 0.4	0.40 ± 1		99
30	120	6.7 ± 0.6	5.4	1.25		127
35	137	15.4	13.2	2.2		153
40	151	24.4	19.1	4.6		175
45	167	32.9	25.2	7.3		200
50	174	42.1	31.7	10.4		216
55	184	46.8	31.5	14.0		231
60	189	54.1	37.5	15.8	0.89	243
70	192	62.8	44.4	17.0	1.42	255
80	196	70.2	47.9	19.9	2.24	267
90	197	77.1	48.1	25.1	3.77	274
100	197	78.8	50.6	24.7	3.49	275
125	192	81.9	49.9	28.6	3.21	273
150	184	80.8	50.2	27.4	2.93	265
200	169	73.7	43.8	26.7	3.06	243
250	155	68.0	40.6	24.6	2.84	223
300	140	60.1	38.5	19.1	2.33	200
400	124	50.1	30.9	16.8	2.32	174
500	111	42.4	26.5	13.9	2.03	153
600	98	38.2	22.8	13.9	1.47	136
800	81	30.1	19.0	10.0	1.32	111
1000	70	25.2	16.9 ± 4.2	7.6 ± 2.3	0.69 ± 0.35	95

From Lindsay and Mangan (2003).

4.3.3. Dissociative attachment

Dissociative attachment in NO has been a hot topic over the years, stimulated by controversy regarding the decay channels that are open and the products that can result. The lowest energy *possibilities* are (with threshold energies bracketed):

$$e + NO \rightarrow (NO^*)^- \rightarrow O^-(^2P) + N(^4S) \quad [5.036\ eV] \tag{10a}$$

$$e + NO \rightarrow (NO^*)^- \rightarrow O^-(^2P) + N(^2D) \quad [7.420\ eV] \tag{10b}$$

$$e + NO \rightarrow (NO^*)^- \rightarrow O^-(^2P) + N(^2P) \quad [8.611\ eV] \tag{10c}$$

$$e + NO \rightarrow (NO^*)^- \rightarrow O(^3P) + N^-(^1D) \quad [7.95\ eV]. \tag{10d}$$

Rapp and Briglia (1965) made an absolute measurement of total anion production in the region near 10 eV incident electron energy. They observed a broad peak with two humps and a sharp onset near 7 eV. Their measured peak cross section

was 1.12×10^{-18} cm^2. Chantry (1968) added the capabilities of kinetic energy analysis and mass identification and was able to show that O^- was the dominant ion produced. He saw no evidence for channel (10d). Subsequent measurements, which were capable of mass analysis [see e.g. Krishnakumar and Srivastava (1988) and Chu et al. (1998a)] have also failed to detect any long-lived N^-. Both Chantry and Chu et al. present evidence that the O^- yield curve, as a function of incident electron energy, depends sensitively on the ion extraction field. Thus detailed arguments, such as those of Sambe and Ramaker (1991), suggesting that some of the structure in the curve was due to long-lived N^-, should be received with caution.

Detection of DA channel (10a) has been controversial. Earlier studies [Chantry (1968), Krishnakumar and Srivastava (1988) and references therein] failed to see any sign of this but Orient and Chutjian (1995), who carried out their measurements in a 6 T magnetic field and monitored their ions using a trochoidal analyzer immersed in this field, claimed that it was the most abundant channel. A number of studies have been carried out since 1995 using a variety of experimental arrangements, and, in all cases, they confirm that (10b) is by far the dominant channel. Channel (10c) provides a much smaller (<20%) contribution [see Chu et al. (1998a), Denifl et al. (1998), Illenberger and Märk (1999) and Allan (2004)]. Trevisan et al. (2005) made a detailed theoretical study of the problem and showed that the cross section for (10a) was very small unless the target NO was vibrationally excited. Thus the weight of evidence seems to point away from the Orient and Chutjian result unless some "new" physics is occurring in the strong magnetic field of their experiment.

Krishnakumar and Srivastava (1988) are the only workers to present DA cross section data at incident electron energies above 15 eV. They indicate that the cross section for the ion pair production channel ($O^- + N^+$) has a threshold around 19.5 eV. It rises to a fairly constant value of approximately 2×10^{-19} cm^2 between 25 and 55 eV.

Chu et al. (1998a,b) have studied DA involving NO clusters as well as isolated molecules. They find that the same reaction mechanisms are active in both cases.

4.3.4. Dissociation into ground or neutral metastable state fragments

Apart from the dissociative attachment work discussed above, no measurements are available for dissociation into ground state or metastable fragments (including Rydbergs) except the work of LeClair et al. (1996) on O(^{1}S) production. From their TOF data, they demonstrated that two channels contributed to O(^{1}S) production, with kinetic releases peaking near 3.4 and 7 eV. Signals were too weak to allow any energy threshold or excitation cross section measurements to be carried out.

4.3.5. Dissociative excitation

Emission of optical radiation following electron impact on NO consists mainly of a large number of molecular band systems of which the most widely studied are the gamma bands ($A\,^2\Sigma^+ - X\,^2\Pi$) (Imami and Borst (1975), Ajello et al. (1989a,b), Schappe et al. (2002) and references therein).

The only contribution to dissociative excitation since the review by van der Burgt et al. (1989) is the extensive and detailed experiment by Ajello et al. (1989a) who measured the cross sections of a large number of atomic and ionic transitions at 200 eV incident electron energy in the wavelength range 40–170 nm. No measurements on atomic transitions in the visible or near-IR spectral regions have been made apart from the measurement by Lawrence (1970) on the 844.7 nm OI feature. He reported an emission cross section for this transition of 5.5×10^{-19} cm^2 at 100 eV.

In the VUV below 125 nm, emissions are entirely atomic or ionic in nature. Above 140 nm the spectrum contains mainly the NO^+ Baer-Miescher ($A\,^1\Pi \rightarrow X\,^1\Sigma^+$) bands, except for the strong NI transitions at 149.3 and 174.3 nm. A considerable body of absolute cross section data is available: Ajello et al. present 200 eV data on over 50 features; Mentall and Morgan (1972) studied 8 prominent OI and NI features; Stone and Zipf (1972) give data for the 130.4 nm OI multiplet and 3 NI features including the 120 nm resonance line; Lawrence (1970) studied OI, 130.4 nm.

Unfortunately there is rather poor agreement on the magnitude of the emission cross sections even though the shapes of the excitation functions (where presented) agree rather well. Thus, for example, there is reasonable (within 20%) agreement on the magnitude of the 130.4 nm emission cross section but, for the 120 nm NI multiplet, results from the different groups differ by more than a factor of two [see Ajello et al. (1989a)]. For the NI multiplets, some systematic differences are observed between the different laboratories highlighting the difficulty of absolute calibration in this spectral region. Of the three groups Mentall and Morgan's data are always the largest, while Ajello et al.'s are the lowest. Comparison between the different laboratories is made more difficult because measurements were presented at different electron energies and only in a limited number of cases were excitation functions presented to allow data at other energies to be obtained. Two possibly significant differences between Ajello et al.'s experiment and the other workers were (1) a crossed beam rather than a static gas system was used and (2) a strong magnetic field was used to confine the electron beam. With such a system difficulties could arise in ensuring identical interaction volumes between calibrating (H_2) and test (NO) gases.

Excitation functions exhibited a typical shape, which is illustrated in Fig. 17 for excitation of OI (130 nm). As can be seen, the cross section exhibits structure suggesting that two major processes are contributing to the excitation. From appearance energy measurements, Mentall and Morgan suggest that, for this multiplet, these processes are dissociative excitation and ionization–dissociative excitation as given below:

$$e + NO(X\,^2\Pi) \rightarrow O(^3S) + N(^4S) + e' \quad [16.0\ \text{eV}] \tag{11a}$$

$$e + NO(X\,^2\Pi) \rightarrow O(^3S) + N^+(^3P) + e' \quad [30.5\ \text{eV}]. \tag{11b}$$

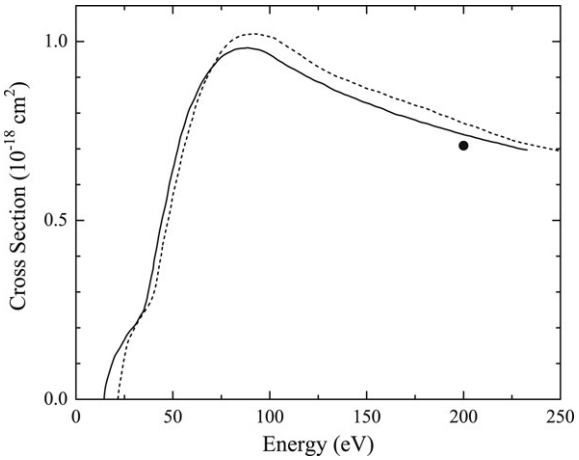

Fig. 17. Emission cross section of the O(130.4 nm) multiplet following dissociative excitation of NO. Solid line, Mentall and Morgan (1972); dashed curve, Lawrence (1970). The single datum point at 200 eV is from Ajello et al. (1989a). Note that the Ajello et al. datum has been renormalized by a factor 7.02/7.29 = 0.963 to reflect changes in the Lyman-α from H_2 calibration standard (see Section 2.2). Mentall and Morgan normalized their data to a cross section of 3.3×10^{-18} cm^2 for 100 eV excitation of the 130.4 nm multiplet from O_2. To reflect our suggested changes to this secondary standard (see Table 7), these data have been normalized by a factor $2.93/3.3 = 0.89$.

In many cases comparison of observed and predicted thresholds indicated that there was considerable kinetic energy release in the dissociation process, suggesting highly-repulsive, parent, excited NO states.

4.4. H_2O and isotopes

Because water is such an important and abundant molecule in a wide variety of planetary and space environments as well as on Earth, a detailed knowledge of its dissociative processes following electron impact is vital to our understanding and modelling of these environments. Secondary electron production in interstellar or cometary ices can influence subsequent chemistry (Gerakines et al., 1995, 2000; Allamandola et al., 1999). In addition water is recognized for its vital role in supporting life, being the dominant component of the biological cell. Electron collisions have been demonstrated to be effective instruments in causing structural damage in biological molecules such as DNA [e.g. Boudaiffa et al. (2000)] and so knowledge of these interactions is important for a proper understanding of radiation damage. The recent discoveries of water reservoirs on such planetary bodies as Mars, Europa and Enceladus have raised the anticipation level that larger molecules, which might be life precursors, could also be discovered in some of these environments. Electron-driven plasmas are important also in terrestrial situations such as in the safe destruction and disposal of toxic wastes (Becker et al., 2000). Because of its importance the water molecule has been identified as a so-called "benchmark" target for electron–molecule studies, where experimental effort can be focused to obtain reliable quantitative data of high accuracy and where theoretical advances can be checked (Becker et al., 2000).

There have been a large number of papers reporting cross section and other data involving $e^- + H_2O$ interactions. A number of reviews, written from the points of view of various scientific communities, are available. The most recent of these is that of Itikawa and Mason (2005), which deals specifically with the water molecule and considers work published up to the end of 2003. Others such as those of Karwasz et al. (2001) and Shirai et al. (2001) and the compilation edited by Itikawa (2003) are more broadly based but contain data concerning electron–water collisions. The IAEA Committee Report (1995) on atomic and molecular data relevant to radiation research is also helpful as is the bibliographical information of Hayashi (2003).

The importance of dissociation in the interaction of electrons with water is borne out by a number of observations:

1. A glance at an energy loss spectrum, e.g. Chutjian et al. (1975), or at the more recent threshold electron spectrum of Jureta (2005) or of Thorn et al. (2007b), reveals the dominance of broad features characteristic of excitation to continuum states.
2. The ionization data of, for example, Straub et al. (1998) show that approximately 40% of ionizing collisions result in break-up of the molecule.
3. Harb et al.'s (2001) data for the dissociation of H_2O resulting in ground state OH indicates that this channel alone accounts for approximately half of the total cross section above 100 eV.
4. By far the dominant features in optical spectra excited by electron impact on H_2O are atomic or molecular features resulting from dissociative excitation. [See Itikawa and Mason (2005).]

In the following sections we discuss the different dissociative processes and associated physics.

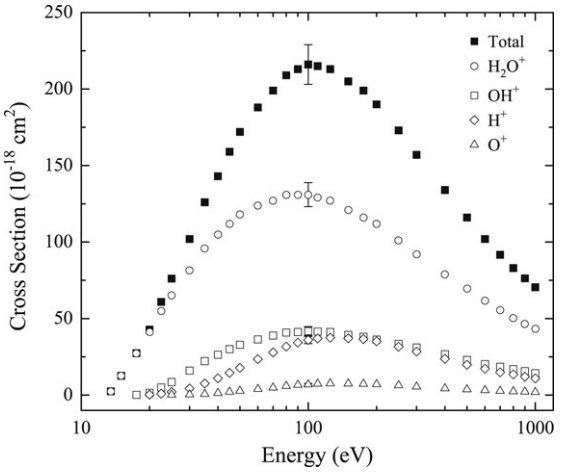

Fig. 18. Partial ionization cross sections of H_2O/D_2O by electron impact. Note that the target gas was actually D_2O. Data from Table 14.

Table 14
$H_2O(D_2O)$ partial and total ionization cross sections

Energy (eV)	$\sigma(H_2O^+)$ (10^{-18} cm^2)	$\sigma(OH^+)$ (10^{-18} cm^2)	$\sigma(O^+)$ (10^{-18} cm^2)	$\sigma(O^{2+})$ (10^{-18} cm^2)	$\sigma(H_2^+)$ (10^{-18} cm^2)	$\sigma(H^+)$ (10^{-18} cm^2)	σ(total) (10^{-18} cm^2)
13.5	2.5						2.5
15	12.6						12.6
17.5	27.2	0.13					27.4
20	41.1	1.45				0.24	42.8
22.5	54.9	5.00				0.91	60.9
25	65.2	8.55	0.22			2.07	76.1
30	81.5	16.0	0.37		0.018	4.33	102
35	95.8	22.2	0.70		0.039	7.59	126
40	105	26.4	1.32		0.057	11.0	143
45	112	30.0	2.07		0.070	14.5	159
50	118	32.9	2.75		0.065	17.8	172
60	124	36.4	3.94		0.066	23.5	188
70	127	38.9	4.84		0.069	27.9	199
80	131	40.9	5.94		0.063	31.7	209
90	131	41.2	6.66	0.008	0.078	34.3	213
100	131	41.8	6.95	0.019	0.075	36.0	216
110	129	41.5	7.38	0.046	0.073	37.0	215
125	127	41.2	7.63	0.069	0.064	37.5	213
150	121	39.3	7.52	0.116	0.077	37.1	205
175	116	38.1	7.31	0.178	0.071	36.6	199
200	112	36.3	7.07	0.179	0.054	35.1	190
250	101	33.4	6.34	0.195	0.050	31.6	173
300	92.1	31.1	5.51	0.179	0.045	28.4	157
400	78.9	26.6	4.34	0.134	0.040	23.7	134
500	69.6	23.0	3.73	0.105	0.032	19.8	116
600	61.8	20.3	3.13	0.096	0.029	17.2	102
700	55.5	18.5	2.71	0.080	0.033	14.9	91.7
800	50.2	16.9	2.40	0.080	0.022	13.5	83.0
900	46.5	15.6	2.20	0.060	0.032	12.0	76.3
1000	43.2	14.3	1.94	0.066	0.024	10.9	70.5

From Itikawa and Mason (2005).

4.4.1. *Dissociative ionization*

For H_2O, Lindsay and Mangan (2003) recommend the data presented by Straub et al. (1998) based on the simplicity of their parallel plate technique coupled to a short TOF mass spectrometer, and the fact that all the quantities needed for the determination of the cross sections could be directly measured. Complete collection of all fragment ions could be demonstrated. Due to a recalibration of their apparatus, the data included in Lindsay and Mangan (2003) and listed in Itikawa and Mason (2005) have been decreased by a few percent from the original Straub et al. data set. These recommended data are listed in Table 14 and shown graphically in Fig. 18.

There is general agreement among workers that there are no isotopic effects involved in the ionization processes in water. Thus, the cross sections for fragment ion production from H_2O and D_2O parents are identical and the cross sections listed

in Table 14 can be applied to either target. Lindsay and Mangan (2003) indicate that the apparent difference in $\sigma(H_2^+)$ and $\sigma(D_2^+)$, which had been noted by Straub et al., was in fact an experimental artefact.

The uncertainties in $\sigma(H_2O^+)$, $\sigma(OH^+)$, $\sigma(O^+)$, $\sigma(H^+)$ and σ (total) are ±6%, ±7%, ±9%, ±6.5% and ±6%, respectively. The uncertainties in $\sigma(O^{2+})$ and $\sigma(H_2^+)$ are ±13% and ±16% respectively. There is good agreement between the recommended data and the partial cross sections measured by Tarnovsky et al. (1998) using a fast neutral beam technique. We note also the good agreement that exists between the total (sum of the partial) cross sections listed in Table 14 and the measurements of Djuric et al. (1988) and Schutten et al. (1966).

There have been a number of calculations of total and partial ionization cross sections in water. Kim and Rudd (1994) and Hwang et al. (1996) developed the so-called "binary encounter dipole" (BED) and "binary encounter Bethe" (BEB) models, which gave a semi-empirical description of the ionization process. These calculations were limited to singly differential and total ionization cross sections. They were found to lie close to the recommended values (Lindsay and Mangan, 2003) though some differences were evident particularly at energies near the peak of the total ionization cross section. Partial cross sections for dissociative ionization were calculated by Khare and Meath (1987) and Khare et al. (1999) also using a semi-empirical approach. The level of agreement with experiment was poorer than when the total ionization cross section was considered. Recently, Champion et al. (2002) have calculated differential and total ionization cross sections within the framework of the distorted wave Born approximation. No adjustable parameters were used and quite good agreement with experiment was obtained where comparisons were possible. No information on partial cross sections was possible. Earlier quantum mechanical studies [e.g. Turner et al. (1982), Jain and Khare (1976), Long et al. (1989)] gave only qualitative agreement with experiment.

4.4.2. Appearance energies and fragment energy distributions

As discussed in Section 2 (experimental considerations), a knowledge or measurement of the appearance energy of a particular ion or fragment locates the particular repulsive curve or surface in the Franck–Condon region. If the end products of the dissociation are known, the kinetic energies of the fragments can often be estimated. Alternatively, if the fragment energies can be measured, dissociation limits can often be established and unknown dissociation products identified.

There have been a large number of measurements relative to H_2O break-up following both photon and electron impact. Prior to 1980, the most careful and comprehensive work, and the one done with the best electron energy resolution, seems to be that of Lefaivre and Marmet (1978). They reference earlier work. Recently, Hanel et al. (2002) have used a set-up very similar to Lefaivre and Marmet, namely a monochromatic electron source in tandem with a quadrupole mass spectrometer, to study the threshold behaviour of fragment ion production in H_2O and D_2O. Their data agree with those of Lefaivre and Marmet (1978) though at poorer energy resolution. However Hanel et al. (2002) provide additional information particularly with respect to the deuterated target. Zavilopulo et al. (2005a) have studied the near-threshold region and give appearance energies for the main ionic fragments. They do not give any error estimates but their electron impact ionizer had an energy spread of approximately 0.5 eV.

Ruscic et al. (2002) have done a very careful experimental and theoretical study to fix the photoionization threshold for OH^+ production at 18.116 ± 0.003 eV. This agrees very well with the earlier photoionization work of McCulloh (1976) and demonstrates that this ion appears with no additional kinetic energy.

A number of further points can be made. First, it is clear that the fragment ions appear as soon as it is energetically feasible for them to do so. This defines the position of the potential surfaces involved in the Franck–Condon region. Second, care should be taken when considering the onset of H^+ production. The value of 16.95 eV given by Lefaivre and Marmet (1978) and quoted by Itikawa and Mason (2005) refers to the ion pair production channel ($H^+ + OH^-$). This is a very minor channel and, in fact, Lefaivre and Marmet were only able to observe it after very prolonged data acquisition. For the more conventional ($H^+ + OH$) channel, their measurement agrees very well with Hanel et al. (2002) and with the value calculated based on the ionization energy of H and the H–OH dissociation energy. A final point to make is with regard to production of $H_2^+(D_2^+)$. This is clearly a very minor channel with a poor level of agreement between the published data. The measurement of Snegursky and Zavilopulo (1997) for D_2^+ is questionable as discussed by Hanel et al. (2002).

Fragment ion kinetic energies have been investigated by a number of workers, Ehrhardt and Kresling (1967), Appel and Durup (1973), Tan et al. (1978), Cordaro et al. (1986) and more recently by Fremont et al. (2005). Both TOF and electrostatic energy analysers have been used. In many cases plots of appearance energy (AE) versus fragment kinetic energy (FKE) have been made allowing conclusions regarding the parent molecular states involved (see Section 2.2). Workers have identified a large number of channels leading to fragmentation with a variety of end products. A large number of the ions have very low (fractions of an eV) kinetic energies but a significant number are released with energies as high as 10 eV or more, when the incident energy is sufficiently high. This indicates very steep repulsive surfaces, sometimes involving Coulomb explosions. [Note also the discussion of atom kinetic energies following dissociative excitation in Section 4.4.6.]

4.4.3. Dissociative attachment

Dissociative attachment (DA) in water vapour has been widely studied though there does not seem to have been any absolute cross section measurements carried out since Melton's (1972) experiments. Itikawa (2003) and Itikawa and Mason (2005) recommend Melton's data, particularly as there is good agreement (5%) between his data set and the earlier

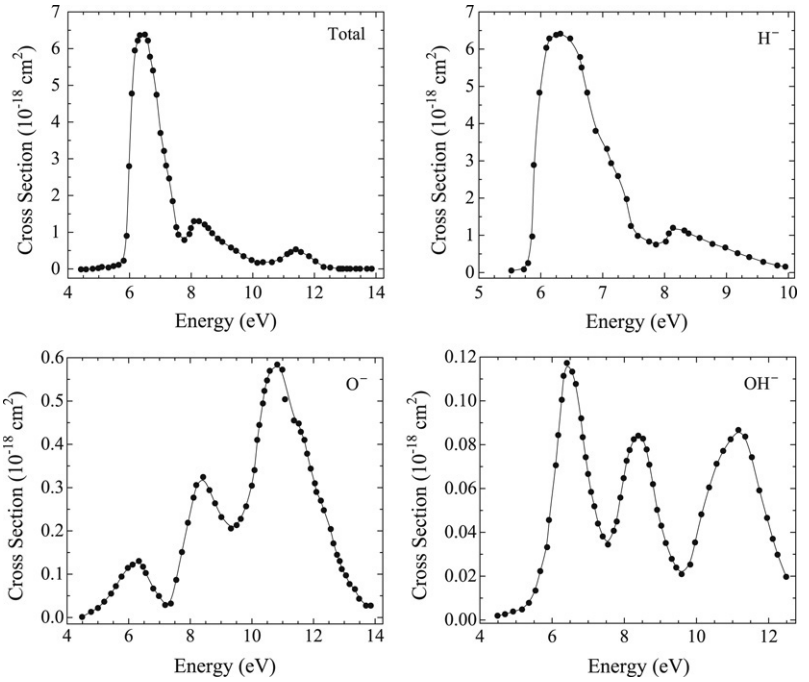

Fig. 19. Dissociative attachment cross sections in H_2O. Adapted from Melton (1972).

independent work of Compton and Christophorou (1967). Melton references earlier measurements. A summary of Melton's data is given in Fig. 19.

Belic et al. (1981) extended the investigations into the DA process by measuring angular and energy distributions of the anionic fragments. They were able to confirm the designation of the temporary negative ion states involved. The fact that the fragment ions have quite a wide energy distribution, extending over several eV, adds to the difficulty of the absolute cross section measurements. Belic et al. (1981) were able to show that the third peak in the H^- production channel at 11.8 eV was lower than the first one by a factor of 600. This is almost certainly the reason why this peak was not measured by Melton, who only observed two lower-energy peaks for production of this species.

More recently, Curtis and Walker (1992) have studied DA in D_2O, paying particular attention to the fragment kinetic energies and dissociation dynamics.

The three distinct $(H_2O^-)^*$ states that have been observed are Feshbach resonances, which are peaked at 6.5, 8.6 and 11.8 eV. They generate H^-, O^- and OH^-, although the cross sections for O^- and OH^- production are quite low. The measured angular distributions of H^- are consistent with resonances of symmetry $^2B_1$ (6.5 eV), $^2A_1$ (8.6 eV), and $^2B_2$ (11.8 eV) (Belic et al., 1981). The energies of these DA resonances are essentially unchanged upon isotopic substitution. However, the cross section for D^- production from D_2O is reduced by a factor of ∼0.6 from that of H^- from H_2O, and the widths of the resonances are reduced by ∼0.3 eV (Compton and Christophorou, 1967).

Recently there has been considerable theoretical effort put into this difficult problem. Haxton et al. (2004a,b) have carried out a very detailed study of the DA process via the $^2B_1$ resonance state. They were able to treat the process in full dimensionality using their local complex potential model. For the $H^- + OH$ channel they found substantial agreement with experiment with regard to total cross section and vibrational excitation of the OH fragment. They presented cross sections for DA into individual ro-vibrational states. Isotope effects were also examined but with poorer agreement with experimental findings. Gorfinkiel et al. (2005) have applied the *R*-matrix approach to study DA via all three of the low-lying resonances. A time-dependent method is used to calculate the nuclear dynamics subsequent to electron impact. So far no direct comparison with experimental data is available.

Very recently, there have been additional significant contributions. Fedor et al. (2006) have re-examined the DA of H_2O and D_2O using two different crossed-beam sets of apparatus. They measured ion yields as a function of incident electron energy and also the kinetic energies of the anions involved. Fig. 20 shows a comparison of their data with the earlier measurements of Melton (1972), Compton and Christophorou (1967) and Jungen et al. (1979). For both H^- and O^- production, agreement in the relative magnitude of the different features is very good though there are differences in the positions of the peaks. It appears that the calibration of the energy scales is different for the different workers with Melton's data, for example, being displaced by about 0.5 eV from those of Fedor et al. Significant discrepancies were observed also between the fragment kinetic energy measurements of Belic et al. (1980) and Fedor et al. (2006). Some of this may be attributed to energy discrimination effects in the ion detection systems. Fedor et al. (2006) suggest that the Belic et al. (1980) data should be preferred. Rawat et al. (2007) used an apparatus that eliminated discrimination effects due to kinetic energy

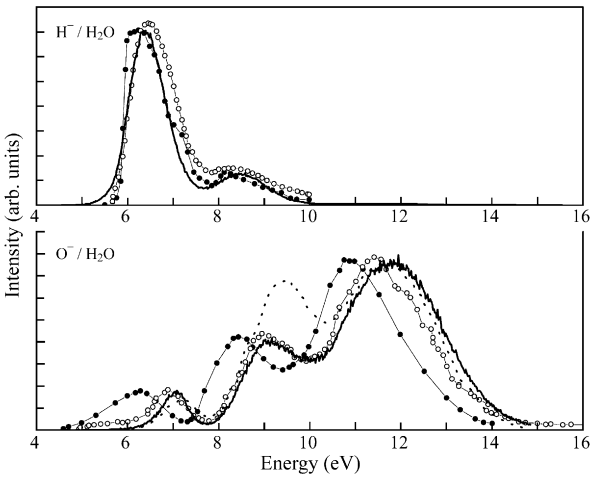

Fig. 20. Production of H^- and O^- from H_2O following electron impact. Solid line, Fedor et al. (2006); solid circles, Melton (1972); open circles, Compton and Christophorou (1967); dashed curve, Jungen et al. (1979). From Fedor et al. (2006).

or angular distribution of the ions. They calibrated their data against O^- production from O_2 using a relative flow technique and the absolute data of Rapp and Briglia (1965) for that process. They looked in detail at the higher energy resonances and at isotopic effects between H_2O and D_2O targets. They noted significant differences to earlier work, particularly with regard to O^- production.

Haxton et al. (2007a,b) have calculated dissociative electron attachment (DEA) cross sections using a multiconfiguration Hartree method within their local complex potential model. They obtained qualitative agreement with the experiments cited for the major fragmentation channels.

Because of its biological significance (Boudaiffa et al., 2000), DA is a very important process that has been studied extensively in the condensed phases also. Thus electron-stimulated desorption (ESD) of H^- and D^- via DA has been observed in thin films of condensed H_2O and D_2O respectively, and in sub-monolayer water films adsorbed on noble gas multilayers, (Rowntree et al., 1991; Tronc et al., 1996; Simpson et al., 1997). [For additional references see also Johnson et al. (2005a,b), Lane and Orlando (2007).] The H^- (D^-) ESD yield has a threshold at ∼5.5 eV and it peaks at ∼7.4 eV, with a shoulder at ∼9 eV. This structure in the anion yield was attributed to excitation of the $^2B_1$ and $^2A_1$ DA resonances, respectively, which are ∼1 eV higher in energy and broader than in the gas phase. The energy shift was attributed to perturbations of the electronic structure of water upon condensation, Rowntree et al. (1991). When D_2O is substituted for H_2O, the main ($^2B_1$) DA resonance narrows in the same manner as is seen in the gas phase, indicating that inelastically scattered electrons do not contribute significantly to the width of the resonance. Simpson et al. (1997) observed a broad fourth feature in their spectra at higher energies (>16 eV), which they attributed to the formation of a transient anion state that dissociates and/or decays into a dissociative excited state.

Energy- and angle-resolved D^- ESD measurements from D_2O multilayers reveal additional differences between anion production in gas- and condensed-phase water. At low incident energy, the most probable kinetic energy of the desorbing anions increases linearly with electron energy, having a slope close to that seen in the gas phase (0.4 eV/eV) (Tronc et al., 1996). However, the anion kinetic energy distributions are shifted down by ∼0.5 eV and are noticeably broader. In addition, the measured angular distributions of the desorbing ions do not reflect the symmetry of the transient excited states, as they do in the gas phase. Instead, they peak in the surface normal direction (Tronc et al., 1996). Finally, electron energy-loss measurements of H_2O multilayers indicate that condensation opens up an additional decay channel for the $^2B_1$ Feshbach resonance, which can couple via long range dipole interactions to intermolecular vibrational modes of the surrounding film (Michaud and Sanche, 1987).

4.4.4. Dissociation into ground state fragments

When electrons interact with water molecules and dissociation occurs, the simplest outcome is when the resultant fragments are unexcited. For two-fragment break-up there are two possibilities:

$$e + H_2O \rightarrow OH(X) + H(^2S_{1/2}) + e' \tag{12a}$$

$$\rightarrow OH(X) + H^-. \tag{12b}$$

Reaction (12b), where a charged particle is one of the products, has already been discussed under "Dissociative Attachment" above and will not be considered further. Reaction (12a) is extremely difficult to monitor as the fragments possess neither electronic internal energy nor charge. To solve this problem Harb et al. (2001) developed a laser-induced-fluorescence technique to probe the nascent OH(X). They used a pulsed cross-beam system involving gas, electron and laser

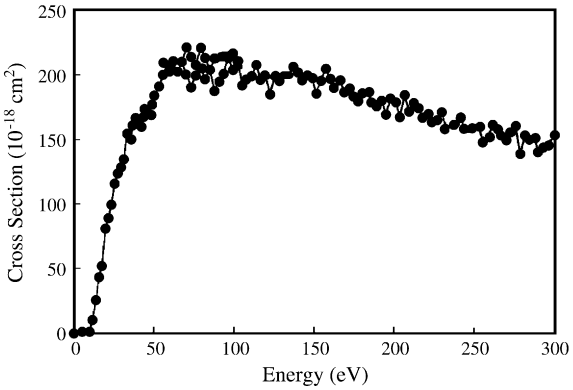

Fig. 21. Absolute cross section for production of OH(X) from H_2O as a function of incident electron energy. From Harb et al. (2001).

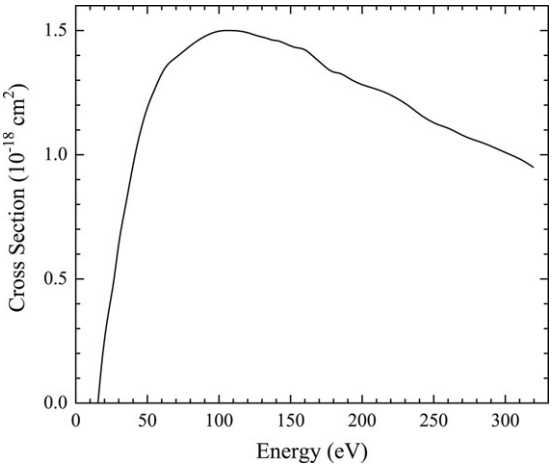

Fig. 22. Absolute cross section for production of O(^{1}S) from H_2O or D_2O as a function of electron impact energy. From Kedzierski et al. (1998).

Table 15
Cross sections for production of OH(X) from H_2O by electron impact

Energy (eV)	Cross section (10^{-18} cm^2)
10	15
15	48
20	70
30	130
50	190
75	210
100	205
150	198
200	175
250	160
300	140

From Harb et al. (2001).

beams. To simplify the spectroscopy, the gas beam was supersonically cooled. They took advantage of the fact that reaction (12b) also occurred in the collisions and thus could be used as a convenient way to calibrate the system. This is a resonance channel with a cross section peaking at 6.5 eV, just below the threshold of process (12a). The LIF diagnostics enabled the excitation of individual rotational levels of the lowest vibrational state to be studied as a function of electron energy.

Because of the tricky nature of the experiment and the difficulty of maintaining long term stability of the system, Harb et al. (2001) quote an error of 36%. This includes the uncertainty in the calibrating cross section [process (12b)]. Their data are listed in Table 15 and displayed in Fig. 21. A broad maximum in the cross section occurs around an electron energy of 100 eV. Significantly, its magnitude is comparable to the total ionization cross section at this energy. Thus at these energies and higher where elastic scattering is falling off more rapidly with energy, this channel represents a very significant fraction of the total scattering cross section.

Table 16
Absolute cross sections for the production of $O(^1S)$ following electron impact on H_2O

Energy (eV)	Cross section (10^{-18} cm^2)	Energy (eV)	Cross section (10^{-18} cm^2)
18.6	0.2	157.2	1.43
22.5	0.36	161.1	1.42
26.5	0.48	165.1	1.40
30.4	0.67	173.0	1.36
34.4	0.78	177.0	1.34
42.3	1.04	180.9	1.33
50.2	1.20	184.9	1.33
54.2	1.25	192.8	1.30
62.1	1.36	196.8	1.29
70.0	1.39	200.7	1.28
81.9	1.45	212.6	1.26
93.8	1.49	220.5	1.24
101.7	1.50	232.4	1.20
105.7	1.50	240.3	1.16
113.6	1.50	252.2	1.12
121.5	1.49	260.1	1.11
125.5	1.48	272.0	1.07
133.4	1.47	283.9	1.05
137.4	1.46	291.8	1.03
141.3	1.46	303.7	1.00
145.3	1.45	311.6	0.98
153.2	1.43	319.5	0.95

From Kedzierski et al. (1998).

Calculations of the excitation of OH(X) have been made by a number of authors, most recently by Gorfinkiel et al. (2005) who used an *R*-matrix approach. They also made an attempt to take account of nuclear motion by means of an adaptation of the adiabatic nuclei approximation. Earlier work by Morgan (1998) (*R*-matrix), Gil et al. (1994) (complex Kohn), Lee et al. (1993) (distorted wave) and Pritchard et al. (1990) (Schwinger variational) all used a fixed nuclei approximation. Gorfinkiel et al. calculate cross sections for the first four excited states, two singlet and two triplet, which dissociate to yield OH(X). These are $^3B_1$, $^1B_1$, $^3A_1$ and $^1A_1$. Agreement between different theories, even the two *R*-matrix ones, is not good. Evidence for strong resonance effects is obtained. Compared to the experimental data of Harb et al. (2001), the theoretical data are all larger, with the best agreement being with the Gil et al. results. Very recently Thorn et al. (2007a,b) have measured differential and integral cross sections for the dissociative electronic states involved over the energy range 20–200 eV. Their data are an order of magnitude less than Harb et al. or theory. A clear need for additional work on this problem, both experimentally and theoretically, is indicated.

4.4.5. Dissociation into neutral metastable fragments

Apart from high-Rydberg species, the possible metastable fragments that can result from electron impact on H_2O are (O^1D_2, $^1S_0$, and ^5S) and H(2s $^2S_{1/2}$). The latter two with internal energies of 9.15 and 10.2 eV respectively can be detected with conventional surface detectors, e.g. a channel electron multiplier; the former two with internal energies of 1.9 and 4.2 eV respectively, require special detection techniques. To date no measurements or calculations of $O(^1D_2)$ production from water targets have been reported.

As outlined in Section 2.2, the Windsor group developed a special surface matrix detector, which is selectively sensitive to $O(^1S_0)$ (LeClair and McConkey, 1993, 1994). Derbyshire et al. (1997) and Kedzierski et al. (1998) applied it to a study of the fragmentation of water yielding this species. Their data are listed in Table 16 and displayed in Fig. 22. The excitation function for production of $O(^1S_0)$ has a broad shape, which is characteristic of an optically allowed transition in the parent molecule, and has a maximum value of 1.5×10^{-18} cm^2 near 105 eV incident electron energy. The energetics of the break up near threshold allowed the dominant parent repulsive state to be positively identified as $^1A_1$. The other fragments can only be ground state H atoms in this case. Significant isotopic effects between H_2O and D_2O targets were observed in the fragment kinetic energy spectra but not in the total cross section for production of $O(^1S_0)$.

Freund (1971a) used detectors that allowed him to study both Rydberg fragments and fragments possessing significant internal energy such as $O(^5S)$ and H(2s $^2S_{1/2}$). His TOF results were quite different to earlier data of Clampitt and Newton (1969). No absolute cross section data were presented in either case. Further work is required to resolve these discrepancies.

4.4.6. Dissociative excitation

When electrons interact with water, radiation is emitted over a wide spectral range. While some measurements have been made of excitation cross sections involving H_2O^* and even H_2O^{+*} (Müller et al., 1993; Kuchenev and Smirnov, 1996) by far the dominant emissions involve the excited fragments, OH*, H* and O*. It is convenient to split a discussion of these into two sections covering the VUV and the near-UV and longer wavelength regions respectively. Avakyan et al. (1998) have reviewed the availability of cross section data prior to 1998 and Itikawa and Mason's (2005) review includes data published up to the end of 2003. There have been some important measurements subsequently, as discussed below.

Table 17
Absolute emission cross sections, in units of 10^{-18} cm^2, at 19 eV of the OH(A–X) bands

A state (v')	X state (v'')					
	0	1	2	3	4	Level
0	**7.66**	<0.049	0.001	0.000	0.000	7.71
1	1.20	**2.14**	0.018	0.001	0.000	3.36
2	0.012	**0.085**	<0.088	0.001	0.000	0.19
3	0.002	0.025	<**0.073**	<0.076	0.000	<0.18

The bold transition cross sections were used to scale the relative discharge emission or transmission rates for a given v'. Italicized cross sections were from the transition rates; the (0, 1) cross section was from discharge data. The last column contains the apparent level cross sections for the vibrational levels of the A state. From Schappe and Urban (2006).

4.4.6.1. Near-UV, visible and near-IR regions. The dominant emissions in this region are the OH($A\,^2\Sigma - X\,^2\Pi$) bands between 280 and 350 nm, the Balmer series of atomic hydrogen and the prominent atomic oxygen lines at 777.4 and 844.7 nm, resulting from the transitions 3p ^{5}P–3s ^{5}S and 3p ^{3}P–3s ^{3}S respectively. As pointed out by Itikawa and Mason (2005), the most extensive measurements are by de Heer's group (Beenakker et al., 1974; Möhlmann and de Heer, 1979). We note that the 100 eV measurement by Lawrence (1970) for the 844.7 nm transition lies 30% lower than that of Beenakker et al. (1974). More recent data, Müller et al. (1993), covered the region from 280 to 500 nm but only presented absolute data at 100 eV. For the Balmer series Müller et al. (1993) lie consistently lower in magnitude (by some 32% on average) than Möhlmann and de Heer (1979), which is barely covered by the joint error bars. Itikawa and Mason (2005) provide tabular and graphical comparative data for all of these emissions.

For the OH bands Müller et al.'s measurement at 100 eV is lower than that of Beenakker et al. (1974) by a factor of 1.72. The minimum ratio that could be accommodated, taking account of the joint error limits, is 1.22. Thus the measurements are in significant disagreement.

Makorov et al. (2004) carried out an extensive investigation of dissociative excitation in water including the OH(A – X) system. They normalized their excitation function (covering the wavelength range 306.2–307.8 nm) to that of Beenakker and deHeer (1974) at 100 eV assuming that their data represent the whole $\Delta v = 0$ sequence. They argue that there should be no difference in *shape* between the two and, in fact, they demonstrate that, for their data, this is the case. (However see further discussion on this point below.)

Very recently Schappe and Urban (2006) have carried out a careful study of the excitation of the OH bands. They were able to obtain data on eight of the vibrational transitions between 280 and 330 nm. These involved levels $v = 0$–3 of the upper $A\,^2\Sigma^+$ state. To accomplish this they used a combination of emission measurements and a fitting procedure involving synthetically generated spectra. They obtain quite good agreement with the data of Beenakker et al. (1974) both in the position of the peak in the cross section (17–19 eV) and its absolute value. Further, if they make the reasonable assumption that the Beenakker et al. data apply to the $\Delta v = 0$ group of bands rather than to the individual (0, 0) transition, then even better agreement is obtained. Their data are given in Table 17 and are recommended for modelling and other purposes.

A number of significant details have been noted about the dissociation leading to OH(A). Strong rotational population development has been noted by many workers [see e.g. Makorov et al. (2004) and Müller et al. (1993)]. Both spin allowed (singlet) and spin forbidden (triplet) excitation channels in the parent H_2O molecule contribute to the population of OH(A). The triplet dissociation path, which peaks just above threshold, is found to produce lower rotational states whereas, at higher electron energies, higher rotational states are preferentially populated via the singlet path, which has a broad maximum at 40 eV (Möhlmann et al., 1976). Thus, at electron energies near threshold the lower rotational states are preferentially populated, making the emission near the bandhead more intense relative to the red-degraded tail; at higher energies the higher rotational states are favoured, which causes the relative intensities near the bandhead to drop while enhancing the tail. Since the shape of the vibrational band changes as the electron energy increases, the experimental determination of the energy dependence must include the entire band. Schappe and Urban (2006) agree with Becker et al. (1980a,b) that the energy dependence of the cross section is independent of the upper state vibrational number. However, they noted that if a small bandpass was used, such that it did not encompass the entire vibrational band, then the energy dependence of the cross section varied markedly depending on which wavelength interval within the band was being sampled. Both Müller et al. (1993) and Makorov et al. (2004) concluded that optically allowed excitation of the bent H_2O ground state into the linear B^1A_1 excited state is the main precursor for the formation of highly rotationally excited OH($A\,^2\Sigma^+$) fragments.

A second significant factor that should be noted is the rapid increase of predissociation effects as the A state vibrational quantum number increases, leading to a rapid diminishing of apparent level cross sections with increasing v'. Schappe and Urban (2006) estimate that this is about a 5% effect for $v' = 0$ but increases rapidly, becoming a 50% effect for $v' = 1$, a factor of 51 for $v' = 2$ and a very much larger factor for $v' \geq 3$. Thus a careful distinction must be drawn between the *emission* cross sections such as in Table 17 (and apparent level cross sections deduced from these), and true production cross sections, which are significantly larger for higher v'.

Schappe and Urban (2006) have also investigated possible cascade contributions from higher lying states, such as $B\,^2\Sigma^+$ or $C\,^2\Sigma^+$, or background contributions from OH^+ transitions. Both were found to be negligible.

Kouchi et al. (1979) studied the translational kinetic energies of H(D) ($n = 3$) following dissociative excitation of H_2O and D_2O, by means of a Doppler profile analysis of the Balmer-α transition. They found that slow 0.4 ± 0.2 eV and fast 4 ± 1 eV

groups of atoms resulted and, within experimental uncertainties, similar distributions were obtained from H_2O and D_2O. Kawazumi and Ogawa (1987) used similar Doppler profile techniques to monitor the translational energy distributions of the OH(X) produced. They found three components with most probable energies of 0, 0.09 and 0.22 eV. They were able to suggest the identities and symmetries of the parent states involved in the dissociation.

Kurawaki et al. (1983) extended the earlier work of Kouchi et al. (1979) and included Doppler profile analysis of the Balmer-β line to probe the H(D) ($n = 4$) behaviour. The translational energy distributions broadened and became more structured as the incident electron energy was increased. They were able to identify four distinct components with peak energies around 0.5, 2, 4 and 6–8 eV. In addition they measured threshold appearance energies for the different processes at about 18.7, 25.5, 31.3 and 38.9 eV. The most likely dissociation mechanisms involved excitation of Rydberg states converging to some of the ionic states of water or, in the case of the most energetic fragments, to doubly ionized states. Of note, Ogawa et al. (1991) refined and extended this work by using angular difference Doppler interferometry to gain additional information about the symmetries of the parent repulsive states.

We note that Makorov et al. (2004) measured similar atom kinetic energies in their study of VUV atomic emissions (see Section 4.4.6.2).

Furuya et al. (1997a,b) have investigated the dissociation of H_2O, D_2O and HOD into OH(A), OD(A) and H and D ($n = 4$). They carefully measured intensity ratios of the excited fragments from the different parent species and they found that the emission cross section for production of OD(A) from HOD was approximately twice that for production of OH(A). As expected, production of D ($n = 4$) from D_2O was twice as likely as from HOD targets.

4.4.6.2. VUV region. The only recent work reported on dissociative excitation resulting in VUV transitions is that of Makorov et al. (2004). The review by van der Burgt et al. (1989) represents a full discussion of the available data base prior to this. The main emissions are H (Lyman series) and the O resonance multiplet at 130.4 nm, though data on a large number of H, O, O^+ and O^{2+} transitions in the wavelength range 40–280 nm, excited at a single energy of 200 eV, have been given by Ajello (1984). The more recent measurements from this group (Makorov et al., 2004) give extensive data on thirty seven spectral features of H, O and O^+ in the range 40–140 nm excited at 100 and 200 eV electron energy. They also present excitation functions for the H and O resonance lines at 121.6 and 130.4 nm respectively. Absolute calibration was achieved by using the Lyman-α from H_2 transition to normalize their data set coupled with a determination of how their detection sensitivity varied with wavelength. The value of the Lyman-α cross section was taken from the earlier work of Ajello (1984) corrected by a factor 7.16/8.18 to take account of new measurements of Lyman-α from H_2 (Liu et al., 1998). Additional data are given by Böse and Sroka (1973) but these are of questionable accuracy, as pointed out by van der Burgt et al. (1989).

Much of the earlier data had been normalized to a secondary standard, often H (Lyman-α) from H_2, and so had to be renormalized to take account of re-measurements of this standard, as discussed by van der Burgt et al. (1989), Makorov et al. (2004) and in Section 4.1.6.2. Considering post-1970 data for the H and O resonance lines, the most careful measurements of the main transitions seem to be those of Morgan and Mentall (1974). They calibrated their data using a value of 3.3×10^{-18} cm^2 for the 100 eV cross section of OI 130.4 nm from O_2. Taking our recommended value of 2.93×10^{-18} cm^2 for this transition (Section 4.1.6.2) means that their data must be corrected by a factor $2.93/3.3 = 0.888$. Morgan and Mentall's renormalized results lie very close in magnitude to the average of the available (renormalized where necessary) post-1970 data (Lawrence, 1970; Morgan and Mentall, 1974; Möhlmann et al., 1978; Ajello, 1984; Makorov et al., 2004). Thus we recommend the Morgan and Mentall renormalized, 100 eV, cross sections for OI 130.4 nm and HI 121.6 nm of 2.84×10^{-19} cm^2 and 7.81×10^{-18} cm^2 respectively. We note that these numbers differ from those recommended by Itikawa and Mason (2005).

Makorov et al. (2004) carried out a careful analysis of the line profiles of the main emissions as a function of incident electron energy. From these they were able to deduce the following. Three distinct populations of H(2p) atoms, with mean kinetic energies of 0.2, 2.0 and 7 eV, result from the dissociative excitation process and indicate that various repulsive surfaces are involved especially at the higher incident electron energies. They suggested that the lowest energy component probably came from total fragmentation of the molecule whereas the 2 eV atoms resulted from two-fragment break-up into OH + H. The 7 eV atoms were only observed at higher incident electron energies and were probably associated with a dissociative ionization process. For O, measurements on the 115.2 and 130.4 nm transitions indicated an upper limit to the mean kinetic energies of the ^{1}D and ^{3}S atoms involved of 1 eV or less. This is to be expected given the fact that the bonds to both H atoms have to be broken if O atoms are to result.

4.4.7. OH targets

Although a broad data base exists for electron collisions with H_2O, this is not the case for the hydroxyl radical (OH, OD). It appears that the only work to date is that of Tarnovsky et al. (1998), who measured absolute partial cross sections for electron impact ionization and dissociative ionization of OD from threshold to 200 eV using their fast neutral beam technique. They found that the ionization was dominated by formation of the parent ion with dissociative ionization accounting for 5% or less of the total single ionization cross section. They found quite good agreement between their measurements and a calculated cross section based on a modified additivity rule (Deutsch et al., 1997). Joshipura et al. (2001) estimated the single ionization cross section of OH based on a semi-empirical calculation of the total inelastic cross section and obtained results that agreed quite well with the experimental data.

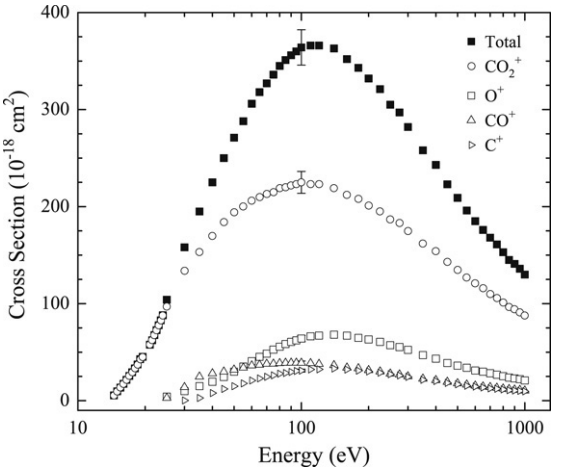

Fig. 23. CO_2 electron impact ionization cross sections. Data from Table 18.

4.5. CO_2

Carbon dioxide (CO_2) is a very important molecule for a variety of reasons. Primarily, it is one of the fundamental constituents of planetary atmospheres. In particular, it is the most abundant molecule in the atmospheres of Venus and Mars. On Earth, its level in the atmosphere has been increasing steadily since the industrial revolution and it is known to contribute to the atmospheric greenhouse effect and possibly to current global warming scenarios. It controls the atmospheric oxygen level through the photosynthesis process. In the laboratory, CO_2 is widely used in lasers, gaseous discharges and low-temperature plasma devices. Being a simple, linear, triatomic molecule, electron interactions with CO_2 are of interest also from the point of view of fundamental atomic and molecular physics.

Electron collisions with CO_2 have been studied both theoretically and experimentally by many authors since the 1920s and a large number of papers have been published reporting cross section and other data. Various reviews have been published over the years such as Itikawa and Shimizu (1971), Tawara (1992), Shirai et al. (2001) and Itikawa (2002, 2003). These have zeroed in on recommending cross section data for various applications. In addition Karwasz et al. (2001) published a review article on the electron impact cross sections of a number of polyatomic molecules, including CO_2, with particular emphasis on total cross sections but including dissociation data where they were important. These publications contain copious references to earlier work.

4.5.1. Dissociative ionization

Lindsay and Mangan (2003) carried out a critical review of the measured data and, for the total ionization cross section, recommended the Rapp and Englander-Golden (1965) data set below 25 eV and the recalibrated data set of Straub et al. (1996a) at higher energies up to one keV. These two data sets were in very good agreement in the near-threshold region but Rapp and Englander-Golden provided additional data points. Tian and Vidal (1998a) presented measurements from threshold up to 300 eV, which were in very good overall agreement with the work of Straub et al. (1996a). For the fragment ions their cross sections were a few percent higher (up to 15% for CO^+) than those of Straub et al., but still in agreement within the error limits. Table 18 lists the recommended total and partial ionization cross sections and Fig. 23 shows plots for the major dissociative ionization channels with production of O^+, CO^+ and C^+. At 100 eV these ions were formed in the ratio 1:0.61:0.48. Their combined cross section accounted for 37% of the total ionization cross section at this energy. We note that measurements were also made of doubly charged ion production.

Straub et al. (1996a) and Tian and Vidal (1998a) were the only two groups who were able to demonstrate total collection of the fragment ions with greater than thermal kinetic energies. All earlier experiments had serious energy discrimination effects and hence ended up presenting fragment ionization cross sections, which were significantly too small. Tian and Vidal (1998a) were able to monitor the translational kinetic energy distributions for the fragment ions as discussed in the next section. Using a covariance mapping technique, Tian and Vidal (1998b) were able to quantify numerous dissociation channels following single, double and multi-ionization of the target CO_2 as a function of incident electron energy between 25 and 600 eV. Coincidence momentum imaging techniques have also been used by Sharma and Bapat (2006) and Bapat and Sharma (2007) to probe CO_2 break-up at 1300 eV incident electron energy.

4.5.2. Appearance energies and fragment energy distributions

A number of different laboratories have contributed data of relevance to these topics. Fragment ion appearance energies have been studied by Appel et al. (1966), Ehrhardt and Kresling (1967), Crowe and McConkey (1974), Bussieres and Marmet (1977), Armenante et al. (1985), Locht and Davister (1995) and Zavilopulo et al. (2005a). Fragment kinetic energies have

Table 18
CO_2 partial and total ionization cross sections

Energy (eV)	$\sigma(CO_2^+)$ (10^{-18} cm^2)	$\sigma(CO^+)$ (10^{-18} cm^2)	$\sigma(C^+)$ (10^{-18} cm^2)	$\sigma(O^+)$ (10^{-18} cm^2)	$\sigma(CO_2^{2+})$ (10^{-18} cm^2)	$\sigma(C^{2+})$ (10^{-18} cm^2)	$\sigma(O^{2+})$ (10^{-18} cm^2)	σ(total) (10^{-18} cm^2)
14.5	5.5							5.5
15	9.7							9.7
15.5	13.5							13.5
16	17.4							17.4
16.5	21.5							21.5
17	25.5							25.5
17.5	29.3							29.3
18	33.3							33.3
18.5	37.3							37.3
19	42.8							42.8
19.5	45.2							45.2
21	57.7							57.7
21.5	62.3							62.3
22	67.6							67.6
22.5	72.7							72.7
23	77.7							77.7
23.5	82.8							82.8
24	88.0							88.0
25	96.9	2.79		4.19				104
30	134	13.9	0.240	9.86				158
35	153	24.7	2.80	15.0				195
40	170	28.1	7.82	19.5				225
45	184	29.9	12.1	24.5	0.166			250
50	194	31.9	14.9	29.9	0.393			271
55	200	33.9	17.8	35.2	0.686			288
60	206	36.2	20.8	40.7	1.06			306
65	210	36.9	22.9	45.2	1.26			318
70	213	37.9	24.6	48.5	1.59			327
75	215	38.0	26.1	52.6	1.72			336
80	219	38.6	27.8	55.6	2.06	0.0179		345
85	220	38.9	28.5	58.4	2.19	0.0215		351
90	222	39.0	29.6	60.6	2.27	0.0311		356
95	223	39.0	30.6	62.2	2.46	0.0506	0.0169	360
100	225	38.9	31.0	64.0	2.65	0.0520	0.0197	364
110	223	38.6	32.2	66.3	2.85	0.0751	0.0324	366
120	223	37.8	32.3	67.1	2.90	0.108	0.0721	366
140	219	36.5	33.1	68.0	2.94	0.157	0.133	363
160	212	34.0	32.1	67.0	2.90	0.186	0.159	352
180	208	33.3	30.9	64.7	2.85	0.249	0.217	343
200	201	31.4	30.1	63.1	2.72	0.279	0.233	332
225	195	30.0	28.8	60.6	2.57	0.256	0.271	321
250	187	27.8	27.3	57.2	2.32	0.291	0.286	305
275	183	26.9	26.0	55.3	2.31	0.247	0.304	297
300	175	25.0	24.5	52.4	2.03	0.252	0.276	282
350	162	22.6	21.5	47.0	1.83	0.216	0.249	258
400	154	21.1	20.2	43.3	1.75	0.224	0.215	243
450	143	19.3	18.3	38.8	1.65	0.198	0.193	223
500	135	17.8	16.9	36.1	1.41	0.177	0.192	209
550	127	16.5	15.4	33.9	1.28	0.184	0.168	196
600	121	15.4	14.5	31.1	1.25	0.145	0.156	185
650	116	14.5	13.6	29.9	1.13	0.169	0.142	176
700	110	13.9	12.7	28.3	1.06	0.147	0.176	168
750	106	13.2	12.3	26.8	0.986	0.157	0.147	161
800	101	12.4	11.6	25.2	0.961	0.139	0.127	153
850	96.4	11.9	10.8	23.8	0.883	0.129	0.127	145
900	94.1	11.3	10.5	22.9	0.823	0.0965	0.100	141
950	90.9	11.0	10.1	22.2	0.741	0.0897	0.116	136
1000	87.6	10.3	9.64	20.9	0.723	0.0984	0.103	130

From Lindsay and Mangan (2003).

been measured by Zhukov et al. (1990) and Locht and Davister (1995) using retarding potential techniques, while Velotta et al. (1994) and Tian and Vidal (1998a) deduced kinetic energies from their TOF mass spectroscopy data. Only Locht and Davister (1995) made kinetic energy measurements at incident electron energies between 19 and 40 eV.

Regarding fragment kinetic energies, it is difficult to make a quantitative comparison between the different data sets because of the sometimes poor statistical quality of the data and because of differences in impact energies used, and in the transmission and collection functions of the different detection systems, but a number of general conclusions can be drawn:

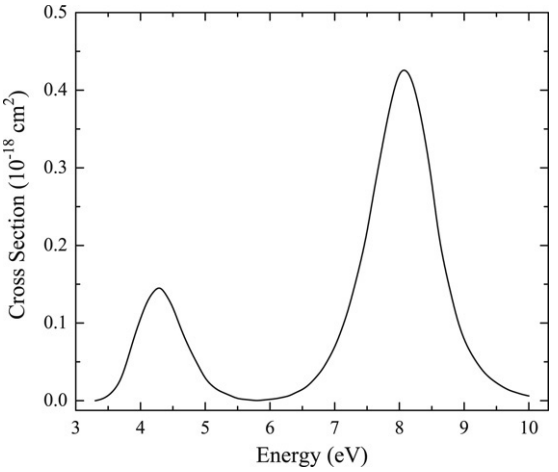

Fig. 24. Attachment cross section for production of O^- from CO_2 at a target gas temperature of 300 K. From Lindsay and Mangan (2003).

1. Near threshold the energy distributions of the major fragment ions, O^+, CO^+ and C^+ are all sharply peaked at zero kinetic energy.

2. As the incident electron energy is increased, faster ions become apparent and the distributions extend from zero to about 5 eV at 50 eV electron energy. Some structure is evident also.

3. At higher electron energies, the "tails" of the distributions continue to broaden, reaching more than 10 eV for O^+ (somewhat less for C^+ and CO^+) by 100 eV.

Tian and Vidal (1998a) obtain broader distributions than some of the other workers. They suggest that their detection system is less discriminating against higher energy fragments. They also present data for C^{2+} and O^{2+}. Both these ions have very broad kinetic energy distributions extending up to 12 eV, and more than 16 eV respectively, when the incident electron energy was 200 eV.

Regarding appearance energies for the various fragments, there are wide discrepancies among the early published data. Crowe and McConkey (1974) list data going back to the earliest measurements (Smyth and Stueckelberg, 1930), which illustrate this fact. This seems to be due to wide differences both in detection sensitivities and in ion energy discrimination effects. Bussieres and Marmet (1977) were the only workers to observe the three dominant fragment ions at their spectroscopic threshold values. This is probably due to the very good sensitivity of their apparatus to low energy ions and to the excellent statistical quality of their data. Locht and Davister (1995), who also had demonstrated high sensitivity to thermal energy ions, measured initial thresholds for the three ions that were within a few tenths of an eV of the spectroscopic values. Zavilopulo et al. (2005a) only list values for C^+ production. They observe two thresholds, at 22.70 and 27.80 eV, in excellent agreement with Bussieres and Marmet (1977) and with values for the two dissociation channels based on spectroscopic data. These channels are:

$$\begin{aligned} e + CO_2 &\rightarrow C^+ + O_2 + 2e \quad [E_a = 22.70\ \text{eV}] \\ &\rightarrow C^+ + 2O + 2e \quad [E_a = 27.80\ \text{eV}]. \end{aligned} \tag{13}$$

A number of workers (Ehrhardt and Kresling, 1967; Armenante et al., 1985; Locht and Davister, 1995) measured ion kinetic energies and associated appearance energies. They then used the technique discussed in Section 2 (see Fig. 1) to deduce the dissociation limits for the processes involved. These works demonstrated that a large number of break-up processes contributed to the ionization signal but, unfortunately, there was considerable disagreement in identifying the individual channels and in specifying the dissociation dynamics.

4.5.3. Dissociative attachment

There have been numerous studies of dissociative attachment in CO_2. These have been reviewed by Itikawa (2002, 2003) who recommend that the original data set of Rapp and Briglia (1965) be preferred. They measured total anion production but it was shown by Orient and Srivastava (1983a,b) that O^- was by far the dominant anion. The recommended data are given in Table 19 and shown in Fig. 24. Data are appropriate to room temperature (300 K) targets. Overall the anion cross sections are small and make less than a 0.1% contribution to the total scattering cross section. Two main peaks are observed, at 4.4 and 8.2 eV. Other workers have observed much weaker features (due to O^-, O_2^- and C^-) at higher energies (Spence and Schulz, 1974; Orient and Srivastava, 1983a,b).

Structure in the 4.4 eV peak was studied by Stamatovic and Schulz (1973), Abouaf and Fiquet-Fayard (1976), Dressler and Allan (1985a,b) and Cicman et al. (1998). This was due to vibrational excitation either of the CO_2^- parent resonance state or of the accompanying CO fragment that resulted from the dissociation process.

Table 19
Cross sections for production of O^- from CO_2 at a target gas temperature of 300 K

Energy (eV)	Cross section (10^{-18} cm^2)	Energy (eV)	Cross section (10^{-18} cm^2)	Energy (eV)	Cross section (10^{-18} cm^2)
3.3	0	5.6	0.00176	7.9	0.396
3.4	0.00176	5.7	0.000880	8.0	0.424
3.5	0.00616	5.8	0	8.1	0.428
3.6	0.0141	5.9	0.000880	8.2	0.413
3.7	0.0273	6.0	0.00176	8.3	0.380
3.8	0.0528	6.1	0.00264	8.4	0.336
3.9	0.0818	6.2	0.00440	8.5	0.283
4.0	0.106	6.3	0.00616	8.6	0.215
4.1	0.128	6.4	0.0106	8.7	0.172
4.2	0.141	6.5	0.0141	8.8	0.136
4.3	0.148	6.6	0.0202	8.9	0.102
4.4	0.136	6.7	0.0290	9.0	0.0783
4.5	0.121	6.8	0.0387	9.1	0.0616
4.6	0.0976	6.9	0.0528	9.2	0.0484
4.7	0.0774	7.0	0.0686	9.3	0.0369
4.8	0.0598	7.1	0.0897	9.4	0.0290
4.9	0.0440	7.2	0.114	9.5	0.0229
5.0	0.0282	7.3	0.145	9.6	0.0176
5.1	0.0194	7.4	0.178	9.7	0.0132
5.2	0.0132	7.5	0.216	9.8	0.0106
5.3	0.00968	7.6	0.267	9.9	0.00792
5.4	0.00616	7.7	0.312	10.0	0.00616
5.5	0.00264	7.8	0.357		

From Lindsay and Mangan (2003).

The O^- kinetic energy release following dissociative attachment via the 4.4 and 8.2 eV bands was studied by Dressler and Allan (1985a,b) and earlier by Chantry (1972) and Tronc et al. (1982). They found that the O^- fragments possessed a significant kinetic energy distribution extending from zero to 1 eV (in the case of the 8.2 eV band). The structure mentioned in the previous paragraph was dependent on which part (zero or non-zero energy) of the fragment kinetic energy distribution was emphasized.

DEA to vibrationally excited CO_2 has been studied by Srivastava and Orient (1983) while electron attachment including dissociative attachment to CO_2 clusters has been studied by numerous workers including Klots and Compton (1978), Stamatovic et al. (1985), Knapp et al. (1986), Leber et al. (2000), Fabrikant and Hotop (2005) and Vostrikov and Dubov (2006). As some of these authors have pointed out, cluster anion formation is predominantly mediated by rather narrow vibrational Feshbach resonances [see also Barsotti et al. (2002) and Hotop et al. (2003)]. Such data are of considerable environmental and biological interest [see e.g. Fabrikant and Hotop (2005)].

4.5.4. Dissociation into ground state fragments

Apart from situations where a ground state fragment accompanied a charged partner fragment or fragments, for example in Sections 4.5.1 and 4.5.3, there has not been any specific monitoring of ground state species.

4.5.5. Dissociation into neutral metastable fragments

Metastable fragments play an important role in the dissociation of CO_2 under electron impact. Species that have been identified and studied are $O(^5S)$, (^1S) and O(R), oxygen high-Rydberg species, and CO ($a\,^3\Pi$) (Freund, 1971a,b,c; Wells et al., 1972; Misakian et al., 1975; Allcock and McConkey, 1976; Barnett et al., 1992; LeClair and McConkey, 1994). Unfortunately, because of different detector geometries and sensitivities, lack of accurate knowledge of the lifetimes involved and the fact that the fragments often possessed significant amounts of kinetic energy, the data obtained are largely qualitative and sometimes conflicting.

The only quantitative measurement is that of LeClair and McConkey (1994) on the production of $O(^1S)$ using their xenon matrix surface detector. Their data, covering the energy range from threshold to 1 keV, are given in Table 20 and displayed in Fig. 25. The excitation function has a threshold at 11.0 ± 0.5 eV and a maximum at 50 eV where the cross section reaches a value of 1.69×10^{-17} cm^2 with an uncertainty of 12%. They found evidence for at least six different $O(^1S)$ production channels. Kinetic energies of the oxygen fragments ranged from near zero up to 5 eV. The only channel that could be positively identified was that where initial excitation took place to the $1\,^1\Sigma_u^+$ state of CO_2 and where ground state CO(X) is also released in the dissociation process according to

$$e + CO_2(X\,^1\Sigma_g^+) \rightarrow CO_2(1\,^1\Sigma_u^+) + e' \rightarrow CO(X\,^1\Sigma^+) + O(^1S) + e'. \quad (14)$$

They estimated that this channel accounted for approximately one third of total $O(^1S)$ production.

The CO($a\,^3\Pi$) metastable particle, produced in electron collisions with CO_2, emits the important Cameron bands, which are bright emission features in the atmospheres of both Mars and Venus. A number of workers Clampitt and Newton (1969),

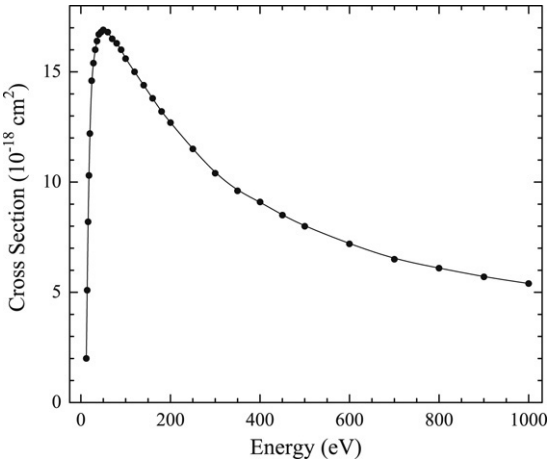

Fig. 25. Electron impact dissociation cross section for the production of $O(^1S)$ from CO_2. Data from Table 20.

Table 20
Absolute cross sections for the production of $O(^1S)$ following electron impact on CO_2

Energy (eV)	Cross section (10^{-18} cm^2)	Energy (eV)	Cross section (10^{-18} cm^2)
11	Threshold	100	15.6
12	2.0	120	15.0
14	5.1	140	14.4
16	8.2	160	13.8
18	10.3	180	13.2
20	12.2	200	12.7
24	14.6	250	11.5
28	15.4	300	10.4
32	16.0	350	9.6
36	16.4	400	9.1
40	16.7	450	8.5
45	16.8	500	8.0
50	16.9	600	7.2
60	16.8	700	6.5
70	16.5	800	6.1
80	16.3	900	5.7
90	16.0	1000	5.4

From LeClair and McConkey (1994).

Freund (1971c), Misakian et al. (1975), Allcock and McConkey (1976), Barnett et al. (1992), LeClair and McConkey (1994) have studied the process,

$$e + CO_2(X\,^1\Sigma_g^+) \rightarrow CO(a\,^3\Pi) + O + e' \tag{15}$$

using surface detectors that were sensitive to this species, while Erdman and Zipf (1983b) studied the Cameron band fluorescence. Unfortunately lack of precise knowledge of such factors as detector sensitivity, particle lifetimes and hence in-flight decay probabilities, prevented quantitative production cross sections being obtained.

Both Freund (1971c) and LeClair and McConkey (1994) present relative excitation functions for $CO(a\,^3\Pi)$ production and there is quite good agreement regarding the shape and the threshold energy. The cross section is observed to rise rapidly from the threshold (indicative of a spin flip in the initial excitation) and then fall off slowly towards higher energies (as would be expected from optically allowed excitation processes). Clearly a number of channels, both optically allowed and forbidden, are contributing to the overall picture. Freund (1971c) made an approximate estimate of the peak cross section of 4×10^{-17} cm^2. This may be compared with Erdman and Zipf's (1983b) estimate of 2.4×10^{-16} cm^2 based on an analysis of their fluorescence data, a factor of 6 higher. They suggested that their result might be a factor of 2 in error given the uncertainties in some of the experimental parameters. Clearly new measurements are required to resolve this situation. Because of the lack of reliable numbers, no recommended cross sections are given by Itikawa (2002, 2003).

In his comprehensive study of $CO(a\,^3\Pi)$ production, Freund (1971c) shows from appearance energy measurements that the first open channel involves a ground state O-atom partner,

$$e + CO_2(X\,^1\Sigma_g^+) \rightarrow CO(a\,^3\Pi) + O(^3P) + e' \quad [E_a = 11.45\ \text{eV}]. \tag{16}$$

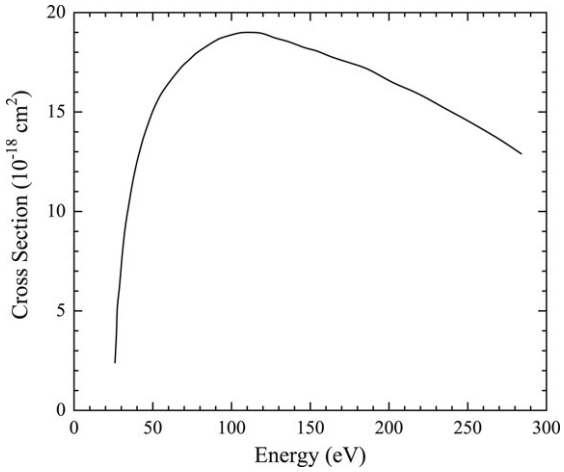

Fig. 26. Cross section for production of the CO^+ first negative ($B\ ^2\Sigma^+ - X\ ^2\Sigma^+$) system following electron impact on CO_2. Data from Table 21.

Evidence for production via a channel that also leads to $O(^5S)$ has been presented by Misakian et al. (1975) and Allcock and McConkey (1976). Thus:

$$e + CO_2(X\ ^1\Sigma_g^+) \rightarrow CO(a\ ^3\Pi) + O(^5S) + e' \quad [E_a = 20.6\ \text{eV}]. \tag{17}$$

Structure on excitation function curves suggest that many other channels lead to $CO(a\ ^3\Pi)$ but it was not possible to identify specific details or quantify relative importance.

Kinetic energies of the $CO(a\ ^3\Pi)$ fragments were in the range 0–1.2 eV (Freund, 1971c). Vibrational excitation of the CO was also occurring as evidenced by the Cameron band emission spectra of Erdman and Zipf (1983b).

Various TOF experiments (Misakian et al., 1975; Allcock and McConkey, 1976; Barnett et al., 1992) revealed the presence of fast atomic O fragments, identified as $O(^5S)$ and O(R) high-Rydberg species. Many different excitation channels contributed to the observations. There was reasonable agreement regarding the kinetic energy spectra of these fast atoms. The distribution extended to 10 eV and higher at incident electron energies above about 60 eV. Peaks in the distribution occurred at around 2 and 3 eV. Information about the nature, symmetries and multiplicities of the parent CO_2^* repulsive states was extracted from fragment angular distributions (Misakian et al., 1975), from excitation function shapes, and from specific knowledge of the fragments.

We note that dissociation of CO_2 clusters with production of fluorescence or metastable fragments has been studied by, for example, Kedzierski et al. (1998a) and Khmel and Sharafutdinov (1997b).

4.5.6. Dissociative excitation

There have not been any new data relevant to dissociative excitation of CO_2 since the recent review by Itikawa (2002). As he pointed out, the level of agreement between existing data sets is far from satisfactory. This is expanded on in the following sections.

4.5.6.1. Near-UV and visible region. Apart from the studies of Cameron band excitation discussed in Section 4.5.5, the only reports of dissociative emission cross sections at wavelengths longer than 200 nm are those of Ajello (1971) and Zipf (1984). Ajello studied the excitation of the $(CO_2)^+$ emission bands in the region 280–450 nm, the Cameron band system and the fourth positive ($A\ ^1\Pi - X\ ^1\Sigma^+$) systems of CO, which occur in the 135–250 nm region, and the CO^+ first negative ($B\ ^2\Sigma^+ - X\ ^2\Sigma^+$) system in the 190–250 nm region with its (0, 0) band at 218.9 nm. Since the strongest bands of the fourth positive system lie in the VUV below 200 nm, it will be dealt with in the next section. Zipf (1984) lists 100 eV emission cross section data for the OI lines at 533, 777.4 and 844.6 nm and for the CI line at 538 nm, in addition to data for numerous lines in the vacuum ultraviolet spectral region, which will be dealt with below.

Ajello's (1971) data for the CO^+ first negative ($B\ ^2\Sigma^+ - X\ ^2\Sigma^+$) system are given in Table 21 and displayed in Fig. 26. The cross section of one band from each v' progression was measured and the Franck–Condon factors of Nicholls (1962) were then used to estimate the total emission cross section of the entire system. Relative calibration of the detection system was established using the molecular branching ratio technique. Absolute calibration was made at wavelengths greater than 260 nm using a standard lamp. A peak cross section of 1.9×10^{-18} cm^2 was obtained at an electron energy of 110 eV. A useful experimental check on this procedure would be to employ the technique used by Schappe and Urban (2006) for OH emissions from H_2O of monitoring the relative intensities of the bands of individual v' progressions from a low pressure discharge source.

Table 21
Cross sections for production of the CO^+ first negative ($B\ ^2\Sigma^+ - X\ ^2\Sigma^+$) system following electron impact on CO_2

Energy (eV)	Cross section (10^{-18} cm^2)	Energy (eV)	Cross section (10^{-18} cm^2)
26.0	2.40	76.5	17.9
26.7	3.46	80.2	18.1
27.2	4.40	84.0	18.3
27.3	5.21	88.0	18.5
28.6	5.94	92.3	18.7
29.3	6.63	96.7	18.8
30.0	7.29	101	18.9
30.7	7.91	106	19.0
31.4	8.45	111	19.0
32.1	8.97	117	19.0
32.9	9.42	122	18.9
33.7	9.84	128	18.7
34.5	10.2	134	18.6
35.3	10.6	141	18.4
37.0	11.4	147	18.2
39.6	12.4	154	18.1
41.6	13.0	162	17.8
43.6	13.6	170	17.6
45.7	14.1	178	17.4
47.9	14.6	186	17.2
50.2	15.1	195	16.8
52.6	15.5	204	16.4
55.1	15.9	214	16.1
57.8	16.2	224	15.7
60.5	16.5	235	15.2
63.4	16.8	247	14.7
66.5	17.1	258	14.2
69.7	17.4	271	13.6
73.0	17.6	284	12.9

From Itikawa (2002).

We note that Ajello's data are somewhat suspect at higher energies because his electron beam was contaminated with a secondary electron component [see Finn and Doering (1976), Ajello and Shemansky (1985) and Johnson et al. (2005a,b)]. However any effect due to this will be less serious for the CO^+ bands because of the broad shape of their excitation function.

We note that Kanik et al. (1993a) report possible contributions to their atomic line emission cross sections from Rydberg transitions in CO and CO^+ (see the following section).

4.5.6.2. VUV region.

CO, Cameron band system. This has already been discussed under 4.5.5.

CO, fourth positive system,($A\ ^1\Pi - X\ ^1\Sigma^+$) these bands were investigated by two groups, Mumma et al. (1971) and Ajello (1971). Both groups measured one band from each v' progression and then used calculated Franck–Condon factors to obtain the total emission cross sections for the different vibrational levels of the $A\ ^1\Pi$ state. Mumma et al. quote a value of 1.4×10^{-18} cm^2 ± 17% for the summed cross sections of $v' = 0 - 4$ at an energy of 300 eV. Applying a correction factor of 0.59 [see van der Burgt et al. (1989) and Section 4.1.6.2 earlier], to take account of the new Lyman-α from H_2 calibration, reduces this to 0.83×10^{-18} cm^2 ± 17%. This value is in reasonable agreement with the data of Ajello, taking into account the fact that Ajello's data contain a contribution from bands with $v' = 5$ (estimated at approximately 7% of the total). Bands with $v' > 5$ added a negligible contribution [see Ajello (1971)]. Mumma et al. noted that there were small differences in the different v' level cross section shapes with the peak occurring at approximately 40 eV. Ajello assumed that the shape of the (0, 1) band cross section was representative of the entire system.

Atomic emissions. Data have been reported by Sroka (1970), Ajello (1971), Mumma et al. (1972), Zipf (1984) and Kanik et al. (1993a). Sroka's calibration of the relative response of his system with wavelength was questionable so his work is more useful for obtaining the emission cross section shapes rather than their absolute magnitudes. There was also a possibility that his data might have been affected by slow secondary electrons in his electron beam [see Mumma et al. (1972)] leading to distortion in the high energy behaviour of his excitation functions. Ajello (1971) and Mumma et al. (1972) made measurements at wavelengths above 125 nm whereas Kanik et al. (1993a) covered the range 40–125 nm and Zipf (1984) the range 95–135 nm. A complete listing of the data prior to 1989 is given in the review by van der Burgt et al. (1989).

Below 125 nm, measured cross sections were small, the most intense features in Kanik et al.'s spectrum being the OI lines at 99.0, 102.7 and 115.2 nm and the CI multiplet at 119.4 nm. The largest emission cross section, measured at 200 eV incident energy, was 3.59×10^{-19} cm^2 for the 99 nm transition. The broad shape of the excitation function suggested that the initial excitation to the parent repulsive state(s) of the molecule was dipole allowed. Zipf (1984) lists a 100 eV cross section for the 99 nm multiplet of 5.6×10^{-19} cm^2. Using the measured cross section shape of Kanik et al. to obtain an estimate of the

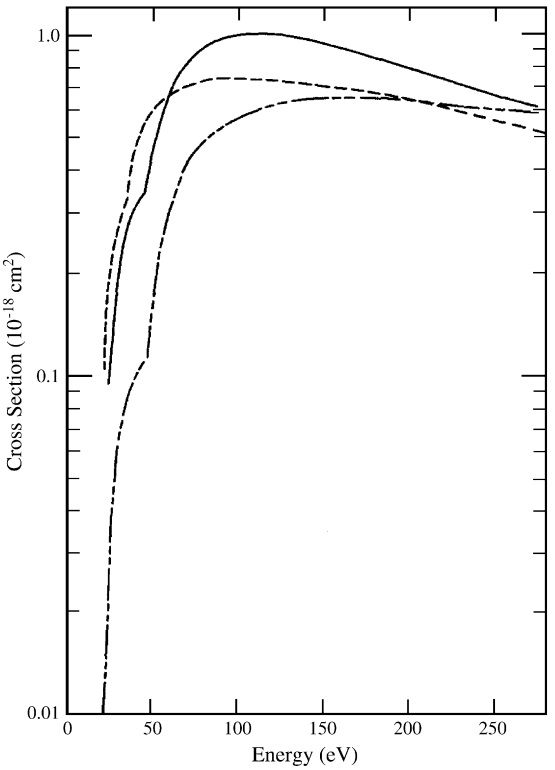

Fig. 27. Absolute cross sections for dissociative excitation of the OI (130.4 nm) multiplet by electron impact on CO_2. Solid line, Mumma et al. (1972); dashed line, Ajello (1971); broken line, Sroka (1970). Note that no renormalizations of the original data sets have been applied (see text for discussion). Reused with permission from M. J. Mumma, Journal of Chemical Physics, 57, 68 (1972).

cross section at 200 eV and applying the correction factor of 0.59 to take account of the revisions to the Lyman-α standard (see Section 4.1.6.2), gives a 200 eV cross section of 3.1×10^{-19} cm^2 in quite good agreement with the data of Kanik et al. A similar level of agreement is obtained for the 102.7 nm feature but not for the one at 115.2 nm where agreement is good *before* this correction to Zipf's data is applied.

Above 125 nm, Ajello (1971) reports 100 eV data on 10 CI multiplets, the most intense being the 165.7 nm ($3s\ ^3P^0 \rightarrow\ ^3P$) feature with a cross section of 1.3×10^{-18} cm^2 at this energy. Mumma et al. (1972) give data on two CII and three CI multiplets including the one at 165.7 nm. Their renormalized cross section of 0.8×10^{-18} cm^2 for this multiplet agrees with Ajello's value (1.31×10^{-18} cm^2) within the error bars of 23% and 30% respectively.

The features above 125 nm for which most data are available are the OI multiplet at 130.4 nm and the CII multiplet at 133.5 nm (Mumma et al., 1972; Sroka, 1970; Ajello, 1971). Fig. 27, taken from Mumma et al. (1972), reveals the extent of the differences between different groups for the OI multiplet, particularly below 50 eV. We note that, if Mumma et al.'s data are reduced by the 0.59 factor, based on revised data for the Lyman-α from H_2 calibration cross section, the low energy differences between their data and Ajello's are exaggerated. For the CII 133.5 nm multiplet the differences in shapes are not so pronounced but the revised peak cross sections differ by a factor of 1.4 [see Table V of Mumma et al. (1972)]. The onset energies of the C emissions are consistent with total fragmentation of the parent molecule to give $C^* + 2O$.

Clearly there is a need for new measurements of the various emission cross sections to clarify some of the issues raised above. A quantitative measurement of $O(^5S)$ production is also a priority.

4.5.7. CO_2^+

Bahati et al. (2001) have measured electron impact dissociation of CO_2^+ to form C^+ and O^+ fragments in the energy range from threshold to 2500 eV. Maximum cross sections are close to 3.5×10^{-17} cm^2 and occur below 100 eV incident electron energy. Threshold energies and fragment kinetic energies were also measured and found to be similar to previously published data obtained in electron impact ionization experiments of neutral CO_2 (see Section 4.5.1).

4.6. N_2O

Nitrous oxide is an important atmospheric constituent involved in the nitrogen cycle. It also plays an important role in stratospheric photochemistry, particularly with regard to ozone, and in the overall global radiation budget (Wang and Sze,

Table 22
Partial and total ionization cross sections of N_2O by electron impact

Energy (eV)	$\sigma(N_2O^+)$ (10^{-18} cm^2)	$\sigma(N_2^+)$ (10^{-18} cm^2)	$\sigma(NO^+)$ (10^{-18} cm^2)	$\sigma(N^+)$ (10^{-18} cm^2)	$\sigma(O^+)$ (10^{-18} cm^2)	σ(total) (10^{-18} cm^2)
14	6.7 ± 0.8					6.7 ± 0.8
16	26.9 ± 2.2					26.9 ± 2.2
18	41.1 ± 2.9		1.31 ± 0.26			42.4 ± 3.2
20	52.7	0.66 ± 0.20	5.64		0.66 ± 0.26	59.7
22.5	68.4	1.7 ± 0.5	13.6	0.23 ± 0.06	1.63 ± 0.20	85.5
25	82.7	4.7 ± 1.2	23.7	0.59 ± 0.06	3.15 ± 0.32	115
27.5	92.2	9.7 ± 2.0	30.3	1.87 ± 0.19	4.07 ± 0.41	138
30	102	14.1	34.4	2.37 ± 0.24	4.66 ± 0.47	157
35	117	22.3	47.1	9.58	8.60	204
40	129	27.2	52.3	17.3	11.5	238
50	141	32.3	65.4	28.2	16.7	284
60	148	36.3	73.5	37.5	24.0	320
70	154	38.7	80.9	46.7	28.5	349
80	157	37.2	86.4	52.6	31.9	365
90	156	39.8	85.4	59.6	32.0	373
100	156	37.9	86.5	61.8	34.7	377
120	153	36.5	86.5	66.3	34.1	377
140	151	33.0	88.2	65.7	35.7	374
160	146	31.8	86.6	62.7	34.7	362
200	139	29.7	81.9	58.5	33.7	343
250	130	25.2	77.5	52.5	30.5	316
300	122	25.3	71.2	48.6	26.5	294
400	106	19.1	63.4	37.7	23.2	250
500	95.0	17.1	56.9	32.0	20.2	221
600	84.4	15.2	50.7	26.9	17.1	194
800	73.1	13.8	40.0	22.8	11.7	161
1000	66.6	11.7	35.3	20.3	8.07	142

From Lindsay et al. (2003).

1980). In the ground state it has a linear, asymmetric (N–N–O) configuration with a small (0.28 D) dipole moment. Despite its importance, there are major gaps in the cross section data base for this molecule.

The most recent review that has dealt with its dissociation is that of Karwasz et al. (2001). Data relevant to some aspects are included in the Landolt–Börnstein compilation (Itikawa, 2003).

4.6.1. Dissociative ionization

There have been relatively few measurements of dissociative ionization in N_2O. Rapp and Englander-Golden (1965) measured the cross section for production of fragment ions with kinetic energies greater than 0.25 eV whereas Iga et al. (1996a,b) used a pulsed ion extraction technique that, they claimed, enabled them to ensure total collection of all fragment ions (but see below). As might be expected the Rapp and Englander-Golden results lie lower in magnitude but there is good agreement on the shape of the total dissociative ionization cross section over the entire energy range up to 1000 eV. Iga et al. also present data for fragmentation into NO^+, N_2^+, N^+ and O^+ and state that cross sections for production of doubly ionized fragments are negligible. NO^+ is the dominant fragment ion produced. Semi-empirical models (Deutsch et al., 1997; Kim et al., 1997) agree well with the measurements.

More recently Lindsay et al. (2003) have presented extensive data for production of the various fragment ions from threshold to 1 keV. They use a technique that is demonstrated to be free from discrimination against fragments with significant amounts of kinetic energy. Although they agree reasonably well with Iga et al. (1996b) regarding the cross sections for production of N_2^+ and NO^+ where little kinetic energy is involved, they show serious disagreement with Iga et al. for N^+ and O^+ production. Here the Lindsay et al. (2003) data are about a factor of 2 larger at medium energies (100–200 eV), probably because of incomplete collection of fast fragment ions in the Iga et al. (1996b) work. In addition, Lopez et al. (2003) have used their fast neutral beam technique to obtain dissociative ionization cross sections for incident energies up to 200 eV. They agree well with the data of Iga et al. (1996b) except in the low energy region below 50 eV where the Lopez et al. data are consistently higher and display lower appearance energies.

We conclude therefore that considerable uncertainty still exists regarding the fragmentation cross sections, particularly in the low energy region. Further work is necessary to clarify this situation. The Lindsay et al. (2003) data set is given in Table 22 as is it demonstrably free of ion kinetic energy effects.

A number of coincidence techniques have been used to study some of the finer details of the dissociative ionization process, e.g. production of $N_2^+(B)$. See Matsuo et al. (1999) for details and references.

4.6.2. Appearance energies and fragment energy distributions

Rapp et al. (1965) found that, of all the molecules they studied, the ionization cross section for the N_2O molecule demonstrated the largest fraction (∼35%) due to dissociated ions with kinetic energies in excess of 0.25 eV. More recent works (Iga et al., 1996b; Lopez et al., 2003; Lindsay et al., 2003) bear out the importance of this observation.

Olivier et al. (1984) carried out a detailed study of the dissociative ionization of N_2O using ion kinetic energy and mass analysis. They studied all four ion production channels, NO^+, N_2^+, O^+ and N^+, in the impact energy range up to 40 eV. Maximum ion energies of 1.5, 2.5, 2.25 and 5 eV respectively were observed for these four channels at 40 eV impact energy. Predissociation of parent N_2O^+ states was shown to be an important mechanism. At least four different channels contributed to the production of each fragment ion.

4.6.3. Dissociative attachment

Early work on dissociative attachment over 30 years ago [see Karwasz et al. (2001) for references] was augmented by Krishnakumar and Srivastava (1988) and by Brüning et al. (1998). O^- is the only anion formed. The room temperature cross section is peaked at an incident energy of 2.2–2.4 eV with a value of 8.6×10^{-18} cm^2. More recently, Aflatooni and Burrow (2000) reported a somewhat lower value for this cross section peak of $7.6(6) \times 10^{-18}$ cm^2 at a target gas temperature of 338 K. Lower energy structure was confirmed as a definite peak at 0.55 eV by Brüning et al. (1998). They also demonstrated that this low energy peak shifted to lower energies as the target gas temperature increased, becoming a dominant zero energy peak at temperatures above 600 K. This behaviour is well understood in terms of the overlap between the neutral and anion states of N_2O. Brüning et al. (1998) demonstrated also that the kinetic energy carried away from the dissociative attachment process by the two fragments is only about 0.25 eV on average leaving the N_2 with considerable vibrational excitation. Allan and Skalicky (2003) demonstrated the presence of vibrational Feshbach resonances in the cross section for O^- formation at electron energies below about 0.7 eV.

Weber et al. (1999) have studied negative ion formation in very low energy (<180 meV) collisions between electrons and N_2O clusters. They find strikingly narrow peaks due to nuclear-excited Feshbach resonances of temporary cluster anions $(N_2O)_N^-$ ($N = 5$–10) dissociating into $(N_2O)_qO^-$ ($q < N$). These occur just below the onsets of vibrational modes in N_2O. Hanel et al. (2001) have studied the production of $(N_2O)_nO^-$ in the energy range up to 25 eV for small clusters with $n \leq 7$.

4.6.4. Dissociation into ground state fragments

No work has been reported on dissociation into two ground state neutral fragments. Dissociation into N + NO(X) could be readily probed using LIF techniques on the NO fragment, though the cross section would be expected to be much smaller than the $N_2(X)$ + O channel because of the increased bond strength involved.

4.6.5. Dissociation into neutral metastable fragments

LeClair and McConkey (1993) have used their solid Xe matrix detector to study the production of $O(^1S_0)$ over the energy range from threshold to 1 keV. They found that the production of $O(^1S_0)$ was via a single channel, the repulsive $D\,^1\Sigma^+$ (or $2\,^1\Sigma^+$) state of the parent molecule. Since the optical oscillator strength for this channel was accurately known from photoabsorption measurements, LeClair and McConkey were able to use the Bethe–Born procedure to put their data on an absolute basis at better than the 10% accuracy level. Their data are shown in Fig. 28 and listed in Table 23. Marinkovic et al. (1986) measured differential cross sections for the $D\,^1\Sigma^+$ state and from these obtained the integral cross section at 80 eV impact energy. Their value of 1.9×10^{-17} cm^2 is very close to the LeClair and McConkey value of 2.1×10^{-17} cm^2 at the same energy. However in later work, Marinkovic et al. (1999) used a different calibration procedure and scaled their 80 eV data upwards by a factor of 2.5, making the comparison with the LeClair and McConkey results much worse. Brunger et al. (2003) reanalyzed the differential cross section data of Marinkovic et al. (1999) using a Molecular Phase Shift Analysis procedure to extract integral cross sections as a function of impact energy. Their recommended excitation function has a maximum at just over 30 eV followed by a minimum around 60 eV. Since the transition in the parent molecule is optically allowed, an excitation function shape, such as that given by LeClair and McConkey (1993), seems much more probable. Additional work is required to clarify this unsatisfactory situation.

Using TOF analysis, LeClair and McConkey (1993) were able to monitor the amount of kinetic energy that went into translational motion of the fragments. From this and knowledge of the potential energy surface involved, they concluded that the N_2 fragment acquired considerable vibrational excitation in the dissociation process.

A considerable amount of effort went into a study of dissociative excitation into other, higher lying metastable states. Early work was referenced and discussed by Allcock and McConkey (1978a,b). Subsequently Mason and Newell (1989) examined the production of $N_2(a\,^1\Pi_g)$ and $O(^5S)$ and Barnett et al. (1991) looked at $N_2(A\,^3\Sigma_u^+)$.

Because of the large number of possible dissociation channels, special detection arrangements were used to isolate particular species. Thus Allcock and McConkey (1978a,b) used a Rydberg detector, with mass spectroscopic analysis, which enabled them to unambiguously identify N or O Rydberg species. They also used a low work function Auger detector that allowed detection of $N_2(A\,^3\Sigma_u^+)$ but, because this was located some 43 cm from the interaction region, most of any $N_2(a\,^1\Pi_g)$ metastables produced decayed in flight and were not detected. Mason and Newell (1989) used a much shorter (5.5 cm) path length to their channel electron multiplier detector so that they detected $N_2(a\,^1\Pi_g)$ efficiently but the work function was

Table 23
Absolute cross sections for the production of $O(^1S)$ following electron impact on N_2O

Energy (eV)	Cross section (10^{-18} cm^2)	Energy (eV)	Cross section (10^{-18} cm^2)
12	5.12	120	18.9
14	9.52	140	18.0
16	13.8	160	17.1
20	18.1	180	16.3
24	20.5	200	15.6
28	21.7	250	13.9
32	22.2	300	12.8
36	22.4	350	11.8
40	22.4	400	11.0
45	22.5	450	10.3
50	22.4	500	9.60
60	22.2	600	8.63
70	21.7	700	7.91
80	21.1	800	7.39
90	20.6	900	6.88
100	20.1	1000	6.49

From LeClair and McConkey (1993).

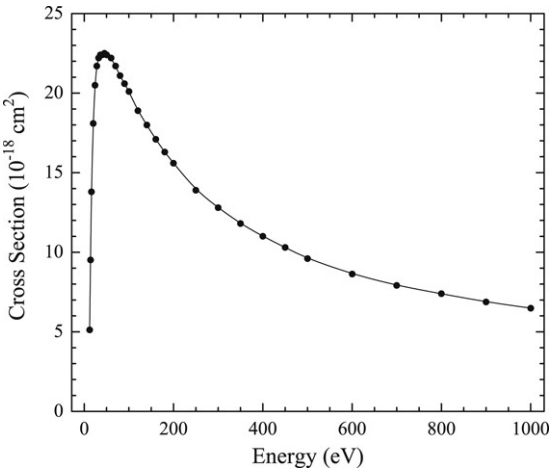

Fig. 28. Plot of absolute cross section data for production of $O(^1S)$ from N_2O as a function of electron energy. Data from Table 23.

high enough that any contribution from $N_2(A\,^3\Sigma_u^+)$ was negligible unless cascade or collisional excitation of high vibrational levels was occurring [see Johnson et al. (2005a)]. Thus they had a filter for detection of $N_2(a\,^1\Pi_g)$. Barnett et al. (1991) used a heated tantalum surface, which detected all metastable species with internal energies greater than about 5 eV and found that $N_2(A\,^3\Sigma_u^+)$ production dominated their measured spectra even though the detector was more sensitive to $N_2(a\,^1\Pi_g)$. This indicated that the cross section for production of $N_2(A\,^3\Sigma_u^+)$, either directly or via cascade, is much larger that that for production of $N_2(a\,^1\Pi_g)$. However, no absolute cross section data were presented by any of these authors. Allcock and McConkey obtained some evidence from their Rydberg detector of two-fragment break-up yielding NO(X) + N(R) but by far the dominant metastable production mechanisms involved breaking the NN = O bond.

All of the experiments discussed above were capable of velocity analysis of the fragments and so it was possible to monitor the fragment kinetic energies. For N_2 molecular fragments, these energies peaked at a few tenths of an eV and for the atomic fragments, broad distributions with widths of several eV and peaking at several eV are observed. These distributions changed with incident energy. In the molecular fragment case, the fact that the energy distribution was finite at zero kinetic energy indicated that the initial excitation was to the inner repulsive wall of a bound molecular state (see Section 2). On the other hand, the energy distribution of O (^5S) clearly indicated that the parent state was purely repulsive in the Franck–Condon region.

A large number of dissociation channels lead to metastable fragments [see for example the table given by Allcock and McConkey (1978a,b)]. In some cases it was possible to identify the parent excited states involved. Thus, from a consideration of the appearance energy and the sharp rise of the excitation function near threshold, Mason and Newell (1989) were able to identify the parent state of N_2O, responsible for $N_2(a\,^1\Pi_g)$ + O (^3P) production, as being either $^3\Sigma$ or $^3\Pi$. Further work by Furuhashi et al. (1997), who measured the angular distribution of the metastable fragments, showed that the latter possibility is preferred.

Recently, Malone et al. (2000) carried out a detailed study of the break-up of N_2O molecules and medium-sized (∼100 molecules) clusters following electron impact over the energy range from threshold to 200 eV. They found that their data

were relatively insensitive to the degree of clustering in the target beam with only minor differences being observed between clustered and non-clustered beams. Metastable fragments and VUV photons were used as diagnostics. Their findings were consistent with the conclusion that when a molecule in the cluster interacted with an electron, dissociation occurs as though the molecule was decoupled from the cluster. This is reasonable given the strength of the interatomic bonds in the molecule compared with the weak van der Waals bonds holding the molecules in the cluster. The finding that similar spectral emissions are obtained from clustered and non-clustered beams was consistent with earlier work by Khmel and Sharafutdinov (1997a,b). Three main interactions were observed to yield fast atomic fragments, most likely O (^{5}S). In each case the original transition in the parent molecule was optically allowed. Production of metastable N_2 ($a\,^1\Pi_g$) molecules was observed in two ways, either through their Lyman–Birge–Hopfield decay fluorescence or through Auger decay at the detector surface.

4.6.6. Dissociative excitation

Electron impact on N_2O leads predominantly to excitation of the ($A\,^2\Sigma^+ - X\,^2\Pi$) system of N_2O^+ and the earliest N_2O emission cross section data (Latimer and McConkey, 1965) were for this system. More recent works, such as Koppe et al. (1975), Gerzanich et al. (1976), van Sprang et al. (1978), have emphasized that dissociative excitation processes are relatively minor for this species.

4.6.6.1. Near-UV, visible and near-IR regions. The most extensive work in this spectral region is that of van Sprang et al. (1978). They observed the emission of NO ($B\,^2\Pi - X\,^2\Pi$) bands in the spectral region 220–330 nm. The total emission cross section of the bands is $2.3 \pm 0.3 \times 10^{-18}$ cm^2 at 100 eV incident electron energy, over 20 times smaller than the total cross section for the N_2O^+ bands. From the shape of the excitation function, they demonstrated that the initial excitation in the parent molecule was optically allowed. From the appearance energy they concluded that excitation was to a strongly repulsive state of N_2O. Although no measurement of fragment kinetic energies was made, it is very likely that these were significant, probably comparable to the metastable fragment kinetic energies discussed in Section 4.6.5.

van Sprang et al. (1978) also made measurements at a single energy (100 eV) of the emission cross sections of the 391.4 nm band of N_2^+, of OI multiplets at 777.4 and 844.7 nm and NI multiplets at 821.1 and 869.1 nm. Good agreement with Gerzanich et al. (1976) for the N_2^+ emission was obtained.

Koppe et al. (1975) studied the fluorescence obtained in the spectral region 388–600 nm using electron impact energies in the range 0.4–6 keV. In addition to the N_2O^+ bands, they list cross section data at 4 keV for a number of emissions from neutral and singly ionized O and N atoms. An important question about the reliability of these data comes from the fact that their values for the ($0 \rightarrow 2$) N_2O^+ band are in serious disagreement with all other measurements of this cross section (Latimer and McConkey, 1965; Gerzanich et al., 1976; van Sprang et al., 1978). Gerzanich et al. (1976) mention weak emissions in the 200–900 nm range from atoms and ions due to dissociative excitation but do not list any absolute data.

4.6.6.2. VUV region. Prior to the very recent work of Malone et al. (2008a,b) there was even less information available relative to dissociative excitation in this spectral region than in the visible. The only work was that of Sroka and Zietz (1973). They presented a spectrum showing atomic emissions from N and O in the spectral region between 105 and 130 nm, together with a partial excitation function for the excitation of N ($3s\,^4$P) monitored by its decay fluorescence at 120 nm. No absolute data were presented.

Malone et al. (2008a) present a detailed study of emissions in the 80–180 nm region for electron energies from threshold up to 300 eV. Calibrated spectral data are presented at 100 eV incident energy and detailed excitation functions are presented for all the major features. The dominant emission is the NI ($3s\,^4\text{P} \rightarrow {}^4$S) multiplet at 120 nm with a maximum emission cross section of $2.2 \pm 0.3 \times 10^{-18}$ cm^2 at 100 eV. We note that this is equivalent to the total emission cross section of the NO ($B \rightarrow X$) system discussed in Section 4.6.6.1.

Electron-induced fluorescence from N_2O clusters in the VUV has been studied by Malone et al. (2000) who reference other work involving electron impact on N_2O clusters.

4.7. NO_2

Nitrogen dioxide (O–N–O) is a very important pollutant molecule in Earth's troposphere and stratosphere where it is involved in ozone chemistry. Its reactions with electrons have not been studied extensively. For example, the recent data compilations of Karwasz et al. (2001) and Itikawa (2003) could not include any absolute data on dissociative attachment, integral elastic or momentum transfer processes.

4.7.1. Dissociative ionization

Recent work on NO_2 ionization by Lindsay et al. (2000) and Lukic et al. (2001) have established the total ionization cross section from threshold to 1 keV to an accuracy of better than 5%. The good agreement between these two data sets obtained on different sets of apparatus using different techniques, combined with the good agreement that is obtained also with the BEB calculations of Kim et al. (1997), implies that a high degree of confidence can be placed in the data. Lindsay et al. (2000) have also measured the dissociative ionization cross sections into NO^+, N^+, O^+, N^{2+} and O^{2+} although with reduced

Table 24
NO_2 partial and total ionization cross sections

Energy (eV)	$\sigma(NO_2^+)$ (10^{-18} cm^2)	$\sigma(NO^+)$ (10^{-18} cm^2)	$\sigma(N^+ + O^+)$ (10^{-18} cm^2)	$\sigma(N^+)$ (10^{-18} cm^2)	$\sigma(O^+)$ (10^{-18} cm^2)	$\sigma(N^{2+} + O^{2+})$ (10^{-18} cm^2)	σ(total) (10^{-18} cm^2)
13.5	9.09	5.5					14.6
16	15.9	14.8					30.8
20	24.4	401	2.2		2.2		66.7
25	31.7	612	6.1		6.1		99.0
30	38.9	906	15.5	1.5	14.0		145
35	43.6	114	27.2	5.5	21.7		185
40	45.4	130	42.8	11.4	31.4		218
50	52.5	157	64.2	18.9	45.3		274
60	54.6	177	84.9	23.4	61.5		316
80	56.1	189	112	33.7	77.8		357
100	54.2	195	126	36.5	89.2	0.140	375
120	54.3	195	135	40.7	93.8	0.238	384
160	50.7	186	131	38.6	92.7	0.433	369
200	47.0	176	124	39.7	84.3	0.614	347
250	43.2	163	114	36.0	77.6	0.640	321
300	39.9	151	102	32.7	69.0	0.615	293
400	35.3	132	85.0	27.5	57.4	0.507	253
500	31.1	117	71.9	22.1	49.8	0.452	221
600	27.8	106	63.1	20.2	42.9	0.413	197
800	23.5	88.6	51.6	13.6	38.0	0.330	164
1000	20.1	75.6	42.2	11.7	30.5	0.211	138

From Lindsay and Mangan (2003).

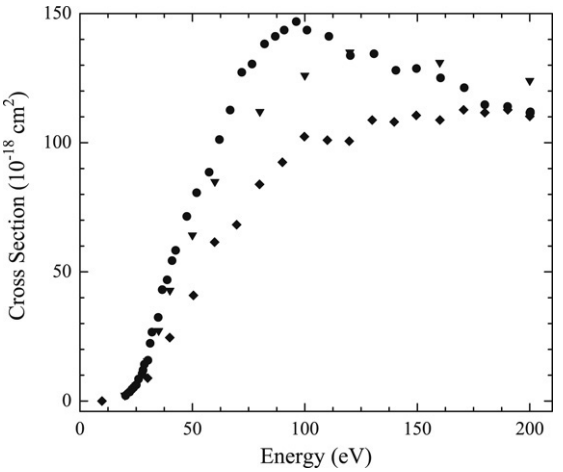

Fig. 29. $[N^+ + O^+]$ partial ionization cross sections of NO_2 from threshold to 200 eV. Diamonds, Lopez et al. (2003); inverted triangles, Lindsay and Mangan (2003); solid circles, Jiao et al. (2002). Adapted from Lopez et al. (2003).

accuracy. Lindsay et al.'s data set are given in Table 24. These results suggest that the earlier data of Stephan et al. (1980), which differed by a factor of two from the Lindsay et al. (2000) results, were unreliable.

Jiao et al. (2002) have used Fourier-transform mass spectroscopy to measure total and partial ionization cross sections over an energy range up to 200 eV. They obtain good agreement with Lindsay et al. (2000) on the total cross section up to 100 eV but deviate at higher energies. Their data for the partial cross sections show significant differences in both shape and magnitude from the Lindsay et al. (2000) results. This may be due at least partly to uncertainties in dealing with fast fragment ions.

More recently, Lopez et al. (2003) have studied the electron impact ionization of NO_2 from threshold to 200 eV using their fast neutral beam technique. Their data for NO_2^+ production agree well with the earlier data of Lindsay et al. (2000) and Lukic et al. (2001) for energies above 100 eV but differ significantly in both magnitude and shape of the cross section at lower energies. For NO^+ production, good agreement with the earlier work is obtained. For $(N^+ + O^+)$ production, agreement with earlier work is poor in both the shape and magnitude of the cross section below 200 eV. This is shown in Fig. 29. Because of the greater simplicity of the experimental method we suggest that the Lindsay et al. data set be preferred.

4.7.2. Appearance energies and fragment energy distributions

Both Lindsay et al. (2000) and Lukic et al. (2001) report an ionization potential for NO_2 close to 10 eV in agreement with the determination of Haber et al. (1988) using a multi-resonant optical absorption technique. Lindsay et al. find appearance potentials for NO^+ and O^+ at energies consistent with the photoionization data reported by Dibeler et al. (1967), namely 12.34 and 16.8 eV respectively. Their appearance energy for $(N^{2+} + O^{2+})$ occurred close to 80 eV.

No quantitative measurements of fragment ion kinetic energies have been reported but it is clear from the widths of the peaks in the TOF data of Lindsay et al. (2000) that a considerable amount of kinetic energy is imparted to fragments in the dissociation process. In their coincidence dissociation work, Au and Brion (1997) comment on the fact that their fragment ion peaks are considerably broadened due to the kinetic energies involved. They did not present any quantitative estimates of the kinetic energies but noted that they increased as the incident electron energy increased up to about 80 eV. The fragment kinetic energy was due to the direct dissociation process or to the Coulomb explosion of multiply charged parent ions.

4.7.3. Dissociative attachment

DA has been studied by a number of workers. Stockdale et al. (1969) summarized work prior to that date and more recent studies are by Abouaf et al. (1976) and by Rangwala et al. (2003). Only the latter workers present absolute data. O^- is the dominant fragment anion with an appearance energy of 1.61 ± 0.05 eV (Abouaf et al., 1976) and a peak in the formation cross section some 0.2 eV higher (Stockdale et al., 1969; Abouaf et al., 1976). The later work of Rangwala et al. (2003) positioned this maximum in the cross section versus energy curve between 1.4 and 1.5 eV, without a well defined onset. This is probably due to the poorer energy resolution in the Rangwala et al. experiment, where an unselected electron gun was used. Abouaf et al. (1976) point out that the theoretical onset, based on known values for the dissociation and attachment energies, for the process,

$$e^- + NO_2\ (X) \rightarrow O^-\ (^2P) + NO(^2\Pi) \tag{18}$$

is at 1.65 eV. Structure in this cross section peak, which was observed by Abouaf et al. (1976) and some earlier workers, was attributed to vibrational effects in the parent $(NO_2)^-$ state. It is noteworthy that the maximum cross section value is quite large, almost 1% of the total cross section at this energy.

Rangwala et al. (2003) found subsidiary maxima in the O^- production cross section at 3.0 and 8.2 eV while Abouaf et al. (1976) put these secondary, and much weaker, maxima at 3.5 and 8.5 eV. It appears that some of the differences between Rangwala et al. (2003) and the earlier workers are due to energy resolution and calibration problems.

NO^- and O_2^- anions are also produced but with much lower intensity (less than 1%). This has been investigated by Abouaf et al. (1976), who used a conventional magnetic mass spectrometer. [Rangwala et al. (2003) did not have sufficient resolution to separate these two anions in their TOF apparatus.] Cross sections for production of these two species were shown to peak near 3.2 and 4.35 eV respectively. Fig. 30 shows the energy dependence of the cross sections for the production of the different anions, as presented by Abouaf et al. (1976).

No measurements of fragment ion kinetic energies following dissociative attachment have been carried out, so little knowledge of the detailed shapes and positions of the molecular potential surfaces involved is available.

4.7.4. Dissociation into ground state fragments

No data are available for dissociation into neutral ground state fragments with the exception of the case discussed above Eq. (18) where O^- is the other fragment. As with the case of N_2O break-up, NO $(^2\Pi)$ should be accessible using LIF techniques.

4.7.5. Dissociation into neutral, excited or metastable fragments

Although various aspects of the photodissociation of NO_2 have been studied [see e.g. Hakala et al. (1974), Calvert et al. (1987), Slanger (1989), Davies et al. (2000), Hancock and Morrison (2005)], no parallel work has been carried out using electron impact. The broad features in the inelastic electron energy loss spectrum (Au and Brion, 1997) below the ionization threshold are very typical of dissociation channels. Clearly these lead to neutral fragments. The authors are not aware of any emission cross section measurements involving this molecule.

4.8. SO_2

Sulfur dioxide is a bent (C_{2v}) molecule with a ground state molecular configuration of $5(a_1)^2 \ldots (5b_2)^2(1a_2)^2(8a_1)^2$ and a large permanent dipole moment (1.63305 D). It has a 1.4308 Å and 119.329° bond length (O–S) and angle (O–S–O), respectively, and a positive electron affinity of 1.107 ± 0.008 eV (Lide, 2007). Sulfur dioxide is an important atmospheric molecule, which is involved in acid rain, and is produced through man-made combustion activities and natural (volcanic) sources (Seinfeld and Pandis, 1997). Volcanic releases of SO_2 have also been observed in other planetary systems, for example, Venus (Esposito, 1984) and the Jovian moon Io. On Io, approximately one metric ton of SO_2 per second is generated volcanically and is the ultimate source of material for Io's atmosphere (Krupp, 2007; Retherford et al., 2007). Geissler et al. (2004) determined that the visible emissions of the Io aurorae are predominantly due to $e^- + SO_2$ and that the principal source of oxygen atoms during eclipse (by Jupiter) is electron impact dissociation of SO_2. On Earth, interest in

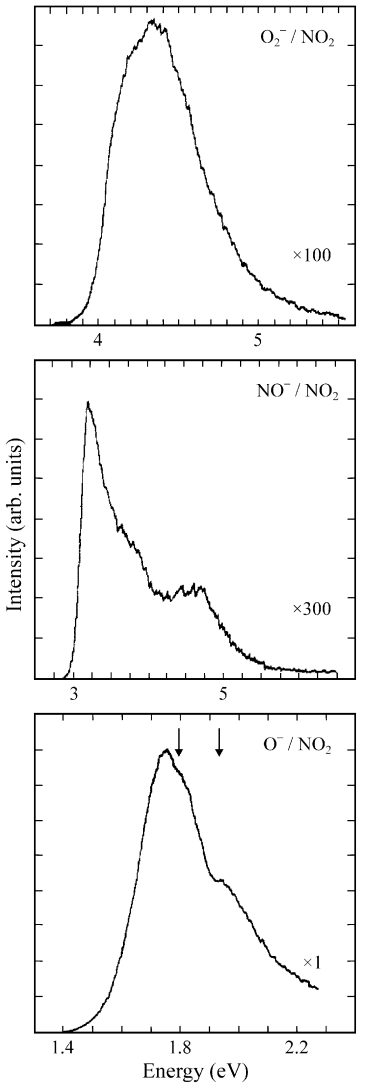

Fig. 30. Relative cross sections for production of O_2^-, NO^- and O^- following electron impact on NO_2. Adapted from Abouaf et al. (1976).

the mitigation and removal of SO_2 and other oxygen–sulfur compounds (see Section 4.8.7) from industrial applications is ongoing, with recent studies of removal mechanisms using dielectric barrier discharges (Saveliev et al., 2007) and plasma-chemical oxidation in air using a pulsed electron beam (Novoselov et al., 2001).

Bhardwaj and Michael (1999) reviewed cross sections for electron impact of sulfur dioxide while modelling electron degradation in SO_2 gas; they utilized some alternate data sets compared to those recommended by Lindsay and Mangan (2003) and presently. Abuain et al. (1985) investigated near-threshold electron impact excitation of SO_2 using a trapped-electron spectrometer and provided energy-loss data for scattered inelastic electrons and negative ions.

4.8.1. Dissociative ionization

The Lindsay and Mangan (2003) review recommended the data of Lindsay et al. (1996) and provided recalibrated partial and total ionization cross sections from threshold to 1 keV. These are listed in Table 25. The recalibrated data of Lindsay et al. were recommended largely due to the demonstrated complete detection of fragment ions. Basner et al. (1995) also presented the total and partial ionization cross sections of SO_2 from threshold to 200 eV using two different experimental techniques: neutralized fast beam and mass spectrometry. The separation of partial ionization cross sections for the S^+ and O_2^+ fragment ions was enabled by the high resolution double-focusing sector-field mass spectrometer. Production of SO_2^{2+} was not observed by Basner et al. below approximately 90 eV. Consequently, the semi-partial cross section of $S^+ + O_2^+ + SO_2^{2+}$, below 90 eV, listed in Table 25 can be partitioned by the $S^+ + O_2^+$ cross section ratio of Basner et al.

Table 25
SO_2 partial and total ionization cross sections

Energy (eV)	$\sigma(SO_2^+)$ (10^{-18} cm^2)	$\sigma(SO^+)$ (10^{-18} cm^2)	$\sigma(S^+ + O_2^+ + SO_2^{2+})$ (10^{-18} cm^2)	$\sigma(O^+)$ (10^{-18} cm^2)	$\sigma(SO^{2+})$ (10^{-18} cm^2)	σ(total) (10^{-18} cm^2)
15	26	0.5				26
20	78	21				99
25	113	71	2.9	0.8		188
30	140	112	19.2	2.0		273
35	150	126	39.5	5.0		320
40	160	135	55.8	11.4	0.03	362
50	173	144	71.9	27.8	0.58	418
60	183	152	82.5	42.3	1.24	461
80	190	155	89.0	61.2	2.03	497
100	192	159	90.9	71.6	2.40	516
120	189	155	85.5	73.7	2.53	505
160	179	145	77.0	71.2	2.30	475
200	172	139	71.0	66.9	2.28	451
250	158	126	62.2	59.2	1.97	407
300	149	119	55.6	53.8	1.74	379
400	130	103	45.4	44.1	1.49	324
500	114	90	37.9	36.7	1.21	280
600	101	79	32.2	31.2	1.05	245
800	85	66	25.9	24.9	0.74	202
1000	73	56	21.8	20.4	0.62	172

From Lindsay and Mangan (2003).

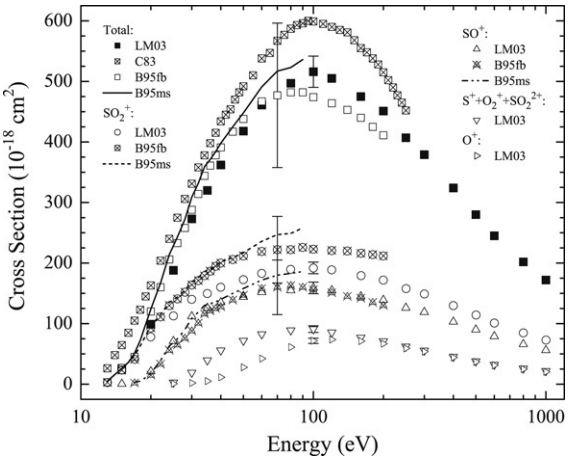

Fig. 31. Total and partial ionization cross sections in SO_2. Data are identified in the legend where LM03 represents Lindsay and Mangan (2003), B95fb and B95ms represent the fast beam and mass spectrometer results, respectively, of Basner et al. (1995), and C83 represents Cadez et al. (1983).

Fig. 31 shows the recommended total and partial ionization cross sections from Table 25. The total, SO_2^+, and SO^+ cross sections agree well with the data of Basner et al. The large uncertainty of the Basner et al. data was partially due to challenges in source stability of their fast beam method, with possible minor S_2 contamination. This may be why the SO_2^+ partial cross section is slightly larger than the recommended cross section. Also shown are the total cross section data of Cadez et al. (1983).

Kim et al. (1997) performed BEB calculations from threshold to 1 keV for the total cross section, which agree well with the recommended data. However, the additivity calculation of the total cross section from Basner et al. does not demonstrate acceptable agreement. More recently, Pal and Prakash (1998) calculated total and partial cross sections using a semi-empirical approach. They agree well with the recommended total and SO^+ cross sections. Other experimental efforts generally have much poorer agreement. The cross sections of Orient and Srivastava (1984) were in some cases (e.g. SO_2^+) too large by roughly a factor of two and had strange double-peaked shapes between threshold and 200 eV, while other partial cross sections (e.g. SO^+) were in reasonable agreement. Smith and Stevenson (1981) measured cross sections up to 40 eV, but generally were too small by a factor of approximately two to three.

Scheier et al. (1988) and Märk et al. (1989) investigated multiply charged SO_2 clusters using mass spectrometry. Ionization of the cluster beam occurred at 120 eV electron impact, inducing fragmentation of the SO_2 clusters, with multiple fragment ions observed. They observed the parent ions, $(SO_2)_n^+$, along with $(SO_2)_nSO^+$, $(SO_2)_nS^+$, and $(SO_2)_nO^+$, ordered by decreasing intensities; doubly and triply ionized fragments were also observed. Appearance energies for various multiply charged cluster ions were determined.

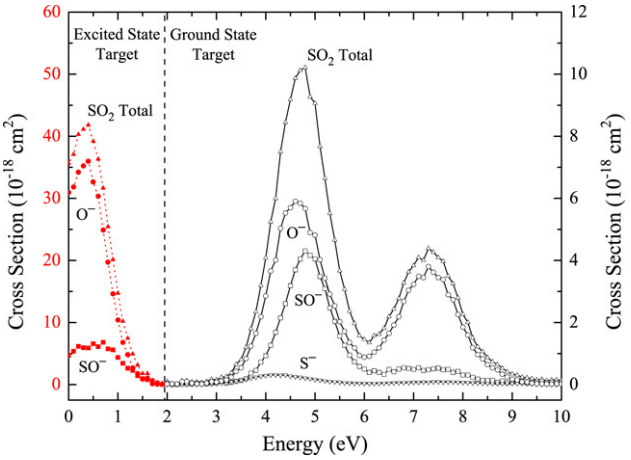

Fig. 32. Partial and total attachment cross sections (right) following electron impact on SO_2. Also shown (left; red) are the partial and total cross sections from an excited SO_2 target (see text). Digitized from Krishnakumar et al. (1997).

4.8.2. Appearance energies and fragment energy distributions

The NIST Chemistry WebBook (2005) lists appearance energies for SO^+, O^+, S^+, and O_2^+ fragments from $e^- + SO_2$ and gives the appropriate references.

For electron impact dissociative ionization of SO_2, the NIST Chemistry WebBook lists appearance energies of 16.5 ± 0.5 eV by Orient and Srivastava (1984) and 16.2 ± 0.2 eV by Smith and Stevenson (1981) for $SO^+ + O$, with respective values of 15.81 ± 0.02 eV and 15.930 ± 0.005 eV by photoionization and photoelectron methods. Basner et al. consistently measured 16.6 ± 0.4 eV for the appearance energy and concluded (based on thermochemical minimum energy arguments) that the SO^+ fragment ions were formed with little excess kinetic energy. The NIST Chemistry WebBook lists values for the $O^+ + SO$ fragmentation process of 23.5 ± 0.5 eV by Orient and Srivastava and 20.6 eV by Reese et al. (1958). Basner et al. report a consistently obtained value of 25.0 ± 1.0 eV. Basner et al. provide a discussion of their relatively small intensity ion results ($<1 \times 10^{-18}$ cm^2), that extended downwards in energy to around 20 eV: $SO_2 \rightarrow S+O+O^+$ has a thermochemical minimum energy of 24.4 ± 0.2 eV and $SO_2 \rightarrow SO+O^+$ has 19.3 ± 0.2 eV. This is an important issue due to the unsatisfactory agreement for many partial ionization cross sections, particularly with the O^+ fragment, which potentially suffer from kinetic energy discrimination effects. Lastly, the combined (typically unresolved) $S^+ + O_2^+$ fragment ion signal has listed appearance energy values of 16.5 ± 0.5 eV by Orient and Srivastava, 22 eV by Smith and Stevenson (possibly process $S^+ + 2O$), and 17.5 ± 0.3 eV by Reese et al. The photoelectron value is 16.334 eV. Basner et al. measured appearance energies of 17.2 ± 0.5 eV (fast beam) and 17.0 ± 0.3 eV (mass spectrometer). They note the close agreement to the lowest thermochemical threshold for both $S^+ + O_2$ (16.1 eV) and $O_2^+ + S$ (17.8 eV).

Appearance and kinetic energies were investigated for dissociation of SO_2 into neutral fragments by van der Burgt et al. (1992), Kedzierski et al. (2000), and Vatti Palle et al. (2004) [see Sections 4.8.5 and 4.8.6].

4.8.3. Dissociative attachment

There have been many studies of electron attachment to SO_2 over the years, though fewer dissociative studies have been carried out. Table 26 lists the recommended cross sections of Krishnakumar et al. (1997) for production of O^-, S^-, and SO^- from the ground state of SO_2, along with the total attachment cross section. They used a multi-element time-of-flight mass spectrometer system with additional focusing to improve ion collection. (This data set was also recommended by Lindsay and Mangan (2003) though they appear to have shifted the energy scale downwards by 0.1 eV.) Fig. 32 shows the Krishnakumar et al. (1997) data up to 10 eV electron impact energy, with the O^- fragment having the largest cross section and S^- production relatively small. Also shown in Fig. 32 are anion cross sections out of an electronically excited SO_2 target (see below).

Other determinations of DEA (dissociative electron attachment) with SO_2 were performed by, for instance, Sauers et al. (1993), Spyrou et al. (1986), Orient and Srivastava (1983a,b), and Cadez et al. (1983). The observed peak positions are in reasonable agreement, but the cross section magnitudes are in poor agreement. Earlier studies [e.g. Harland et al. (1973)] investigated the relative DEA intensities and provided translational energy assessments. Spyrou et al. (1986) and Orient and Srivastava (1983a,b) directly measured the cross sections for O^-, S^-, and SO^-, but showed the SO^- fragment having a larger cross section than the O^- fragment, in contrast with the results of Krishnakumar et al. (1997) and Cadez et al. (1983). Orient and Srivastava provided a DEA cross section for S^- in agreement with the recommended values, though their agreement was poor for the O^- and SO^- fragments. Spyrou et al.'s cross sections for O^- and S^- were in poor agreement with the recommended cross sections, though their SO^- cross section was in very good agreement. Their total DEA cross section was ~35% lower than the recommended value at the 4.6 eV peak. Spyrou et al. also investigated the effect of temperature changes on the target gas and found increasing cross sections with larger temperatures.

Table 26
SO_2 partial and total electron attachment cross sections

Energy (eV)	$\sigma(O^-)$ (10^{-18} cm^2)	$\sigma(S^-)$ (10^{-18} cm^2)	$\sigma(SO^-)$ (10^{-18} cm^2)	σ(total) (10^{-18} cm^2)	Energy (eV)	$\sigma(O^-)$ (10^{-18} cm^2)	$\sigma(S^-)$ (10^{-18} cm^2)	$\sigma(SO^-)$ (10^{-18} cm^2)	σ(total) (10^{-18} cm^2)
2.8	0.048	0.017	0.031	0.102	6.5	1.65	0.045	0.490	2.19
2.9	0.096	0.020	0.043	0.170	6.6	1.92	0.054	0.415	2.43
3.0	0.076	0.032	0.053	0.153	6.7	2.19	0.054	0.501	2.78
3.1	0.114	0.047	0.095	0.238	6.8	2.68	0.062	0.543	3.27
3.2	0.153	0.060	0.043	0.257	6.9	3.04	0.059	0.521	3.63
3.3	0.238	0.089	0.073	0.378	7.0	3.23	0.071	0.490	3.84
3.4	0.428	0.112	0.106	0.652	7.1	3.49	0.069	0.543	4.10
3.5	0.542	0.138	0.138	0.805	7.2	3.45	0.079	0.458	4.01
3.6	0.836	0.173	0.191	1.20	7.3	3.80	0.074	0.479	4.39
3.7	1.24	0.206	0.373	1.80	7.4	3.62	0.085	0.511	4.27
3.8	1.65	0.234	0.458	2.35	7.5	3.45	0.088	0.533	4.10
3.9	2.19	0.270	0.724	3.19	7.6	3.38	0.077	0.479	3.98
4.0	2.86	0.289	0.926	4.08	7.7	2.90	0.081	0.490	3.50
4.1	3.66	0.310	1.27	5.24	7.8	2.74	0.079	0.393	3.26
4.2	4.01	0.310	1.68	6.00	7.9	2.26	0.072	0.426	2.79
4.3	5.04	0.300	2.15	7.50	8.0	1.85	0.067	0.308	2.26
4.4	5.53	0.305	2.61	8.45	8.1	1.60	0.063	0.308	2.00
4.5	5.70	0.271	3.19	9.18	8.2	1.19	0.055	0.233	1.51
4.6	5.90	0.250	3.70	9.87	8.3	0.970	0.047	0.181	1.22
4.7	5.84	0.232	4.05	10.1	8.4	0.827	0.043	0.138	1.06
4.8	5.67	0.210	4.30	10.2	8.5	0.647	0.036	0.138	0.873
4.9	4.89	0.188	4.17	9.27	8.6	0.542	0.033	0.138	0.736
5.0	4.82	0.160	4.05	9.06	8.7	0.475	0.031	0.073	0.652
5.1	4.03	0.138	3.48	7.68	8.8	0.332	0.032	0.116	0.531
5.2	3.43	0.117	3.09	6.65	8.9	0.247	0.033	0.063	0.411
5.3	2.92	0.096	2.47	5.52	9.0	0.181	0.037	0.085	0.342
5.4	2.54	0.086	2.03	4.66	9.1	0.153	0.033	0.095	0.307
5.5	2.02	0.071	1.57	3.67	9.2	0.086	0.033	0.106	0.238
5.6	1.71	0.052	1.27	3.07	9.3	0.076	0.027	0.053	0.222
5.7	1.36	0.047	0.948	2.37	9.4	0.048	0.020	0.073	0.189
5.8	1.18	0.040	0.734	1.97	9.5	0.029	0.014	0.063	0.153
5.9	0.941	0.039	0.586	1.58	9.6	0.029	0.009	0.106	0.170
6.0	0.883	0.033	0.501	1.46	9.7	0.020	0.008	0.053	0.120
6.1	0.912	0.032	0.393	1.35	9.8	0.010	0.003	0.073	0.153
6.2	1.05	0.034	0.446	1.58	9.9	0.029	0.000	0.063	0.153
6.3	1.18	0.035	0.393	1.63	10.0	0.020	0.000	0.063	0.137
6.4	1.44	0.042	0.330	1.82	.				

Data digitized from diagrams in Krishnakumar et al. (1997).

Cadez et al. (1983) measured a total dissociative cross section, which was ∼40% lower than the recommended value at the 4.6 eV peak, and used earlier published data (peak positions and relative intensities) to estimate the partial cross sections. Sauers et al. (1993) measured relative DEA intensities and placed them on an absolute scale by normalization to Wan et al.'s (1993) absolute total DEA cross section. Sauers et al. suggested peak cross sections of 4.5×10^{-18} cm^2, 5.4×10^{-18} cm^2, and 0.2×10^{-18} cm^2 for O^-, S^-, and SO^-, respectively. Note that the recommended total attachment cross section in Table 26 agrees well with the results of Wan et al. Krishnakumar et al. (1997) provide further detailed discussion on possible causes for the generally poor cross section agreement between different groups.

As shown in Fig. 32, DEA was reported by Krishnakumar et al. (1996, 1997) and Krishnakumar (1998) for an electronically excited neutral SO_2 target. Cross sections of 36×10^{-18} cm^2 at 0.4 eV for O^- and 6.6×10^{-18} cm^2 at 0.6 eV for SO^- were measured. Interestingly, the ∼7 eV peak from the ground state target, which would appear at ∼3 eV from the excited target, was not observed. The absence of the second peak was attributed to selection rules governing the electron capture process. Jaffke et al. (1993) also reported DEA cross sections for excited SO_2 using a quadrupole mass spectrometer and observed approximately the same ∼4 eV shifted peak positions as compared to the ground state. However, Jaffke et al. reported an O^- cross section roughly a factor of 30 times larger than that of Krishnakumar et al. (1997). This discrepancy illustrates the difficult challenges (i.e. relative number densities, different detection efficiencies, etc.) encountered with excited state targets. Kumar et al. (2004) extended the DEA measurements to vibrationally excited SO_2 in the Clements band. They demonstrated that the DEA (to a first approximation) was independent of the vibrational levels in this band, in contrast with the typical case where vibrational levels of the ground state were considered.

Märk et al. (1987) and Stamatovic et al. (1987) presented relative electron attachment cross sections (i.e. intensities) from neutral $(SO_2)_n$ clusters, for $n < 9$, up to roughly 12 eV and observed three homologous cluster ion series: $(SO_2)_n^-$, $(SO_2)_n\,O^-$, and $(SO_2)_nSO^-$ for $n < 10$. Two noteworthy observations were the detection of SO_2^-, which is absent in typical low pressure SO_2 gas experiments but can be found at elevated pressures (Rademacher et al., 1975), and an additional resonance feature at around 11 eV as compared to the non-clustered case. SO_2^- was found to be more abundant than SO_2 O^- and SO_2SO^-.

Stamatovic et al. also observed various DEA cross sections up to 40 eV that were judged to be due to ion pair processes and not auto-scavenging via secondary processes in the collision gas.

4.8.4. Dissociation into ground state fragments

Apart from situations where a ground state fragment accompanied a charged partner fragment or fragments, for example in Sections 4.8.1 and 4.8.3, there have not been any specific monitoring of ground state species.

4.8.5. Dissociation into neutral metastable fragments

The production of metastable fragments by electron impact dissociation of SO_2 molecules was studied by van der Burgt et al. (1992) and Kedzierski et al. (2000) using direct detection techniques. No other results appear to be available. van der Burgt et al. used a channel electron multiplier to detect Rydberg fragments of S, O, and SO up to an impact energy of 300 eV. The non-selective nature of their surface detector resulted in the inability to distinguish between different states or decay channels. Their surface detector was also able to observe O($3s\ ^5S^o$) metastable fragments (9.14 eV onset), but was limited by its ∼8 eV work function. Consequently, they were not able to observe metastable atoms with lower onset energies. Excitation functions displayed up to about 60 eV were determined for composite metastable features of specific kinetic energy ranges, but could not be made absolute. From the excitation function data, numerous onset energies were documented. A comparison of the fragment energies versus appearance potentials enabled the identification of (at least) 11 processes, which were extensively discussed. They concluded that most observed fragments were atomic Rydbergs (S and O) with some contributions from SO and O_2 Rydberg fragments.

Kedzierski et al. (2000) used their Xe matrix surface detector to selectively and sensitively study O(^{1}S) metastable fragments from $e^- + SO_2$. Fragment kinetic energy distributions were obtained from the time-of-flight data and the cross section for production of O(^{1}S) metastables was studied in the energy range from threshold to 400 eV. The relative cross section for production of O($3p\ ^3P$ and $3p\ ^5P$) emissions was also studied (see Section 4.8.6.1). The time-of-flight and fragment kinetic energy data indicated at least three contributing channels to the O(^{1}S) production. They were also able to demonstrate that production of O($3p\ ^3P$ and $3p\ ^5P$) was accompanied by SO fragments with significant vibrational or electronic excitation. The O(^{1}S) cross section had a maximum of about 2.2×10^{-18} cm^2 at 150 eV and a broad shape that indicated optically allowed excitation out of the ground state of the parent molecule.

4.8.6. Dissociative excitation

There have been several important new articles relevant to dissociative excitation of SO_2 since the review of the cross sections by Bhardwaj and Michael (1999). The recent emission work of Ajello and coworkers along with the selective surface technique of McConkey and coworkers are the main contributions.

4.8.6.1. Middle-UV and visible optical near-IR region. There have been several electron impact dissociative excitation studies of emissions in the middle-ultraviolet (MUV) and visible optical near-infrared (VOIR) spectral regions. The MUV spectral region is largely composed of broad band molecular features and can be partitioned into the MUV1 (∼238.5–267 nm) and MUV2 (∼267–600 nm) regions. This was based upon observed features: the MUV1 emission features are from SO(A, B → X), including the SO_2 quasicontinuum; the MUV2 emission features are from $SO_2(\tilde{A}, \tilde{B}, \tilde{a} \rightarrow \tilde{X})$, $SO_2^+(\tilde{C} \rightarrow \tilde{X})$, and SO(B → X), plus over 100 candidate OI, OII, SI, and SII emissions.

The MUV emission cross sections have been summarized by Bhardwaj and Michael (1999). Briefly, Ajello et al. (1992b) measured the MUV1 and MUV2 (up to 430 nm) spectral regions up to 1 keV. Earlier investigations of the MUV and visible spectral regions were by Miller and Becker (1987) and Johnson et al. (1987a,b). Ajello et al. (2002) extended the spectral range of previous emission measurements to capture more of the MUV2 contributions (200–600 nm) with electron impact energies up to ∼100 eV. They benefited from a better spectral calibration, higher instrumental resolution, and higher signal-to-noise compared to previous measurements. Kedzierski et al. (2000) (see Section 4.8.5) also obtained a low resolution (uncalibrated) spectrum covering 350–850 nm at 100 eV incident electron energy, which clearly showed the MUV2 emissions. Ajello et al. (2008) measured the MUV region (displayed 210–380 nm at 100 eV) while covering an extended spectral range into the near-IR (see below) and demonstrated excellent agreement with the results of Ajello et al. (2002). Ajello et al. (2008) did not observe molecular emission features beyond 600 nm and determined that OII and SII emissions heavily outweigh neutral atomic emissions between 390 and 600 nm.

Kedzierski et al. were seemingly the first to observe the OI 777.4 nm and 844.7 nm atomic emissions from $e^- + SO_2$, which dominated the low resolution spectrum into the VOIR region. At low energies (∼10 eV) they also observed a hitherto unidentified triplet state of SO_2 that emitted weakly in the near-IR, centred near 700 nm. Kedzierski et al. provided a combined relative emission cross section for the OI (777.4 nm + 844.7 nm) transitions from threshold to 400 eV. It had a broad, optically-allowed shape with multiple onsets evident from near-threshold to about 50 eV and a maximum near 125 eV. Kiehling et al. (2001) studied proton impact-induced emissions (380–800 nm) and found the molecular features to be weak relative to the many observed OI, OII, SI, and SII lines.

Ajello et al. (2008) investigated emissions from $e^- + SO_2$ in the range 200–1100 nm at medium resolution (∼0.25 nm FWHM) with incident electron energies of 25 eV and 100 eV. They calibrated their spectrometer and three-grating system using standard deuterium and tungsten spectral irradiance lamps over the 200–1200 nm spectral range and placed it on

Table 27
Absolute cross sections for electron impact dissociative excitation of SO_2

Selected features	Wavelength (nm)	Cross section at 25 eV (10^{-18} cm^2)	Cross section at 100 eV (10^{-18} cm^2)
MUV1 Total[a]	238.5–267.0	2.43	2.09
MUV2 Total[b]	267.0–600.0	7.0	10.0
Atomic VOIR Total[c]	390.0–571.0	>0.0411	0.8303
OI(^{1}S)[d]	–	∼0.9	2.0
OI(3s ^{5}S–3p ^{5}P)[c]	777.34	0.390	4.20
OI(3s ^{3}S–3p ^{3}P)[c]	844.67	0.215	2.60
SI(4s ^{5}S–4p ^{5}P)[c]	921.29	0.363	1.80
SI(4s ^{3}S–4p ^{3}P)[c]	1045.94	0.442	1.06
VOIR total[c]	571.0–1100.0	2.90	17.62

From Ajello et al. (1992b, 2002, 2008) and Kedzierski et al. (2000).
[a] Ajello et al. (1992b) identified the MUV1 emission features from SO(A, B → X), including the SO_2 quasicontinuum.
[b] Ajello et al. (2002) identified the MUV2 emission features (at 98 eV) from $SO_2(\tilde{A}, \tilde{B}, \tilde{a} \rightarrow \tilde{X})$, $SO_2^+(\tilde{C} \rightarrow \tilde{X})$, and SO(B → X), plus over 100 candidate OI, OII, SI, and SII emissions.
[c] Ajello et al. (2008) identified a multitude of atomic (OI, OII, SI, and SII) emission features. The atomic lines within 390–571 nm occur on top of the MUV2 continuum.
[d] Kedzierski et al. (2000) measured the cross section of O(^{1}S) from all production channels.

an absolute scale by comparison with the emission cross sections of H_α from H_2. Cross sections were presented at incident electron energies of 25 eV (i.e. negligible ion contributions) and 100 eV for many OI, SI, OII, and SII multiplet emission features between approximately 390–1100 nm, with about a dozen measured features within 570–1100 nm not found in the NIST atomic database. The 570–1100 nm spectral region was dominated by OI and SI emissions.

Table 27 summarizes the absolute cross sections at 25 eV and 100 eV for selected features in the MUV and VOIR from electron impact excitation of SO_2. The "total" cross sections from Ajello et al. (2008) represent a lower bound since an unknown number of weak features were not included in the summation; however, the weak features presumably contribute only a small amount. Also included is the O(^{1}S) cross section from all production channels by Kedzierski et al. (2000). It is evident that the OI and SI states (^{3,5}P) that cascade to significant VUV emitting levels (^{3,5}S) dominate the VOIR spectral region. The short-lived atomic emission levels (indicated as Atomic VOIR Total in Table 27) make a minimal contribution to the MUV2 spectral region, in striking contrast to the 40% estimation of Ajello et al. (2002). The MUV1 and MUV2 contributions increase substantially at lower impact energies (∼10–20 eV) (Ajello et al., 2002).

4.8.6.2. VUV region. The vacuum ultraviolet (VUV) spectral region is typically partitioned into the extreme-ultraviolet (EUV) and far-ultraviolet (FUV) regions: roughly 40–120 nm and 120–200 nm, respectively. Vatti Palle et al. (2004) have recently carried out a high resolution, optically-thin FUV/EUV emission (85–170 nm) study of electron impact dissociative excitation of SO_2 up to 800 eV. They observed many SI, SII, OI, and OII multiplets and provided cross sections for all emission features from medium resolution (1.5 Å FWHM) spectra at 200 eV. High resolution (0.6 Å or 95 mÅ FWHM) spectra at 30 eV and 100 eV electron impact energies were obtained for the most important and intense multiplets (intended for modelling Io observations by the Hubble Space Telescope) with the fine-structure lines resolved. This enabled the determination of cross sections up to 800 eV for the following emission lines: SII (125.6 nm), OI (130.4 nm), SI (142.9 nm), and SI (147.9 nm). Table 28 lists emission cross sections for OI (130.4 nm) and SI (142.9 nm) from Vatti Palle et al. (2004). Note that these cross sections were originally made absolute by comparison to the OI (130.4 nm) cross section from $e^- + O_2$ as measured by Kanik et al. (2003). The 130.4 nm and 147.9 nm values listed in Table 28 have been renormalized to reflect the newly recommended 130.4 nm emission cross section from O_2 (see Table 7). We note a possible weakness in the calibration procedure of Vatti Palle et al. (2004) in that they did not measure their SO_2 and O_2 pressures absolutely. The magnitude of Vatti Palle et al.'s (2004) OI (135.6 nm) emission cross section should be used with caution, due to the long lifetime involved and consequent uncertainty in their field-of-view correction factor.

Previous measurements in the EUV and FUV were by Ajello et al. (1992a) and Becker et al. (1983). Becker et al. studied EUV emissions in the spectral range 45–110 nm for incident electron energies up to 500 eV. Ajello et al. (1992a) investigated EUV and FUV emissions in the spectral range 40–200 nm for incident electron energies up to ∼2 keV, with cross sections for all observed features provided at 200 eV. The results of Becker et al. and Ajello et al. appear to be consistent within stated uncertainties and are summarized by Bhardwaj and Michael (1999). Table 28 also lists the emission cross sections for OI (98.9 nm) and SII (91.1 nm) from Ajello et al. (1992a), which have been renormalized using the cross sections of Vatti Palle et al. (2004) that were themselves renormalized to the newly recommended 130.4 nm cross section (see above and Table 7). Fig. 33 shows the emission cross sections from Table 28. These represent the larger emission cross sections in the VUV with many more dissociative fragments (neutral and ionized) emitting with smaller cross sections.

Vatti Palle et al. (2004) observed high resolution line profiles of some atomic S and O emissions and used a Doppler broadening deconvolution technique to determine kinetic energies of the emitting fragments. They stated peak kinetic energies of 2.0 ± 0.8 eV and 1.8 ± 0.5 eV for OI (115.2151 nm) and limits were also provided for SII (91.0485 nm), OI (135.5598 nm), and SI (147.3990 nm).

Table 28
Emission cross sections for SII (91.1 nm), OI (98.9 nm), OI (130.4 nm), and SI (147.9 nm) from SO_2

Energy	Cross section				Energy	Cross section			
(eV)	OI (130.4 nm) (10^{-18} cm^2)	SI (147.9 nm) (10^{-18} cm^2)	OI (98.9 nm) (10^{-18} cm^2)	SII (91.1 nm) (10^{-18} cm^2)	(eV)	OI (130.4 nm) (10^{-18} cm^2)	SI (147.9 nm) (10^{-18} cm^2)	OI (98.9 nm) (10^{-18} cm^2)	SII (91.1 nm) (10^{-18} cm^2)
17.5	0.01	0.00			85	2.32	1.64	1.19	0.442
20	0.04	0.10	0.002		90	2.29	1.66	1.23	0.486
22.5	0.09	0.26	0.008		95	2.30	1.64	1.25	0.511
25	0.19	0.52	0.019		100	2.30	1.63	1.27	0.557
27.5	0.24	0.74	0.032		125			1.27	0.628
30	0.31	0.94	0.050		150	2.01	1.57	1.24	0.682
32.5	0.37	1.01	0.070		175	1.91	1.48	1.14	0.715
35	0.48	1.03	0.094		200	1.73	1.36	1.07	0.673
37.5	0.74	1.04	0.135	0.009	225	1.60	1.28	0.990	0.645
40	0.98	1.06	0.177	0.034	250	1.50	1.13	0.922	0.618
42.5	1.16	1.08	0.269	0.071	275	1.41	1.09	0.871	0.574
45	1.51	1.16	0.383	0.105	300	1.34	1.00	0.802	0.531
47.5	1.64	1.21	0.475	0.145	350	1.21	0.92	0.727	0.503
50	1.80	1.22	0.625	0.187	400	1.10	0.80	0.672	0.427
52.5	1.91	1.39	0.724	0.229	450	1.01	0.73	0.620	0.385
55	2.01	1.46	0.785	0.243	500	0.95	0.63	0.527	0.356
57.5	2.09	1.49	0.857	0.278	550	0.88	0.61	0.485	0.331
60	2.10	1.54	0.917	0.293	600	0.84	0.56	0.428	0.303
65	2.16	1.59	0.967	0.319	650	0.77	0.52	0.402	0.288
70	2.22	1.60	1.02	0.353	700	0.74	0.48	0.376	0.289
75	2.26	1.62	1.08	0.396	750	0.70	0.44	0.362	0.280
80	2.27	1.63	1.14	0.417	800	0.65	0.43	0.338	0.268

The OI (130.4 nm) and SI (147.9 nm) data (from Vatti Palle et al. (2004)), which were normalized to the 130.4 nm from O_2 emission cross section of Kanik et al. (2003) at 100 eV, have been renormalized by a factor of 1.01 to reflect the new recommended value for the 130.4 nm emission cross section (see Table 7). The SII (91.1 nm) and OI (98.9 nm) data (from Ajello et al. (1992a)) have been renormalized (at 200 eV) to the renormalized data of Vatti Palle et al. (2004).

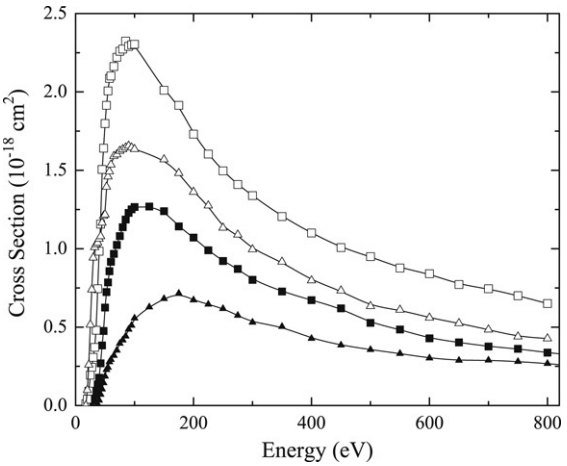

Fig. 33. Absolute emission cross sections for OI (130.4 nm) [open squares], SI (147.9 nm) [open triangles], OI (98.9 nm) [solid squares], and SII (91.1 nm) [solid triangles] from SO_2. Data from Table 28.

4.8.7. Other O–S targets

In addition to SO_2, electron impact dissociative processes with other sulfur/oxygen compounds are relevant. The SO free radical is an obvious example of a derivative O–S target species. Apps et al. (1997) and Akhmatskaya et al. (1997) investigated the adsorption interactions of SO_2 and SO_3 with large water clusters using 70 eV electron impact ionization. They observed multiple fragments, including H_2SO_4 production, a component of acid rain. Further, it was observed that SO_3 sticks to water clusters at much smaller cluster sizes (i.e. number of clustered water molecules) than was typically appreciated for atmospheric aerosols. This indicated that SO_2 derivatives can have a more serious environmental impact than previously thought, especially in drier regions. It is noteworthy that sulfur is the element with the largest number of binary oxides (S_nO_2) (Steudel, 2003).

4.8.7.1. Sulfur/oxygen radicals. Electron impact investigations with targets of sulfur/oxygen radicals (e.g. SO, SO_3, S_2O, and S_2O_2) are infrequent largely due to target preparation difficulties. However, many of these O–S targets are important in a

Table 29
Cross sections for production of O^+, S^+, and SO^+ from SO

Energy (eV)	$\sigma(O^+)$ (10^{-18} cm^2)	$\sigma(S^+)$ (10^{-18} cm^2)	$\sigma(SO^+)$ (10^{-18} cm^2)	$\sigma(\text{total}_{\text{expt.}})$ (10^{-18} cm^2)	$\sigma(\text{total}_{\text{theory}})$ (10^{-18} cm^2)
11			8	8	
12			23	23	
13			41	41	
14			58	58	
15			76	76	
16			91	91	
17		9	114	123	
18		28	133	161	
19		40	154	194	
20		58	175	233	323
22		73	189	262	
24	4	88	209	301	
26	10	101	219	330	
28	17	110	227	354	
30	24	115	236	375	440
32	27	120	242	389	
34	30	122	250	402	
36	33	124	260	417	
38	37	125	271	433	
40	40	127	279	446	462
45	42	129	300	471	
50	44	130	317	491	468
55	45	132	322	499	
60	45	134	326	505	470
70	45	132	325	502	470
80	44	129	322	495	470
90	42	125	319	486	
100	40	120	310	470	449
120	38	116	292	446	441
140	34	107	272	413	417
160	30	96	255	381	404
180	28	87	234	350	380
200	26	72	214	312	360

Also included is the derived experimental total and the calculated total (via the modified additivity rule) single ionization cross sections. From Tarnovsky et al. (1995).

number of circumstances ranging from Io's aurorae emissions to acid rain production. This is particularly the case for SO_3, which is an important pollutant acting as the primary agent in acid rain generation along with the conversion of SO_2 with water aerosols (Apps et al., 1997; Akhmatskaya et al., 1997; Seinfeld and Pandis, 1997). The NIST Chemistry WebBook lists ionization and appearance energies for fragments from many sulfur/oxygen target compounds, including SO, S_2O, and SO_3.

Tarnovsky et al. (1995) obtained a ground state target of SO via the neutralized fast beam method. Electron impact ionization from threshold to 200 eV produced expected fragments: SO^+, S^+, and O^+. Absolute total and partial ionization cross sections were obtained, as listed in Table 29. Fig. 34 shows the partial ionization cross sections, dominated by the parent ion (SO^+), and the experimental total ionization cross section. A modified additivity rule was used to obtain a theoretical estimate of the total ionization cross section. The appearance potential of the parent ion was consistent with Lias et al. (1988), but the onsets for the dissociative ions (S^+ and O^+) were slightly larger. All ions had well defined onsets. This indicated that the dissociative ions were both formed with a minimum excess kinetic energy of about 2 eV per ionic fragment and there was negligible vibrationally excited SO in the target beam.

Other electron impact dissociative studies have involved targets of SO, SO_3, S_2O, and S_2O_2. Smith and Stevenson (1981) obtained partial and total ionization cross sections for $e^- + SO_3$ from threshold to 30 eV, and $e^- + SO_2$ (see Section 4.8.1), over several temperatures using a quadrupole mass spectrometer. Target purity via SO_2 contamination is a realistic concern. Note that their SO_2 ionization cross sections were generally too small by a factor of approximately two to three. They also correctly expressed concern with fragment kinetic energy issues.

Field et al. (2005) utilized a microwave discharge, along with variable production conditions via inlet pressure changes of the He/SO_2 mixture, to generate a mixed target of SO, S_2O, and S_2O_2, along with SO_2, which was probed using a time-of-flight mass spectrometer. With the discharge off, they were able to observe consistent results with previous measurements of DEA to SO_2 (see Section 4.8.3). Significant variation in radical intensity was realized using different inlet pressure conditions. Non-trivial analysis was used to deconvolute the mixed target DEA spectra. They did not observe any resonance structure attributable to the SO radical; however, rough estimates were provided for numerous DEA cross sections from the S_2O and S_2O_2 radical targets.

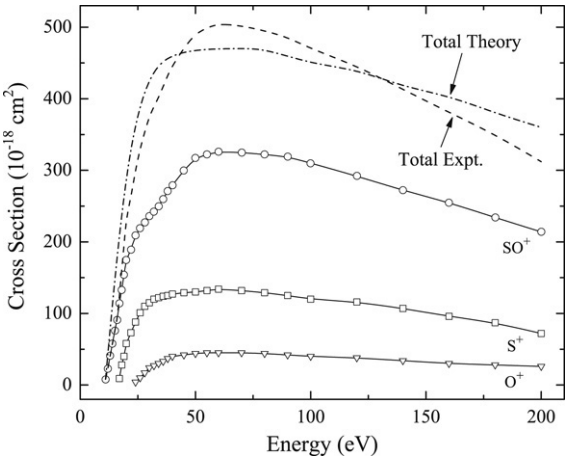

Fig. 34. Absolute cross sections for the formation of the SO^+ parent ions and S^+ and O^+ fragment ions from SO as a function of electron impact energy. Also shown are the experimental and calculated (modified additivity rule) total single ionization cross sections of SO. Data from Table 29.

4.8.7.2. SO_2^-. Studies of electron collisions with anions are relatively scarce. Seiersen et al. (2003) found no evidence for dissociation or dianion production for $e^- + SO_2^-$, only detachment excitation functions and estimated cross sections were determined.

4.9. OCS

OCS is a linear triatomic molecule with a permanent dipole moment. It is a minor pollutant in our own atmosphere, where it is believed to play a role in the atmospheric sulfur cycle (Polanyi and Young, 1990), Hines and Morrison (1992), and it is known to play a subtle role in the carbon and sulfur chemistries in such astrophysical environments as diffuse and dark interstellar clouds (van Dishoeck, 1998). It is also found as a pollutant in some low-temperature plasmas (Kawada et al., 2000).

The photoabsorption and photodissociation of OCS have been very widely studied [see, for example, Itakura et al. (2000), Sugita et al. (2000), Richter et al. (1998), Suzuki et al. (1998), Hikosaka et al. (1997), Sivarkumar et al. (1988), Tabche-Fouhaile et al. (1983), van Veen et al. (1983), Wu and Judge (1982), Eland and Berkowitz (1979), and references therein]. There have been no parallel investigations involving electron impact. Relatively little information is thus available and major gaps exist in our knowledge of various electron impact processes. However, there have been a number of significant developments since the reviews by Karwasz et al. (2001) and by Itikawa (2002). These are discussed fully below.

4.9.1. Dissociative ionization

No systematic investigation of the dissociative ionization has been carried out, and, in fact, there is considerable disagreement between the earlier measurement of the *total* ionization cross section [Srivastava, unpublished, quoted in Kim et al. (1997) and in Lindsay and Mangan (2003)] and the recent work of Hudson et al. (2004). The latter's data agree reasonably well with the DM calculations of Margreiter et al. (1990, 1994) while the former set agrees quite well with the BEB calculations of Kim et al. (1997). Hudson et al. (2004) present arguments, based on a systematic study of a number of molecules, that the DM calculations should be preferred in the case of OCS though later work (Hudson et al., 2005) casts some doubt on this conclusion. A recent single measurement at 200 eV (Wang and Vidal, 2003) is more in accord with the BEB calculations at that energy. Thus the total ionization picture for OCS is still far from being firmly established.

The only quantitative data on dissociative ionization seems to be the recent work of Wang and Vidal (2003) at a single energy of 200 eV. Using covariance mapping coincidence techniques, they obtained absolute data for the production of a wide range of fragment ions, both singly and doubly charged. The dominant fragment ion produced was S^+ followed by CO^+, C^+, O^+ and CS^+ in that order. Cross sections for other ions were very small, down by at least two orders of magnitude from that for S^+ production. Table 30 shows their results in detail. They were able to identify many of the fragmentation pathways but were unable to give any information about neutral fragments. It is perhaps worth pointing out that a lot of parallel work on the photodissociation of OCS has been carried out using coincidence techniques and synchrotron radiation [see for example Masuoka (1993), Masuoka and Doi (1993), Ankerhold et al. (1997a,b)], or atomic discharge lamps [Hsieh and Eland (1997), Eland et al. (1986)]. All of these photodissociation channels will be open for electron impact also, in addition to the spin forbidden channels that are accessible with the charged projectile.

No work has been reported on electron impact ionization of OCS clusters apart from that of Buck et al. (1991). They found evidence for dissociation of OCS in the cluster yielding S atoms, which reacted rapidly to form S_2 according to $S + OCS \rightarrow CO + S_2$. The S_2 was subsequently ionized and detected. This occurred even for very small clusters. As the cluster size increased, evidence emerged that more complicated chemical reactions were taking place. This work parallels

Table 30
Cross sections (10^{-18} cm^2) for electron impact dissociative ionization of OCS at 200 eV: (A) for the dissociation channels $OCS^+ \rightarrow X^+ + n$ or $OCS^{2+} \rightarrow X^{2+} + n$; (B) for the dissociation channels $OCS^{2+} \rightarrow X^+ + Y^+ + n$ or $OCS^{3+} \rightarrow X^{2+} + Y^+ + n$

Fragment X	σ(A)	σ(B)	$\sigma(C^{2+})$	$\sigma(O^{2+})$	$\sigma(C^+)$	$\sigma(CO^{2+})$	$\sigma(O^+)$	$\sigma(S^{2+})$	$\sigma(CO^+)$
OCS^+	152.0	152.0							
SO^+	0.258	0.244			0.014				
CS^+	11.6	10.7		0.005			0.900		
S^+	209.0	192.0	0.069	0.043	4.58	0.026	2.69		7.86
OCS^{2+}	10.1	10.1							
CO^+	63.7	55.3						0.557	
CS^{2+}	0.215	0.174					0.041		
S^{2+}							0.522		
O^+	39.6[a]	28.4[b]	0.076		4.15[c]				
CO^{2+}	0.070	0.044							
C^+	47.4	36.9		0.033					
O^{2+}	0.213	0.132							
C^{2+}	0.390	0.245							

Here, n represents the remaining columns. See the original paper for more details. From Wang and Vidal (2003).
[a] Including S^{2+}.
[b] Including $OCS^{2+} \rightarrow S^{2+} + n$.
[c] Including $OCS^{3+} \rightarrow C^+ + S^{2+} + O$.

that of Prinslow and Vaida (1989) who studied the photodissociation of $(OCS)_2$ and again found evidence for significant production of S_2.

4.9.2. Appearance energies and fragment energy distributions

Early work on dissociative ionization by electron impact was limited to measurements of fragment ion appearance energies and the spectroscopic information, for example about fragment heats of formation, which can be derived from these (Hubin-Franskin et al., 1978). These authors measured appearance energies for S^+, O^+, and CS^+. They identified the observed thresholds as being due to two-fragment break-up, with the production of a ground state ion in each case. The other partner was a ground state neutral partner, except in the case of O^+, where ion pair production occurred with a CS^- anion.

Cooks et al. (1974) carried out ion appearance and kinetic energy measurements following impact ionization to OCS^{2+} with subsequent Coulomb decay to CO^+ and S^+. They were able to identify the particular ion states involved and found that over 90% of the available energy appeared as translational kinetic energy of the fragments.

As mentioned above, considerable photoionization work is available, establishing thresholds, branching ratios etc. for the dipole allowed channels, e.g. Masuoka and Doi (1993).

4.9.3. Dissociative attachment

Dissociative attachment is very strong in OCS, relatively much more so than in the sister molecule, CO_2. S^- is the main anion formed; others such as O^- and C^- have been noted but have cross sections that are less by some two orders of magnitude (Hubin-Franskin et al., 1976; Iga et al., 1996a). Iga et al. (1996a) observed four resonance peaks leading to S^- production. These occurred at 1.4, 4.7, 7.0 and 10.2 eV. All except the 4.7 eV channel had been observed in earlier work [Dillard and Franklin (1968), MacNeil and Thynne (1969), Ziesel et al. (1975), Hubin-Franskin et al. (1976)]. The resonance peak at 1.4 eV is the strongest with an intensity about two orders of magnitude greater than the others. Good agreement in the magnitude of the peak cross section at 1.4 eV is obtained between Iga et al. (1996a) [2.6×10^{-17} cm^2] and Ziesel et al. (1975) [2.9×10^{-17} cm^2].

The energetics involved allows the dissociative attachment process represented by the 1.4 eV peak to be specified as:

$$e + OCS\ (X) \rightarrow OCS^-\ (^2\Pi) \rightarrow CO(X\,^1\Sigma^+, v) + S^-\ (^2P_u). \tag{19}$$

Abouaf and Fiquet-Fayard (1976) presented evidence that vibrational quanta up to $v = 4$ were excited. Using better energy resolution, Abouaf et al. (1994) confirmed and extended this work. The 4.7 and 7.0 eV peaks resulted in the same fragments but in each of these cases a few eV of energy was shared between kinetic energy of the fragments and ro-vibrational energy of the ground state CO(X). The 10 eV peak resulted in the formation of CO in an excited electronic state. Again some 3 eV of excess energy is shared between kinetic energy of the fragments and internal ro-vibrational excitation of the CO.

Iga et al. (1996a) also monitored the formation of the ion pair, S^- and CO^+, with an appearance energy of 15.0 eV. This agrees very well with the known threshold of 15.09 eV.

Dissociative and associative cluster anion formation have been studied with high resolution for electron attachment to OCS clusters at low energies (<0.2 eV) by Barsotti et al. (2004). They found prominent vibrational Feshbach resonances similar to the situation for CO_2 and N_2O clusters.

4.9.4. Dissociation into ground state fragments

Apart from the limited work discussed above in connection with dissociative ionization and attachment, there have been no electron impact measurements of neutral ground state fragment production in $e^- + OCS$ collisions.

4.9.5. Dissociation into neutral metastable fragments

van Brunt and Mumma (1975) studied the break-up of OCS into energetic metastable fragments. By using different types of Auger surface detectors, which were preferentially sensitive to metastables of different internal energies, they were able to observe a variety of metastable fragments including $CO(a\,^3\Pi)$, $S(^5S)$ and $O\,(^5S)$ in addition to atomic and molecular Rydberg fragments. Unfortunately they were unable to uniquely determine the particular fragments being observed. From appearance energy measurements they could be definitive about the final states of the dissociation products for only one process, namely $CO(a\,^3\Pi) + S(^3P)$. Fragment kinetic energies were typically a few eV but, again, inability to uniquely determine the fragment identity meant that the kinetic energies could not be defined more accurately. Barnett et al. (1992) carried out a very similar experiment to that of van Brunt and Mumma (1975) with rather similar conclusions. They presented evidence for a rather short ($\sim$10 μs) lifetime for $S(^5S)$ such that only a small fraction would survive to activate the detector in either experiment.

Kedzierski et al. (2001) overcame the problem of fragment identification by using their xenon matrix surface detector where they could unambiguously select $S(^1S_0)$ or $O(^1S_0)$ [see Section 2.2]. Thus they were able to demonstrate that the former species predominated, that it possessed a range of kinetic energies between 0.2 and 1.2 eV and that there was a maximum production cross section of 3.3×10^{-17} cm^2 at an electron energy of 55 eV. From the shape of the excitation function they concluded that the initial excitation in the parent molecule was optically allowed and from threshold energy measurements they were able to assign the partner fragment as CO(X) with possibly some vibrational excitation. Not remarkably, their findings were similar to those obtained from photodissociation studies (Ondrey et al., 1983; Strauss et al., 1989; Itakura et al., 2000; Wu et al., 2005).

It is well known from photodissociation studies [e.g. Kim et al. (2004)] that $S(^1D_2)$ is produced with high efficiency using photon energies around 5 eV. Clearly this channel will be open for electron impact as well.

4.9.6. Dissociative excitation

Dissociative excitation of OCS by electron impact, leading to subsequent emission from the excited fragments, is a relatively untouched field. There are no data available on emissions in the VUV. The only quantitative measurement seems to be that of Tikue et al. (1994) who measured the emission cross sections of the CS(A $\rightarrow$ X) bands in the 245–275 nm interval and for electron energies from threshold to 120 eV. They measured a band emission cross section of $0.75 \pm 0.15 \times 10^{-18}$ cm^2 at 100 eV. Although no data were obtained regarding other fragment emissions, these authors reported that the CO^+(A $\rightarrow$ X) and (B $\rightarrow$ X) bands were prominent, at 100 eV incident energy, in the wavelength regions 400–450 and 190–250 nm respectively. As part of their work on $S(^1S)$ production from OCS, Kedzierski et al. (2001) show a rich, low-resolution, emission spectrum covering the wavelength interval 350–850 nm with identified emissions from CO, CO^+, O and S. They show a relative emission cross section function for the combined 777 and 844 nm OI lines, which demonstrated that they are produced via optically allowed transitions in the parent molecule. Taylor and Eland (2005) in their photoionization experiment involving coincidences between ions, electrons and photons, demonstrated that O^+, S^+, CO^+ and CS^+ fragments all emitted photons in the wavelength range 200–500 nm. Clearly, these emissions would be expected from electron impact as well.

Tikue et al. (1994) showed from appearance energy measurements that the OCS dissociation which they were monitoring was $OCS(X) \rightarrow CS(A\,^1\Pi) + O(^3P)$. A second onset near 25 eV was probably due to the opening of the $O^+(^4S)$ production channel. Their results showed a wide range of vibrational excitation in the CS fragment and also that kinetic energy releases were significant, amounting to a few (3–4) eV. Their results suggested that the linear geometry of the molecule was preserved during the dissociation process. Clearly much work is needed to obtain a more quantitative understanding of the excited state fragmentation dynamics of OCS.

4.10. O_3

Because of its fundamental importance in the Earth's atmosphere, photon absorption and electron scattering by ozone are very relevant. Electrical discharges involving ozone are also of interest (Eliasson and Kogelschatz, 1986; Lukes and Locke, 2005). Despite this importance, the data base for electron–ozone interactions is incomplete mainly due to the difficulties involved in its production and use [see e.g. Newson et al. (1995)]. Thus in the Landolt–Börnstein data compilation (Itikawa, 2003), no *total* cross sections could be recommended. [This situation has been remedied somewhat for energies above 350 eV by the work of De Pablos et al. (2002) and Joshipura et al. (2002).] There seems to be considerable uncertainty also in the ionization cross sections (Lindsay and Mangan, 2003), both with regard to the absolute calibration and with the assigning of realistic error bars. The Karwasz et al. (2001) review included no references to any post-1999 publications. Mason (2003) summarized available data at that time and also gave references to electron impact work on O_3 clusters.

Table 31
O_3 partial ionization cross sections

Energy (eV)	Partial ionization cross section (10^{-18} cm^2)		
	O_3^+	O_2^+	O^+
40	137.4 ± 3.6	108.6 ± 2.9	17.0 ± 1.2
45	138.0	111.0 ± 2.7	24.0 ± 0.7
50	148.2 ± 5.1	126.1 ± 3.9	31.3 ± 1.4
55	155.9 ± 7.3	132.6 ± 3.4	36.6 ± 1.4
60	166.9 ± 9.2	149.4 ± 2.9	44.0 ± 2.0
65	169.5 ± 8.3	148.1 ± 2.2	46.9 ± 1.7
70	173.9 ± 5.5	163.7 ± 3.1	51.8 ± 3.4
75	174.2 ± 2.2	158.8 ± 1.4	55.1 ± 2.2
80	179.9 ± 4.6	168.6 ± 2.2	59.3 ± 3.1
85	178.5 ± 4.4	164.4 ± 3.1	60.5 ± 3.7
90	179.7 ± 4.2	166.6 ± 2.1	63.4 ± 3.9
95	179.9 ± 4.8	164.6 ± 3.1	64.1 ± 4.1
100	180.2	168.3	64.3 ± 2.4
152	171.2 ± 6.1	147.2 ± 3.2	62.0 ± 6.3
200	163.0 ± 1.9	143.5 ± 5.3	56.8 ± 5.3
259	154.9 ± 6.1	140.6 ± 4.8	53.4 ± 3.9
306	145.2 ± 6.8	129.4 ± 2.0	47.8 ± 2.7
355	135.5 ± 4.6	119.0 ± 1.9	44.2 ± 2.4
413	128.7 ± 9.2	115.4 ± 1.7	42.5 ± 1.9
462	115.9 ± 9.9	96.0 ± 0.7	37.6 ± 1.9
509	117.3 ± 3.6	110.3 ± 0.8	39.3 ± 2.7

Data are from Newson et al. (1995) renormalized by a factor of 1.7 as discussed in the text.

4.10.1. Dissociative ionization

The only experimental data available on dissociative ionization cross sections are those of Siegel (1982) and Newson et al. (1995). The latter data were normalized to the former at 100 eV and cover the range 40–509 eV. Siegel (1982) used a modulated beam quadrupole mass spectrometer system for his measurements. His absolute calibration was by means of comparison with rare gas cross sections, particularly that of argon at 60 eV incident energy. His system was not ideal for absolute cross section determination because of potential problems with target density determination (e.g. some Ar could have been frozen out in the liquid oxygen-cooled trap in the gas inlet line), beam profile differences for different gases and efficiency of detection of fragments with non-thermal energies. Recent determinations [see Straub et al. (1995)] of the Ar reference cross section are slightly higher (∼10%) than adopted by Siegel (1982) and thus some increase in the ozone data is warranted based on that factor alone. However it appears that a more significant correction factor of 1.7 should be applied.

The rationale for this correction factor is as follows: the semi-empirical BEB model of Kim et al. (1997) would be expected to give a good representation of the total ionization cross section based on its performance for similar triatomic molecules like N_2O or SO_2; in fact it suggests numbers that are higher than the experimental ones by the factor given. Further, recent theoretical work by Joshipura et al. (2002) agrees very well with the predictions of Kim et al. Finally, if these higher values are accepted for the ionization cross sections and used with other calculated values, which go to make up the total electron scattering cross section, then good agreement is achieved with the total cross section measurements of De Pablos et al. (2002).

Based on this we present, in Table 31 and Fig. 35, renormalized cross sections for production of O_2^+ and O^+ from O_3 as a function of incident electron energy. No data are available on the production of multiply charged ion fragments. Clearly additional experimental work on O_3 ionization is desirable.

4.10.2. Appearance energies and fragment energy distributions

Siegel's (1982) apparatus was not suitable for accurate appearance energy measurements but he was able to observe thresholds for O_3^+ and O_2^+ production, which were consistent with photoionization [Rosenstock et al. (1977)] data (12.67 and 13.14 eV respectively). His measured appearance energy for O^+ production was a few eV higher than expected, leading Siegel to suggest that the ion-pair production channel, namely

$$e + O_3 \rightarrow O^+ + O^- + O + e' \tag{20}$$

could be dominant near threshold. Alternatively, his apparatus might have discriminated against super-thermal fragments, which could have resulted from two-fragment break-up.

More recently, Probst et al. (2002) obtained a value of 12.70 ± 0.02 eV for the electron impact appearance potential of the O_3^+ cation but, because of background contamination problems with O_2, they were unable to measure threshold values for the other ionic fragments. They were able to get data for the dimer species also. There is a clear need for more work in this area.

Table 32
Cross sections for production of O^- and O_2^- from O_3

Energy (eV)	$\sigma(O^-)$ (10^{-18} cm^2)	$\sigma(O_2^-)$ (10^{-18} cm^2)	σ(total) (10^{-18} cm^2)	Energy (eV)	$\sigma(O^-)$ (10^{-18} cm^2)	$\sigma(O_2^-)$ (10^{-18} cm^2)	σ(total) (10^{-18} cm^2)
0.0	8.06	2.00	10.06	5.1	1.31	0.14	1.45
0.1	7.50	2.22	9.72	5.2	1.03	0.14	1.17
0.2	6.92	1.80	8.72	5.3	0.72	0.15	0.87
0.3	8.20	2.00	10.20	5.4	0.59	0.16	0.75
0.4	10.01	2.16	12.17	5.5	0.76	0.17	0.93
0.5	11.94	3.06	15.00	5.6	1.06	0.17	1.23
0.6	14.69	4.02	18.71	5.7	1.27	0.19	1.46
0.7	18.70	6.24	24.94	5.8	1.39	0.20	1.59
0.8	20.87	8.64	29.51	5.9	1.37	0.21	1.58
0.9	24.88	11.88	36.76	6.0	1.67	0.22	1.89
1.0	28.24	13.26	41.50	6.1	1.82	0.24	2.06
1.1	31.58	15.00	46.58	6.2	2.12	0.25	2.37
1.2	36.21	16.80	53.01	6.3	2.31	0.27	2.58
1.3	37.03	15.48	52.51	6.4	2.56	0.28	2.84
1.4	37.21	14.16	51.37	6.5	2.79	0.30	3.09
1.5	36.47	11.52	47.99	6.6	3.07	0.31	3.38
1.6	34.67	9.30	43.97	6.7	3.92	0.32	4.24
1.7	31.29	6.96	38.25	6.8	3.72	0.32	4.04
1.8	27.97	4.68	32.65	6.9	4.36	0.33	4.69
1.9	23.78	3.96	27.74	7.0	4.98	0.34	5.32
2.0	21.11	2.28	23.39	7.1	5.56	0.34	5.90
2.1	19.05	1.86	20.91	7.2	5.71	0.34	6.05
2.2	15.99	1.56	17.55	7.3	6.01	0.33	6.34
2.3	13.30	1.20	14.50	7.4	6.31	0.33	6.64
2.4	11.51	0.60	12.11	7.5	5.71	0.32	6.03
2.5	11.25	0.69	11.94	7.6	6.08	0.31	6.39
2.6	9.59	0.30	9.89	7.7	5.86	0.30	6.16
2.7	8.93	0.24	9.17	7.8	5.03	0.29	5.32
2.8	8.63	0.24	8.87	7.9	5.35	0.29	5.64
2.9	9.18	0.18	9.36	8.0	5.30	0.26	5.56
3.0	8.47	0.18	8.65	8.1	4.07	0.25	4.32
3.1	8.94	0.18	9.12	8.2	3.89	0.23	4.12
3.2	8.25	0.19	8.44	8.3	3.58	0.22	3.80
3.3	8.20	0.20	8.40	8.4	2.58	0.20	2.78
3.4	7.85	0.21	8.06	8.5	2.46	0.18	2.64
3.5	7.66	0.20	7.86	8.6	1.81	0.16	1.97
3.6	6.86	0.20	7.06	8.7	1.37	0.14	1.51
3.7	6.62	0.19	6.81	8.8	1.35	0.13	1.48
3.8	6.12	0.18	6.30	8.9	1.01	0.11	1.12
3.9	6.29	0.18	6.47	9.0	0.79	0.10	0.89
4.0	5.53	0.17	5.70	9.1	0.60	0.08	0.68
4.1	4.62	0.16	4.78	9.2	0.43	0.07	0.50
4.2	4.00	0.16	4.16	9.3	0.38	0.06	0.44
4.3	3.85	0.16	4.01	9.4	0.31	0.06	0.37
4.4	2.84	0.16	3.00	9.5	0.19	0.05	0.24
4.5	2.77	0.15	2.92	9.6	0.42	0.05	0.47
4.6	2.34	0.14	2.48	9.7	0.31	0.05	0.36
4.7	2.10	0.14	2.24	9.8	0.19	0.05	0.24
4.8	2.00	0.14	2.14	9.9	0.16	0.04	0.20
4.9	1.77	0.14	1.91	10.0	0.17	0.04	0.21
5.0	1.08	0.14	1.22				

The total attachment cross section is given also. From Lindsay and Mangan (2003).

4.10.3. Dissociative attachment

Of all the possible interactions between electrons and ozone, the one that has received most study is the dissociative attachment channel. This is understandable given its importance in both atmospheric and industrial settings, Senn et al. (1999a,b,c,d). Equations that govern the excitation and decay of the molecular resonance yielding anions are:

$$O_3 + e^- \rightarrow [O_3^-] \rightarrow O^- + O_2 \tag{21a}$$

$$\rightarrow O_2^- + O. \tag{21b}$$

Karwasz et al. (2001) have pointed out in their review that there is reasonable agreement between the recent measurements for the energy positions of the peaks in the dissociative attachment cross section and in the magnitude of the prominent O^- peak at 1.3 eV. However, Lindsay and Mangan (2003) recommend the data set of Rangwala et al. (1999) because of their ability to measure ions efficiently over a wide kinetic energy range. Allan et al. (1996a,b) and Walker et al. (1996) showed that many of the anions formed possessed considerable (1–2 eV) kinetic energies, particularly the

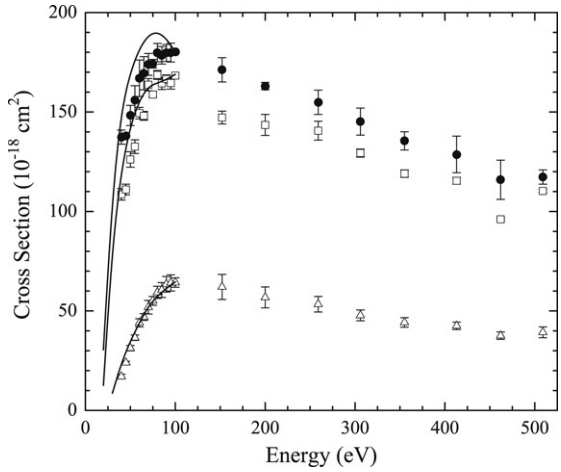

Fig. 35. Ionization in ozone leading to O_3^+ [solid circles], O_2^+ [open squares], and O^+ [open triangles]. Data from Newson et al. (1995) [Table 31] and Siegel (1982) [solid lines] renormalized as discussed in the text.

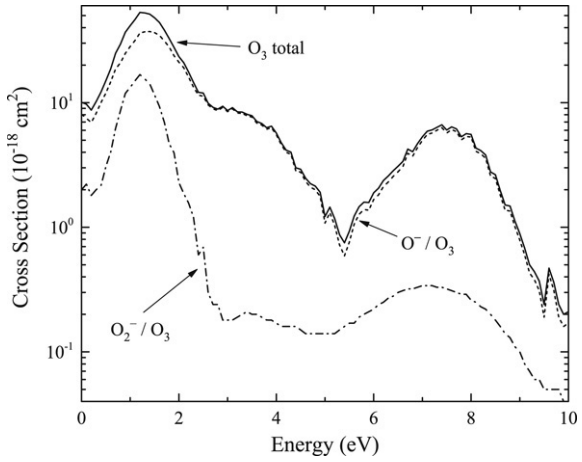

Fig. 36. Partial and total attachment cross sections following electron impact on ozone. From Lindsay and Mangan (2003).

ones observed at higher (∼10 eV) incident electron energies. Recently, Cicman et al. (2003) did a careful analysis of the ion trajectories in their system and found that the previous data of Senn et al. (1999a) had to be significantly adjusted to take account of ion discrimination effects, which occurred for ions with significant amounts of kinetic energy. Their revised data are now in quite good agreement with those of Rangwala et al. (1999). Nestmann et al. (2005a,b) have provided theoretical insight for the identification of the resonance responsible for the 1.3 eV peak.

Table 32 and Fig. 36 give the partial and total attachment cross sections of ozone. We note that Senn et al. (1999a) found a very sharp peak in the O^- production spectrum at zero incident electron energy when they were using energy resolutions of approximately 30 meV, considerably better than was used in much of the previous work. Senn et al. estimated that the cross section for production of this feature was at least 4 times greater than the feature at 1.3 eV, which had previously dominated the spectrum. However, later work by this group (Cicman et al., 2007) revealed that this low energy peak was an artefact of the apparatus.

As mentioned above, many of the anions are released with considerable kinetic energy. This was investigated by Allan et al. (1996a,b) and, with poorer energy resolution, by Walker et al. (1996). They found that the O^- anions formed at the higher incident energies had kinetic energies of $\geq$2 eV. Most of the anions produced via the 1.3 eV peak had energies less than 0.2 eV. Allan et al. also showed data which strongly suggested that the partner molecule in (21a) was vibrationally excited.

4.10.4. Dissociation into ground state fragments

Apart from some of the ionization processes discussed above where the accompanying fragment was in its electronic ground state, there do not appear to be any direct measurements of ground state fragment production following electron impact.

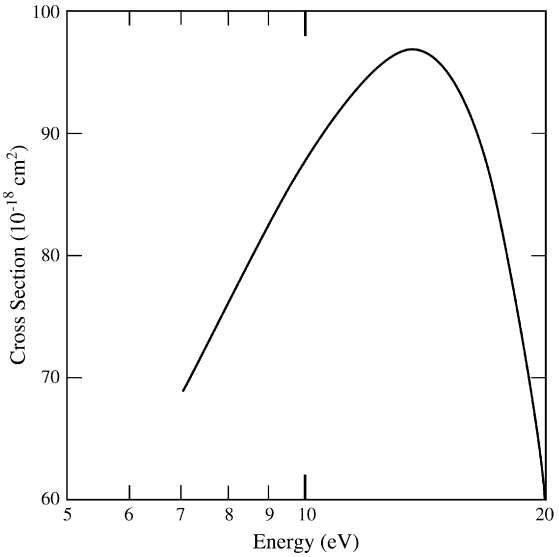

Fig. 37. Integral cross section for electron impact excitation of the Hartley band of O_3. From Brunger et al. (2003).

4.10.5. Dissociation into neutral metastable fragments

Although it is well known that UV Hartley-band dissociation of ozone around 254 nm results in $O(^1D_2)$ and $O_2(^1\Delta_g)$ metastable production [see e.g. Qu et al. (2005)], there have been no quantitative investigations of this electron impact dissociation channel apart from the energy-loss measurements of Sweeney and Shyn (1996) and Allan et al. (1996b). These works were not able to specify the end products of the electron–ozone interaction. The recommended integral cross sections for Hartley-band excitation are shown in Fig. 37 adapted from Brunger et al. (2003).

4.10.6. Dissociative excitation

To the authors' knowledge there have been no quantitative reports of photon emission in any wavelength region following dissociative excitation of ozone by electrons.

4.11. OClO

The OClO molecule is bent and belongs to the C_{2v} symmetry group. At the equilibrium geometry, the Cl–O bond length is 1.471 Å and the angle OClO is 117.5° [Flesch et al. (1993)]. Chlorine dioxide plays an important part in the ozone chemistry of the Earth's stratosphere as it acts as a night-time Cl reservoir, which then releases Cl for ozone destruction during the day. Like ozone, it is tricky to handle experimentally because of its tendency to decompose on surfaces and because of its explosive character. This may be the reason why there are relatively few studies of its dissociation, particularly when electron impact is involved. A particular example of the difficulties introduced into measurements involving this target gas is seen when considering total cross section measurements. Gulley et al. (1998) reported data for total cross sections in the electron energy range 9 meV–10 eV. Two years later, this group realized that there were problems with the purity of their gas source and increased their cross section data by a factor of 3.8 (Field et al., 2000). These authors caution that their revised results represent a lower limit to the cross section. No recommended data are listed in the Landolt–Börnstein compilation (Itikawa, 2003).

4.11.1. Dissociative ionization

Relatively little work has been reported on cation production in OClO following electron impact. A 150 eV mass spectrum obtained by O'Connor et al. (1998) indicates that O^+, O_2^+, Cl^+, ClO^+ and their Cl isotopes are all detected, with ClO^+ being the dominant fragment species. These authors measured relative partial ionization cross sections for electron energies from 30–450 eV. They noted that their apparatus discriminated against ions with non-thermal kinetic energies but argued that the majority of their ions had energies <0.3 eV. They also carried out coincidence measurements to show that the following reactions occurred:

$$e + OClO \rightarrow OClO^{2+} + 2e' \rightarrow O^+ + ClO^+ + 2e' \quad (22a)$$

$$\rightarrow O^+ + Cl^+ + O + 2e'. \quad (22b)$$

Significant fragment kinetic energies were observed in these Coulomb explosion-type reactions.

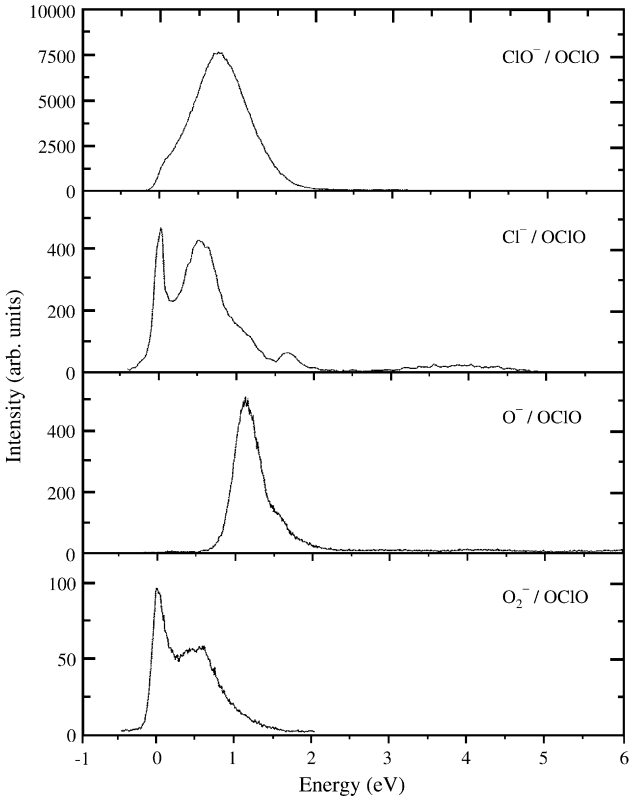

Fig. 38. Negative ion production in OClO as a function of incident electron energy. From Senn et al. (1999a,b,c,d).

4.11.2. Appearance energies and fragment energy distributions

Probst et al. (2002) have measured the appearance energy of ClO^+ and found good agreement between their value (13.37 ± 0.03 eV) and data obtained by photoionization techniques. They were not able to make similar measurements for the O^+ and O_2^+ ions because of background O_2 impurity in their target. These authors also made some measurements with the dimer species, $(OClO)_2$. Probst et al.'s appearance energy measurement for ClO^+ was slightly lower than earlier electron impact values, namely 13.5 ± 0.1 eV (Fisher, 1967) and 13.55 eV (Baluev et al., 1963). Appearance energies for the other fragment ions have been measured by Rockland et al. (1995).

4.11.3. Dissociative attachment

There have been no recent studies of dissociative attachment since the works of Marston et al. (1998) and Senn et al. (1999b). The data of Marston et al. were seriously contaminated with a Cl_2 impurity but they were able to confirm peaks in the attachment cross section at energies of 0.7, 4.3 and 8 eV in agreement with earlier work (Meinke et al., 1991). Both symmetric and non-symmetric dissociation processes seemed to be involved.

Senn et al. (1999b) have updated and extended their earlier work (Meinke et al., 1991). They identified four different anion fragments as given in (23)(a)–(d),

$$e + OClO \rightarrow O + ClO^- \quad (23a)$$

$$\rightarrow O_2 + Cl^- \quad (23b)$$

$$\rightarrow Cl + O_2^- \quad (23c)$$

$$\rightarrow ClO + O^-. \quad (23d)$$

Fig. 38 shows the negative ion production as a function of incident electron energy. The dominant channel, more than twenty times larger than any of the others, is for ClO^- production with a peak at an electron energy of 0.7 eV. Distinct peaks are observed near zero energy on the Cl^- and O_2^- curves. It is unclear whether these are connected with the structure observed near zero energy in the total scattering work of Gulley et al. (1998) and Field et al. (2000). Senn et al. (1999b) note also the presence of weak signals at 4 and 8 eV in both the Cl and O anion production channels. These peaks are in agreement in energy position with Marston et al. (1998). We note that, since these higher energy peaks are more likely to be associated with substantial kinetic energy releases, their magnitude may be underestimated in the work of Senn et al. (1999b). We recall that this problem was evident in the work of this group with ozone (Cicman et al., 2003) (see Section 4.10.3). It is

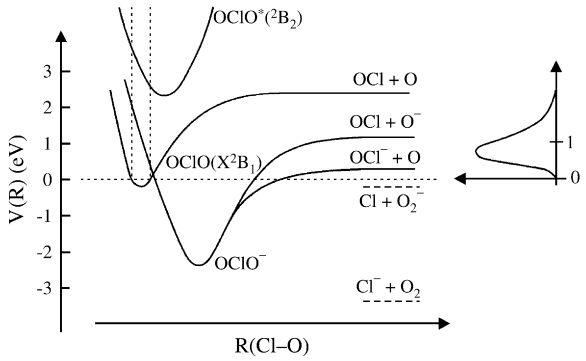

Fig. 39. Schematic potential energy diagram illustrating dissociative attachment along the OCl–O coordinate. Reproduced with permission from Senn et al. (1999b).

likely that these higher energy resonances are core excited resonances associated with electronically excited neutral states in the 2.5–4.5 eV region and with optically forbidden quartet states near 8 eV (Marston et al., 1998). Baluja et al. (2001) have carried out *R*-matrix calculations of OClO excitation by electrons. They predict a number of shape resonances above 2.5 eV whose energies agree approximately with those measured experimentally in this energy region. We note that there is a sharp peak in the Cl^- yield at 1.7 eV, which is the threshold for complete fragmentation into $Cl^- + O + O$, Senn et al. (1999b).

Senn et al. (1999b) estimate the magnitude of the dissociative attachment cross section at the 0.7 eV peak to be 8×10^{-16} cm^2. They appear to have used the SF_6 thermal attachment cross section to normalize their data. No estimate of the error involved in this procedure is given. Wecker et al. (1981) used an ECR technique to obtain an absolute value for the attachment rate coefficient of *thermal* electrons to OClO of $k_a = (1.5 \pm 0.5) \times 10^{-10}$ cm^3 s^{-1} corresponding to an attachment cross section of 1.5×10^{-17} cm^2. In view of the uncertainties here, it is desirable that a new quantitative measurement of the dissociative attachment cross section in OClO at 0.7 eV be carried out.

Since formation of OCl^- or O^- results from a simple O–ClO bond cleavage, these mechanisms may be represented by the two-dimensional potential energy diagram shown in Fig. 39. This illustrates dissociative attachment occurring along the OCl–O coordinate. From the energetics of the situation, Senn et al. (1999b) argue that all four ion production channels are associated with the same shape resonance representing ground state $OClO^-$. Estimates of the kinetic energy distributions of the various ions indicate that average kinetic energies are below 1 eV. In the case of channel (23b), where some 4 eV is available, this means that the O_2 molecular partner must possess considerable vibrational excitation. Similar arguments indicate that the molecular partner in process (23c) will only be moderately excited.

4.11.4. Dissociation into neutral fragments

Apart from the processes discussed above, where ground state neutral fragments were produced with an ionized partner, there are no direct measurements of dissociation into neutral ground or metastable fragments.

4.11.5. Dissociative excitation

Dissociation of OClO with production of short-lived fragments emitting optical radiation anywhere in the spectral range from VUV to near-IR has not been studied. This remains an obvious gap in our knowledge base relative to this molecule.

4.12. Alcohols, CH_3OH, C_2H_5OH, etc

There has been interest in the electron impact cross sections of the alcohols because of their many industrial applications, because of their discovery in interstellar space and in the atmospheres of the planets (Keating et al., 1987; Kissel and Kruger, 1995; Allamandola, 1992)) and because of their importance in understanding radiation damage in biological systems (Bouchiha et al., 2007). As far as electron impact interactions are concerned, few studies are available. Methanol (CH_3OH) has received the most attention, as discussed in the following sections. Other alcohols such as ethanol (C_2H_5OH), propanol (C_3H_7OH), butanol (C_4H_9OH) and allyl alcohol (C_3H_5OH) have also been considered. Helpful information relative to fragmentation patterns etc. is available from the NIST Database (Mallard and Linstrom, 2000).

4.12.1. Dissociative ionization

Cation production in the alcohols following electron impact has been studied by Djuric et al. (1989) and Hudson et al. (2003) (total ionization cross sections only), by Srivastava et al. (1996) (methanol only), by Rejoub et al. (2003) (total and partial cross sections for methanol, ethanol and l-propanol) and by Zavilopulo et al. (2005a,b) (fragment ion appearance energies and relative cross sections for methanol, ethanol and butanol). Lindsay and Mangan (2003) recommend cross

Table 33
Absolute partial ionization cross sections for electron impact on methanol, where $n = 0$–4

Energy (eV)	$\sigma(CH_nO^+)$ (10^{-18} cm^2)	$\sigma(CH_n^+ + H_nO^+)$ (10^{-18} cm^2)	$\sigma(H^+)$ (10^{-18} cm^2)	$\sigma(H_2^+)$ (10^{-18} cm^2)	σ(total) (10^{-18} cm^2)
13	15.1 ± 1.2				15.1 ± 1.2
14	33.5 ± 2.7				33.5 ± 2.7
16	60.9 ± 4.3	1.5 ± 0.3			62.4 ± 4.3
18	91.3	6.3 ± 0.6			97.6
20	122	11.5 ± 0.9			133
22.5	160	21.4 ± 1.7			181
25	195	29.8			225
30	239	42.8	3.79 ± 0.30	0.32 ± 0.08	286
35	274	56.3	8.92	0.93 ± 0.09	341
40	298	67.3	15.2	1.59 ± 0.13	382
50	328	82.1	26.2	3.28 ± 0.26	440
60	339	90.1	35.5	4.72	470
80	348	99.8	48.8	6.04	503
100	337	101	53.0	6.45	498
125	330	98.0	55.3	6.02	489
150	318	93.0	54.0	5.66	471
200	286	84.7	46.8	4.88	422
300	241	68.6	35.4	3.55	349
400	205	57.1	27.0	2.77	291
500	179	48.8	22.3	2.16	252
600	162	43.5	18.6	1.89	226
800	133	35.2	14.2	1.40	184
1000	114	29.5	11.7	1.13	157

From Rejoub et al. (2003).

Table 34
Absolute partial ionization cross sections for electron impact on ethanol, where $n = 0$–6

Energy (eV)	$\sigma(C_2H_nO^+)$ (10^{-18} cm^2)	$\sigma(CH_nO^+ + C_2H_n^+)$ (10^{-18} cm^2)	$\sigma(CH_n^+ + H_nO^+)$ (10^{-18} cm^2)	$\sigma(H^+)$ (10^{-18} cm^2)	$\sigma(H_2^+)$ (10^{-18} cm^2)	σ(total) (10^{-18} cm^2)
16	86 ± 16	82 ± 22				168 ± 27
18	94 ± 11	142 ± 28				236 ± 30
20	107 ± 9	174 ± 17				281 ± 19
22.5	119 ± 10	209 ± 21				328 ± 23
25	132 ± 11	243 ± 24				375 ± 26
30	143	303	24 ± 5			470
35	149	349	42 ± 9	0.48 ± 0.11		540
40	159	385	58 ± 10	7.0 ± 0.6		609
50	168	427	83 ± 10	18.2 ± 1.5	2.00	698
60	174	452	97	28.2	3.30	755
80	173	469	112	41.5	4.45	800
100	170	454	114	48.2	4.84	791
125	163	432	109	45.5	4.77	754
150	156	398	96.5	40.0	4.11	695
200	140	364	81.7	30.4	3.85	620
300	124	319	61.8	23.3	3.16	531
400	109	272	51.2	19.2	2.88	454
500	97.7	242	45.7	15.8	2.26	403
600	88.8	221	41.9	14.1	1.91	368
800	74.3	191	35.3	10.7	1.83	313
1000	63.5	172	31.6	9.48	1.58	278

From Rejoub et al. (2003).

section values for total ion production and also for certain fragment ions that could be readily identified. These partial ionization cross sections are given in Tables 33–35, while Fig. 40 gives a sample of the graphed data.

When the partial ionization cross sections are summed, there is quite good agreement between the different experiments for methanol and ethanol but not for l-propanol. The semi-classical DM calculation of Deutsch et al. (2000) reproduces the measured methanol total cross section quite well.

Rejoub et al.'s apparatus was limited in mass resolution so they were only able to present data for groups of ions of similar mass. In the case of methanol, Srivastava et al. obtained much better mass resolution (see Fig. 41) using a quadrupole mass analyzer but may have had some detection efficiency problems and seem to have incorrectly identified their H_2^+ peak. They do not mention any H^+ production even though this species is clearly more evident on Rejoub et al.'s spectra than H_2^+. Rejoub et al. suggest that the most accurate partial cross sections for the heaviest mass fragment ions can be obtained by combining their composite cross sections with the relative abundances of the individual ions reported by Srivastava et al. It is important that data be obtained for the other alcohols with sufficient resolution that the cross sections for all the fragment ions can be

Table 35
Absolute partial ionization cross sections for electron impact on l-propanol, where $n = 0$–8

Energy (eV)	$\sigma(C_3H_nO^+)$ (10^{-18} cm^2)	$\sigma(C_2H_nO^+ + C_3H_n^+)$ (10^{-18} cm^2)	$\sigma(CH_nO^+ + C_2H_n^+)$ (10^{-18} cm^2)	$\sigma(CH_n^+ + H_nO^+)$ (10^{-18} cm^2)	$\sigma(H^+)$ (10^{-18} cm^2)	$\sigma(H_2^+)$ (10^{-18} cm^2)	σ(total) (10^{-18} cm^2)
16	53 ± 18		130 ± 35				183 ± 39
18	49 ± 12	22 ± 22	171 ± 38				242 ± 46
20	73 ± 18	41 ± 20	253 ± 56				367 ± 62
22.5	64 ± 11	51 ± 11	291 ± 35				406 ± 38
25	89 ± 11	69 ± 12	387 ± 43				545 ± 46
30	92 ± 11	117 ± 20	536 ± 48				745 ± 53
35	103 ± 12	130 ± 16	637 ± 51				870 ± 55
40	112 ± 13	136 ± 16	683		10 ± 5		941
50	118 ± 14	142 ± 17	711	46 ± 14	17.1 ± 2.7	0.9 ± 0.5	1035
60	119	148 ± 15	718	63 ± 19	24.9 ± 3.0	5.0 ± 1.5	1078
80	117	144 ± 14	728	74	33.4	4.2	1101
100	108	146	695	76	41.1	4.7	1071
125	101	143	676	72	39.5	4.2	1036
150	94.1	133	654	69	37.4	3.7	991
200	87.9	122	597	63	34.4	3.5	908
300	72.8	99.9	503	51	27.2	3.1	757
400	64.5	79.8	421	37	23.1	2.4	628
500	56.1	72.6	370	31	18.2	1.6 ± 0.8	550
600	52.1	69.7	337	26 ± 8	16.3		501
800	46.3	63.6	301	34 ± 22	12.6		458
1000	40.2	58.2	283	30 ± 15	10.3 ± 1.2		422

From Rejoub et al. (2003).

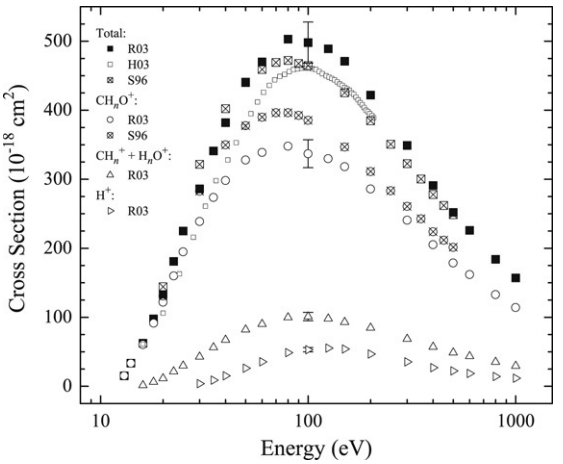

Fig. 40. Total and partial ionization cross sections in methanol. Data are identified in the legend where R03 represents Rejoub et al. (2003), H03 represents Hudson et al. (2003), and S96 represents Srivastava et al. (1996).

quantified. Zavilopulo et al. (2005a,b) present a mass spectrum of butanol, which seems to have adequate resolution but no quantitative cross section data are given.

For all alcohols studied the dominant fragment cation species was CH_3O^+. CH_3OH^+ was observed to be strong following methanol ionization but was weak or absent when other parents were considered. Clear groupings of fragment ions were observed with all of the targets. These were H_x, CH_x, C_xH_y, CH_xO and C_xH_yO, where x and y could have various values depending on the target molecule. A significant limitation in these studies follows from the difficulty of unambiguous identification of the fragments. Thus CO^+ and $C_2H_4^+$, with identical masses, could not be distinguished nor could HCO^+ and COH^+.

Rejoub et al. (2003) compared data from methanol and deuterated methanol targets and found identical cross sections to within ± 2% for most of the comparable fragments. However they did note that the cross section for CH_x^+ production from CH_3OH was about 15% smaller than CD_x^+ from CD_3OD. Further experiments with better mass resolution are needed to clarify this situation.

We note that alcohol, particularly methanol, clusters have been widely studied also [see e.g. El-Shall et al. (1992), Vaidyanathan et al. (1992), Choi et al. (1993), Ahmed et al. (1994, 1995), Buck and Huisken (2000), Yang et al. (2005)].

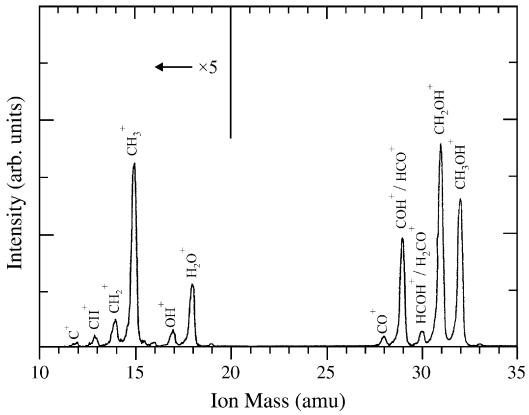

Fig. 41. Mass spectrum of CH_3OH at 100 eV incident electron energy. Note that the relative intensities have not been corrected for any variation of detection efficiency with mass. Reused with permission from S.K. Srivastava, Journal of Geophysical Research, 101, 26155 (1996).

4.12.2. Appearance energies and fragment energy distributions

Appearance energies for eleven different cationic fragments from methanol have been given by Srivastava et al. (1996), see Fig. 41. Zavilopulo et al. (2005b) list appearance energy data for four cations from methanol, seven from ethanol and one (CH_3O^+) from butanol, though they claim to have measured appearance energies for many more. For the listed appearance energies, reasonable (within 0.5 eV) agreement was obtained with the NIST data set (Lias, 2003). Zavilopulo et al. (2005b) do not give error estimates but list their appearance energies to a precision of 10 meV. This does not seem to be consistent with the quoted energy resolution of their ionizing electron beam of approximately 0.5 eV. Srivastava et al.'s (1996) appearance energy data are often significantly higher than earlier work. For example, their onset for CH_3^+ was 17.56 eV, some 4 eV higher than the data of Haney and Franklin (1968). Similarly, their value for the appearance energy of CH_3O^+ was 13.12 eV compared to the average value of seven determinations listed in the NIST compendium (Lias, 2003) of 11.65 eV. This last number is in close agreement with the photoionization threshold value of 11.649 ± 0.003 eV listed by Lias (2003). This lack of precise knowledge of the appearance energies precludes any definite conclusions regarding the particular dissociation channels that are open at threshold and the energy that might be released as kinetic energy of the fragments. Clearly additional work is required in this area.

4.12.3. Dissociative attachment

Apart from some very early work of Von Trepka and Neuert (1963) the most extensive dissociative attachment work reported prior to 1990 seems to be that of Kühn et al. (1988). They investigated the formation and dissociation of negative ion resonances in methanol, different deuterated methanol molecules and allyl alcohol using a combination of TOF and quadrupole mass spectroscopy. They were able to identify the different anions and measure their kinetic energy. They studied O^-, OH^- and CH_3O^- production but, for experimental reasons, were unable to monitor H^-. Von Trepka and Neuert (1963) had identified H^- as one of the products of dissociative attachment and this was confirmed by Prabhudesai et al. (2005b) who found that three resonances were involved at 6.4, 7.9 and 10.2 eV. Very similar resonance positions were obtained by Skalicky and Allan (2004) and in recent *R*-matrix calculations (Bouchiha et al., 2007).

Kühn et al. (1988) found that electron attachment by methanol (and the deuterated species) predominantly occurred within a resonance near 10.5 eV. The more recent works of Curtis and Walker (1992) and Prabhudesai et al. (2005b) indicate strong resonances at lower energies also that produce H^-. Measurements on the deuterated species indicated that H^- produced via the 10.5 eV resonance originated from the C site whereas H^- produced via the lower energy resonances came from the O site.

In allyl alcohol, Kühn et al. (1988) found that negative ion formation occurred via a low energy resonance (at 1.7 eV) in addition to contributions at higher energies. This is in distinct contrast to what Kühn et al. had observed in the other alcohols. Another contrasting fact was that O^- production did not occur at all in allyl alcohol while it was the most abundant ion generated in the other alcohols. Clearly additional quantitative work remains to be done in this important area so that the different formation and decay channels can be put on an absolute basis.

4.12.4. Dissociation into ground state fragments

The only work reported here seems to be the preliminary studies by the Windsor Group (Darrach and McConkey, 1992; Harb, 2003). They used LIF techniques to probe OH(X) produced in electron impact dissociation of methanol but were not able to put their data on a reliable quantitative footing.

4.12.5. Dissociation into neutral metastable fragments

No measurements have been reported on dissociation into neutral metastable or Rydberg fragments.

4.12.6. Dissociative excitation

Donahue et al. (1977) have studied optical emission following electron impact dissociation of methanol in the energy range from threshold to 2 keV and in the spectral range from 180–500 nm. Regrettably no results in the VUV or IR regions, where the main O emissions are located, are available. Emissions from atomic H (Balmer series) and C, in addition to bands of $CH(A \rightarrow X)$, $CH^+(B \rightarrow A)$, $OH(A \rightarrow X)$ and $CO^+(B \rightarrow X)$ were studied. The threshold and high energy behaviour of the various features were investigated but no absolute data were obtained. Onsets for fragment emissions were found to be considerably higher than the thermodynamic limits indicating that a considerable amount of excess energy was available for translational or internal energy of the fragments. Both optically allowed and optically forbidden processes were identified from the high-energy Fano plots.

4.13. N_2O_5

Dinitrogen pentoxide, N_2O_5, plays a major role in Earth's atmospheric chemistry. In the stratosphere it is one of the major reservoir molecules for nitrogen oxides, NO_x, which are intimately involved in stratospheric ozone depletion (Solomon et al., 1986; Tolbert and Toon, 2001). At lower altitudes in the troposphere N_2O_5 is a key component of acid rain and is involved in the atmospheric circulation of other minor species such as $ClNO_2$ (Hoffman et al., 2003). It exists in equilibrium with NO_3, the major night-time oxidant (Thrush, 1988).

Despite its importance, very little quantitative information is available on N_2O_5 dissociation pathways and cross sections. This is at least partly due to the difficulty of preparing it in pure form and to its tendency to decompose on surfaces. The information that is available is limited to cation and anion production as discussed below.

4.13.1. Dissociative ionization

Apart from some very early work (Liuti et al., 1968) in which the fragment ions NO^+ and NO_2^+ were observed following electron impact on N_2O_5 at a nominal energy of 11.5 eV, only three attempts have been made to obtain detailed ionization information. O'Connor et al. (1996) reported relative partial ionization cross sections for incident energies between 35 and 444 eV. They point out that their system discriminates strongly against ions with translational energies greater than 0.3 eV but they claim, based on comparisons with other smaller triatomic molecules, that such ions were a negligible fraction of the total. In addition to the ions observed in the earlier work, they identified O^+ and N^+ fragments. O^+ but not N^+ had been observed in earlier *photo*-dissociation work (Jochims et al., 1992). O'Connor et al. (1997) extended this work using coincidence techniques to study electron impact double ionization of N_2O_5 with subsequent Coulomb explosion into ion pairs. Five different channels were identified with different resultant ion pairs. They argued that their data were consistent with initial break-up into $NO_3^+ + NO_2^+$ followed by subsequent dissociation to produce the detected ion pairs. More recently, Abedi et al. (2004) actually observed the NO_3^+ ion fragment in the single ionization process and measured its appearance energy (see the next section). No quantitative ionization cross section data were presented by any of the groups. Total ionization cross sections have been calculated by Antony et al. (2004) using a spherical complex potential formalism and, very recently, by Joshipura et al. (2007a) using a similar approach. This method was shown to give quite good agreement with experimental results for the other nitrogen oxides where quantitative data were available.

4.13.2. Appearance energies and fragment energy distributions

Abedi et al. (2004) used a trochoidal monochromator to study the ionization up to about 25 eV. They measured the appearance energies of the NO_2^+, NO^+, O^+ and NO_3^+ fragment ions to be 12.2 ± 1.1, 13.09 ± 0.25, 16.74 ± 0.36 and 13.25 ± 0.30 eV respectively in good agreement with photoionization studies (Jochims et al., 1992). O'Connor et al. (1996) measured an appearance energy for N^+ of 36 ± 2 eV while O'Connor et al. (1997) determined appearance energies for forming the $NO^+ + NO_2^+$ and $NO^+ + O^+$ ion pairs to be 34.5 ± 2 and 48 ± 2 eV respectively.

Although no actual measurements were made of fragment kinetic energies, O'Connor et al. (1996) argued that these should be small (<0.3 eV) for single ionization fragmentation, given the size and complexity of the molecule. In ion pair production, fragment kinetic energies should be much higher and, in fact, O'Connor et al. (1997) deduced released kinetic energies of 6–7 eV from the width of the TOF peaks in their mass spectra.

4.13.3. Dissociative attachment

To date the only report of anion production in N_2O_5 is the recent one by Cicman et al. (2004). They used a trochoidal monochromator with an energy resolution of 100–150 meV as their electron source. This was coupled to a quadrupole mass spectrometer for ion detection and analysis. Incident energies between a few meV (nominal) and 10 eV were used. Several anionic fragments (NO_3^-, NO_2^-, NO^-, O^- and O_2^-) were detected with the first two listed being by far the most intense. Both the NO_3^- and NO_2^- anion cross sections exhibit a large cross section at "zero" incident electron energy, with a shoulder evident above 1 eV and a small secondary maximum around 4 eV. This suggests that three distinct dissociation channels

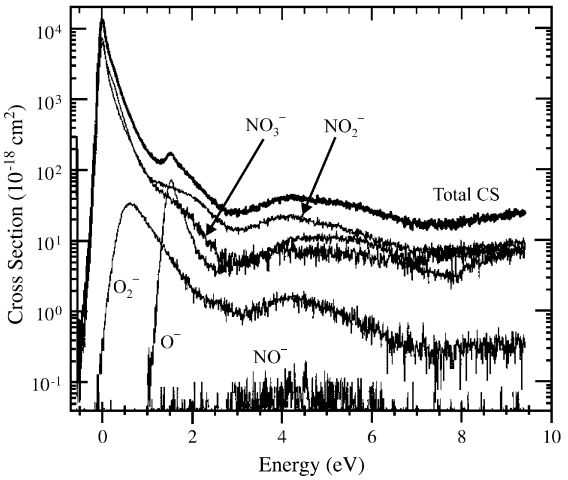

Fig. 42. Total and partial electron attachment cross sections in N_2O_5. From Cicman et al. (2004).

contribute to the measured cross section. An approximate calibration of their system was made using Cl^- from CCl_4 as a secondary standard (Klar et al., 2001). Their total and partial cross sections are shown in Fig. 42 and are seen to be very large around zero incident electron energy. The magnitudes of the cross sections close to zero eV are somewhat uncertain as they depend on the energy resolution of the electron source.

4.14. Organic acids, HCOOH, CH_3COOH, amino acids

Formic (HCOOH) and acetic (CH_3COOH) acids are minor constituents in Earth's atmosphere and have also been observed in the interstellar medium and in cometary comas [see e.g. Harvey et al. (2005), Mehringer et al. (1997), Crovisier et al. (2004), Irvine et al. (1989)]. Along with ammonia, they may form the basic building blocks for the formation of biomolecules such as the amino acid, glycine (CH_3COONH_2). Little quantitative information is available for these molecules and no data are listed in the Landolt–Börnstein compilation (Itikawa, 2003). Very recently the photophysics of formic and acetic acids was studied (Schwell et al., 2002; Leach et al., 2006)) and information was given on fragmentation, fluorescence and ionization of the molecules in the photon energy range 6–23 eV. Also using synchrotron radiation, Boechat-Roberty et al. (2005) investigated the break-up of formic acid by 200–310 eV X-rays. Available electron impact data seem to be limited to the dissociative ionization and attachment work discussed below.

4.14.1. Dissociative ionization

Pilling et al. (2006a,b) have investigated the ionization and dissociation of formic acid by electrons of energy ranging from 500 eV to 2 keV. Comparisons were drawn with data obtained for proton projectiles of equal velocities. Rather similar ion fragmentation patterns were obtained with the two projectiles, though there were some differences in the relative intensities of the fragments. CO^+ was the dominant ion observed for electron impact at 500 eV and higher. We note that a quite different fragmentation pattern is given by the NIST Chemistry WebBook (2005). Here the data were obtained at an energy of 70 eV and the dominant fragment was HCO^+. This is in agreement with the very early work of Mariner and Bleakney (1947) using 65 eV electron impact.

Estimates were made by Pilling et al. (2006b) of the absolute cross sections involved based on the so-called additivity rule where the assumption is made that the large molecule cross section is equal to the sum of the cross sections of its constituents. These partial cross sections were obtained from theoretical estimates of Kim and Rudd (1994). It is important that direct absolute measurements of dissociative ionization be made to extend the current data base and check these estimates.

To the authors' knowledge, no information is available on dissociative ionization cross sections of acetic acid or more massive molecules in this sequence. Fragmentation patterns may be obtained from the NIST Chemistry WebBook (2005).

4.14.2. Appearance energies and fragment energy distributions

The first measurements of appearance energies following electron impact on formic acid seem to have been made by Mariner and Bleakney (1947). They obtained a value of 11.0 ± 0.1 eV for the appearance energy of the parent $HCOOH^+$ ion. This is somewhat less than the accepted photoionization threshold of 11.31 eV [Knowles and Nicholson (1974)], though this may be a result of the way Mariner and Bleakney identified the actual threshold on their curves. Nishimura et al. (1989) used a combination of photoelectron and mass spectroscopy to identify the thresholds of the main fragment ions from HCOOH following photon impact. They also list data from earlier work.

For acetic acid, ion appearance energies under electron impact have been given by Holmes and Losing (1980), who compare with earlier work. Very recently Leach et al. (2006) discuss its dissociative ionization in detail and give extensive comparisons with earlier work using both photon and electron projectiles. Additional electron impact work is necessary.

Pilling et al. (2006a,b) were able to make deductions about the translational kinetic energies of the fragment ions in the case of formic acid targets. At 500 eV incident electron energy, H^+, O^+, OH^+ and COH^+ all showed mean kinetic energy releases of approximately 1 eV or a significant fraction of this amount. All the other fragment ions possessed near-thermal translational energies in the meV region.

We note that Nishimura et al. (1989) in their study of HCOOH photoionization using photons in the 11–19 eV energy range found evidence of HCO^+ kinetic energies of up to 2 eV, though peaking at lower energies close to zero. Near-threshold measurements of kinetic energy releases in fragment ion formation following electron impact are not available at the present time.

4.14.3. Dissociative attachment

Mariner and Bleakney (1947) seem to have been the first to demonstrate that dissociative attachment was occurring in electron impact on HCOOH. They tentatively identified OH^- fragments but with such a low intensity that "*it did not seem worthwhile to investigate them further*"! Recently the situation has changed and detailed investigations have been carried out by Pelc et al. (2002a,b, 2003a, 2004) by Sailer et al. (2003) and by Prabhudesai et al. (2005a,b) on formic, acetic and propanoic (C_2H_5COOH) acids.

In HCOOH, Pelc et al. (2002a,b, 2003a) observed a prominent resonance at an energy of 1.25 eV, which decayed into $HCOO^- + H$. Much weaker resonances at higher energies were associated with OH^- and O^- production. Their data are shown in Fig. 43. Using Cl^- from CCl_4 as a calibration standard, they estimated a peak cross section for $HCOO^-$ production of $1.7 \pm 0.6 \times 10^{-18}$ cm^2. As can be seen from Fig. 43, the cross sections for OH^- and O^- are less than this by one or two orders of magnitude respectively. Rather similar data for $COOH^-$ were obtained by Prabhudesai et al. (2005a,b). They were able to demonstrate also that fast H^- was a very significant product of the 7.3 eV feature with a peak production cross section of 1.2×10^{-19} cm^2. This may not have been observed by Pelc et al. because of energy discrimination effects in their detection system. We note that if any dimers were present in the target gas, then these cross sections would represent upper limits [see Martin et al. (2005) and Scheer et al. (2007)]. The simplified potential energy diagram (Fig. 44) illustrates the main resonance process and indicates that some energy is available either as translational energy of the fragments or as internal energy of the $HCOO^-$ anion.

Sailer et al. (2003) and Pelc et al. (2004) found a more complicated situation with acetic and propanoic acid targets. For acetic acid they observed no less than nine different fragment anions, the most intense being CH_3COO^- and $CH_2O_2^-$. These were suggested to be the product of two shape resonances, peaking at 1.5 and 0.75 eV respectively. An approximate cross section for peak CH_3COO^- production was estimated to be 6×10^{-19} cm^2. Most of the other, less intense, anion fragments were thought to be formed through higher energy core-excited Feshbach resonances. They were unable to observe a parent anion that had been observed in earlier studies by Hadjiontoniou et al. (1973) at somewhat higher pressure.

For propanoic acid, ten different anion products were identified, the most intense being $C_3H_5O_2^-$ and $CH_2O_2^-$. Once more, Prabhudesai et al. (2005b) demonstrated that H^- was produced strongly also.

Total dissociative electron attachment cross sections for the amino acids, glycine, alanine, proline, phenylalanine and tryptophan at incident electron energies below 10 eV, have been measured very recently by Scheer et al. (2007) who also present extensive references to earlier work on these molecules. Cross section magnitudes were determined by comparison with signals for corresponding total positive ion formation calculated in the BEB formalism (Hwang et al., 1996). Fig. 45 shows the DEA data of Scheer et al. (2007).

Some similarities with the simpler HCOOH molecule are evident, namely a 1.2 eV shape resonance feature and some higher energy core excited resonances above 4 eV. Mass analysis indicates that the low energy feature in each case is due to $[M–H]^-$, the parent molecular anion minus an H atom. Major contributions to the spectrum at higher energies come from such fragments as $COOH^-$ and OH^- and possibly also H^- [see Scheer et al. (2007)]. The lighter fragments may possess a considerable amount of translational energy.

Very recently, Abouaf (2008) has studied the $(M - H)^-$ peaks of glycine, alanine and propanoic acid at higher energy resolution. No absolute cross section data are given.

4.15. Nitroalkanes, CH_3NO_2, $C_2H_5NO_2$, ...

The nitroalkanes, nitromethane (CH_3NO_2), nitroethane ($C_2H_5NO_2$) and nitropropane ($C_3H_7NO_2$) are of great interest for a number of reasons. Not only are they involved in atmospheric chemistry but they also have significant industrial potential as explosives or propellants. They have been used as fuels by high altitude aircraft to help solve flameout and re-ignition problems [see Jiao et al. (2003)]. Relatively little work has been carried out on their response to electron impact interactions and no recommended cross section data have appeared in data compilations as of mid-2007.

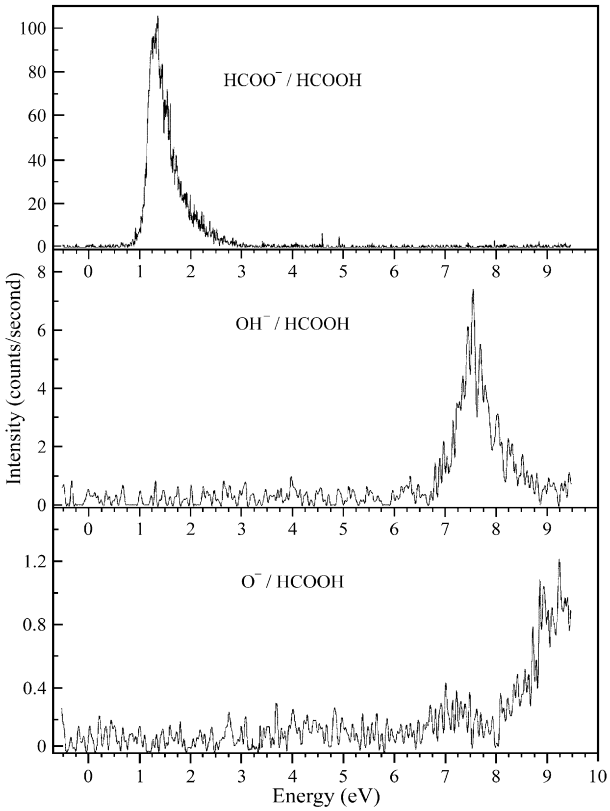

Fig. 43. Relative negative ion production in formic acid as a function of incident electron energy. The electron energy resolution was 140 meV. From Pelc et al. (2002b).

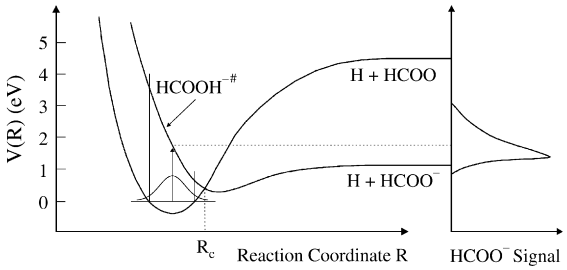

Fig. 44. Schematic potential energy diagram illustrating $HCOO^-$ formation following electron impact on HCOOH. From Pelc et al. (2002b).

4.15.1. Dissociative ionization

Apart from measurements of fragmentation patterns taken at a specific electron energy, such as are compiled by the NIST Mass Spec Data Center and published in the NIST Chemistry WebBook (2005), there have been few measurements giving details of the dissociative ionization of these targets. Recently, Jiao et al. (2003) have studied both positive and negative ion formation in nitromethane over an electron energy range from threshold to 200 eV using Fourier Transform Mass Spectroscopy. They find a similar fragmentation pattern to what is suggested by the NIST data set except they observe significantly less of the parent ion. The most important fragment ion is NO^+ followed by CH_3^+, NO_2^+ and CH_2NO^+. Fig. 46 presents their absolute cross section data and illustrates the wide range of fragment ions that are observed.

No cross section data seem to be available for nitroethane or the higher nitroalkanes.

4.15.2. Appearance energies and fragment energy distributions

Using a commercial mass spectrometer, Kandel (1955) investigated the break-up of nitromethane under electron impact and measured the appearance energies of the various fragment ions. Energy calibration was achieved using known ionization energies of argon and krypton. Most of the observed ions had very low, essentially thermal, kinetic energies but a notable exception to this was CH_3^+, which was observed to have over 1 eV of translational kinetic energy. Jiao et al. (2003) had a similar finding.

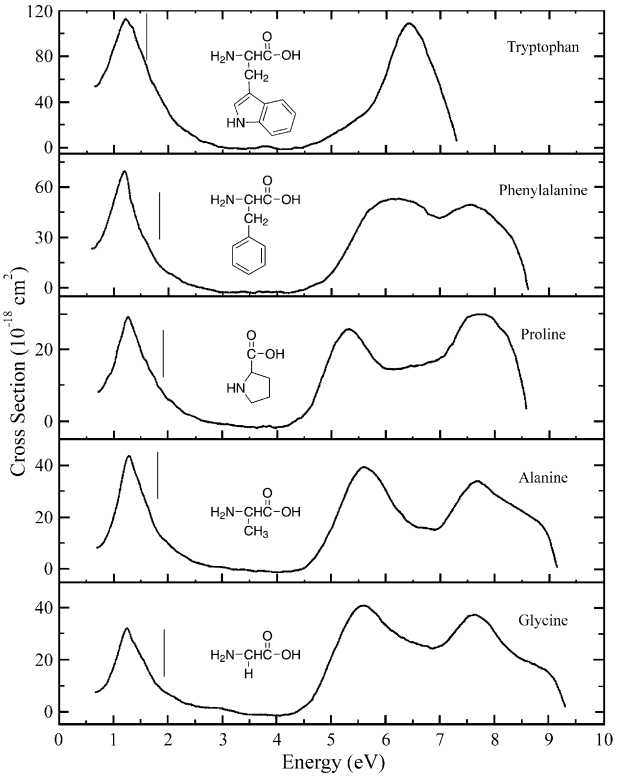

Fig. 45. Total dissociative electron attachment cross sections of glycine, alanine, proline, phenylalanine, and tryptophan. Chemical structures of the parent molecules are shown. The vertical lines indicate the vertical attachment energies into the π^* orbital of the −COOH group. The sharp decreases in anion current at the higher energies reflect the onset of positive ionization. From Scheer et al. (2007).

These latter workers did not specifically measure appearance energies but from Fig. 46, it seems clear that many of these thresholds will be larger than 15 eV. If this is the case, then some disagreements with Kandel's data are indicated. He presented appearance energies for most ions that were less than 15 eV. As an example, we note that for CH_3^+, the data of Jiao et al. (2003) suggest a threshold close to 20 eV whereas Kandel (1955) give a value in close agreement with some other values quoted by the NIST Chemistry WebBook (2005). For the main fragment ion, NO^+, the agreement seems to be much better.

For nitroethane, the NIST Chemistry WebBook (2005) lists values for the appearance energies of just two cations, the dominant one, $C_2H_5^+$, and $C_2H_5O^+$. These energies are 11.0 and 10.62 ± 0.07 eV respectively.

4.15.3. Dissociative attachment

A number of studies of dissociative electron attachment in nitromethane have been carried out over the years and the most abundant anions have been identified to be NO_2^-, O^-, OH^-, CN^-, CNO^- and CH^- [see Sailer et al. (2002) for a listing of earlier references]. Good agreement is obtained regarding the energy positions of the transient negative ion resonances, which give rise to the various anions. Sailer et al. (2002) were able to obtain estimates of the partial production cross sections, using the production of Cl^- from CCl_4 as a secondary standard, and assuming constant transmission and detection efficiencies for the various anions. No estimates of the kinetic energies of the fragments, or consequent possible discrimination effects, were made. The maximum cross section (for NO_2^- production) was $\sim 10^{-17}$ cm^2 at 0.62 eV. Sailer et al. (2002) observed production of OH^-, CN^-, and CNO^- at very low energy (∼0 eV) in contrast to what had been noted in earlier studies [e.g. Walker and Fluendy (2001) and Modelli and Venuti (2001)].

In the case of nitroethane, two studies (Jager and Henglein, 1967; Tsuda et al., 1969) were reported prior to the recent work of Pelc et al. (2003a,b). Estimates of partial production cross sections for the different anions were made by Jager and Henglein (1967) and by Pelc et al. (2003a,b). There were significant disagreements in the data from the two groups, sometimes approaching an order of magnitude. Possible production mechanisms were discussed in detail. Additional independent measurements are desirable.

4.15.4. Dissociative excitation

Some data on the near-UV/visible fluorescence of nitromethane and nitropropane following 100 eV electron impact on low pressure gaseous targets have been given by Wehry et al. (1987). Their work indicates that the H Balmer series is strongly

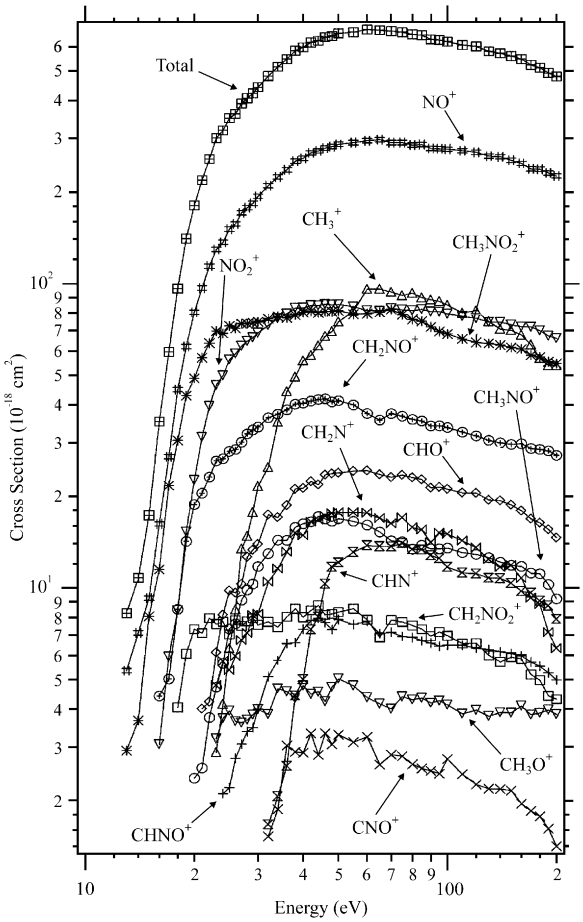

Fig. 46. Absolute cross sections for ionization of nitromethane by electron impact. Errors are estimated at ±15% for the total ionization cross section. From Jiao et al. (2003).

excited as are the CH($A\ ^2\Delta - X\ ^2\Pi$) band at 431.4 nm and the CN($B\ ^2\Sigma^+ - X\ ^2\Sigma^+$) band at 388.3 nm. Unfortunately no quantitative cross section data are available. Electron energy loss spectra (Flicker et al., 1980) show many broad features indicative of the occurrence of dissociation. Additional electron scattering information is available from the work of Walker and Fluendy (2001).

4.16. Biological molecules

Ever since the pioneering recognition by Sanche and co-workers (Boudaiffa et al., 2000) that low energy electrons could cause significant damage in DNA molecules via dissociative attachment events, there has been a rapid increase in work directed towards a fuller understanding of the interaction of electrons, with energies less than 30 eV, with biological molecules. Motivation for this work comes from the need to understand the mechanisms involved in radiation damage. Most of the energy deposited in biological material by high energy radiation goes into production of secondary electrons, the majority of which possess energies of less than 30 eV. Progress was reviewed by Sanche (2005) and there have been a large number of publications since. As will be evident below, most of the activity on the experimental side has involved dissociative attachment but other data has been included where relevant. Measurements have been made both in the gaseous phase or where very thin films were deposited on clean surfaces of gold or other suitable substrate materials.

One way of attacking the problem, the so-called "bottom up" approach (Swiderek, 2006), is to isolate and study in detail smaller sections of the DNA molecule, e.g. the four bases [adenine (A), thymine (T), guanine (G) and cytosine (C)] or the sugar and phosphate units. Uracil (U) is also of interest as it replaces thymine when RNA is being considered. Fig. 47, adapted from Sanche (2005), shows a segment of DNA illustrating the basic structure. It can be seen that three of the four bases, T, G and C, are oxygen containing as, of course, are the sugar-phosphate components of the DNA backbone and uracil.

Table 36 lists some recent publications involving electron collisions with DNA and RNA bases and related molecules. A number of comments can be made. First, the increasing level of interest and activity in this sub-field in the last few years is evident. This is certainly a "hot" area of research at the moment. Second, it is broadly based with very active groups in Canada,

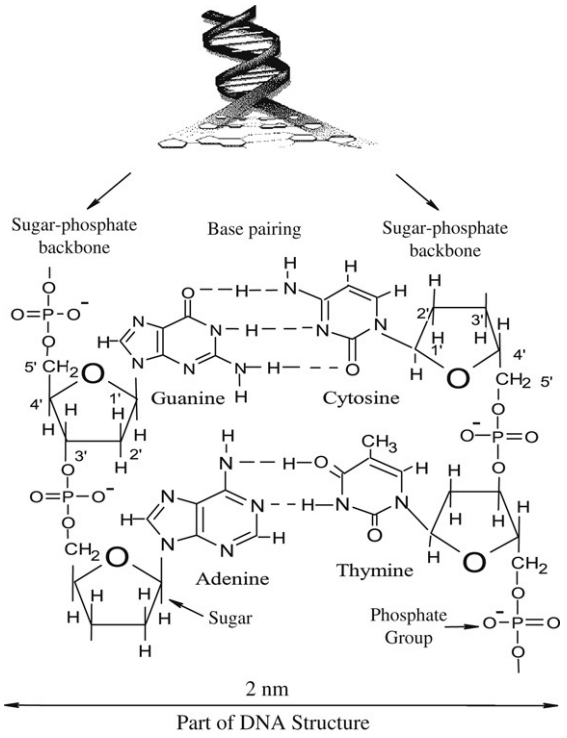

Fig. 47. Segment of DNA containing the four bases: guanine (G), cytosine (C), adenine (A), and thymine (T). From Sanche (2005).

the USA, and Europe. Third, activity to date has been largely experimental, highlighting the difficulty of handling these large molecules theoretically. Fourth, the majority of the experimental studies involved DEA. Fewer than 20% dealt with cation production while very limited information is available on electronic excitation and nothing on dissociative excitation leading to photon emission in any spectral region. We note that although no emission cross section data have been published, the first data on dissociative excitation of these biological molecules were presented at the 25th ICPEAC Conference, Freiburg (Erdevdy et al., 2007; Shafranyosh et al., 2007) and by Shafranyosh and Sukhoviya (2007).

In the data discussion below we limit ourselves to a presentation of what quantitative, gas phase, collisional data are available. For further details readers are referred to the original papers and the review by Sanche (2005) who deals also with thin film targets. These also give additional references to related work.

A word of caution is timely at this point where consideration of non-volatile materials, such as most bio-molecules, is considered. These readily condense on chamber walls and so the pumping speeds for these species can be quite different from those of volatile gases, such as SF_6 or CCl_4, which may be used as calibrants. This leads to difficulty in establishing actual relative gas densities in the target region. When this is coupled to the discrimination effects often introduced by the use of quadrupole mass spectrometers, a high probability of erroneous measurements can occur. Some of the discrepancies noted in the following sections may be due to such effects. Hence much of the 'absolute' data should be treated with caution. For this reason we have not included absolute scales on the DEA figures of this section. The technique used by Burrow and co-workers (e.g. Aflatooni et al. (2006)), in which currents are measured directly and where comparison of anion and cation signals obtained under identical source conditions is used for calibration, is likely to give the most accurate cross section values.

4.16.1. Cytosine ($C_4H_5N_3O$)

Data available for cytosine include dissociative ionization and DEA. Unfortunately the data from different groups are conflicting. For example Shafranyosh et al. (2006) measure a maximum total cation production cross section of $7.8 \pm 0.8 \times 10^{-16}$ cm^2 at 78 eV incident electron energy, whereas Aflatooni et al. (2006) normalize to a peak cross section of 14.58×10^{-16} cm^2 based on BEB calculations (Bernhardt and Paretzke, 2003; Mozejko and Sanche, 2005). Shafranyosh et al. (2006) present data for 23 cationic fragments at 78 eV, the parent ion being responsible for only 21% of total ionization at this energy. This highlights the importance of dissociative ionization. Shafranyosh et al. indicate a threshold energy for positive ion production of 9.0 ± 0.2 eV, which is consistent with data in the NIST Chemistry WebBook (2005).

Since anion production cross sections are often obtained by normalization to cation signals, it is not surprising that data from different groups are found to differ significantly. However this cannot account for the huge differences in measurements of DEA. For example, Aflatooni et al.'s measurement of the total DEA at the 1.5 eV peak is 2.2×10^{-19} cm^2 while Shafranyosh et al.'s value is 4.2×10^{-18}cm^2, some 19 times larger. Denifl et al. (2004b) measure 2.3×10^{-16} cm^2,

Table 36
Some recent publications involving electron collisions with biologically-related molecules

Reference	Molecules	Processes studied[a]	Incident energy (eV)	Experiment/theory[b]
Allan (2007)	tetrahydrofuran	elastic, inelastic scattering	0.1–20	E
Xie and Cao (2007)	adenine, guanine	DEA	0–3	T
Bald et al. (2007)	TAR	DEA	0–12	E/T
Sommerfeld (2007)	fructose	DEA	0–0.5	T
Panajtovic et al. (2007)	adenine	HREEL	0–7	E
Kim and Schaefer (2007)	cytosine	EA	0–2	T
Bachorz et al. (2007)	uracil	EA	0–1	T
Scheer et al. (2007)	amino acids	DEA	0–10	E
Imhoff et al. (2007)	uracil, 5-bromouracil	DI	70	E
Dampc et al. (2007)	tetrahydrofuran	EEL	6–20	E
Colyer et al. (2007)	tetrahydrofuran	EEL	6.5–50	E
Aflatooni et al. (2006)	thymine, cytosine, adenine, tetrahydrofuran, 3-hydroxytetrahydrofuran, trimethylphosphate	DEA	0–10	E
Bouchiha et al. (2006)	tetrahydrofuran	elastic, inelastic scattering	1–10	T
Park et al. (2006)	tetrahydrofuran	DEA	0–12	E
Zheng et al. (2006)	single strand DNA (film)	bond breaking	0–15	E
Konig et al. (2006)	dibutyl phosphate, triethyl phosphate	DEA	0–12	E
Ptasinska and Sanche (2006)	single strand DNA (film)	anion desorption	3–15	E
Pan and Sanche (2006)	NaH_2PO_4 (film)	anion desorption	0–19	E
Huber et al. (2006)	adenine	DEA	0–15	E
Shafranyosh et al. (2006)	cytosine	DI	0–200	E
		DEA	0–5	E
Ptasinska et al. (2006)	thymidine	DEA	0–12	E
Winstead and McKoy (2006)	uracil	elastic scattering, excitation	0–20	T
Tonzani and Greene (2006)	uracil, thymine, cytosine, adenine, guanine	elastic scattering	0–14	T
Burrow et al. (2006)	uracil, thymine	DEA	0–4	E
Sulzer et al. (2006)	furan, tetrahydrofuran, fructose	DEA	0–12	E
Bald et al. (2006)	D-ribose	DEA	0–2	E
Imhoff et al. (2005)	thymine	DI	70	E
Ptasinska et al. (2005a)	thymine, uracil	DEA	4–14	E
Mozejko and Sanche (2005)	DNA, RNA	elastic scattering	50–2000	T
		I	0–4000	T
Abouaf and Dunet (2005)	uracil, thymine, halouracils	elastic scattering, DEA	0–3	E
Pan and Sanche (2005)	DNA (film)	anion desorption (OH)	0–19	E
Abdoul-Carime et al. (2005)	adenine, guanine	DEA	0–16	E
Levesque et al. (2005)	pyrimidine (film)	EEL	0–12	E
Denifl et al. (2005)	5-bromouridine (film)	DI	0–13	E
		DEA	0–12	E
Ptasinska et al. (2005b)	alanine	DEA	0–14	E
Li et al. (2004)	uracil, thymine, cytosine	DEA	–	T
Scheer et al. (2004)	uracil, halouracils	total scattering	0–5	E/T
Ptasinska et al. (2004)	deoxyribose	DI	0–70	E
		DEA	0–14	E
Denifl et al. (2004a)	cytosine, thymine	DEA	0–14	E
Martin et al. (2004)	DNA (film)	DEA	0–4	E
Berdys et al. (2004)	cytosine	DEA	0.2–1.5	T
Feil et al. (2004)	uracil	DI	0–1000	E
		DEA	0–14	E
Denifl et al. (2004b)	uracil, thymine, cytosine	DEA	0–14	E
Denifl et al. (2004c)	uracil	I, DI	5–18	E
Grandi et al. (2004)	uracil	DEA	6–12	T
Gianturco and Lucchese (2004)	glycine	DEA	0–14	T
Mozejko and Sanche (2003)	DNA and RNA bases	elastic scattering	50–4000	T
		I	0–5000	T
Denifl et al. (2003)	5-chloro uracil	EA, DEA	0–14	E
Pan et al. (2003)	DNA (film)	anion desorption	3–20	E
Ptasinska et al. (2003)	glycine	DEA	0–12	E
Hanel et al. (2003)	uracil	DEA	0–12	E
Abouaf et al. (2003a,b)	thymine, 5-bromouracil	HREEL	0–100	E

Table 36 (*continued*)

Reference	Molecules	Processes studied[a]	Incident energy (eV)	Experiment/theory[b]
Coupier et al. (2002)	uracil/water	DI	0–200	E
Abdoul-Carime and Sanche (2002)	DNA (film)	dissociation, DEA	1–30	E
Abdoul-Carime et al. (2001)	5-halouracils	DEA	0–3	E
Du Penhoat et al. (2001)	thymine (film), uracil (film)	DEA	0–38	E
Boudaiffa et al. (2000)	DNA	DEA	0–20	E

[a] Processes studied: DEA: Dissociative Electron Attachment; HREEL: High Resolution Electron Energy Loss; EA: Electron Attachment; DI: Dissociative Ionization; EEL: Electron Energy Loss; I: Ionization.
[b] E = Experiment; T = Theory.

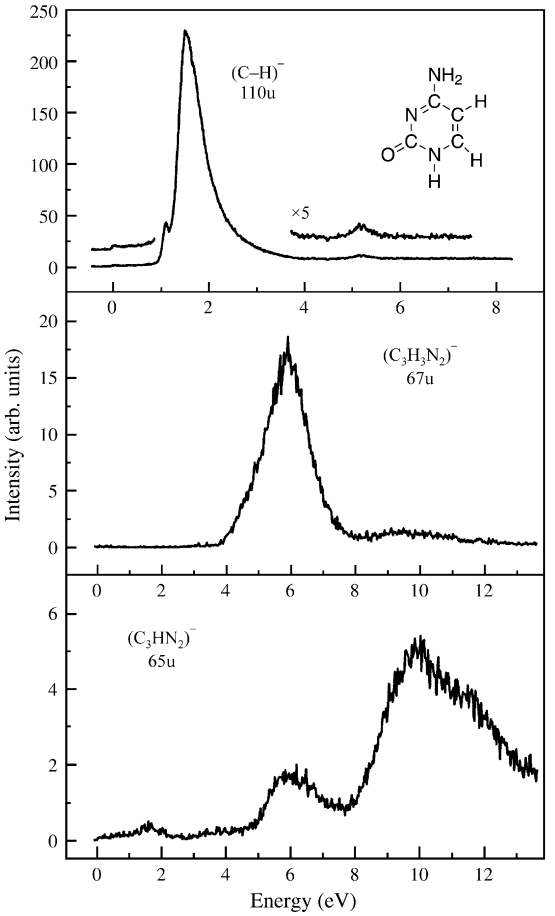

Fig. 48. Relative ion yield of $(C–H)^-$, $(C_3H_3N_2)^-$, and $(C_3HN_2)^-$ formed via dissociative electron attachment to cytosine (shown as the inset chemical structure). From Denifl et al. (2004a).

55 times larger again. Denifl et al. suggest that their cross sections are accurate to about one order of magnitude while Aflatooni et al. indicate error bars of ±50% below 4 eV and ±25% at higher energies. Aflatooni et al. suggest that differences in cross section values may be due to the difficulty of accurately determining molecular densities in the interaction region. This highlights the difficulties of dealing with these biological molecules. As discussed in Section 4.16, we suggest that the measurements of Aflatooni et al. (2006) are to be preferred.

A second peak in anion production was observed by Aflatooni et al. (2006) at an electron energy of 5.48 eV and with a cross section of 2.2×10^{-19} cm^2, i.e. of comparable magnitude to the 1.5 eV peak. Other workers, namely Huels et al. (1998) and Denifl et al. (2004a,b), observed additional, but much smaller peaks at energies above 4 eV. Using mass analysis, these peaks were identified as being due to DEA processes yielding a variety of anion fragments. The main peak at 1.5 eV was due to the parent molecular anion minus a hydrogen atom $(C–H)^-$. Figs. 48 and 49, adapted from Denifl et al. (2004a), illustrate the peak structure.

As discussed by numerous authors, the low energy, 1.5 eV, peak may be largely due to the formation of a temporary negative ion state where the electron occupies an empty π^* orbital. However, recent high-resolution work on the DNA

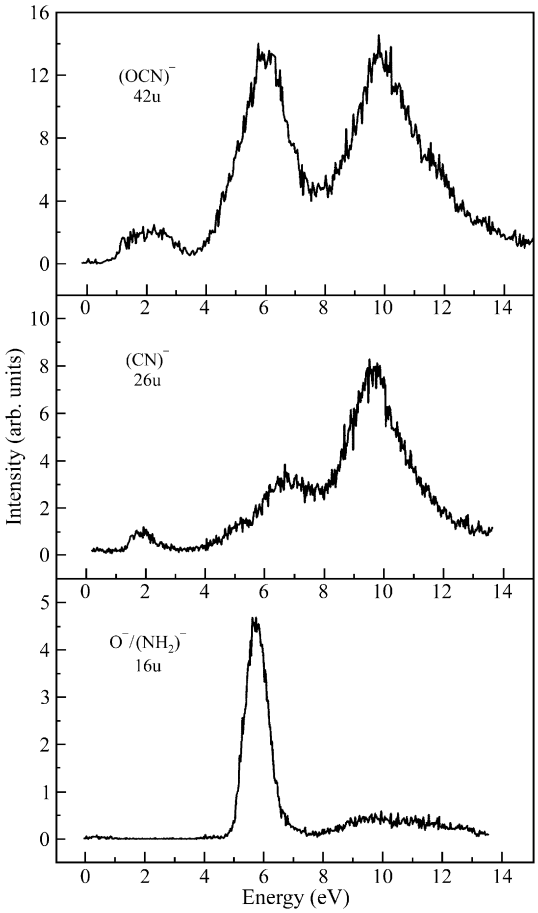

Fig. 49. Relative ion yield of $(OCN)^-$, $(CN)^-$, and $O^-/(NH_2)^-$ formed via dissociative electron attachment to cytosine. From Denifl et al. (2004a).

and RNA bases, (Burrow et al., 2006), reveals that sharp structures on the primary peak are due to vibrational Feshbach resonances. The higher energy peaks, above 4 eV, are due to the formation of core-excited negative ion states.

4.16.2. Thymine ($C_5H_6N_2O_2$)

Collisional dissociation studies of thymine parallel the work already discussed for cytosine. Imhoff et al. (2005) present positive ion fragmentation patterns following 70 eV electron impact. The parent ion is observed together with a wide range of fragments, the most intense of which is CO^+ and/or $HNCH^+$.

Aflatooni et al. (2006) present total DEA cross sections for electron energies up to 9 eV. The data indicate a double peak in the low energy region (below 3 eV) and a broad peak at higher energies, 5–9 eV. Absolute calibration was again based on a theoretical BEB cross section (Bernhardt and Paretzke, 2003; Mozejko and Sanche, 2005) for direct cation production. The cross section reached a maximum value of 4.7×10^{-19} cm^2 at an energy of 1.01 eV. This value is 2500 times smaller than the 1.2×10^{-15} cm^2 reported by Denifl et al. (2004a,b,c) for $(T–H)^-$ production in their mass analysed data. Abouaf et al. (2003b) indicate a peak cross section for $(T–H)^-$ in the region of 10^{-15} cm^2 in rough agreement with Denifl et al. but give no details of their calibration procedure. This highlights, again, the difficulty of absolute calibration when using these molecular species. For the same reasons as discussed in the previous section, we suggest that the Aflatooni et al. (2006) data be preferred.

Using mass analysis Denifl et al. (2004a,b,c) identified nine different DEA channels and studied their variation with incident electron energy. Their findings are illustrated in Figs. 50–52. The channel with the largest cross section is that for $(T–H)^-$ production in which a hydrogen atom is released. Interestingly the yield of neutral H atoms was found to be site selective. Using deuterium substitution, Abdoul-Carime et al. (2005) found that H loss occurred only from the nitrogen positions not from the carbon ones. Further, it was shown that the mechanisms of H-atom release from the two possible nitrogen sites were quite different. Thus from the so-called N_1 site, sharp vibrational Feshbach resonances (VFRs) are involved whereas from the N_3 site the H atoms are produced by coupling between the temporary anion states associated with the π^* and σ^* valence orbitals owing to out-of-plane vibrational motion [see Burrow et al. (2006)].

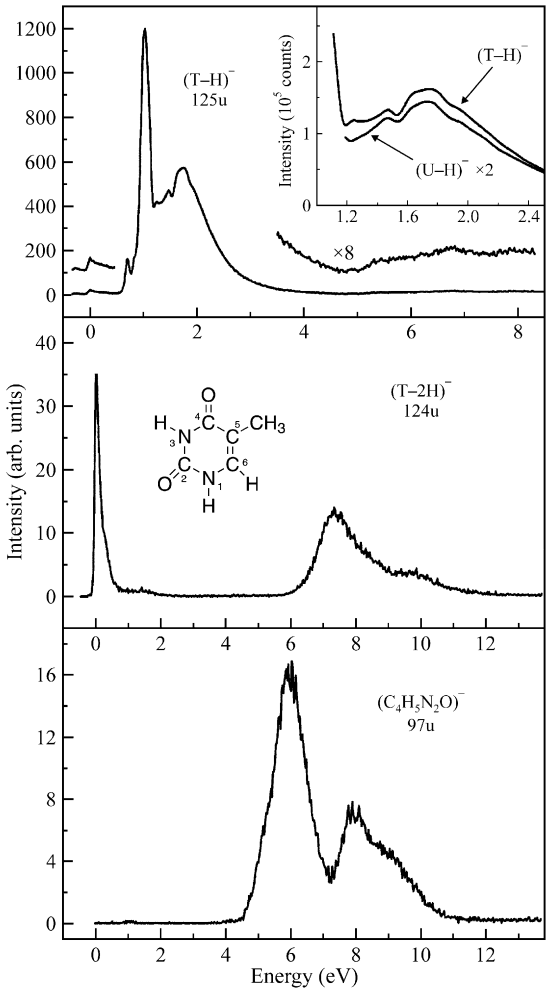

Fig. 50. Relative ion yield of $(T–H)^-$, $(T–2H)^-$, and $(C_4H_5N_2O)^-$ formed via dissociative electron attachment to thymine (shown as the inset chemical structure). The inset figure illustrates the peak structure of ion yields from thymine and uracil (U) at high resolution. From Denifl et al. (2004a).

Above 4 eV, the cross sections for anion production are about two orders of magnitude smaller and the anion fragments are produced through the formation of core-excited negative ion states. In addition to the channels illustrated in Figs. 50–52, Ptasinska et al. (2005a) have investigated H^- production and have shown that it is both bond and site selective.

Denifl et al. (2006) have investigated dissociative electron attachment to adenine and thymine molecules and clusters imbedded in superfluid helium droplets. They find significant differences to what is observed in the gas phase with individual molecules.

Shafranyosh et al. (2007) and Shafranyosh and Sukhoviya (2007) have presented the first electron-excited fluorescence data from this target. They present spectral data for bands excited in the wavelength range 200–600 nm, with electrons of energies in the range 0–200 eV.

4.16.3. Guanine ($C_5N_5H_5O$)

Table 36 indicates that guanine has not been studied as much as some of the other bases. This may be due in part to the difficulty of getting pure uncontaminated guanine in the gas phase by evaporation. We note that Trofimov et al. (2006) did not include guanine in their study of the photo-electron properties of the nucleobases because they could not get a pure target. For this reason cross section estimates should be treated with caution.

Abdoul-Carime et al. (2005) have used mass spectroscopy to study the various DEA processes that occur with this molecule and have shown that it possesses some unique features. Thus the de-hydrogenation reaction, which was the dominant DEA process in the other bases, is comparatively weak (about 5% of the total yield) while five other decomposition reactions are observed from the low energy π^* precursor resonances at energies below 3 eV. This is illustrated in Fig. 53, which shows some of their data. At higher incident electron energies, CN^- and O^- and/or NH_2^- structures are evident at 7.5 and 6.2 eV respectively and are due to core excited resonances.

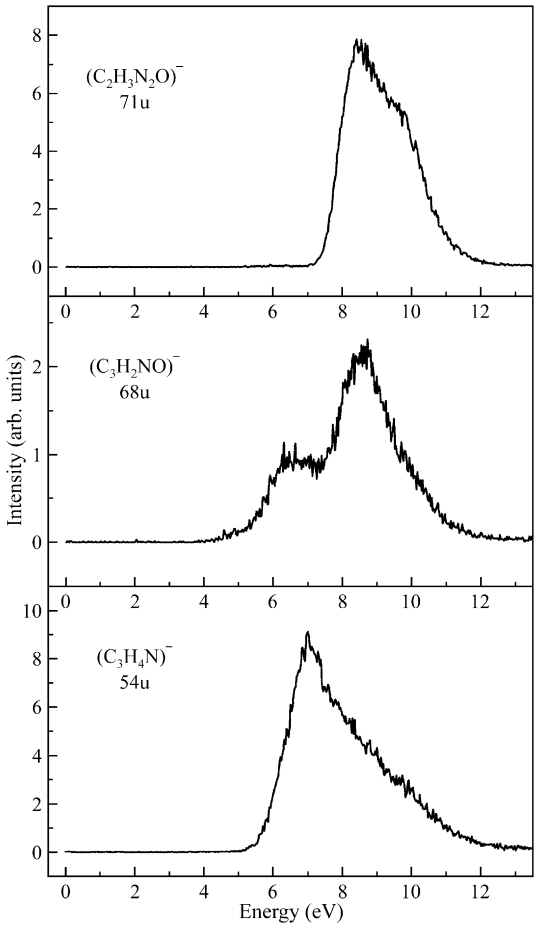

Fig. 51. Relative ion yield of $(C_3H_2N_2O)^-$, $(C_3H_2NO)^-$, and $(C_3H_4N)^-$ formed via dissociative electron attachment to thymine. From Denifl et al. (2004a).

We note that Erdevdy et al. (2007) have presented first results on dissociative excitation of guanine. They observed emission spectra in the range 300–500 nm following 52 eV electron impact. The most prominent band was the CN ($B\ ^2\Sigma^+ - X\ ^2\Sigma^+$) band at 387 nm.

4.16.4. Uracil ($C_4N_2H_4O_2$)

Uracil, which replaces thymine when RNA rather than DNA is being considered, has been widely studied as indicated in Table 36. Both positive and negative ion formation have been studied. Imhoff et al. (2007) report the fragmentation pattern for 70 eV electron impact. Feil et al. (2004) report positive ion production cross sections over an energy range from threshold to 1000 eV whereas Denifl et al. (2004c) have studied the threshold region in detail and have obtained accurate appearance energies for all the main ions produced. Normalization of the Feil et al. data was to a calculated total single ionization cross section using the semi-classical Deutsch–Märk formalism (Deutsch et al., 2000, 2004). This gave cross sections for large molecules that were accurate to 20% or better. The parent ion U^+, had the largest cross section, peaking at 4.4×10^{-16} cm^2 at 100 eV incident energy. The two fragment ions with the largest cross sections were $C_3NH_3O^+$ and OCN^+. Both had maximum cross sections of around 2×10^{-16} cm^2 at 100 eV incident energy.

Denifl et al. (2004c) measured the appearance energies of eight fragment ions as well as the parent ion. These all lay in the range 9–15 eV. The measured appearance energy for U^+ production (9.59 ± 0.08 eV) agreed well with a large number of previous determinations [see Denifl et al. (2004c)].

DEA has been discussed in detail by various authors: Feil et al. (2004), Abouaf and Dunet (2005), Burrow et al. (2006). An overview of the results obtained is shown in Fig. 54, adapted from Feil et al. [See also insert in Fig. 50.] Note that we have chosen not to display an absolute cross section scale here or in the cases of the other DNA bases. This is because of the difficulties involved in absolute calibration of the data as discussed in previous sections. The cross section values of Feil et al. (2004) were reduced by an order of magnitude from what was presented in earlier work from this laboratory (Hanel et al., 2003). At low electron energies, less than 3 eV, the DEA structure obtained is very similar to that obtained with thymine and similar mechanisms are involved. The primary DEA process leading to de-hydrogenation is both bond and site specific. A full discussion of the different mechanisms involved at the N_1 and N_3 sites is given by Burrow et al. (2006).

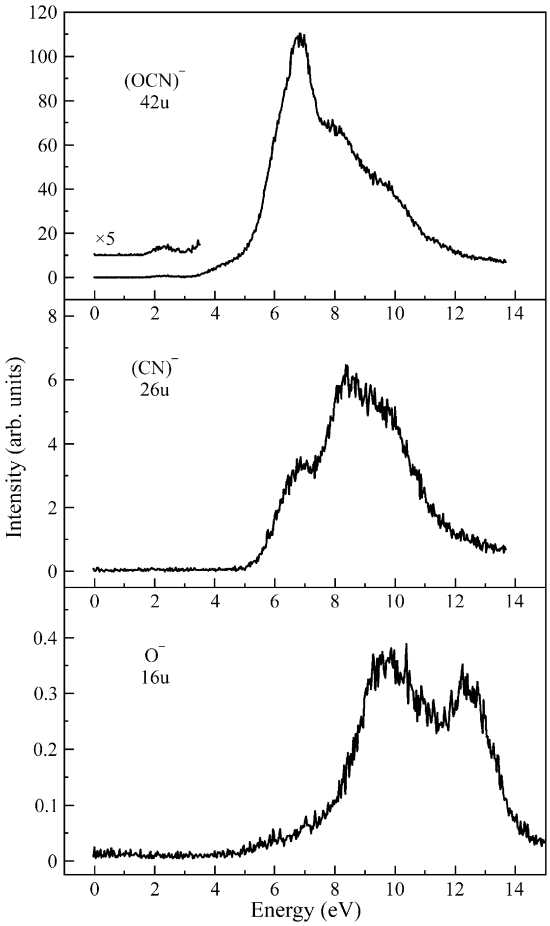

Fig. 52. Relative ion yield of $(OCN)^-$, $(CN)^-$, and O^- formed via dissociative electron attachment to thymine. From Denifl et al. (2004a).

The other main fragment ions observed, namely $C_3NH_2O^-$, OCN^- and CN^- are evident at incident energies above 4 eV. As with thymine these are the product of core-excited negative ion states. From the positions of the resonances in the cross section curves, Denifl et al. (2004c) suggest that more than one of the anions may arise from the same parent resonance. In addition to those fragments shown on Fig. 54, H^- production has been studied by Ptasinska et al. (2005a), who observed four overlapping resonances between 5 and 12 eV. By using methylation and deuteration techniques they showed that each resonance corresponds to H^- loss from a specific site in the molecule. Thus the two lowest energy resonances at 5.5 and 6.8 eV yield H anions from the N_1 and N_3 sites respectively while the higher energy resonances are related to H^- loss from the C atoms. The cross section curves were not calibrated and no measurements of fragment kinetic energies were carried out.

4.16.5. Sugars: deoxyribose ($C_5H_{10}O_4$), D-ribose ($C_5H_{10}O_5$), fructose ($C_6H_{12}O_6$)

Deoxyribose (or pentose) occupies a central position in the chemical structure of DNA. It links the phosphate groups into the backbone of the macromolecule and provides links for the DNA bases (see Fig. 47).

To date, the only gas phase study of electron interactions with this molecule seems to be the work of Ptasinska et al. (2004). They studied both cation and anion production paying particular attention to the energy region below 20 eV. A positive ion spectrum taken at 70 eV shows the same fragment ions as in the NIST Chemistry WebBook (2005) though with a slightly different mass distribution. These differences could be accounted for by mass-dependent, or ion kinetic energy dependent, effects in the quadrupole mass spectrometer. The small relative abundance of the parent cation compared to the fragment ions indicates the fragility of the furanose ring of deoxyribose and highlights the importance of dissociative ionization. Ptasinska et al. (2004) were able to measure appearance energies for sixteen different positive ions. A further factor that needs to be considered is possible fragmentation of the parent molecules by thermal heating during vaporization in the source.

DEA also was studied by Ptasinska et al. (2004) in the electron energy range 0–14 eV. Within the detection limit of their apparatus, they detected seven different anions. By far the strongest channel, nominally at zero eV energy, was where two

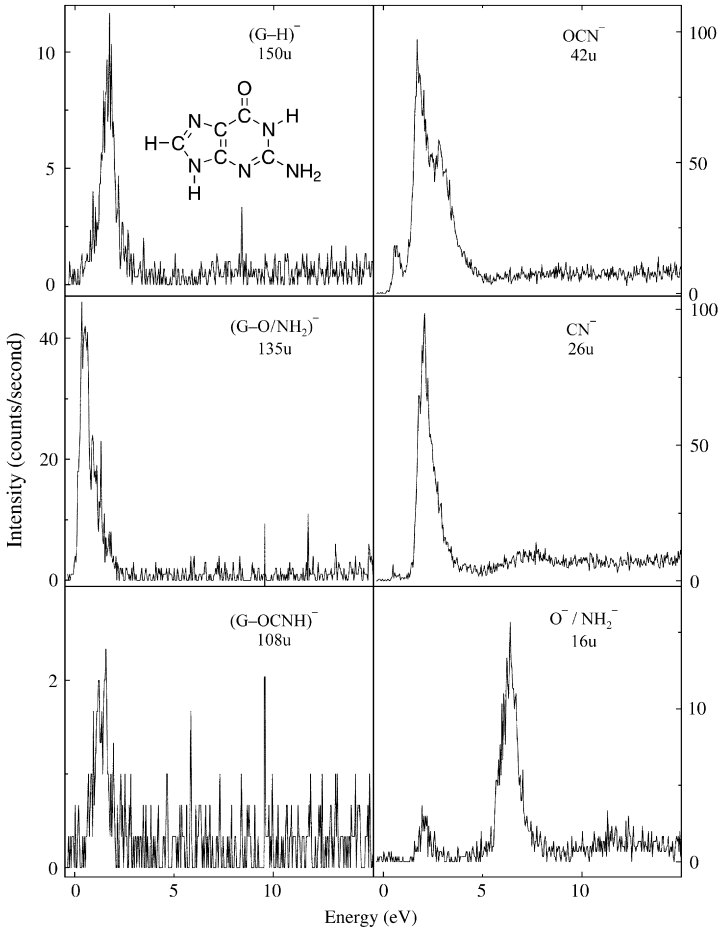

Fig. 53. Relative ion yield of $(G–H)^-$, $(G–O/NH_2)^-$, $(G–OCNH)^-$, $(OCN)^-$, $(CN)^-$ and $(O/NH_2)^-$ formed via dissociative electron attachment to guanine (shown as the inset chemical structure). From Abdoul-Carime et al. (2005).

molecules of water were released. Thus:

$$e + D \rightarrow (D)^{-*} \rightarrow (C_5H_6O_2)^- + 2(H_2O). \tag{24}$$

This is in contrast to the situation with the bases discussed above where dehydrogenation accompanied the most intense DEA channel. A sample of their data is shown in Fig. 55. Except in the case of O^- production, all fragment anions show a resonance peak very close to zero eV. This again contrasts with what was observed with the nucleobases where only a few fragment anions showed evidence of such low energy resonances.

Other sugars that have been investigated recently in connection with their interactions with low energy electrons are D-ribose, fructose and tetra-acetylribose (TAR). In all cases, only DEA was studied (Bald et al., 2006, 2007; Sulzer et al., 2006). All were gas-phase experiments. The results obtained were rather similar to what had been observed with deoxyribose (Ptasinska et al., 2004): the dominant resonant behaviour took place at very low energy, close to zero eV, where major dissociation channels saw the loss of water molecules — one or two in the case of D-ribose and up to three from fructose. A wide range of other fragment anions were produced. With TAR targets, the dominant fragment anion was CH_3COO^-, which occurred via cleavage of a C–O bond. Further strong π^* resonances were observed in the 1.6–1.8 eV region. (Not surprisingly, these were not seen in the pure sugars, which are saturated compounds without π bonds). Weaker resonant contributions, probably σ^* in nature, were observed in the 7–11 eV incident energy region.

In the case of fructose, light anions, H^-, O^- and OH^-, were observed at electron energies greater than 5 eV. In these cases, the precursor ions are of the core-excited type and, for H^- and OH^- production, they are the result of simple bond cleavages leaving the rest of the fructose molecule unchanged. Using isotopic labelling techniques, Bald et al. (2006) were able to specify the site in the target molecule involved in the reaction under consideration. Thus they were able to show that the $(C_4H_5O_3)^-$ anion appeared from a reaction in which the C5 atom of the original molecule is excised while the C1 atom and the hydrogen at the C1 position remain on the negative ion.

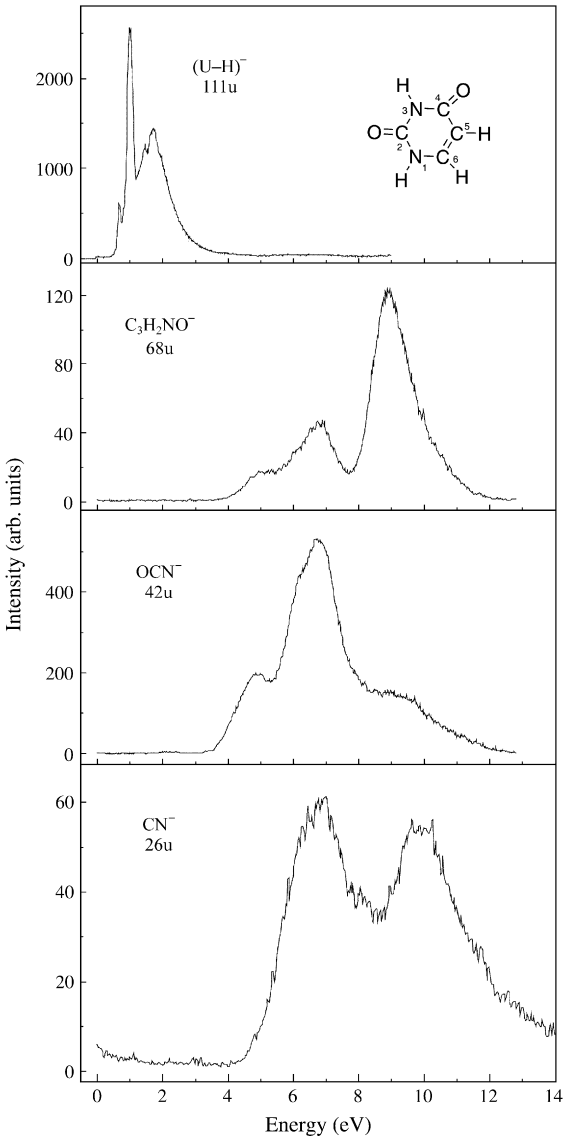

Fig. 54. Relative partial cross sections for dissociative electron attachment to uracil (shown as the inset chemical structure) as a function of electron energy. $(U–H)^-$ refers to the $(C_4H_3N_2O_2)^-$ anion. From Feil et al. (2004).

It is worth mentioning that, unlike some of the other molecules discussed in this section, the sugar ring in DNA does not have any OH groups hanging on it. Aflatooni et al. (2006) showed that the presence of an OH group on tetrahydrofuran increased the DEA cross section substantially.

4.16.6. Phosphates

Phosphates are of intense interest currently because of the key role the phosphate group plays in the backbone of the DNA molecule where it connects to adjacent sugar units. Cleavage of any of the P–O–C bonds would result in a single strand break in the DNA (see Fig. 47). Three different phosphate molecules have been studied recently in an attempt to elucidate what role phosphate units might have in the interaction of low energy electrons with DNA, particularly via the DEA process. Aflatooni et al. (2006) measured total cross sections for the DEA process in trimethyl phosphate (TMP) $[(H_3CO)_3PO]$, while Konig et al. (2006) studied the same process in dibutyl phosphate (DBP) $[(C_4H_9O)_2P(O)OH]$, and triethyl phosphate (TEP) $[(C_2H_5O)_3PO]$. Aflatooni et al. did not observe any DEA occurring at energies below about 3 eV and noted a broad structure at higher energies with a maximum cross section of 1.8×10^{-20} cm^2 at 7.4 eV. Konig et al., on the other hand, found that for their targets most of the DEA occurred at low energies below 2 eV with another, smaller, resonance near 8 eV. In DBP they found that the dominant anion production process was accompanied by dehydrogenation of the parent molecule. The second dominant fragment was the hydroxyl anion, with a peak at 0.2 eV, likely due to direct cleavage of the P–OH bond.

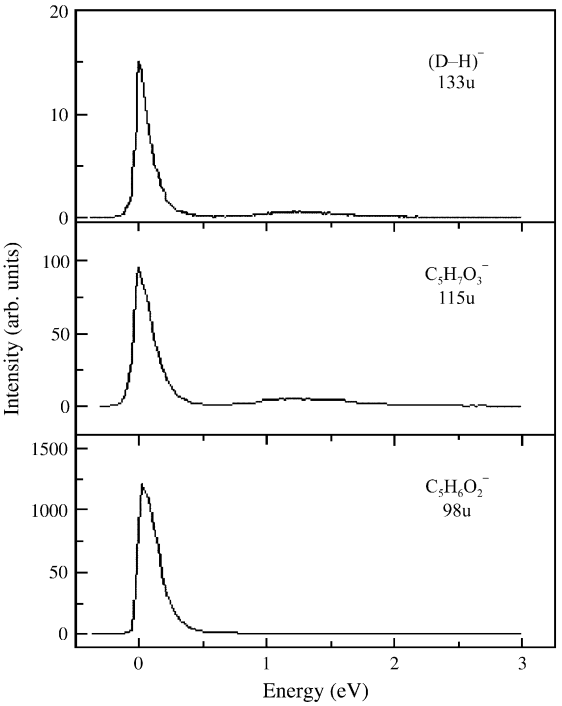

Fig. 55. Relative partial cross sections for production of $(D–H)^-$, $(C_5H_7O_3)^-$, and $(C_5H_6O_2)^-$ via dissociative electron attachment to deoxyribose as a function of electron energy. From Ptasinska et al. (2004).

In addition to these single bond cleavage processes, multiple bond cleavages, yielding such anions as PO^-, PO_3^- and $H_2PO_3^-$, were also observed. In TEP, these three anions were observed also but the de-hydrogenation reaction did not occur. This strongly suggests that loss of hydrogen occurs from the O–H site. An additional anion, observed with TEP, was $(C_2H_5O)_2PO^-$, which involved the loss of a complete C_2H_5O group from the precursor ion.

Kumar and Sevilla (2007) have used density functional theory to investigate DEA in 5-thymidine monophosphate, a simple model for DNA.

4.16.7. Furans

Furans, such as tetrahydrofuran (C_4H_8O) and 3-hydroxy-tetrahydrofuran ($C_4H_8O_2$), are commonly used as surrogates for study of the deoxyribose group in DNA and so there has been interest in how they respond to low-energy electron impact (Sanche, 2005). Thus, Aflatooni et al. (2006) have measured total DEA cross sections for these molecules and Sulzer et al. (2006) have used mass analysis to study the individual anion channels. Antic et al. (1999) and Park et al. (2006) have studied H^- desorption and electron trapping respectively following irradiation of thin films of these targets by low energy electrons. Bouchiha et al. (2006) have reported calculated integral scattering cross sections for tetrahydrofuran over the electron energy range 0–10 eV using an *ab initio R*-matrix technique.

In tetrahydrofuran, Sulzer et al. (2006) and Aflatooni et al. (2006) agree that DEA cross sections are small and, unlike the DNA bases, the process proceeds mainly via core excited resonances at energies above 5.5 eV.

Very recently absolute, differential elastic scattering measurements with tetrahydrofuran targets have been carried out by Allan (2007), Colyer et al. (2007) and Dampc et al. (2007) in the energy range below 50 eV. Reasonable agreement with the complex Kohn variational calculations of Trevisan et al. (2005) and the Schwinger multichannel calculations of Winstead and McKoy (2006), as well as with some earlier measurements of Milosavljevic et al. (2005), has been obtained. Allan (2007) also measured vibrational excitation cross sections from threshold up to 16 eV.

In addition to their biological uses, the furans have many industrial applications. Tetrahydrofuran is widely used as an industrial solvent and 2,5-dimethylfuran (C_6H_8O) has potential as a bio-fuel (Roman-Leshkov et al., 2007; Zhao et al., 2007).

4.17. Molecules of technological interest

In addition to NO_2, H_2O and O_2 itself, there are other oxygen-containing molecules of technological relevance particularly to the plasma processing and semiconductor communities. TEOS (tetraethoxysilane) and HMDSO (hexamethyldisiloxane) are frequently used in various plasma-assisted deposition and polymerization applications. HMDSO is often employed as a precursor for plasma-enhanced chemical vapour deposition of silicon oxide films and is frequently used in silicon integrated circuit technology. The silicon oxides, SiO and SiO_2 are of obvious interest also.

Fragmentation following electron impact is a primary process in electrical discharges involving these species and accurate quantification of the various processes involved is of fundamental interest and importance. To date, information is limited to some dissociative ionization and fluorescence studies. No information on dissociative attachment is available. Some information on neutral particle production in TEOS by electron impact has been inferred by Aumaille et al. (2000) while a total electron impact dissociation coefficient has been estimated by Vallee et al. (2000). Morgan et al. (2002) have developed a consistent set of low energy electron collision cross sections for TEOS based on a combination of calculations and experimental observations. These include a total dissociation cross section from threshold up to 50 eV.

4.17.1. *TEOS* [$Si(OCH_2CH_3)_4$]

4.17.1.1. Dissociative ionization. The only ionization cross section data for TEOS are those reported by Holtgrave et al. (1993) using Fourier-transform mass spectroscopy and, more recently, by Basner et al. (2000) using a double focusing mass spectrometer. The latter work covers a wider energy range but is still limited to incident energies below 100 eV. Dissociative ionization dominates over parent ionization and the cracking pattern is very complicated with a large number of fragment ions with appreciable cross sections. Table 37, adapted from Basner et al., gives a listing of the most intense ions, their appearance energies and partial ionization cross sections at 70 eV. Only those ions with relative intensities greater than 1% of the most abundant ion are presented. Holtgrave et al. (1993) only present data for the 20 most abundant ions. However, their summed cross sections for these ions agree well with the summed cross sections of Basner et al. for the same ions. Probst et al. (2001) find reasonable agreement between their calculated total cross sections and the data of Basner et al. (2000) using either the DM formalism or a Modified Additivity Rule (MAR), at least for energies below 50 eV.

4.17.1.2. Appearance energies and fragment energy distributions. Appearance energies for the various ions have been presented by both Holtgrave et al. (1993) and Basner et al. (2000). According to Basner et al., these range from 7.2 ± 0.3 eV for the parent ion to energies of 25 eV and larger for some of the lighter fragments (see Table 37). Holtgrave et al.'s data suggest that the appearance energies lie in a much smaller range between 10.6 and 16 eV. There may have been some fragment energy discrimination effects occurring, which could account for these differences. Since some appearance energies are quite low (below 12 eV in many cases), it is clear that a small TEOS admixture with Ar (where the ionization energy is much higher) in a plasma can drastically affect the ionization balance.

Many of the smaller fragment ions were observed to possess significant amounts of kinetic energy but no quantitative data were given.

4.17.1.3. Dissociative attachment. Holtgrave et al. (1993) looked for but saw no evidence for any negative ions produced by electron impact on TEOS.

4.17.1.4. Dissociative excitation. The only studies to date of the dissociative excitation of TEOS under controlled single-collision conditions seem to be those of Ducrepin et al. (1993) in the 200–800 nm region and of Kurunczi et al. (1998) in the VUV.

Kurunczi et al. found that the VUV emissions were dominated by the hydrogen Lyman series and they measured emission cross sections of 11 and 2×10^{-19} cm^2, respectively, for the Lyman-α and β members of this series at 100 eV incident electron energy. Detailed studies of the near-threshold regions indicated the existence of numerous break-up channels that contributed to the observed emissions. The lowest appearance energy indicated that excited H atoms in the $n = 2$ state were being removed from the parent molecule. Based on a detailed analysis of the near-threshold excitation functions and also on some direct measurements of the H Balmer lines, they estimated that cascade contributions to the Lyman emissions were significant.

In the near-UV–visible spectral region Ducrepin et al. (1993) found that the TEOS emission spectrum showed very few features. Apart from the H Balmer series, which was observed weakly, the only emissions were the CH($B\ ^2\Sigma^- - X\ ^2\Pi$) and ($A\ ^2\Delta - X\ ^2\Pi$) bands at 390 and 430 nm, respectively. Kurunczi et al. (1998) measured a Balmer-β cross section of 3.4×10^{-19} cm^2 at 100 eV. Some of their earlier work on H Balmer emission cross sections could have been over-estimates resulting from thermal decomposition of TEOS at the heated filament of the electron gun producing background H_2 [see Kurunczi et al. (1998)].

Initially it was thought that an atomic Si emission had been observed at 390 nm but this assignment was subsequently found to be incorrect [see Kurunczi et al. (1996)].

4.17.2. *HMDSO* [$(CH_3)_3SiOSi(CH_3)_3$]

4.17.2.1. Dissociative ionization. Some early work on ion fragmentation patterns in this molecule by Drake et al. (1979) and Seefeldt et al. (1985) has been supplemented recently by detailed studies over the impact energy range from threshold to 100 eV by Basner et al. (1998) and to 200 eV by Jiao et al. (2005). Whereas there is reasonable agreement in the cross sections for the major ions between the Jiao et al. and Basner et al. data sets, the earlier data of Seefeldt et al. seem to be too low. This may have been due to difficulties in target gas density determination in the earlier work [see Basner et al. (1998)]. Fig. 56 presents a sample of the Jiao et al. results and their data for the five most prominent ion fragmentation channels are given

Table 37
Measured appearance energies and partial ionization cross sections at 70 eV for the various ions produced following electron impact on TEOS

m/z [u]	Ion	Appearance energy (eV)	Cross section (10^{-18} cm^2)
208	$SiO_4C_8H_{20}^+$	7.2 ± 0.3	163
207	$SiO_4C_8H_{19}^+$	8.7 ± 0.4	48
193	$SiO_4C_7H_{17}^+$	8.4 ± 0.3	572
179	$SiO_4C_6H_{15}^+$	8.2 ± 0.3	139
177	$SiO_4C_6H_{13}^+$	13.3 ± 0.5	6.9
165	$SiO_4C_5H_{13}^+$	10.1 ± 0.5	42
151	$SiO_4C_4H_{11}^+$	10.4 ± 0.4	17
137	$SiO_4C_3H_9^+$	12.5 ± 0.5	12
123	$SiO_4C_2H_7^+$	13.1 ± 0.6	17
163	$SiO_3C_6H_{15}^+$	12.2 ± 0.3	320
149	$SiO_3C_5H_{13}^+$	11.4 ± 0.3	449
147	$SiO_3C_5H_{11}^+$	14.1 ± 0.8	12
135	$SiO_3C_4H_{11}^+$	11.5 ± 0.7	107
133	$SiO_3C_4H_9^+$	15.9 ± 0.7	17
121	$SiO_3C_3H_9^+$	13.5 ± 0.8	31
107	$SiO_3C_2H_7^+$	15.3 ± 0.4	67
105	$SiO_3C_2H_5^+$	21.4 ± 0.8	20
103	$SiO_3C_2H_3^+$	25.5 ± 1.0	3
93	$SiO_3CH_5^+$	16.9 ± 0.6	22
91	$SiO_3CH_3^+$	25.1 ± 0.8	13
89	SiO_3CH^+	18.4 ± 0.8	13
79	$SiO_3H_3^+$	19.3 ± 0.5	282
119	$SiO_2C_4H_{11}^+$	15.2 ± 0.6	173
118	$SiO_2C_4H_{10}^+$	16.6 ± 1.0	9.3
117	$SiO_2C_4H_9^+$	16.8 ± 1.0	9.2
105	$SiO_2C_3H_9^+$	16.6 ± 0.8	29
103	$SiO_2C_4H_7^+$	19.2 ± 1.0	12
91	$SiO_2C_2H_7^+$	17.1 ± 0.7	56
90	$SiO_2C_2H_6^+$	19.8 ± 0.8	15
89	$SiO_2C_2H_5^+$	19.4 ± 0.8	13
77	$SiO_2CH_5^+$	18.8 ± 0.6	22
76	$SiO_2CH_4^+$	22.8 ± 0.8	4.8
75	$SiOC_2H_7^+$	24.4 ± 0.8	1.4
63	$SiO_2H_3^+$	21.8 ± 0.5	152
62	$SiO_2H_2^+$	23.4 ± 0.7	68
61	SiO_2H^+	29.7 ± 1.2	5.3
75	$SiO_2C_2H_7^+$	23.1 ± 0.8	6.7
74	$SiOC_2H_6^+$	15.8 ± 0.8	4.8
73	$SiOC_2H_5^+$	21.8 ± 0.8	12.4
61	$SiOC_2H_5^+$	24.1 ± 0.9	3.4
47	$SiOH_3^+$	25.4 ± 1.0	5.1
45	$SiOH^+$	26.1 ± 0.9	79
45	$C_2H_5O^+$	11.1 ± 0.9	13
43	$C_2H_3O^+$	14.0 ± 0.7	35
31	CH_3O^+	13.1 ± 0.7	7.1
29	CHO^+	15.1 ± 0.7	29
29	$C_2H_5^+$	22.1 ± 0.7	251
28	$C_2H_4^+$	10.8 ± 0.7	55
27	$C_2H_3^+$	16.3 ± 0.3	156
26	$C_2H_2^+$	13.6 ± 0.3	27
15	CH_3^+	15.6 ± 0.5	71
14	CH_2^+	17.3 ± 0.5	9.2
2	H_2^+	15.9 ± 0.8	11
	TEOS	σ(total)	3719

From Basner et al. (2000).

in Table 38. Agreement between the Jiao et al. and Basner et al. data sets is particularly good with regard to the dominant fragment ion, $Si_2OC_5H_{15}^+$ where the ionization is accompanied by the loss of a CH_3 radical. For the smaller fragment ions, agreement between the two data sets is good only at energies <30 eV.

Probst et al. (2001) have calculated the total ionization cross section using two different techniques, the DM and MAR formalisms. They demonstrated that better agreement with the measurements of Basner et al. (1998) [and hence also Jiao et al. (2005)] is achieved using the latter technique. We note that this contrasts with the situation involving TEOS where the DM formalism gave better agreement with experiment.

Table 38
Absolute partial ionization cross sections for electron impact on HMDSO for the production of the five most significant ions

Energy (eV)	$\sigma(SiCH_5^+)$ (m/z 45u) (10^{-18} cm^2)	$\sigma(SiC_2H_7^+)$ (m/z 59u) (10^{-18} cm^2)	$\sigma(SiC_3H_9^+)$ (m/z 73u) (10^{-18} cm^2)	$\sigma(Si_2OC_4H_{11}^+)$ (m/z 131u) (10^{-18} cm^2)	$\sigma(Si_2OC_5H_{15}^+)$ (m/z 147u) (10^{-18} cm^2)	σ(total) (10^{-18} cm^2)
10					2	2
11					44	44
12					110	110
13					190	190
14					260	260
15					400	400
16			1	2	540	550
17			2	3	740	750
18			4	5	870	890
19			6	9	960	990
20			10	14	1070	1110
21	6		15	23	1160	1230
22	9		17	29	1240	1320
23	12	5	22	38	1410	1520
24	18	8	32	48	1480	1630
25	18	15	34	48	1510	1680
26	18	14	37	63	1550	1730
27	37	20	54	64	1610	1880
28	38	27	67	66	1640	1960
29	41	28	76	63	1670	2010
30	40	30	84	72	1700	2070
32	48	31	104	89	1700	2140
34	50	32	111	91	1730	2190
36	50	34	115	85	1710	2190
38	49	34	113	105	1730	2220
40	51	35	114	96	1710	2200
42	53	38	121	101	1740	2280
44	53	39	115	110	1750	2300
46	52	35	130	108	1740	2290
48	51	38	123	111	1750	2300
50	51	40	129	107	1740	2300
55	54	42	129	107	1730	2320
60	52	43	124	111	1760	2340
65	50	39	123	105	1740	2300
70	52	43	125	108	1740	2320
75	52	42	120	103	1730	2310
80	46	40	118	101	1730	2280
90	47	40	113	99	1730	2270
100	43	38	109	94	1710	2210
110	42	38	109	82	1640	2120
120	43	39	103	83	1550	2040
130	37	39	101	72	1470	1930
140	37	34	98	62	1440	1860
150	27	34	93	50	1350	1730
160	23	31	85	48	1330	1680
170	22	24	83	38	1240	1540
180	14	19	71	31	1080	1330
190	13	16	68	15	1040	1220
200	9	13	55	14	940	1080

The total ionization cross sections are also included. From Jiao et al. (2005).

4.17.2.2. Appearance energies and fragment energy distributions. Appearance energies for the thirteen most abundant ions have been tabulated by Basner et al. (1998, 2000). They range from 8.8 to 32.6 eV. Although not explicitly given, the threshold data of Jiao et al. (2005) seem consistent with these.

Basner et al. note that the fragment ions from HMDSO are formed with little, if any, excess kinetic energy. The only exception is the methyl ion, CH_3^+, which is formed with appreciable excess kinetic energy.

The shape of the CH_3^+ ionization cross section curve differs from the other ionization functions in that it has structure, which indicates that at least two dissociation channels are active in the production of this ion. The second, and more efficient, channel has an onset close to 50 eV.

4.17.2.3. Dissociative excitation. Kurunczi et al. (1998) found the same VUV spectral features as they had observed with TEOS targets, namely the H Lyman series. Emission cross sections were smaller, perhaps reflecting the fewer number of H atoms in the parent molecule. They drew similar conclusions regarding the importance of cascade and regarding the complexity of the dissociation processes.

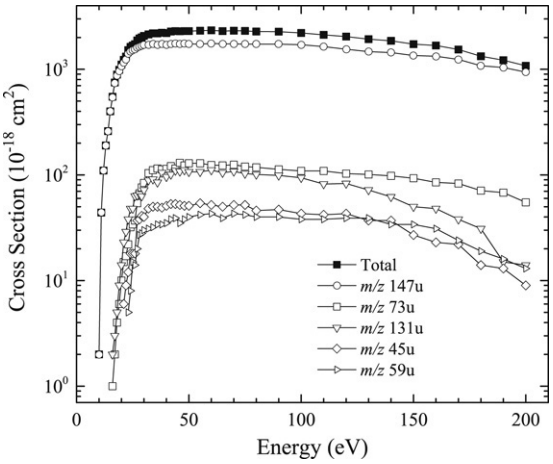

Fig. 56. Absolute cross sections for electron impact ionization of HMDSO. The estimated uncertainty is ±18%. The lines through the data points serve only as a guide to the eye. Data from Table 38.

In the near-UV/visible spectral region, Kurunczi et al. (1996) found that the dominant features were CH molecular emissions together with the hydrogen Balmer series and the atomic Si emissions at 253 and 288 nm. Not unexpectedly, similar features have been observed by Granier et al. (2003) in their study of the optical emission from HMDSO plasmas. Measured emission cross sections were typical of optically allowed channels in the excitation of the parent molecule. In general, cross sections were small, in the 10^{-19} cm^2 range or less. The strongest molecular emission was the so-called "430 nm" CH($A^2\Delta - X^2\Pi$) band, which had an emission cross section of 6.1×10^{-19} cm^2 at 100 eV incident electron energy. The appearance energy of this feature was 33 eV. Weaker molecular emissions observed were the CH($B\ ^2\Sigma^- - X\ ^2\Pi$) and ($C\ ^2\Sigma - X\ ^2\Pi$) bands at 390 and 314 nm respectively. In addition to the molecular features, the Balmer series of atomic hydrogen and some atomic Si lines near 250 nm and one at 288 nm were observed. The cross section for the latter $3s4p\ ^1P^o \rightarrow 3p^2\ ^1D$ transition reached a broad maximum of about 8×10^{-20} cm^2 at 150 eV. Interestingly, no atomic Si emissions were observed from TEOS in the energy range up to 100 eV, probably reflecting the fact that four strong Si–O bonds would need to be broken in this case. The observed appearance energy of the Si line from HMDSO was close to 45 eV.

4.17.3. SiO and SiO_2

A better understanding of the interaction of electrons with these targets is desirable for applications such as Electron Beam Induced Deposition (EBID) on nano-devices [see e.g. Hoffmann et al. (2000)]. Unfortunately very little quantitative information is available. Joshipura et al. (2007b) have calculated total inelastic cross sections in their complex potential formalism and have derived total ionization cross sections from these. He and Leung (2003) have used electron energy loss spectroscopy to study surface effects following ion bombardment of vitreous SiO_2 surfaces. A distinct need for both experimental and theoretical work, particularly regarding electron impact dissociation of these molecules, is evident.

4.17.4. Sulfur/oxygen halides

With new technology come new challenges and data needs. The increased use of SF_6 in the semiconductor industry (e.g. etching process gases) and electric power industry (e.g. compressed gas insulation of power lines, circuit breakers, etc.) has resulted in a need to understand the by-products of SF_6 plasmas (with O_2, H_2O, etc.) in order to increase efficiencies and minimize impediments (Anderson, 1993). Typical by-products from the plasmas include SO_2 along with other O–S compounds (e.g. SOF_2, SOF_4, SO_2F_2, S_2OF_{10}, and $S_2O_2F_{10}$) (van Brunt and Herron, 1994; Antoniotti et al., 2003). Also, for example, the increased use of power-dense lithium batteries has spawned a need for data relevant to the compounds contained inside in order to quantify chemical dynamics: lithium-thionyl chloride batteries utilize $SOCl_2$ as the positive active material.

The total electron impact cross sections for some sulfuryl halides, i.e. sulfuryl fluorochloride (SO_2ClF) and sulfuryl chloride (SO_2Cl_2), were obtained by Szmytkowski et al. (2005, 2006) who provided references to earlier work. Electron impact studies of sulfuryl halides have mainly focused on dissociative electron attachment and total intensity measurements. Wan et al. (1993) investigated the absolute total cross sections, with electrons between 0.2 and 12 eV, of some electrical discharge by-products of SF_6: thionyl fluoride (SOF_2), thionyl tetraflouride (SOF_4), and sulfuryl fluoride (SO_2F_2), along with SO_2 (see Section 4.8.3). Wan et al. also obtained the total electron attachment cross sections for these gaseous compounds. Sauers et al. (1993) essentially provided a complementary study of the same target species and determined relative DEA cross sections for the range 0–14 eV. The total attachment cross sections of Sauers et al. agreed well with the results of Wan et al., who used a different apparatus, enabling estimates of the absolute DEA cross sections. Sauers et al.'s work represents a continuation of the $e^- + SO_2F_2$ work of Datskos and Christophorou (1989), which included the effect of temperature changes

on the target gas. Miletic et al. (1996, 1997) have studied dissociative ionization channels in SO_2F_2. Earlier electron impact studies, with some also including SO_2Cl_2 and SO_2ClF targets, mostly involved DEA and some ionization appearance potential studies: Wang and Franklin (1980); Robbiani and Franklin (1979); Sullivan and Beauchamp (1978); Reese et al. (1958).

Merrill and Cady (1961) were one of the first to study bis-pentafluorosulfur peroxide ($S_2O_2F_{10}$). However, their electron impact work only stated the observed fragments at 70 eV using an early magnetic sector mass spectrometer. More recently, Olthoff et al. (1993) investigated DEA to $S_2O_2F_{10}$ and bis-pentafluorosulfur oxide (S_2OF_{10}), with the negative ion fragment identification by way of a time-of-flight mass spectrometer. No parent anions were observed, which suggested that dissociation occurred even at thermal energies. Amazingly large DEA cross sections ($\sim 10^{-12}$ cm^2) were observed for S_2OF_{10} and $S_2O_2F_{10}$ at energies near 0.1 eV suggesting that trace amounts cannot be immediately discounted as having negligible impact.

4.18. Ethers, dioxins, dioxanes

Ethers are important molecules being widely used for example as solvents and anaesthesia agents. Only a limited amount of electron impact related information seems to be available regarding their dissociation though cracking patterns and appearance energy determinations for the various fragment cations are available from the NIST Chemistry WebBook (2005).

Dissociative attachment data has been given by Bulliard et al. (2001) for methyl vinyl ether (C_3H_6O), ethyl vinyl ether (C_4H_8O), methyl allyl ether (C_4H_8O), benzyl methyl ether ($C_8H_{10}O$) and anisole (C_7H_8O). They discuss the various anion production pathways but no quantitative cross section data are given.

Some information is also available for related dioxin and dioxane compounds, which technically qualify as ethers. Both are heterocyclic organic compounds. In their simplest un-substituted forms, dioxin and dioxane have chemical formulae $C_4H_4O_2$ and $C_4H_8O_2$ respectively. Interest in the interaction of low energy electrons with these species stems not only from their importance in the manufacturing industries but also because they are extremely important as environmental pollutants with carcinogenic properties. Hirota and Kojima (2005) have studied the decomposition behaviour of a number of dioxins in incinerator gases under electron beam irradiation, motivated by the potential importance of such processes in solid waste disposal. Muftakov et al. (2000a,b, 2001) and Khatymov et al. (2004) studied DEA to dibenzo-p-dioxin ($C_{12}O_2H_8$) and its chloro derivatives in the electron energy range 0–10 eV. Cl^- was the dominant anion observed but abstraction of hydrogen or chlorine atoms or the HCl molecule from the parent molecule were also contributing processes. Berkout et al. (1999) studied the production of negative ions, particularly chloride ions, from a number of polychlorodibenzo-p-dioxins (PCDDs) while Furlei et al. (1999) studied negative ion formation in a number of substituted dioxanes.

4.19. Aldehydes and ketones

Aldehydes and ketones are widely used in the chemical industry. Ketones such as acetone, $(CH_3)_2CO$, are widely used as solvents and intermediates. They are often used in perfumes and paints to stabilize the other ingredients so that they do not degrade as quickly over time. These species are also present in the terrestrial atmosphere as minor but active constituents [see Limao-Vieira et al. (2003)].

Most of the available gas phase electron impact work appears to be concentrated in establishing ionization energies of the various targets, fragmentation patterns at a particular impact energy, and appearance energies of the fragment ions [see e.g. Kanomata (1961), Dorman (1965), Movier and Hernandez (1975) and included references]. The most detailed studies of DEA seem to be those of Dressler and Allan (1985a,b, 1986) who studied the decay channels of acetaldehyde, CH_3COH, using negative ion mass spectroscopy; CH_3^-, O^- and H^- were all observed.

Photodissociation work on acetone has been reported by Wei et al. (2005). They were able to establish the dissociation channels for the formation of a number of fragment ions. Lepage et al. (2000) have reported on the production of neutral CO following electron bombardment of thin acetone films in the energy range 2–25 eV.

4.20. Phenols

Phenols are a class of compounds consisting of a hydroxyl (OH) group attached to an aromatic hydrocarbon group. The simplest member has the formula C_6H_5OH. Although similar to alcohols, they have unique properties and are not classified as alcohols because the OH group is not bonded to a *saturated* carbon atom. They have a wide range of uses from disinfectants and herbicides to food flavouring [see e.g. Muftakov et al. (2000a,b)].

Muftakov et al. (2000a,b) studied DEA to phenol and parachlorophenol in the electron energy range 0–12 eV. They showed that the dominant negative ion production process in each case was associated with hydrogen atom abstraction at electron energies close to 1 eV. Evidence for other anions such as Cl^- was demonstrated and many Feshbach and shape resonances were observed. Khatymov et al. (2003a,b) extended this work to other chlorophenols. They were able to quantify the different dissociation channels and discuss the various mechanisms involved.

4.21. Esters

Esters consist of an inorganic or organic acid in which at least one hydroxy (OH) group is replaced by an alkoxy (O-alkyl) group. They have a wide range of applications in commerce and industry ranging from perfume manufacture to solvents and plastics. For esters derived from the carboxylic acids, the traditional name for the acid is generally retained, e.g. formate, acetate, etc. Alternatively, the systematic name of the acid is used with the suffix –*oate*. Thus methyl formate may also be called methyl methanoate.

There seems to be a scarcity of data available for gas phase studies of low energy electron interactions with esters leading to dissociation. A notable exception to this is the work of Pariat and Allan (1991) who have studied DEA to methyl acetate (CH_3OCOCH_3). Eight fragment anions were observed in the energy range 0–12 eV and production mechanisms were discussed. Data were also presented for fragmentation of methyl and ethyl propionate resulting in the CH_3CO^- fragment. Hudson et al. (2006) presented absolute total positive ion cross sections for a number of formates and acetates but no fragmentation data are available.

5. Conclusions

A wide range of oxygen-containing molecules has been surveyed and a quantitative analysis made of the electron impact processes that produce dissociation in these molecules. Data of sufficient quality to be considered "benchmarks" have been identified (see for example Tables 7 and 8) as have areas where no quantitative information is available or where significant levels of disagreement between different experimenters, or between experiment and theory, are evident and hence where additional work is required.

In addition to the molecules discussed here, we should note that sporadic information is available on other oxygen-containing molecules. For example, Voinov et al. (2003) and Feil et al. (2007) discuss ion formation in nitrobenzene ($C_6H_5NO_2$) and nitrotoluene ($C_7H_7NO_2$) respectively and reference earlier work on the dissociation of these molecules by low energy electrons.

Acknowledgements

This work was performed at the Jet Propulsion Laboratory (JPL), California Institute of Technology (Caltech), under a contract with the National Aeronautics and Space Administration (NASA), and at Caltech. We gratefully acknowledge financial support through NASA's Planetary Atmospheres and Outer Planets Research programs as well as from the U.S. Department of Energy, Office of Basic Energy Sciences, and from the Natural Sciences and Engineering Research Council of Canada. This research was performed while CPM and JWMcC held NASA Fellowships at JPL. Kate Mendenhall provided invaluable assistance in the preparation of tabular and graphical material. The authors thank the referee for many helpful suggestions.

References

Aarts, J.F.M, de Heer, F.J., 1970. J. Chem. Phys. 52, 3554.
Aarts, J.F.M, de Heer, F.J., 1971. Physica 56, 294.
Abdoul-Carime, H., Huels, M.A., Illenberger, E., Sanche, L., 2001. J. Amer. Chem. Soc. 123, 5354.
Abdoul-Carime, H., Sanche, L., 2002. Int. J. Rad. Bio. 78, 89.
Abdoul-Carime, H., Langer, J., Huels, M.A., Illenberger, E., 2005. Eur. Phys. J. D 35, 399.
Abedi, A., Cicman, P., Coupier, B., Gulejova, B., Buchanan, G.A., Marston, G., Mason, N.J., Schier, P., Märk, T.D., 2004. Int. J. Mass Spectrom. 232, 147.
Abouaf, R., 2008. Chem. Phys. Lett. 451, 25.
Abouaf, R., Pommier, J., Dunet, H., 2003a. Chem. Phys. Lett. 381, 486.
Abouaf, R., Pommier, J., Dunet, H., 2003b. Int. J. Mass Spectrom. 226, 397.
Abouaf, R., Dunet, H., 2005. Eur. Phys. J. D 35, 405.
Abouaf, R., Fiquet-Fayard, F., 1976. J. Phys. B 9, L323.
Abouaf, R., Paineau, R., Fiquet-Fayard, F., 1976. J. Phys. B 9, 303.
Abouaf, R., Pommier, J., Cvejanovic, S., Saubaméa, B., 1994. Chem. Phys. 188, 339.
Abuain, T., Walker, I.C., Dance, D.F., 1985. J. Chem. Soc.-Faraday Trans. II 81, 1061.
Aflatooni, K., Burrow, P.D., 2000. J. Chem. Phys. 113, 1455.
Aflatooni, K., Scheer, A.M., Burrow, P.D., 2006. J. Chem. Phys. 125, 054301.
Ahmed, M., Apps, C.J., Hughes, C., Whitehead, J.C., 1994. J. Phys. Chem. 98, 12530.
Ahmed, M., Apps, C.J., Hughes, C., Whitehead, J.C., 1995. Chem. Phys. Lett. 240, 216.
Ajello, J.M., 1971. J. Chem. Phys. 55, 3169.
Ajello, J.M., 1984. Geophys. Res. Lett. 11, 1195.
Ajello, J.M., Franklin, B., 1985. J. Chem. Phys. 82, 2519.
Ajello, J.M., Shemansky, D.E., 1985. J. Geophys. Res. A 90, 9845.
Ajello, J.M., Pang, K.D., Franklin, B.O., Howell, S.K., Bowring, N.J., 1989a. J. Geophys. Res. A 94, 9093.
Ajello, J.M., Pang, K.D., Franklin, B.O., Howell, S.K., Bowring, N.J., 1989b. J. Geophys. Res. A 94, 9105.
Ajello, J.M., James, G.K., Kanik, I., Franklin, B.O., 1992a. J. Geophys. Res. 97, 10473.
Ajello, J.M., James, G.K., Kanik, I., 1992b. J. Geophys. Res. 97, 10501.
Ajello, J.M., Hansen, D.L., Beegle, L.W., Terrell, C.A., Kanik, I., James, G.K., Makarov, O.P., 2002. J. Geophys. Res. 107, 1099.
Ajello, J.M., Aguilar, A., Mangina, R.S., James, G.K., Geissler, P., Trafton, L., 2008. J. Geophys. Res. 113, E03002.
Akhmatskaya, E.V., Apps, C.J., Hillier, I.H., Masters, A.J., Palmer, I.J., Watt, N.E., Vincent, M.A., Whitehead, J.C., 1997. J. Chem. Soc.-Faraday Trans. 93, 2775.

Allamandola, L.J., 1992. In: Bohma, D.K., Hebst, H., Kaifu, N., Saito, S. (Eds.), Chemistry and Spectroscopy of Interstellar Molecules. Univ. of Tokyo Press, Tokyo.
Allamandola, L.J., Bernstein, M.P., Sandford, S.A., Walker, R.L., 1999. Space Sci. Rev. 90, 219.
Allan, M., 1995. J. Phys. B 28, 4329.
Allan, M., 2004. J. Phys. B 37, L359.
Allan, M., 2007. J. Phys. B 40, 3531.
Allan, M., Skalicky, T., 2003. J. Phys. B 36, 3397.
Allan, M., Asmis, K.R., Popovic, D.B., Stepanovic, M., Mason, N.J., Davies, J.A., 1996a. J. Phys. B 29, 4727.
Allan, M., Mason, N.J., Davies, J.A., 1996b. J. Chem. Phys. 105, 5665.
Allcock, G., McConkey, J.W., 1976. J. Phys. B 9, 2127.
Allcock, G., McConkey, J.W., 1978a. Chem. Phys. 34, 169.
Allcock, G., McConkey, J.W., 1978b. J. Phys. B 11, 741.
Anderson, W.E. (Ed.) 1993. Research for Electric Energy Systems – An Annual Report. NISTIR 5268, National Inst. of Standards and Technology, Gaithersburg, MD.
Ankerhold, U., Esser, B., von Busch, F., 1997a. J. Phys. B 30, 1207.
Ankerhold, U., Esser, B., von Busch, F., 1997b. Chem. Phys. 220, 393.
Antic, D., Parenteau, L., Lepage, M., Sanche, L., 1999. J. Phys. Chem. B 103, 6611.
Antoniotti, P., Facchini, P., Grandinetti, F., 2003. Chem. Phys. Lett. 372, 455.
Antony, B.K., Joshipura, K.N., Mason, N.J., 2004. Int. J. Mass Spectrom. 233, 207.
Appel, J., Durup, J., Hitz, F., 1966. Adv. Mass Spectrom. 3, 457.
Appel, J., Durup, J., 1973. Int. J. Mass Spectrom. Ion Phys. 10, 247.
Apps, C.J., Watt, N.E., Whitehead, J.C., 1997. Isr. J. Chem. 37, 419.
Armenante, M., Santoro, V., Spinelli, N., Vanoli, F., 1985. Int. J. Mass Spectrom. Ion. Proc. 64, 265.
Au, J.W., Brion, C.E., 1997. Chem. Phys. 218, 109.
Aumaille, K., Granier, A., Schmidt, M., Grolleau, B., Vallee, C., Turban, G., 2000. Plasma Sources Sci. Tech. 9, 331.
Avakyan, A.V., Il'in, R.N., Lavrov, V.M., Ogurtsov, G.N., 1998. Collision Processes and Excitation of UV Emission from Planetary Atmospheric Gases. Gordon and Breach, Newark, NJ, p. 151.
Bachorz, R.A., Klopper, W., Gutowski, M., 2007. J. Chem. Phys. 126, 085101.
Bahati, E.M., Jureta, J.J., Belic, D.S., Rachafi, S., Defrance, P., 2001. J. Phys. B 34, 1757.
Balakrishnan, N., Jamieson, M.J., Dalgarno, A., Li, Y., Buenker, R.J., 2000. J. Chem. Phys. 112, 1255.
Bald, I., Kopyra, J., Illenberger, E., 2006. Angew. Chem. Int. Ed. 45, 4851.
Bald, I., Kopyra, J., Dabkowska, I., Antonsson, E., Illenberger, E., 2007. J. Chem. Phys. 126, 074308.
Baluev, A.V., Nikitina, Z.K., Fedorova, L.I., Rosolovskii, V.Y., 1963. Izv. Akad. Nauk. SSR, Ser. Khi. 1980.
Baluja, K.L., Mason, N.J., Morgan, L.A., Tennyson, J., 2001. J. Phys. B 34, 4041.
Bapat, B., Sharma, V., 2007. J. Phys. B 40, 13.
Bardsley, J.N., 1968. J. Phys. B 1, 349.
Barnett, S.M., Mason, N.J., Newell, W.R., 1991. Chem. Phys. 153, 283.
Barnett, S.M., Mason, N.J., Newell, W.R., 1992. J. Phys. B 25, 1307.
Barsotti, S., Leber, E., Ruf, M.-W., Hotop, H., 2002. Int. J. Mass Spectrom. 220, 313.
Barsotti, S., Sommerfeld, T., Ruf, M.-W., Hotop, H., 2004. Int. J. Mass Spectrom. 233, 181.
Basner, R., Schmidt, M., Deutsch, H., Tarnovsky, V., Levin, A., Becker, K., 1995. J. Chem. Phys. 103, 211.
Basner, R., Foest, R., Schmidt, M., Becker, K., Deutsch, H., 1998. Int. J. Mass. Spectrom. Ion Proc. 176, 245.
Basner, R., Becker, K., Deutsch, H., Schmidt, M., 2000. In: Inokuti, M., Becker, K. (Eds.), Fundamentals of Plasma Chemistry. In: Adv At Mol Opt Phys, vol. 43. Academic Press, New York, p. 147.
Becker, K., Stumpf, B., Schulz, G., 1980a. Chem. Phys. 53, 31.
Becker, K., Stumpf, B., Schulz, G., 1980b. Chem. Phys. Lett. 73, 102.
Becker, K., van Wijngaarden, W., McConkey, J.W., 1983. Planet Space Sci. 31, 197.
Becker, K., McCurdy, C.W., Orlando, T.M., Rescigno, T.N., 2000. Electron-driven processes: Scientific challenges and technological opportunities. US DOE Report.
Beegle, L.W., Ajello, J.M., James, G.K., Dziczek, D., Alvarez, M., 1999. Astron. Astrophys. 347, 375.
Beenakker, C.I.M., de Heer, F.J., Krop, H.B., Möhlmann, G.R., 1974. Chem. Phys. 6, 445.
Belic, D.S., Landau, M., Hall, R.I., 1981. J. Phys. B 14, 175.
Belic, D.S., Yu, D.J., Siari, A., Defrance, P., 1997. J. Phys. B 30, 5535.
Belic, D.S., Landau, M., Hall, R.I., 1980. J. Phys. B 14, 175.
Berdys, J., Anusiewicz, I., Skurski, P., Simons, J., 2004. J. Phys. Chem. 108, 2999.
Berkout, V.D., Mazurkiewicz, P., Deinzer, M.L., 1999. J. Amer. Chem. Soc. 121, 2561.
Bernhardt, Ph., Paretzke, H.G., 2003. Int. J. Mass Spectrom. 223, 599.
Bethe, H., 1930. Ann. Phys. (Leipzig) 5, 325.
Bhardwaj, A., Michael, M., 1999. J. Geophys. Res. 104, 24713.
Boechat-Roberty, H.M., Pilling, S., Santos, A.C.F., 2005. Astronom. Astrophys. 438, 915.
Borst, W.L., Zipf, E.C., 1971. Phys. Rev. A 4, 153.
Böse, N., Sroka, W., 1973. Z. Naturforsch 28a, 22.
Bouchiha, D., Gorfinkel, J.D., Caron, L.G., Sanche, L., 2006. J. Phys. B 39, 975.
Bouchiha, D., Gorfinkel, J.D., Caron, L.G., Sanche, L., 2007. J. Phys. B 40, 1259.
Boudaiffa, B., Cloutier, P., Hunting, D., Huels, M.A., Sanche, L., 2000. Science 287, 1658.
Bray, I., Fursa, D.V., Kheifets, A.S., Stelbovics, A.T., 2002. J. Phys. B 35, R117.
Brunger, M., et al., 2003. In: Itikawa, Y. (Ed.), Photon and Electron Interactions with Atoms, Molecules and Ions. In: Landolt-Börnstein, vol. I/17, Subvolume C. Springer, New York.
Brüning, F., Matejcik, S., Illenberger, E., Chu, Y., Senn, G., Muigg, D., Denifl, G., Märk, T.D., 1998. Chem. Phys. Lett. 292, 177.
Buck, U., Huisken, F., 2000. Chem. Rev. 100, 3863.
Buck, U., Hobein, M., Krohne, R., Linnartz, H., 1991. Z. Phys. D 20, 181.
Bulliard, C., Allan, M., Grimme, S., 2001. Int. J. Mass Specrtom. 205, 43.
Burke, P.G., Berrington, K.A. (Eds.), 1993. Atomic and Molecular Processes: An R-Matrix Approach. IOP Publishing, Bristol.
Burrow, P.D., Gallup, G.A., Scheer, A.M., Denifl, S., Ptasinska, S., Märk, T.D., Scheier, P., 2006. J. Chem. Phys. 124, 124310.
Bussieres, N., Marmet, P., 1977. Canad. J. Phys. 55, 1889.
Cadez, I.M., Pejcev, V.M., Kurepa, M.V., 1983. J. Phys. D 16, 305.
Calvert, J.G., Madronich, S., Gardner, E.P., Davidson, J.A., Cantrell, C.A., Shetter, R.E., 1987. J. Phys. Chem. 91, 6339.
Campbell, L., Green, M.A., Brunger, M.J., Teubner, P.J.O., Cartwright, D.C., 2000. Phys. Rev. A 61, 022706.
Carilli, C.L., Cox, P., Bertoldi, F., Menten, K.M., Omont, A., Djorgovski, S.G., Petric, A., Beelen, A., Issac, K.G., McMahon, R.G., 2002. Astrophys. J. 575, 145.
Champion, C., Hanssen, J., Hervieux, P.A., 2002. J. Chem. Phys. 117, 197.
Chantry, P.J., 1968. Phys. Rev. 172, 125.

Chantry, P.J., 1972. J. Chem. Phys. 57, 3180.
Choi, C.J., Jung, K.W., Kang, W.K., Youn, D.Y., Jung, K.-H., Kim, D., 1993. Org. Mass. Spec. 28, 931.
Chu, Y., Senn, G., Scheier, P., Stamatovic, A., Märk, T.D., Brüning, F., Matejcik, S., Illenberger, E., 1998a. Phys. Rev. A 57, R697.
Chu, Y., Senn, G., Matejcik, S., Scheier, P., Stampfli, P., Stamatovic, A., Illenberger, E., Märk, T.D., 1998b. Chem. Phys. Lett. 289, 521.
Chung, S., Lin, C.C., 1980. Phys. Rev. A 21, 1075.
Chutjian, A., Hall, R.I., Trajmar, S., 1975. J. Chem. Phys. 63, 892.
Cicman, P., Senn, G., Denifl, G., Muigg, D., Skalny, J.D., Lukac, P., Stamatovic, A., Märk, T.D., 1998. Czech J. Phys. 48, 1135.
Cicman, P., Francis, M., Skalny, J.D., Märk, T.D., 2003. Int. J. Mass Spectrom. 223-4, 271.
Cicman, P., Buchanan, G.A., Marston, G., Ulejova, B.G., Skalny, J.D., Mason, N.J., Scheier, P., Märk, T.D., 2004. J. Chem. Phys. 121, 9891.
Cicman, P., Skalny, J.D., Fedor, J., Mason, N.J., Scheier, P., Illenberger, E., Märk, T.D., 2007. Int. J. Mass Spectrom. 260, 85.
Ciocca, M., Kanik, I., Ajello, J.M., 1997. Phys. Rev. A 55, 3547.
Clampitt, R., Newton, A.S., 1969. J. Chem. Phys. 50, 1997.
Colyer, C.J., Vizcaino, V., Sullivan, J.P., Brunger, M.J., Buckman, S.J., 2007. New J. Phys. 9, 41.
Compton, R.N., Christophorou, L.G., 1967. Phys. Rev. 154, 110.
Cooks, R.G., Terwilliger, D.T., Beynon, J.H., 1974. J. Chem. Phys. 61, 1208.
Cooper, C.D., Cobb, G.C., Tolnas, E.L., 1961. J. Mol. Spectrosc. 7, 223.
Cordaro, R.B., Hsieh, K.C., McIntyre Jr., L.C., 1986. J. Phys. B 19, 1863.
Cosby, P.C., 1993. J. Chem. Phys. 98, 7804; 9544; 9560.
Coupier, B., Farizon, B., Farizon, M., Gaillard, M.J., Gobet, F., de Castro Faria, N.V., Jalbert, G., Ouaskit, S., Carre, M., Gstir, B., Hanel, G., Denifl, S., Feketeova, L., Scheier, P., Märk, T.D., 2002. Eur. Phys. J. D 20, 459.
Lide, David R. (Ed.), 2007. CRC Handbook of Chemistry and Physics, 87th edition (Internet Version 2007). CRC Press/Taylor and Francis, Boca Raton, FL.
Crovisier, J., Bockelee-Morvan, D., Colom, P., Biver, N., Despois, D., Lis, D., 2004. Astron. Astrophys. 418, 1141.
Crowe, A., McConkey, J.W., 1974. J. Phys. B 7, 349.
Crutzen, P.J., 1971. J. Geophys. Res. 76, 7311.
Curtis, M.G., Walker, I.C., 1992. J. Chem. Soc. Far. Trans. 88, 2805.
Dampc, M., Milosavljevic, A.R., Linert, I., Marinkovic, B.P., Zubek, M., 2007. Phys. Rev. A 75, 042710.
Darrach, M., McConkey, J.W., 1992. Chem. Phys. Lett. 184, 141.
Datskos, P.G., Christophorou, L.G., 1989. J. Chem. Phys. 90, 2626.
Davies, J.A., Continetti, R.E., Chandler, D.W., Hayden, C.C., 2000. Phys. Rev. Lett. 84, 5983.
De Pablos, J.L., Kendall, P.A., Tegeder, P., Williart, A., Blanco, F., Garcia, G., Mason, N.J., 2002. J. Phys. B 35, 865.
de Heer, F.J., Carrière, J.D., 1971. J. Chem. Phys. 55, 3829.
Denifl, G., Muigg, D., Stamatovic, A., Märk, T.D., 1998. Chem. Phys. Lett. 288, 105.
Denifl, S., Matwejcik, S., Gstir, B., Hanel, G., Probst, M., Scheier, P., Märk, T.D., 2003. J. Chem. Phys. 118, 4107.
Denifl, S., Ptasinska, S., Probst, M., Hrusak, J., Scheier, P., Märk, T.D., 2004a. J. Phys. Chem. A 108, 6562.
Denifl, S., Ptasinska, S., Hanel, G., Gstir, B., Scheier, P., Probst, M., Farizon, B., Farizon, M., Matejcik, S., Illenberger, E., Märk, T.D., 2004b. Phys. Scripta T110, 252.
Denifl, S., Sonnweber, B., Hanel, G., Scheier, P., Märk, T.D., 2004c. Int. J. Mass Spectrom. 238, 47.
Denifl, S., Candori, P., Ptasinska, S., Limao-Vieira, P., Grill, V., Märk, T.D., Scheier, P., 2005. Eur. Phys. J. D 35, 391.
Denifl, S., Zappa, F., Mahr, I., Lecointre, J., Probst, M., Märk, T.D., Scheier, P., 2006. Phys. Rev. Lett. 97, 043201.
Derbyshire, J., Kedzierski, W., McConkey, J.W., 1997. Phys. Rev. Lett. 79, 2229.
Deutsch, H., Becker, K., Märk, T.D., 1997. Int. J. Mass Spectrom. Ion. Proc. 167–168, 503.
Deutsch, H., Becker, K., Matt, S., Märk, T.D., 2000. Int. J. Mass Spectrom. 197, 37.
Deutsch, H., Scheier, P., Becker, K., Märk, T.D., 2004. Int. J. Mass Spectrom. 233, 13.
Dibeler, V.H., Walker, J.A., Liston, S.K., 1967. J. Res. Natl. Bur. Stand. 71A, 371.
Dillard, J.G., Franklin, J.L., 1968. J. Chem. Phys. 48, 2349.
Djuric, N., Cadez, I.M., Kurepa, M.V., 1989. Fizika (Zagreb) 21, 339.
Djuric, N., Cadez, I.M., Kurepa, M.V., 1988. Int. J. Mass. Spectrom. Ion Phys. 83, R7.
Domcke, W., 1991. Phys. Rep. 208, 97.
Donahue, D.E., Schiavone, J.A., Freund, R.S., 1977. J. Chem. Phys. 67, 769.
Donaldson, F.G., Hender, M.A., McConkey, J.W., 1972. J. Phys. B 5, 1192.
Doolittle, P.H., Schoen, R.I., Schubert, K.E., 1968. J. Chem. Phys. 49, 5108.
Dorman, F.H., 1965. J. Chem. Phys. 42, 65.
Dörner, R., Mergel, V., Jagutski, O., Spielberger, L., Ullrich, J., Moshammer, R., Schmidt-Bocking, H., 2000. Phys. Rep. 330, 95.
Drake, J.E., Glavincevski, B.M., Wong, C., 1979. J. Inorg. Nucl. Chem. 42, 175.
Dressler, R., Allan, M., 1985a. Chem. Phys. 92, 449.
Dressler, R., Allan, M., 1985b. Chem. Phys. Lett. 118, 93.
Dressler, R., Allan, M., 1986. J. Electron. Spect. Related Phenom. 41, 275.
Ducrepin, M., Dike, J., Siegel, R.B., Tarnovsky, V., Becker, K., 1993. J. Appl. Phys. 73, 7203.
Du Penhoat, M.-A.H., Huels, M.A., Cloutier, P., Jay-Gerin, J.-P., Sanche, L., 2001. J. Chem. Phys. 114, 5755.
Dunn, G.H., 1962. Phys. Rev. Lett. 8, 62.
Ehrhardt, H., Kresling, A., 1967. Z. Naturforschg 22a, 2036.
Eland, J.H.D., Berkowitz, J., 1979. J. Chem. Phys. 70, 5155.
Eland, J.H.D., Wort, F.S., Lablanquie, P., Nenner, I., 1986. Z. Phys. D 4, 31.
Eliasson, B., Kogelschatz, U., 1986. J. Phys. B 19, 1241.
El-Shall, M.S., Marks, C., Sleck, L.W., Meot-Ner, M., 1992. J. Phys. Chem. 96, 2045.
Erdman, P.W., Zipf, E.C., 1983a. J. Geophys. Res. 88, 7245.
Erdman, P.W., Zipf, E.C., 1983b. Planet Space Sci. 31, 1291.
Erdman, P.W., Zipf, E.C., 1987. J. Chem. Phys. 87, 4540.
Erdevdy, N.M., Vukstich, V.S., Shpenik, O.B., 2007. Abs. Th. 058, ICPEAC XXV, Freiburg.
Esposito, L.W., 1984. Science 223, 1072.
Fabrikant, I.I., Wahehra, J.M., Xu, Y., 2002. Phys. Scripta T96, 45.
Fabrikant, I.I., Hotop, H., 2005. Phys. Rev. Lett. 94, 063201.
Fedor, J., Cicman, P., Coupier, B., Feil, S., Winkler, M., Gluch, K., Husarik, J., Jaksch, D., Farizon, B., Mason, N.J., Scheier, P., Märk, T.D., 2006. J. Phys. B 39, 3935.
Feil, S., Gluch, K., Matt-Leubner, S., Scheier, P., Limtrakul, J., Probst, M., Deutsch, H., Becker, K., Stamatovic, A., Märk, T.D., 2004. J. Phys. B 37, 3013.
Feil, S., Sulzer, P., Mauracher, A., Beikircher, M., Wendt, N., Aleem, A., Denifl, S., Zappa, F., Matt-Leubner, S., Bacher, A., Matejcik, S., Probst, M., Scheier, P., Märk, T.D., 2007. J. Phys.: Conf. Ser. 86, 012003.
Field, D., Jones, N.C., Gingell, J.M., Mason, N.J., Lunt, S.L., Ziesel, J.-P., 2000. J. Phys. B 33, 1039.
Field, T.A., Slattery, A.E., Adams, D.J., Morrison, D.D., 2005. J. Phys. B 38, 255.
Finn, T.G., Doering, J.P., 1976. J. Chem. Phys. 64, 4490.
Fisher, I.P., 1967. J. Chem. Soc., Far. Trans. 63, 684.
Flaherty, D.W., Kasper, M.A., Baio, J.E., Graves, D.B., Winters, H.F., Winstead, C., McKoy, V., 2006. J. Phys. D 39, 4393.

Flesch, R., Ruhl, E., Hottmann, K., Baumgartel, H., 1993. J. Phys. Chem. 97, 837.
Flicker, W.M., Mosher, O.A., Kuppermann, A., 1980. J. Chem. Phys. 72, 2788.
Fremont, F., Leclercq, C., Hajaji, A., Naja, A., Lemennais, P., Boulbain, S., Broquin, V., Chesnel, J.-Y., 2005. Phys. Rev. A 72, 042702.
Freund, R.S., 1971a. Chem. Phys. Lett. 9, 135.
Freund, R.S., 1971b. J. Chem. Phys. 54, 3125.
Freund, R.S., 1971c. J. Chem. Phys. 55, 3569.
Furlei, I.I., Shmakov, V.S., Rakhmankulov, D.L., Zlotskii, S.S., 1999. Russ. Chem. Bull. 48, 2173.
Furuhashi, O., Currell, F.J., Suzuki, H., Ohtani, S., 1997. J. Phys. B 30, 3287.
Furuya, K., Koba, F., Ogawa, T., 1997a. J. Chem. Phys. 106, 1764.
Furuya, K., Koba, F., Ogawa, T., 1997b. J. Chem. Phys. 107, 4979.
Garrett, B.C., Redmon, L.T., McCurdy, C.W., Redmon, M.J., 1985. Phys. Rev. A 32, 3366.
Geissler, P., McEwen, A., Porco, C., Strobel, D., Saur, J., Ajello, J., West, R., 2004. Icarus 172, 127.
Gerakines, P.A., Schutte, W.A., Greenberg, J.M., van Dishoeck, E.F., 1995. Astron. Astrophys. 296, 810.
Gerakines, P.A., Moore, M.H., Hudson, R.L., 2000. Astron. Astrophys. 357, 793.
Gerzanich, G.Yu., Skubenich, V.V., Zapesochnyi, I.P., 1976. Opt. Spectrosc. 41, 315.
Gianturco, F.A., Lucchese, R.R., 2004. J. Phys. Chem., A 108, 7056.
Gil, T.J., Rescigno, T.N., McCurdy, C.W., Lengsfield, B.H., 1994. Phys. Rev. A 49, 2642.
Gilpin, R., Welge, K.H., 1971. J. Chem. Phys. 55, 975.
Gorfinkiel, J.D., Faure, A., Taioli, S., Picarreta, C., Halmova, G., Tennyson, J., 2005. Eur. Phys. J. D 35, 231.
Gousset, G., Ferreira, C.M., Pinheiro, M., Sa, P.A., Touzeau, M., Vialle, M., Loureiro, J., 1991. J. Phys. D 24, 290.
Grandi, A., Gianturco, F.A., Sanna, N., 2004. Phys. Rev. Lett. 93, 048103.
Granier, A., Vervloet, M., Aumaille, K., Vallee, C., 2003. Plasma Sources Sci. Tech. 12, 89.
Gulley, R.J., Field, T.A., Steer, W.A., Mason, N.J., Lunt, S.L., Ziesel, J.-P., Field, D., 1998. J. Phys. B 31, 5197.
Gusten, R., Philipp, S.D., Weiss, A., Klein, B., 2006. Astron. Astrophys. 454, L115.
Hadjiontoniou, A., Christophorou, L.G., Carter, J.G., 1973. J. Chem. Soc., Faraday Trans. II 69, 1704.
Hakala, D., Harteck, P., Reeves, R.R., 1974. J. Phys. Chem. 78, 1583.
Hall, R.I., Cadez, I., Schermann, C., Tronc, M., 1977. Phys. Rev. A 15, 599.
Hancock, G., Morrison, M., 2005. Mol. Phys. 103, 1727.
Hanel, G., Fiegele, T., Stamatovic, A., Märk, T.D., 2001. Int. J. Mass Spectrom. 205, 65.
Hanel, G., Gstir, B., Fiegele, T., Hagelberg, F., Becker, K., Scheier, P., Snegursky, A., Märk, T.D., 2002. J. Chem. Phys. 116, 2456.
Hanel, G., Gstir, B., Denifl, S., Scheier, P., Probst, M., Farizon, B., Farizon, M., Illenberger, E., Märk, T.D., 2003. Phys. Rev. Lett. 90, 188104.
Haney, M.A., Franklin, J.L., 1968. J. Chem. Phys. 48, 4093.
Harb, T., 2003. Ph.D. Thesis. University of Windsor.
Harb, T., Kedzierski, W., McConkey, J.W., 2001. J. Chem. Phys. 115, 5507.
Harland, P.W., Franklin, J.L., Carter, D.E., 1973. J. Chem. Phys. 58, 1430.
Harvey, D.K., Feierabend, K.J., Black, J.C., Vaida, V., 2005. J. Mol. Spectrosc. 229, 151.
Haxton, D.J., Zhang, Z., Meyer, H.-D., Rescigno, T.N., McCurdy, C.W., 2004a. Phys. Rev. A 69, 062714.
Haxton, D.J., Zhang, Z., McCurdy, C.W., Rescigno, T.N., 2004b. Phys. Rev. A 69, 062713.
Haxton, D.J., Rescigno, T.N., McCurdy, C.W., 2005. Phys. Rev. A 72, 022705.
Haxton, D.J., McCurdy, C.W., Rescigno, T.N., 2006. Phys. Rev. A 73, 062724.
Haxton, D.J., McCurdy, C.W., Rescigno, T.N., 2007a. Phys. Rev. A 75, 012710.
Haxton, D.J., Rescigno, T.N., McCurdy, C.W., 2007b. Phys. Rev. A 75, 012711.
Hayashi, M., 2003. Bibliography of electron and photon cross sections with atoms and molecules. In: 20th Century–Water Vapour–NIFS-Data-81, National Institute for Fusion Science, Oroshi-cho, Toki, Japan.
He, Z., Leung, K.T., 2003. Sur. Sci. 523, 48.
Hikosaka, Y., Hattori, H., Hikida, T., Mitsuki, K., 1997. J. Chem. Phys. 107, 2950.
Hines, M.E., Morrison, M.C., 1992. J. Geophys. Res. 97, 16703.
Hirota, K., Kojima, T., 2005. Bull. Chem. Soc. Japan 78, 1685.
Hoffmann, P., Utke, I., Cicoira, F., Dwir, B., Leifer, K., Kapon, E., Doppelt, P., 2000. Mat. Res. Soc. Symp. 624, 171.
Hoffman, R.C., Gebel, M.E., Fox, B.S., Finlayson-Pitts, 2003. Phys. Chem. Chem. Phys. 5, 1780.
Holmes, J.L., Losing, F.P., 1980. J. Amer. Chem. Soc. 102, 3732.
Holtgrave, J., Reichl, K., Abner, D., Haaland, P.D., 1993. Chem. Phys. Lett. 215, 548.
Hotop, H., Ruf, M.-W., Allan, M., Fabrikant, I.I., 2003. Adv. At. Mol. Opt. Phys. 49, 85.
Hsieh, S., Eland, J.H.D., 1997. J. Phys. B 30, 4515.
Huang, Y.-L., Gordon, R.J., 1991. J. Chem. Phys. 94, 5083.
Huber, D., Beikircher, M., Denifl, S., Zappa, F., Matejcik, S., Bacher, A., Grill, V., Märk, T.D., Scheier, P., 2006. J. Chem. Phys. 125, 084304.
Hubin-Franskin, M.J., Katihawa, J., Collin, J.E., 1976. Int. J. Mass. Spectrom. Ion Phys. 20, 285.
Hubin-Franskin, M.J., Huard, D., Marmet, P., 1978. Int. J. Mass. Spectrom. Ion Phys. 27, 263.
Hudson, J.E., Hamilton, M.L., Vallance, C., Harland, P.W., 2003. Phys. Chem. Chem. Phys. 5, 3162.
Hudson, J.E., Vallance, C., Harland, P.W., 2004. J. Phys. B 37, 445.
Hudson, J.E., Vallance, C., Harland, P.W., 2005. J. Phys. B 38, 1077.
Hudson, J.E., Weng, Z.F., Vallance, C., Harland, P.W., 2006. Int. J. Mass Spectrom. 248, 42.
Huels, M.A., Hahndorf, I., Illenberger, E., Sanche, L., 1998. J. Chem. Phys. 108, 1309.
Hwang, W., Kim, Y.-K., Rudd, M.E., 1996. J. Chem. Phys. 104, 2956.
IAEA-TECDOC-799, 1995. Atomic and Molecular Data for Radiotherapy and Radiation Research. International Atomic Energy Agency.
Iga, I., Rao, M.V.V.S., Srivastava, S.K., Nogueira, J.C., 1996a. Int. J. Mass. Spect. Ion Proc. 155, 99.
Iga, I., Rao, M.V.V.S., Srivastava, S.K., 1996b. J. Geophys. Res. 101, E9261.
Illenberger, E., Märk, T.D., 1999. Phys. Rev. Lett. 82, 4364.
Imami, M., Borst, W.L., 1975. J. Chem. Phys. 63, 3602.
Imhoff, M., Deng, Z., Huels, M.A., 2005. Int. J. Mass Spectrom. 245, 68.
Imhoff, M., Deng, Z., Huels, M.A., 2007. Int. J. Mass Spectrom. 262, 154.
Irvine, W.M., Friberg, P., Kaifu, N., Kitamura, Y., Kawaguchi, K., 1989. Astrophys. J. 342, 871.
Itakura, R., Hishikawa, A., Yamanouchi, K., 2000. J. Chem. Phys. 113, 6598.
Itikawa, Y., Shimizu, M., 1971. Bull. Inst. Space Aeronaut. Sci. 7, 64.
Itikawa, Y., Ichimura, A., Onda, K., Sakimoto, K., Takayanagi, K., Hatano, Y., Hayashi, M., Nishimura, H., Tsurubuchi, S., 1989. J. Phys. Chem. Ref. Data 18, 23.
Itikawa, Y. (Ed.), 2003. Photon and Electron Interactions with Atoms, Molecules and Ions. In: Landolt-Börnstein, Volume I/17, Subvolume C. Springer, New York.
Itikawa, Y., Ichimura, A., 1990. J. Phys. Chem. Ref. Data 19, 637.
Itikawa, Y., 2002. J. Phys. Chem. Ref. Data 31, 749.
Itikawa, Y., Mason, N.J., 2005. J. Phys. Chem. Ref. Data 34, 1.
Jaffke, T., Hashemi, R., Christophorou, L.G., Illenberger, E., Baumgartel, H., Pinnaduwage, L.A., 1993. Chem. Phys. Lett. 203, 21.

Jager, K., Henglein, A., 1967. Z. Naturforsch. A 22a, 700.
Jain, D.K., Khare, S.P., 1976. J. Phys. B 9, 1429.
James, G.K., Ajello, J.M., Shemansky, D.E., Franklin, B., Siskind, D., Slanger, T.G., 1988. J. Geophys. Res. 93, 9893.
James, G.K., Ajello, J.M., Kanik, I., Franklin, B., Shemansky, D.E., 1992. J. Phys. B 25, 1481.
Jans, W., Mobus, B., Kühn e, M., Ulm, G., Werner, A., Schartner, K.-H., 1995. Appl. Opt. 34, 3671.
Jans, W., Mobus, B., Kühn e, M., Ulm, G., Werner, A., Schartner, K.-H., 1997. Phys. Rev. A 55, 1890.
Jiao, C.Q., DeJoseph Jr., C.A., Garscadden, A., 2002. J. Chem. Phys. 117, 161.
Jiao, C.Q., DeJoseph Jr., C.A., Garscadden, A., 2003. J. Phys. Chem. A 107, 9040.
Jiao, C.Q., DeJoseph Jr., C.A., Garscadden, A., 2005. J. Vac. Sci. Tech. A23, 1295.
Jochims, H.W., Denzer, W., Baumgartel, H., Losking, O., Wilner, H., 1992. Ber. Bunsenges Phys. Chem. 96, 573.
Johnson, C.A.F., Kelly, S.D., Parker, J.E., 1987a. J. Chem. Soc.-Faraday Trans. II 83, 411.
Johnson, C.A.F., Kelly, S.D., Parker, J.E., 1987b. J. Chem. Soc.-Faraday Trans. II 83, 985.
Johnson, P.V., Malone, C.P., Kanik, I., Tran, K., Khakoo, M.A., 2005a. J. Geophys. Res. A110, 11311.
Johnson, R.E., Cooper, P.D., Quickenden, T.I., Grieves, G.A., Orlando, T.M., 2005b. J. Chem. Phys. 123, 184715.
Jonin, C., Liu, X., Ajello, J.M., James, G.K., Abgrall, H., 2000. Astrophys. J. Suppl. 129, 247.
Joshipura, K.N., Vinodkumar, M., Patel, U.M., 2001. J. Phys. B 34, 509.
Joshipura, K.N., Antony, B.K., Vinodkumar, M., 2002. J. Phys. B 35, 4211.
Joshipura, K.N., Gangopadhyay, S., Vaishnav, B.G., 2007a. J. Phys. B 40, 199.
Joshipura, K.N., Vaishnav, B.G., Gangopadhyay, S., 2007b. Int. J. Mass Spectrom. 261, 146.
Jungen, M., Vogt, J., Staemmler, V., 1979. Chem. Phys. 37, 49.
Jureta, J.J., 2005. Eur. Phys. J. D 32, 319.
Kandel, R.J., 1955. J. Chem. Phys. 23, 84.
Kanik, I., Ajello, J.M., James, G.K., 1993a. Chem. Phys. Lett. 211, 523.
Kanik, I., Trajmar, S., Nickel, J.C., 1993b. J. Geophys. Res. 98, 7447.
Kanik, I., James, G.K., Ajello, J.M., 1995. Phys. Rev. A 51, 2067.
Kanik, I., Noren, C., Makarov, O.P., Vatti Palle, P., Ajello, J.M., Shemansky, D.E., 2003. J. Geophys. Res. 108E, 5126.
Kanomata, I., 1961. Bull. Chem. Soc. Japan 34, 1864.
Kato, H., Kawahara, H., Hoshino, M., Tanaka, H., Brunger, M.J., Kim, Y.-K., 2007. J. Chem. Phys. 126, 064307.
Kawada, M.K., Sueoka, O., Kimura, M., 2000. J. Chem. Phys. 112, 7057.
Kawazumi, H., Ogawa, T., 1987. Chem. Phys. 114, 149.
Karwasz, G.P., Brusa, R.S., Zecca, A., 2001. Rivista Nuovo Cim. 24 (#1), 1.
Keating, G.M., Shorthill, R.W., Masursky, H., Elson, L.S., 1987. Adv. Space Res. 7, 10.
Kedzierski, W., Brennan, M., McConkey, J.W., 1998a. Canad. J. Phys. 76, 985.
Kedzierski, W., Derbyshire, J., Malone, C.P., McConkey, J.W., 1998. J. Phys. B 31, 5361.
Kedzierski, W., Malone, C., McConkey, J.W., 2000. Canad. J. Phys. 78, 617; 78, 1113(E).
Kedzierski, W., Borbely, J., McConkey, J.W., 2001. J. Phys. B 34, 4027.
Khare, S.P., Meath, W.J., 1987. J. Phys. B 20, 2101.
Khare, S.P., Sharma, M.K., Tomar, S., 1999. J. Phys. B 32, 3147.
Khatymov, R.V., Muftakov, M.V., Mazunov, V.A., 2003a. Rapid Comm. Mass Spectrom. 17, 2327.
Khatymov, R.V., Muftakov, M.V., Schukin, P.V., Mazunov, V.A., 2003b. Russ. Chem. Bull. 52, 1974.
Khatymov, R.V., Muftakov, M.V., Schukin, P.V., Mazunov, V.A., 2004. Russ. Chem. Bull. 53, 738.
Khmel, S.Ya., Sharafutdinov, R.G., 1997a. Sov. Phys.–Technol. Phys. 42, 291.
Khmel, S.Ya., Sharafutdinov, R.G., 1997b. Sov. Phys.–Technol. Phys. 42, 775.
Kiefl, H.U., Karl, E., Fricke, J., 1983. J. Phys. B 16, 4165.
Kiehling, J.E., Ammirati, T.F., Moore, M.D., Monce, M.N., Hansel, E.F., 2001. J. Geophys. Res. 106, 26147.
Kim, M.H., Li, W., Lee, S.K., Suits, A.G., 2004. Canad. J. Chem. 82, 880.
Kim, S., Schaefer III, H.F., 2007. J. Chem. Phys. 126, 064301.
Kim, Y.-K., Rudd, M.E., 1994. Phys. Rev. A 50, 3954.
Kim, Y.-K., Hwang, W., Weinberger, N.M., Ali, M.A., Rudd, M.E., 1997. J. Chem. Phys. 106, 1026.
Kimmel, G.A., Orlando, T.M., 1995. Phys. Rev. Lett. 75, 2606.
Kissel, J., Kruger, F.R., 1995. Adv. Space Res. 15, 59.
Klar, D., Ruf, M.-W., Hotop, H., 2001. Int. J. Mass Spectrom. 205, 93.
Kling, M.F., Siedschlag, C., Verhoef, A.J., Khan, J.I., Schultze, M., Uphues, Th., Ni, Y., Uiberacker, M., Drescher, M., Krausz, F., Vrakking, M.J.J., 2006. Science 312, 246.
Klots, C.E., Compton, R.N., 1978. J. Chem. Phys. 69, 1636.
Knapp, M., Echt, O., Kreisle, D., Märk, T.D., Recknagle, E., 1986. Chem. Phys. Lett. 126, 225.
Knowles, D.J., Nicholson, A.J.C., 1974. J. Chem. Phys. 60, 1180.
Köllmann, K., 1975a. Int. J. Mass Spectrom. Ion. Phys. 17, 261.
Köllmann, K., 1975b. J. Chem. Phys. 63, 1314.
Köllmann, K., 1978. J. Phys. B 11, 339.
Konig, C., Kopyra, J., Bald, I., Illenberger, E., 2006. Phys. Rev. Lett. 97, 018105.
Koppe, V.T., Koval, A.G., Danilevskii, N.P., Popova, L.I., 1972. Opt. Spectrosc. 33, 326.
Koppe, V.T., Danilevskii, N.P., Koval, A.G., 1975. Opt. Spectrosc. 39, 447.
Kouchi, N., Ito, K., Hatano, Y., Oda, N., Tsuboi, T., 1979. Chem. Phys. 36, 239.
Kreil, J., Ruf, M.-W., Hotop, H., Ettischer, I., Buck, U., 1998. Chem. Phys. 239, 459.
Krishnakumar, E., Srivastava, S.K., 1988. J. Phys. B 21, L607.
Krishnakumar, E., Srivastava, S.K., 1992. Int. J. Mass Spect. Ion Proc. 113, 1.
Krishnakumar, E., Kumar, S.V.K., Rangwala, S.A., Mitra, S.K., 1996. J. Phys. B 29, L657.
Krishnakumar, E., Kumar, S.V.K., Rangwala, S.A., Mitra, S.K., 1997. Phys. Rev. A 56, 1945.
Krishnakumar, E., 1998. Pramana-J. Phys. 50, 591.
Krupp, N., 2007. Science 318, 216.
Kuchenev, A.N., Smirnov, Y.M., 1996. Canad. J. Phys. 74, 267.
Kühn, A., Fenzlaff, H.-P., Illenberger, E., 1988. J. Chem. Phys. 88, 7453.
Kumar, A., Sevilla, M.D., 2007. J. Phys. Chem. B 111, 5464.
Kumar, S.V.K., Ashoka, V.S., Krishnakumar, E., 2004. Phys. Rev. A 70, 052715.
Kurawaki, J., Ueki, K., Higo, M., Ogawa, T., 1983. J. Chem. Phys. 78, 3071.
Kurunczi, P., Becker, K., Martus, K., 1998. Canad. J. Phys. 76, 153.
Kurunczi, P., Koharian, A., Becker, K., Martus, K., 1996. Contrib. Plasma Phys. 36, 723.
Lane, C.D., Orlando, T.M., 2007. Appl. Surf. Sci. 253, 6646.
Lara, L.-M., Rodrigo, R., Tozzi, G.P., Boehnhardt, H., Leisy, P., 2004. Astron. Astrophys. 420, 371.
Latimer, I.D., McConkey, J.W., 1965. Proc. Phys. Soc. 86, 745.

Lawrence, G.M., 1970. Phys. Rev. A 2, 397.
Leach, S., Schwell, M., Jochims, H.-W., Baumgartel, H., 2006. Chem. Phys. 321, 171.
Leber, E., Barsotti, S., Fabrikant, I.I., Weber, J.M., Ruf, M.-W., Hotop, H., 2000. Eur. Phys. J. D 12, 125.
LeClair, L.R., McConkey, J.W., 1993. J. Chem. Phys. 99, 4566.
LeClair, L.R., McConkey, J.W., 1994. J. Phys. B 27, 4039.
LeClair, L.R., Brown, M.D., McConkey, J.W., 1994. Chem. Phys. 189, 769.
LeClair, L.R., Derbyshire, J.M., McConkey, J.W., 1996. J. Geophys. Res. E 101, 7585.
Lecointre, J., Belic, D.S., Cherkani-Hassani, H., Jureta, J.J., Defrance, P., 2006. J. Phys. B 39, 3275.
Lecointre, J., Belic, D.S., Jureta, J.J., Becker, K., Deutsch, H., Limtrakul, J., Märk, T.D., Probst, M., Defrance, P., 2007. J. Phys. B 40, 85.
Lee, L.C., Slanger, T.G., Black, G., Sharpless, R.L., 1977. J. Chem. Phys. 67, 5602.
Lee, M.T., Michelin, S.E., Machado, L.E., Brescansin, L.M., 1993. J. Phys. B 26, L203.
Lefaivre, D., Marmet, P., 1978. Canad. J. Phys. 56, 1549.
Lepage, M., Michaud, M., Sanche, L., 2000. J. Chem. Phys. 113, 3602.
Levesque, P.L., Michaud, M., Sanche, L., 2005. J. Chem. Phys. 122, 094701.
Li, X., Sevilla, M.D., Sanche, L., 2004. J. Phys. Chem. B 108, 5472 and 19013.
Lias, S.G., 2003. In: Linstrom, P.J., Mallard, W.G. (Eds.), NIST Chemistry WebBook, Standard Ref Database #69. http://webbook.nist.gov.
Lias, S.G., Bartmess, J.E., Lieberman, J.F., Holmes, J.L., Levine, R.D., Mallard, W.G., 1988. J. Phys. Chem. Ref. Data 17, 1.
Ligtenberg R.C.G., McPherson A., Rouze N., Westerveld W.B., Risley J.S., 1985. Proc. 14th Int. Conf. on Phys. of Electronic and Atomic Collisions, Palo Alto, p. 276.
Limao-Vieira, P., Eden, S., Mason, N.J., Hoffmann, S.V., 2003. Chem. Phys. Lett. 376, 737.
Lin, J.J., Huang, D.W., Lee, Y.T., Yang, X., 1998. J. Chem. Phys. 109, 1758.
Lindsay, B.G., Straub, H.C., Smith, K.A., Stebbings, R.F., 1996. J. Geophys. Res. 101, 21151.
Lindsay, B.G., Mangan, M.A., Straub, H.C., Stebbings, R.F., 2000. J. Chem. Phys. 112, 9404.
Lindsay, B.G., Rejoub, R., Stebbings, R.F., 2003. J. Chem. Phys. 118, 5894.
Lindsay, B.G., Mangan, M.A., 2003. Photon and Electron Interactions with Atoms, Molecules and Ions. In: Itikawa, Y. (Ed.), Landolt-Börnstein, vol. I/17, subvolume C. Springer, New York.
Liu, X., Shemansky, D.E., Ahmed, S.M., James, G.K., Ajello, J.M., 1998. J. Geophys. Res. 103A, 26739.
Liuti, G., Dondes, S., Harteck, P., 1968. J. Chem. Phys. 72, 1081.
Locht, R., Schopman, J., Wankenne, H., Momigny, J., 1974. Chem. Phys. 7, 393.
Locht, R., 1977. Chem. Phys. 22, 13.
Locht, R., Durer, J.M., 1975. Chem. Phys. Lett. 34, 508.
Locht, R., Davister, M., 1995. Int. J. Mass Spect. Ion Proc. 144, 105.
Long, R.L., Cox, D.M., Smith, S.J., 1968. J. Res. Nat. Bur. Stand. 72, 521.
Long, K.A., Paretzke, H.G., Müller-Plathe, F., Diercksen, G.H.F., 1989. J. Chem. Phys. 91, 1569.
Lopez, J., Tarnovsky, V., Gutkin, M., Becker, K., 2003. Int. J. Mass Spectrom. 225, 25.
Lukes, P., Locke, B.R., 2005. J. Phys. D 38, 4074.
Lukic, D., Josifov, G., Kurepa, M.V., 2001. Int. J. Mass Spect. 205, 1.
MacNeil, K.A.G., Thynne, J.C.J., 1969. J. Phys. Chem. 73, 2960.
Makorov, O.P., Kanik, I., Ajello, J.M., 2003. J. Geophys. Res. 108, 5125.
Makorov, O.P., Ajello, J.M., Vatti Palle, P., Kanik, I., Festou, M.C., Bhardwaj, A., 2004. J. Geophys. Res. 109, A09303.
Mallard, G., Linstrom, P J, 2000. NIST Standard Reference Database, vol. 69. http://www.webbook.nist.gov.
Malone, C.P., Kedzierski, W., McConkey, J.W., 2000. J. Phys. B 33, 4863.
Malone, C.P., Johnson, P.V., McConkey, J.W., Ajello, J.M., Kanik, I., 2008a. J. Phys. B 41, 095201.
Malone, C.P., Johnson, P.V., McConkey, J.W., Kanik, I., 2008b. J. Geophys. Res. 113, A06309.
Mangan, M.A., Lindsay, B.G., Stebbings, R.F., 2000. J. Phys. B 33, 3225.
Margreiter, D., Deutsch, H., Märk, T.D., 1990. Contrib. Plasma Phys. 30, 487.
Margreiter, D., Deutsch, H., Märk, T.D., 1994. Int. J. Mass Spectrom. Ion Process. 139, 127.
Mariner, T., Bleakney, W., 1947. Phys. Rev. 72, 792.
Marinkovic, B., Szmytkowski, Cz., Pejcev, V., Filipovic, D., Vuskovic, L., 1986. J. Phys. B 19, 2365.
Marinkovic, B., Panajotovic, R., Pesic, Z.D., Filipovic, D., Felfi, Z., Msezane, A.Z., 1999. J. Phys. B 32, 1949.
Märk, T.D., 1975. J. Chem. Phys. 63, 3731.
Märk, T.D., Dunn, G.H., 1985. Electron Impact Ionization. Springer Verlag, Berlin.
Märk, T.D., Scheier, P., Stamatovic, A., 1987. Chem. Phys. Lett. 136, 177.
Märk, T.D., Scheier, P., Lezius, M., Walder, G., Stamatovic, A., 1989. Z. Phys. D 12, 279.
Marston, G., Walker, I.C., Mason, N.J., Gingell, J.M., Zhao, H., Brown, K.L., Motte-Tollet, F., Delwiche, J., Siggel, M.R.F., 1998. J. Phys. B 31, 3387.
Martin, F., Burrow, P.D., Cai, Z., Cloutier, P., Hunting, D., Sanche, L., 2004. Phys. Rev. Lett. 93, 068101.
Martin, I., Skalicky, T., Langer, J., Abdoul-Carime, H., Karwasz, G., Illenberger, E., Stano, M., Matejcik, S., 2005. Phys. Chem. Chem. Phys. 7, 2212.
Mason, N.J., 2003. Physica Scripta 68, C37.
Mason, N.J., Newell, W.R., 1989. J. Phys. B 22, 2297.
Mason, N.J., Newell, W.R., 1990. J. Phys. B 23, 4641.
Massey, H.S.N., Burhop, E.H.S., Gilbody, H.B., 1969. Electronic and Ionic Impact Phenomena, vols I & II. Clarendon Press, Oxford.
Masuoka, T., 1993. J. Chem. Phys. 98, 6989.
Masuoka, T., Doi, H., 1993. Phys. Rev. A 47, 278.
Matejcik, S., Stampfli, P., Stamatovic, A., Scheier, P., Märk, T.D., 1999. J. Chem. Phys. 111, 3548.
Matejcik, S., Kiendler, A., Cicman, P., Skalny, J., Stampfli, P., Illenberger, E., Chu, Y., Stamatovic, A., Märk, T.D., 1997. Plasma Sources Sci. Technol. 6, 140.
Matsumi, Y., Kawasaki, M., 1990. J. Chem. Phys. 93, 2481.
Matsuo, A., Furuya, K., Ogawa, T., 1998. Chem. Phys. Lett. 287, 653.
Matsuo, A., Furuya, K., Ogawa, T., 1999. Chem. Phys. 242, 91.
McCulloh, K.E., 1976. Int. J. Mass Spectrom. Ion Phys. 21, 333.
McCurdy, C.W., Baertschy, M., Rescigno, T.N., 2004. J. Phys. B 37, R137.
McDaniel, E.W., 1989. Atomic Collisions, Electron and Photon Projectiles. John Wiley & Sons, New York.
McPherson, A., Rouze, N., Westerveld, W.B., Risley, J.S., 1986. Appl. Opt. 25, 298.
Mehringer, D.M., Snyder, L.E., Miao, Y., Lovas, F.J., 1997. Astrophys. J. 480, L71.
Meinke, M., Schmale, C., Rühl, E., Illenberger, E., 1991. In: McCarthy, I.E., MacGillivray, W.R., Standage, M.C. (Eds), Abst. 17th Int. Conf. on Physics of Electronic and Atomic Collisions (Brisbane), p. 262.
Melton, C.E., 1972. J. Chem. Phys. 57, 4218.
Mentall, J.E., Morgan, H.D., 1972. J. Chem. Phys. 56, 2271.
Merrill, C.I., Cady, G.H., 1961. J. Amer. Chem. Soc. 83, 298.
Michaud, M., Sanche, L., 1987. Phys. Rev. Lett. 59, 645.
Miletic, M., Neskovic, O., Veljkovic, M., Zimbov, K., 1996. Rapid Comm. Mass Spectrom. 10, 1961.
Miletic, M., Neskovic, O., Veljkovic, M., Zimbov, K., 1997. Rapid Comm. Mass Spectrom. 11, 381.

Miller, K., Becker, K., 1987. Canad. J. Phys. 65, 530.
Milosavljevic, A.R., Giuliani, A., Sevic, D., Hubin-Franklin, M.-J., Marinkovic, B.P., 2005. Eur. Phys. J. D 35, 411.
Misakian, M., Mumma, M.J., Faris, J.F., 1975. J. Chem. Phys. 62, 3442.
Modelli, A., Venuti, M., 2001. Int. J. Mass Spect. 205, 7.
Möhlmann, G.R., de Heer, F.J., 1979. Chem. Phys. 40, 157.
Möhlmann, G.R., Shima, K H, de Heer, F.J., 1978. Chem. Phys. 28, 331.
Möhlmann, G.R., Beenakker, C.I.M., de Heer, F.J., 1976. Chem. Phys. 13, 375.
Moore, J.H., Davis, C.C., Coplan, M.A., 2002. Building Scientific Apparatus. Westview Press, Colorado.
Morgan, H.D., Mentall, J.E., 1974. J. Chem. Phys. 60, 4734.
Morgan, H.D., Mentall, J.E., 1983. J. Chem. Phys. 78, 1747.
Morgan, L.A., 1998. J. Phys. B 31, 5003.
Morgan, W.L., Winstead, C., McKoy, V., 2002. J. Appl. Phys. 92, 1663.
Movier, G., Hernandez, R., 1975. Org. Mass Spectrom. 10, 958.
Mozejko, P., Sanche, L., 2003. Rad. Environ. Biophys. 42, 201.
Mozejko, P., Sanche, L., 2005. Rad. Phys. Chem. 73, 77.
Muftakov, M.V., Khatymov, R.V., Mazunov, V.A., 2000a. Rapid Comm. Mass Spectrom. 14, 1468.
Muftakov, M.V., Khatymov, R.V., Mazunov, V.A., Tachistov, V.V., Ponomarev, D.A., 2000b. Khim. Fiz. 19, 42.
Muftakov, M.V., Khatymov, R.V., Mazunov, V.A., Tachistov, V.V., Ponomarev, D.A., 2001. Engl. Transl. – Chem. Phys. Rep. 19, 2287.
Müller, U., Bubel, Th., Schulz, G., 1993. Z. Phys. D 25, 167.
Mumma, M.J., Zipf, E.C., 1971. J. Chem. Phys. 55, 1661.
Mumma, M.J., Stone, E.J., Zipf, E.C., 1971. J. Chem. Phys. 54, 2627.
Mumma, M.J., Stone, E.J., Borst, W.L., Zipf, E.C., 1972. J. Chem. Phys. 57, 68.
Mundel, C., Berman, M., Domcke, W., 1985. Phys. Rev. A 32, 181.
Nestmann, B.M., Brems, V., Dora, A., Kumar, S., 2005a. J. Phys. B 38, 75.
Nestmann, B.M., Kumar, S.V.K, Peyerimhoff, S.D., 2005b. Phys. Rev. A 71, 012705.
Newson, K.A., Luc, S.M., Price, S.D., Mason, N.J., 1995. Int. J. Mass Spect. Ion Proc. 148, 203.
Nicholls, R.W, 1962. J. Quant. Spect. Rad. Trans. 2, 433.
Nishimura, T., Meisels, G.G., Niwa, Y., 1989. J. Chem. Phys. 91, 4009.
NIST Chemistry WebBook, 2005. In: Linstrom, P.J., Mallard, W.G. (Eds.), NIST Standard Reference Database Number, vol. 69. National Institute of Standards and Technology, Gaithersburg, MD, p. 20899. http://webbook.nist.gov.
Noren, C., Kanik, I., Ajello, J.M., McCartney, P., Makarov, O.P., McClintock, W.E., Drake, V.A., 2001. Geophys. Res. Lett. 28, 1379.
Novoselov, Y.N., Mesyats, G.A., Kuznetsov, D.L., 2001. J. Phys. D 34, 1248.
O'Connor, C.S.S, Jones, N.C, O'Neale, K., Price, S.D., 1996. Int. J. Mass Spect. Ion Proc. 154, 203.
O'Connor, C.S.S., Jones, N.C., Price, S.D., 1997. Chem. Phys. 214, 131.
O'Connor, C.S.S, Tafadar, N., Price, S.D., 1998. J. Chem. Soc. Far. Trans. 94, 1797.
Ogawa, T., Yonekura, N., Tsukada, M., Ihara, S., Yasuda, T., Tomura, H., Nakashima, K., Kawazumi, H., 1991. J. Phys. Chem. 95, 2788.
Ohshima, S., Kondow, T., Fukuyama, T., Kuchitsu, K., 1989. Chem. Phys. 135, 267.
Oliversen, R.J., Doane, N., Scherb, F., Harris, W.M., Morganthaler, J.P., 2002. Astrophys. J. 581, 770.
Olivier, J.L., Locht, R., Momigny, J., 1984. Int. J. Mass Spect. Ion Proc. 58, 293.
Olthoff, J.K., Stricklett, K.L., van Brunt, R.J., Moore, J.H., Tossell, J.A., Sauers, I., 1993. J. Chem. Phys. 98, 9466.
O'Malley, T.F., 1966. Phys. Rev. 150, 14.
O'Malley, T.F., 1967. Phys. Rev. 155, 59.
O'Malley, T.F., Taylor, H.S., 1968. Phys. Rev. 176, 207.
Ondrey, G.S., Kanfer, S., Bersohn, R., 1983. J. Chem. Phys. 79, 179.
Orient, O.J., Chutjian, A., 1995. Phys. Rev. Lett. 74, 5017.
Orient, O.J., Srivastava, S.K., 1983a. Chem. Phys. Lett. 96, 681.
Orient, O.J., Srivastava, S.K., 1983b. J. Chem. Phys. 78, 2949.
Orient, O.J., Srivastava, S.K., 1984. J. Chem. Phys. 80, 140.
Ostrawsky, C., Blum, K., Gillan, C., 1995. J. Phys. B 28, 2269.
Pal, S., Prakash, S., 1998. Rapid Commun. Mass Spectrom. 12, 297.
Pan, X., Cloutier, P., Hunting, D., Sanche, L., 2003. Phys. Rev. Lett. 90, 208102.
Pan, X., Sanche, L., 2005. Phys. Rev. Lett. 94, 198104.
Pan, X., Sanche, L., 2006. Chem. Phys. Lett. 421, 404.
Panajtovic, R., Michaud, M., Sanche, L., 2007. Phys. Chem. Chem. Phys. 9, 138.
Pang, K.D., Ajello, J.M., Franklin, B., Shemansky, D.M., 1987. J. Chem. Phys. 86, 2750.
Pariat, Y., Allan, M., 1991. Int. J. Mass Spectrom. Ion Proc. 103, 181.
Park, Y.S., Cho, H., Parenteau, L., Bass, A.D., Sanche, L., 2006. J. Chem. Phys. 125, 074714.
Parker, D.H., 2000. Acc. Chem. Res. 33, 563.
Pedersen, H.B., Djuric, N., Jensen, M.J., Kella, D., Savran, C.P., Schmidt, H.T., Vejby-Christensen, L., Andersen, L.H., 1999. Phys. Rev. A 60, 2882.
Pelc, A., Sailer, W., Scheier, P., Mason, N.J., Märk, T.D., 2002a. Eur. Phys. J. D 20, 441.
Pelc, A., Sailer, W., Scheier, P., Probst, M., Mason, N.J., Illenberger, E., Märk, T.D., 2002b. Chem. Phys. Lett. 361, 277.
Pelc, A., Sailer, W., Scheier, P., Mason, N.J., Illenberger, E., Märk, T.D., 2003a. Vacuum 70, 429.
Pelc, A., Sailer, W., Matejcik, S., Scheier, P., Märk, T.D., 2003b. J. Chem. Phys. 119, 7887.
Pelc, A., Sailer, W., Scheier, P., Märk, T.D., Illenberger, E., 2004. Chem. Phys. Lett. 392, 465.
Pilling, S., Santos, A.C.F., Boechat-Roberty, H.M, de Souza, G.G.B., Sant' Anna, M.M., Barros, A.L.F., Wolff, W., de Castro Faria, N.V., 2006a. Brazilian J. Phys. 36, 538.
Pilling, S., Santos, A.C.F., Wolff, W., Sant' Anna, M.M., Barros, A.L.F., de Souza, G.G.B., de Castro Faria, N.V., Boechat-Roberty, H.M., 2006b. Mon. Not. R. Astron. Soc. 372, 1379.
Pindzola, M.S., Robicheaux, F., Loch, S.D., Berengut, J.C., Topcu, T., Colgan, J., Foster, M., Griffen, D.C., Balance, C.P., Schultz, D.R., Minami, T., Badnell, N.R., Witthoeft, M.C., Plante, D.R., Mitnik, D.M., Ludlow, J.A., Kleiman, U., 2007. J. Phys. B 40, R39.
Polanyi, J.C., Young, P.A., 1990. J. Chem. Phys. 93, 3673.
Prabhudesai, V.S., Nandi, D., Kelkar, A.H., Parajuli, R., Krishnakumar, E., 2005a. Chem. Phys. Lett. 405, 172.
Prabhudesai, V.S., Kelkar, A.H., Nandi, D., Krishnakumar, E., 2005b. Phys. Rev. Lett. 95, 143202.
Prinslow, D.A., Vaida, V., 1989. J. Phys. Chem. 93, 1836.
Pritchard, H.P., McKoy, V., Lima, M.A., 1990. Phys. Rev. A 41, 546.
Probst, M., Deutsch, H., Becker, K., Märk, T.D., 2001. Int. J. Mass Spect. 206, 13.
Probst, M., Hermansson, K., Urban, J., Mach, P., Muigg, D., Denifl, G., Fiegele, T., Mason, N.J., Stamatovic, A., Märk, T.D., 2002. J. Chem. Phys. 116, 984.
Ptasinska, S., Sanche, L., 2006. J. Chem. Phys. 125, 144713.
Ptasinska, S., Denifl, S., Scheier, P., Märk, T.D., 2004. J. Chem. Phys. 120, 8505.
Ptasinska, S., Denifl, S., Abedi, A., Scheier, P., Märk, T.D., 2003. Biomed. Life Sci. Chem. Mat. Sci. Eng. 377, 1115.
Ptasinska, S., Denifl, S., Grill, V., Märk, T.D., Illenberger, E., Scheier, P., 2005a. Phys. Rev. Lett. 95, 093201.

Ptasinska, S., Denifl, S., Candori, P., Matejcik, S., Scheier, P., Märk, T.D., 2005b. Chem. Phys. Lett. 403, 107.
Ptasinska, S., Denifl, S., Gohlke, S., Scheier, P., Illenberger, E., Märk, T.D., 2006. Angew. Chem. Int. Ed. 45, 1893.
Qu, Z.-W., Zhu, H., Grebenshchikov, S.Y., Schinke, R., 2005. J. Chem. Phys. 123, 074305.
Rademacher, J., Christophorou, L.G., Blaunstein, R.P., 1975. J. Chem. Soc.-Faraday Trans. II 71, 1212.
Rangwala, S.A., Krishnakumar, E., Kumar, S.V.K., Mason, N.J., 1999. J. Phys. B 32, 3795.
Rangwala, S.A., Krishnakumar, E., Kumar, S.V.K., 2003. Phys. Rev. A 68, 052710.
Rapp, D., Briglia, D., 1965. J. Chem. Phys. 43, 1480.
Rapp, D., Englander-Golden, P., 1965. J. Chem. Phys. 43, 1464.
Rapp, D., Englander-Golden, P., Briglia, D.D., 1965. J. Chem. Phys. 42, 4081.
Rawat, P., Prabhudesai, V.S., Aravind, G., Rahman, M.A., Krishnakumar, E., 2007. J. Phys. B 40, 4625.
Reese, R.M., Dibeler, V.H., Franklin, J.L., 1958. J. Chem. Phys. 29, 880.
Rejoub, R., Morton, C.D., Lindsay, B.G., Stebbings, R.F., 2003. J. Chem. Phys. 118, 1756.
Rescigno, T.N., McCurdy, C.W., Orel, A.E., Lengsfield III, B.H., 1995. In: Gianturco, F.A., Huo, W.M. (Eds.), Computational Methods for Electron-Molecule Collisions. Plenum Press, New York.
Retherford, K.D., Spencer, J.R., Stern, S.A., Saur, J., Strobel, D.F., Steffl, A.J., Gladstone, G.R., Weaver, H.A., Cheng, A.F., Parker, J.W., Slater, D.C., Versteeg, M.H., Davis, M.W., Bagenal, F., Throop, H.B., Lopes, R.M.C., Reuter, D.C., Lunsford, A., Conard, S.J., Young, L.A., Moore, J.M., 2007. Science 318, 237.
Ricard, A., Collobert, D., Moisan, M., 1983. J. Phys. B 16, 1657.
Richard-Viard, M., Dutuit, O., Lavollee, M., Govers, T., Guyon, P.M., Durup, J., 1985. J. Chem. Phys. 82, 4054.
Richter, R.C., Rosendahl, A.R., Hynes, A.J., Lee, E.P.F., 1998. J. Chem. Phys. 109, 8876.
Robbiani, R., Franklin, J.L., 1979. J. Amer. Chem. Soc. 101, 3709.
Rockland, U., Baumgärtel, H., Rühl, E., Lösking, O., Müller, H.S.P., Willner, H., 1995. Ber. Bunsenges. Phys. Chem. 99, 969.
Roman-Leshkov, Y., Barrett, C.J., Liu, Z.Y., Dumesic, J.A., 2007. Nature 447, 982.
Rosenstock, H.M., Draxl, K., Steiner, B.W., Herron, J.T., 1977. J. Phys. Chem. Ref. Data 6 (I-S263).
Rowntree, P., Parenteau, L., Sanche, L., 1991. J. Chem. Phys. 94, 8570.
Ruscic, B., Wagner, A.F., Harding, L.B., Asher, R.L., Feller, D., Dixon, D.A., Peterson, K.A., Song, Y., Qian, X., Ng, C.-Y., Liu, J., Chen, W., Schwenke, D.W., 2002. J. Phys. Chem. A 106, 2727.
Sailer, W., Pelc, A., Matejcik, S., Illenberger, E., Scheier, P., Märk, T.D., 2002. J. Chem. Phys. 117, 7989.
Sailer, W., Pelc, A., Probst, M., Limtrakul, J., Scheier, P., Illenberger, E., Märk, T.D., 2003. Chem. Phys. Lett. 378, 250.
Saksena, V., Kushwaha, M.S., Khare, S.P., 1997. Physica B 223, 201.
Sambe, H., Ramaker, D.E., 1991. J. Chem. Phys. 94, 2548.
Sanche, L., 2005. Eur. Phys. J. D 35, 367.
Sato, S., Kiyota, M., Fujioka, T., 1985. J. Appl. Phys. 58, 3991.
Sauers, I., Christophorou, L.G., Spyrou, S.M., 1993. Plasma Chem. Plasma Process 13, 17.
Saveliev, A.B., Pietsch, G.J., Murtazin, A.R., Fried, A., 2007. Plasma Sources Sci. Technol. 16, 454.
Schappe, R.S., Urban, E., 2006. Phys. Rev. A 73, 052702.
Schappe, R.S., Edgell, R.J., Urban, E., 2002. Phys. Rev. A 65, 042701.
Scheer, A.M., Aflatooni, K., Gallup, G.A., Burrow, P.D., 2004. Phys. Rev. Lett. 92, 068102.
Scheer, A.M., Mozejko, P., Gallup, G.A., Burrow, P.D., 2007. J. Chem. Phys. 126, 174301.
Scheier, P., Walder, G., Stamatovic, A., Märk, T.D., 1988. J. Chem. Phys. 90, 1288.
Schiavone, J.A., Smyth, K.C., Freund, R.S., 1975. J. Chem. Phys. 63, 1043.
Schiavone, J.A., Donohue, D.E., Freund, R.S., 1977. J. Chem. Phys. 67, 759.
Schopman, J., Locht, R., 1974. Chem. Phys. Lett. 26, 596.
Schramm, A., Fabrikant, I.I., Weber, J.M., Leber, E., Ruf, M.-W., Hotop, H., 1999. J. Phys. B 32, 2153.
Schulman, M.B., Sharpton, F.A., Chung, S., Lin, C.C., Anderson, L.W., 1985. Phys. Rev. A 32, 2100.
Schutten, J., de Heer, F.J., Moustafa, H.R., Boerboom, A.J.H., Kistemaker, J., 1966. J. Chem. Phys. 44, 3924.
Schwell, M., Dulieu, F., Jochims, H.-W., Fillion, J.-H., Lemaire, J.-L., Baumgärtel, H., Leach, S., 2002. J. Phys. Chem. A 106, 10908.
Seefeldt, V.R., Moller, W., Schmidt, M., 1985. Z. Phys. Chem. (Leipzig) 266, 797.
Seiersen, K., Bak, J., Bluhme, H., Jensen, M.J., Nielsen, S.B., Andersen, L.H., 2003. Phys. Chem. Chem. Phys. 5, 4814.
Seinfeld, J.H., Pandis, S.N., 1997. Atmospheric Chemistry and Physics: From Air Pollution to Climate Change. Wiley-Interscience.
Senn, G., Skalny, J.D., Stamatovic, A., Mason, N.J., Scheier, P., Märk, T.D., 1999a. Phys. Rev. Lett. 82, 5028.
Senn, G., Drexel, H., Marston, G., Mason, N.J., Märk, T.D., Meinke, M., Schmale, C., Tegeder, P., Ruhl, E., Illenberger, E., 1999b. J. Phys. B 32, 3615.
Senn, G., Muigg, D., Denifl, G., Stamatovic, A., Scheier, P., Märk, T.D., 1999c. Euro. Phys. J. D 9, 152.
Senn, G., Muigg, D., Denifl, G., Stamatovic, A., Scheier, P., Märk, T.D., 1999d. Euro. Phys. J. D 9, 159.
Shafranyosh, I.I., Sukhoviya, M.I., Shafranyosh, M.I., 2006. J. Phys. B 39, 4155.
Shafranyosh, I.I., Sukhoviya, M.I., 2007. Opt. Spectrosc. 102, 500.
Shafranyosh, I.I., Sukhoviya, M.I., Margitich, M.O., Shafranyosh, M.I., Shimon, L.L., 2007. Abs Fr 111, ICPEAC XXV, Freiburg.
Sharma, V., Bapat, B., 2006. Eur. Phys. J. D 223.
Shemansky, D.E., Ajello, J.M., Hall, D.T., 1985. Astrophys. J. 296, 765.
Shirai, T., Tabata, T., Tawara, H., 2001. Atomic Data Nucl. Data Tables 79, 143.
Siegel, M.W., 1982. Int. J. Mass Spect. Ion Phys. 44, 19.
Simmons, J.D., Maki, A.G., Houyen, J.T., 1979. J. Mol. Spectrosc. 74, 70.
Simpson, W.C., Sieger, M.T., Orlando, T.M., Parenteau, L., Nagesha, K., Sanche, L., 1997. J. Chem. Phys. 107, 8668.
Sivarkumar, N., Hall, G.E., Houston, P.L., Hepburn, J.W., Burak, I., 1988. J. Chem. Phys. 88, 3692.
Skalicky, T., Allan, M., 2004. J. Phys. B 37, 4849.
Slanger, T.G., 1989. SRI Report –NO_2Photodissociation Dynamics.
Smith, O.I., Stevenson, J.S., 1981. J. Chem. Phys. 74, 6777.
Smyth, H.D., Stueckelberg, E.C.G, 1930. Phys. Rev. 36, 472.
Smyth, K.C., Schiavone, J.A., Freund, R.S., 1973. J. Chem. Phys. 59, 5225.
Smyth, K.C., Schiavone, J.A., Freund, R.S., 1974. J. Chem. Phys. 60, 1358.
Snegursky, A.V., Zavilopulo, A.N., 1997. Nucl. Instrum. Methods Phys. Res. B 126, 301.
Solomon, S.R., Garcia, R.R., Rowland, F.S., Wuebbles, D.J., 1986. Nature 321, 755.
Sommerfeld, T., 2007. J. Chem. Phys. 126, 124301.
Spence, D., Schulz, G.J., 1969. Phys. Rev. 188, 280.
Spence, D., Schulz, G.J., 1974. J. Chem. Phys. 60, 216.
Spyrou, S.M., Sauers, I., Christophorou, L.G., 1986. J. Chem. Phys. 84, 239.
Srinivasa, V., Rees, J.A., 1967. Brit. J. Appl. Phys. 18, 59.
Srivastava, S.K., Orient, O.J., 1983. Phys. Rev. A 27, 1209.
Srivastava, S.K., Krishnakumar, E., Fucaloro, A.F., van Note, T., 1996. J. Geophys. Res. 101, 26155.
Sroka, W., 1970. Z. Naturforsch. A25, 1434.
Sroka, W., Zietz, R., 1973. Z. Naturforsch. A28, 794.
Stamatovic, A., Schulz, G.J., 1970. J. Chem. Phys. 53, 2663.

Stamatovic, A., Schulz, G.J., 1973. Phys. Rev. A 7, 589.
Stamatovic, A., Leiter, K., Ritter, W., Stephan, K., Märk, T.D., 1985. J. Chem. Phys. 83, 2942.
Stamatovic, A., Scheier, P., Märk, T.D., 1987. Z. Phys. D 6, 351.
Stepanovic, M., Pariat, Y., Allan, M., 1994. J. Chem. Phys. 110, 11376.
Stephan, K., Helm, H., Kim, Y.B., Seykora, G., Ramler, J., Grossyl, M., Märk, E., Märk, T.D., 1980. J. Chem. Phys. 73, 303.
Steudel, R., 2003. Top. Curr. Chem. 231, 203.
Stockdale, J.A.D., Deleanu, L., 1973. Chem. Phys. Lett. 22, 204.
Stockdale, J.A.D., Deleanu, L., 1974. Chem. Phys. Lett. 28, 588.
Stockdale, J.A.D., Compton, R.N., Hurst, G.S., Reinhardt, W.P., 1969. J. Chem. Phys. 50, 2176.
Stone, E.J., Zipf, E.C., 1972. J. Chem. Phys. 56, 2870.
Stone, E.J., Lawrence, G.M., Seitel, S.C., 1975. In: Risley, J.S., Geballe, R. (Eds), Electronic and Atomic Collisions: Abstr 9th ICPEAC, University of Washington, Seattle, pp. 816–817.
Stone, E.J., Lawrence, G.M., Fairchild, C.E., 1976. J. Chem. Phys. 65, 5083.
Straub, H.C., Renault, P., Lindsay, B.G., Smith, K.A., Stebbings, R.F., 1995. Phys. Rev. A 52, 1115.
Straub, H.C., Lindsay, B.G., Smith, K.A., Stebbings, R.F., 1996a. J. Chem. Phys. 105, 4015.
Straub, H.C., Renault, P., Lindsay, B.G., Smith, K.A., Stebbings, R.F., 1996b. Phys. Rev. A 54, 2146.
Straub, H.C., Lindsay, B.G., Smith, K.A., Stebbings, R.F., 1998. J. Chem. Phys. 108, 109.
Strauss, C.E., McBane, G C, Houston, P.L., Burak, I., Hepburn, J.W., 1989. J. Chem. Phys. 90, 5364.
Sugita, A., Mashino, M., Kawasaki, M., Matsumi, Y., Bershn, R., Trott-Kriegeskorte, G., Gericke, K-H, 2000. J. Chem. Phys. 112, 7095.
Sullivan, S.A., Beauchamp, J.L., 1978. Int. J. Mass Spectrom. Ion Process 28, 69.
Sulzer, P., Ptasinska, S., Zappa, F., Mielewska, B., Milosavljevic, A.R., Scheier, P., Märk, T.D., Bald, I., Gohike, S., Huels, M.A., Illenberger, E., 2006. J. Chem. Phys. 125, 044304.
Suzuki, T., Katayanagi, H., Nanbu, S., Aoyagi, M., 1998. J. Chem. Phys. 109, 5778.
Sweeney, C.J., Shyn, T.W., 1996. Phys. Rev. A 53, 1576.
Swiderek, P., 2006. Angew. Chem. Int. Ed. 45, 4056.
Szmytkowski, C., Mozejko, P., Kwitnewski, S., Ptasinska-Denga, E., Domaracka, A., 2005. J. Phys. B 38, 2945.
Szmytkowski, C., Mozejko, P., Kwitnewski, S., Domaracka, A., Ptasinska-Denga, E., 2006. J. Phys. B 39, 2571.
Tabche-Fouhaile, A., Hubin-Franskin, M.-J., Delwiche, J.P., Frolich, H., Ito, K., Guyon, P.-M., Nenner, I., 1983. J. Chem. Phys. 79, 5894.
Tan, K.H., Brion, C.E., van der Leeuw, P.E., van der Wiel, M.J., 1978. Chem. Phys. 29, 299.
Tarnovsky, V., Levin, A., Deutsch, H., Becker, K., 1995. J. Chem. Phys. 102, 770.
Tarnovsky, V., Deutsch, H., Becker, K., 1998. J. Chem. Phys. 109, 932.
Tate, J.T., Smith, P.T., 1932. Phys. Rev. 39, 270.
Tawara, H., 1992. Atomic and Molecular Data for H_2O, CO and CO_2 Relevant to Edge Plasma Impurities, National Institute for Fusion Science (NIFS) Report, NIFS-DATA-19.
Taylor, S., Eland, J.H.D., 2005. Chem. Phys. 315, 8.
Teillet-Billy, D., Gauyacq, J.P., 1984. J. Phys. B 17, 3329.
Teillet-Billy, D., Malegat, L., Gauyacq, J.P., Abouaf, R., Benoit, C., 1989. J. Phys. B 22, 1095.
Thorn, P.A., Brunger, M.J., Kato, H., Hoshino, M., Tanaka, H., 2007a. J. Phys. B 40, 697.
Thorn, P.A., Brunger, M.J., Teubner, P.J.O., Diakomichalis, N., Madden, T., Bolorizadeh, M.A., Newell, W.R., Kato, H., Hoshino, M., Tanaka, H., Cho, H., Kim, Y.-K., 2007b. J. Chem. Phys. 126, 064306.
Tronc, M., Malegat, L., Azria, R., 1982. Chem. Phys. Lett. 88, 551.
Thrush, B.A., 1988. Rep. Prog. Phys. 51, 1341.
Tian, C., Vidal, C.R., 1998a. J. Chem. Phys. 108, 927.
Tian, C., Vidal, C.R., 1998b. Phys. Rev. A 58, 3783.
Tian, C., Vidal, C.R., 1998c. J. Phys. B 31, 895.
Tian, C., Vidal, C.R., 1998d. J. Phys. B 31, 5369.
Tikue, I., Kusakabe, M., Ogawa, H., Ito, Y., 1994. J. Phys. Chem. 98, 3588.
Tolbert, M.A., Toon, O.B., 2001. Science 292, 61.
Tonzani, S., Greene, C.H., 2006. J. Chem. Phys. 124, 054312.
Trajmar, S., Williams, W., Kuppermann, A., 1972. J. Chem. Phys. 56, 3759.
Trevisan, C.S., Houfek, K., Zhang, Z., Orel, A., McCurdy, C.W., Rescigno, T.N., 2005. Phys. Rev. A 71, 052714.
Trofimov, A.B., Schirmer, J., Kobychev, V.B., Potts, A.W., Holland, D.M.P., Karlsson, L., 2006. J. Phys. B 39, 305.
Tronc, M., Azria, R., Le Coat, Y., Illenberger, E., 1996. J. Phys. Chem. 100, 14745.
Tsuda, S., Yokohata, A., Kaway, M., 1969. Bull. Chem. Soc. Japan 42, 607, 614 and 1515.
Turner, J.E., Paretzke, H.G., Hamm, R.N., Wright, H.A., Ritchie, R.H., 1982. Radiat. Res. 92, 47.
Ullrich, J., Moshammer, R., Dörner, R., Jagutski, O., Mergel, V., Schmidt-Bocking, H., Spielberger, L., 1997. J. Phys. B 30, 2917.
Vaidyanathan, G., Coolbaugh, M.T., Garvey, J.F., 1992. J. Phys. Chem. 96, 1589.
Vallee, C., Rhallabi, A., Granier, A., Goullet, A., Turban, G., 2000. J. Vac. Sci. Tech. A18, 2728.
van Brunt, R.J., 1974. J. Chem. Phys. 60, 3064.
van Brunt, R.J., Kieffer, L.J., 1974. J. Chem. Phys. 60, 3057.
van Brunt, R.J., Zare, R.N., 1968. J. Chem. Phys. 48, 4304.
van Brunt, R.J., Kieffer, L.J., 1970. Phys. Rev. A 2, 1899.
van Brunt, R.J., Mumma, M.J., 1975. J. Chem. Phys. 63, 3210.
van Brunt, R.J., Lawrence, G.M., Kieffer, L.J., Slater, J.M., 1974. J. Chem. Phys. 61, 2032.
van Brunt, R.J., Herron, J.T., 1994. Phys. Scr. T53, 9.
van der Burgt, P.J.M., Westervelt, W.B., Risley, J.S., 1989. J. Phys. Chem. Ref. Data 18, 1757.
van der Burgt, P.J.M., Antaya, M.E., McConkey, J.W., 1992. Z. Phys. D 24, 125.
van Dishoeck, E.F., 1998. In: Hartquist, T.W., Williams, D.A. (Eds.), The Molecular Astrophysics of Stars and Galaxies. Oxford Science, New York.
van Dishoeck, E.F., Black, J.H., 1988. Astrophys. J. 334, 771.
van Sprang, H.A., Möhlmann, G.R., de Heer, F.J., 1978. Chem. Phys. 33, 65.
van Veen, N., Brewer, P., Das, P., Bersohn, R., 1983. J. Chem. Phys. 79, 4295.
Van Zyl, B., Gealy, M.W., Neumann, H., 1985. Phys. Rev. A 31, 2922.
Vatti Palle, P., Ajello, J.M, Bhardwaj, A., 2004. J. Geophys. Res. 109, A02310.
Velotta, R., Girolamo, P.D., Berardi, V., Spinelli, N., Armenante, M., 1994. J. Phys. B 27, 2051.
Voinov, V.G., Vasil'ev, Y.V., Morre, J., Barofsky, D.F., Dienzer, M.L., Gonin, M., Egan, T.F., Fuhrer, K., 2003. Anal. Chem. 75, 3001.
Von Trepka, L., Neuert, H., 1963. Z. Naturforsch., Teil A 18, 1295.
Vostrikov, A.A., Dubov, D.Y., 2006. Sov. Phys. Tech. Phys. 51, 540.
Vriens, L., 1966. Phys. Rev. 141, 88, and references therein.
Wakiya, K., 1978. J. Phys. B 11, 3913.
Walker, I.C., Fluendy, M.A.D., 2001. Int. J. Mass Spect. 205, 171.
Walker, I.C., Gingell, J.M., Mason, N.J., Marston, G., 1996. J. Phys. B 29, 4749.

Wan, H.X., Moore, J.H., Olthoff, J.K., van Brunt, R.J., 1993. Plasma Chem. Plasma Process 13, 1.
Wang, J.S., Franklin, J.L., 1980. Int. J. Mass Spectrom. Ion Proc. 36, 233.
Wang, W.C., Sze, N.D., 1980. Nature 268, 589.
Wang, P., Vidal, C.R., 2003. J. Chem. Phys. 118, 5383.
Weber, J.M., Leber, E., Ruf, M.-W., Hotop, H., 1999. Phys. Rev. Lett. 82, 516.
Wecker, D., Christodoulides, A.A., Schindler, R.N., 1981. Int. J. Mass Spectrom. Ion Phys. 38, 391.
Wehry, E.L., Hohmann, R., Gates, J.K., Guibault, L.F., Johnson, P.M., Schendel, J.S., Radspinner, D.A., 1987. App. Opt. 26, 3559.
Wei, L., Yang, B., Huang, C., Wang, J., Shan, X., Sheng, L., Zhang, Y., Qi, F., 2005. J. Phys. Chem. A109, 4231.
Wells, W.C., Borst, W.L., Zipf, E.C., 1971. Chem. Phys. Lett. 12, 288.
Wells, W.C., Borst, W.L., Zipf, E.C., 1972. J. Geophys. Res. 77, 69.
Wells, W.C., Borst, W.L., Zipf, E.C., 1978. Phys. Rev. A 17, 1357.
Wilhelmi, O., Schartner, K.-H., 2000. Eur. Phys. J. D 11, 79.
Winstead, C., McKoy, V., 1995. In: Yarkony, D.R. (Ed.), Modern Electronic Structure Theory. World Scientific, Singapore.
Winstead, C., McKoy, V., 2006. J. Chem. Phys. 125, 174304.
Woolsey, J.M., Forand, J.L., McConkey, J.W., 1986. J. Phys. B 19, L493.
Wu, C.Y.R., Judge, D.L., 1982. J. Chem. Phys. 76, 2871.
Wu, S.-M., Yang, X., Parker, D.H., 2005. Mol. Phys. 103, 1797.
Xie, H., Cao, Z., 2007. Int. J. Quant. Chem. 107, 1261.
Yang, S., Brereton, S.M., Wheeler, M.D., Ellis, A.M., 2005. Phys. Chem. Chem. Phys. 7, 4082.
Zavilopulo, A.N., Chipev, F.F., Kokhtych, L.M., 2005a. Nucl. Instrum. Methods B 233, 298.
Zavilopulo, A.N., Chipev, F.F., Kokhtych, L.M., 2005b. Nucl. Instrum. Methods B 233, 302.
Zecca, A., Karwasz, G.P., Brusa, R.S., 1992. Phys. Rev. A 46, 3877.
Zecca, A., Karwasz, G.P., Brusa, R.S., 1996. Riv Nuovo Cimento 19 (#3), 1.
Zhang, Z., Vanroose, W., McCurdy, C.W., Orel, A.E., Rescigno, T.N., 2004. Phys. Rev. A 69, 062711.
Zhao, H., Holladay, J.E., Brown, H., Zhang, Z.C., 2007. Science 316, 1597.
Zheng, Y., Cloutier, P., Hunting, D.J., Wagner, J.R., Sanche, L., 2006. J. Chem. Phys. 124, 064710.
Zhukov, A.I., Zavilopulo, A.N., Snegursky, A.V., Shpenik, O.B., 1990. J. Phys. B 23, 2373S.
Ziesel, J.P., Schulz, G.J., Milhaud, J., 1975. J. Chem. Phys. 62, 1936.
Zipf, E.C., 1984. In: Christophorou, L.G. (Ed.), Electron-Molecule Interactions and their Applications. Academic Press, Orlando, 1, 335.
Zipf, E.C., 1986. J. Phys. B 19, 2199.
Zipf, E.C., McLaughlin, R.W, Gorman, M.R., 1979. Planet Space Sci. 27, 719.
Zipf, E.C., Kao, W.W., McLaughlin, R.W, 1985. Chem. Phys. Lett. 118, 591.